A REVIEW OF RESEARCH ON AERONAUTICAL FATIGUE IN THE UNITED STATES

2001 - 2003

Compiled by
James L. Rudd
Air Force Research Laboratory
Wright-Patterson Air Force Base, Ohio, USA

FOR PRESENTATION AT THE MEETING
OF THE
INTERNATIONAL COMMITTEE ON AERONAUTICAL FATIGUE

5 – 9 MAY 2003

LUCERNE, SWITZERLAND

TABLE OF CONTENTS

9.1. INTRODUCTION

1. Leading government laboratories, universities and aerospace manufacturers were invited to contribute summaries of recent aeronautical fatigue research activities. Their voluntary contributions are compiled here. Inquiries should be addressed to the person whose name accompanies each item. On behalf of the International Committee of Aeronautical Fatigue, the generous contribution of each organization is hereby gratefully acknowledged.

+ Federal Aviation Administration
+ NASA - Langley Research Center
+ Air Force Office of Scientific Research
+ University of Houston
+ Naval Air Systems Command
+ STI Technologies
+ Advanced Structural Technology, Inc.
+ Structural Integrity Engineering
+ Aeronautical Systems Center
+ Air Force Research Laboratory
+ Fatigue Technology Inc.
+ Lockheed Martin Aeronautics Company
+ Georgia Institute of Technology
+ The Boeing Company
+ Lehigh University
+ Analytical Processes/Engineered Solutions
+ Purdue University
+ University of Dayton Research Institute
+ SAIC Ultra Image International
+ University of Puerto Rico
+ Old Dominion University
+ National Institute of Aerospace
+ Mississippi State University
+ Lockheed Martin Engineering and Sciences Corporation
+ U.S. Army Research Laboratory
+ Warner Robins Air Logistics Center
+ Naval Aviation Systems
+ Computational Tools
+ Lambda Research
+ University of Utah

2. The assistance of Ms. Charlotte Burns, Universal Technology Corporation, in the preparation of this review is gratefully appreciated.

3. Reference numbers are indicated as [ ]. For example, [1] is reference 1. References, if any, are listed at the end of each article. Figures are compiled at the end of the review.

9.2. OVERVIEWS

9.2.1 Centennial of Flight (1903-2003)

Robert M. Bader, Consultant

The year 2003 is a historical year as we celebrate the centennial of flight. As we know, the Wright Brothers were the first to fly a manned, powered, heavier-than-air, and controlled aircraft. The first four flights occurred at Kill Devil Hills near Kitty Hawk, North Carolina, on 17 December 1903. The first flight is shown in Figure 9.2.1.1. Because of the broken glass from the lower left corner, Orville Wright preferred the cropped version that is usually shown even though it shows less of the launching area. The original Wright Flyer I is on display in the Smithsonian in Washington, D.C.

Dayton, Ohio claims to be the "Birthplace of Aviation". The United States $.25 coin (quarter of a dollar) commemorating the State of Ohio as the 17th state to enter the Union (United States) refers to Ohio as the "Birthplace of Aviation Pioneers", Figure 9.2.1.2. This coin commemorates the Wright Brothers and Neil Armstrong. By the way, the State of Ohio is celebrating its 200th Birthday in 2003 as it was admitted to the Union in 1803. The State of North Carolina claims the "First Flight" on its coin, Figure 9.2.1.3.

The Wright Brothers conducted their research in Dayton, Ohio. Most of their gliding experiments leading up to the first four flights on 17 December 1903 were conducted at Kill Devil Hills. Starting in 1904, the Wright Brothers perfected flight through their experiments at the Huffman Prairie Flying Field, which is just east of Dayton and now a part of Wright-Patterson Air Force Base. The first "practical" airplane is considered to be the Wright Flyer III, which was built in 1905, and is on display at Carillon Historic Park in Dayton. The Wright Flyer III is the only airplane designated as a National Historic Landmark in the United States.

Figure 9.2.1.4 is a transcript of the patent for their "Flying Machine" that was issued in 1906. Figure 9.2.1.5 is the U. S. Army Signal Corps Specification, No.486 that is the "Advertisement and Specification for a Heavier-Than-Air Flying Machine". Note the *Preliminary* line: "This specification covers the construction of a flying machine supported by the dynamic reaction of the atmosphere and having no gas bag." Figure 9.2.1.6 is the contract between the Government and the Wright Brothers. The Wright 1909 Military Flyer was purchased by the Signal Corps for $30,000 on 21 August 1909. The contract cost of $25,000 was increased by an incentive of $5,000 since the speed requirement was exceeded. The original airplane is on display in the Smithsonian Museum, Washington, DC, and a reproduction of this airplane, Figure 9.2.1.7, in located in the US Air Force Museum, Wright-Patterson Air Force Base.

There are many books, articles and websites that chronicle the life and achievements of the Wright Brothers and there are also many events that are taking place in 2003 that celebrate the centennial of flight. Some of the other interesting historic sites in the Dayton area are as follows:

+ The Wright Brothers originally lived at 7 Hawthorne Street. This house was moved to Greenfield Village, Dearborn, Michigan by Henry Ford in 1937 – 1938. A replica of the Wright home is nearing completion on the original site in Dayton.

+ Close to Hawthorne Street at 22 Williams Street is one of the buildings where the Wright Cycle Company was located. This building is in its original location and open to the public. The Wright Cycle Company building where the Wright Brothers conducted their research and built the 1903 Flyer was located at 1127 W. Third St. in Dayton. This building was moved to Greenfield Village at the same time the Hawthorne Street home of the Wright Brothers was moved. A replica of this building is located at the Carillon Historic Park in Dayton.

+ Their new home, Hawthorne Hill, Figure 9.2.1.8, was completed in 1914. Katherine Wright, the Wright Brothers' sister, and Orville lived at Hawthorne Hill. Wilber died before the home was completed.

+ Overlooking Wright Patterson Air Force Base and the Huffman Prairie Flying Field is the Wright Memorial, Figure 9.2.1.9, which is located on Wright Brothers Hill. Adjacent to the Wright Memorial is a new National Park Service Interpretative Center, Figure 9.2.1.10. The Interpretative Center and the Huffman Prairie Flying Field have just recently been opened to the public.

These are some of the sites in the Dayton, Ohio area related to the Wright Brothers that you might find interesting to include in your itinerary on your next visit to Dayton, Ohio.

Acknowledgements:

Figures 9.2.1.1, 9.2.1.4, 9.2.1.5, 9.2.1.6 and 9.2.1.7: Photos/information courtesy of the US Air force Museum
Figures 9.2.1.2 and 9.2.1.3: Reference the US Mint website, http://www.usmint.gov
Figures 9.2.1.8, 9.2.1.9 and 9.2.1.10: Photos by R. M. Bader

9.2.2 Corrosion Enhanced Fatigue, MSD, and Framework and Methodology for Design and Prognostics

Robert P. Wei, D. Gary Harlow, Lehigh University (Research supported by the Air Force Office of Scientific Research)

Research on aging aircraft over the past ten years under programs sponsored by the U. S. Air Force, and those by the Fereral Aviation Administration and ALCOA, at Lehigh University have shown that a science based probability approach can be brought to bear on the life-cycle design of aircraft and their pronostics/sustainment. The feasibility and efficacy of the approach (vis-à-vis, the current experientially based statistical approaches) have been demonstrated. Inspite of the aggressive use of CPP (corrosion protection and prevention) programs, corrosion cannot be avoided, and must be incorporated into the design and maintenance of aircraft. As such, a transformation in approach for aircraft design and sustainment, to integrate corrosion analysis into structural integrity and durability assessments, is urgently needed. It is hoped that ICAF will take the lead in effecting this transformation.

The impact of localized (pitting) corrosion in enhancing the early onset of fatigue crack growth and the resulting reduction in fatigue life have been demonstrated. The feasibility of formulating science-based probability models for pitting corrosion and corrosion fatigue crack growth and of using such models in predicting response in service have been shown.

Models for pitting corrosion, based on galvanic coupling between aluminum and constituent particles in the alloys have been developed and validated. The good agreement between the observed distribution in pit size, following 192 h of immersion in a 0.5M NaCl solution at room temperature, and that from model prediction is shown in Figure 9.2.2.1. (The prediction was made using data on particle size and distribution, particle density, and electrochemical data estimated from laboratory measurements).

Based on the pit size distribution, estimates of fatigue lives and distribution were made. Figure 9.2.2.2 shows that the predicted distribution matched well with the experimentally measured values. The agreement indicates the variability in the fatigue lives of pre-corroded specimens reflected principally the variability in the crack nucleating pit size, which can be effectively predicted from a science-based model.

The feasibility for using laboratory (design) data to predict long-term service was shown through comparisons of model predictions with damage measured on retired aircraft. For example, by integrating models for contituent particle induced pitting and fatigue crack growth and using laboratory data, an estimate of the distribution in damage was made and was found to match well with that measured from a Boeing 707-321B aircraft that had been in commercial service for 22,533 flight cycles, or about 24 years (see Figure 9.2.2.3). Using the same basic data, estimates of the evolution and distribution of damage with time (or flight cycles) can be made and are also shown in Figure 9.2.2.3.

To further illustrate the approach, the evolution and spatial distribution in damage may be estimated through successive Monte Carlo simulations, using the distributions shown in Figure 9.2.2.3, and are shown in Figure 9.2.2.4. (It should be noted that in this simplified model, crack-crack interactions were not taken into account. The data are presented for illustration only; refinements are needed to reflect actual response for large damge sizes and life times.) By using the same seed number in the random number generator, the set of randomly selected key data for each damage location would remain the same, and the predicted results shown in Figure 9.2.2.4 represent one realization (*i.e.*, a single simulation) over the indicated flight cycles. The impact of damage is reflected (simplistically) through the loss of section, over all 1,000 holes or over the most heavily damaged 25 neighboring holes, in Figure 9.2.2.5. In practice, the distribution would be represented by the averages of many thousands of separate simulations; the number being dictated by the desired confidence level.

This approach provides the means for assessing the evolution and distribution of damage over a given area, separate areas, in an aircraft, or in a fleet of aircraft. It also provides a scientific basis for MSD (multiple site damage) analysis. It needs to be broadened and validated to better reflect operating environments. It is hoped that the community and the cognizant agencies would rise to the challenge to further develop and implement this approach.

REFERENCES

[1] Robert P. Wei and D. Gary Harlow, “Aging Aircraft and Life-Cycle Engineering and Management of Engineered Systems”, Fatigue 2002, Proceedings of the Eigth International Fatigue Congress, ed. A. F. Blom, Vol. 1/5 (2002), pp. 71-78.

[2] Robert P. Wei, “Corrosion/Corrosion Fatigue and Life-Cycle Management”, Materials Science Research International, Vol. 7, No. 3 (2001) pp.147-156.

[3] Robert P. Wei and D. Gary Harlow, “Corrosion Enhanced Fatigue and MSD”, AIAA Journal (to appear 2003).

9.2.3 Focused Life Assessment Models Using Holistic Concepts

C.L. Brooks, K.T. Honeycutt, T. Mills and S. Prost Domasky, Analytical Processes/Engineered Solutions, APES, Inc., St. Louis MO

In recent years, a fracture mechanics-based analytical life assessment process has been developed that has the potential to improve estimates of a structural component's cradle-to-grave service life by including contributions of both operational and time environments. This "holistic" process evolved by focusing on the fundamental role and function of the component, the mechanics and modes of damage, material behaviors, exposures, and driving forces, Figure 9.2.3.1. This life assessment capability: 1) includes design philosophies that are traditionally outside the scope of crack growth analysis (such as strain-life with hysteresis behavior, short-crack behavior, and intrinsic material discontinuities), and 2) incorporates effects of age-based structural degradation mechanisms (such as pitting, multi-site damage, corrosion topographies, pillowing, sustained stresses) as well as fatigue degradation mechanisms, Figure 9.2.3.2.

This focus assessment process, using holistic considerations, has been developed to provide evaluations of the structure from multiple perspectives: durability, damage tolerance, residual strength, corrosion tolerance, WSFD & MSD, and economic life. Where achievable, the whole of the holistic process should be used, but in other cases, partitions of the holistic process can be used to implement assessment techniques that enable potentially significant improvements to design processes through optimization of materials, design configurations, manufacturing processes, maintenance programs, usage variations, and general aircraft utilization.

While the inclusion of age degradation effects in systems requirements is not new, the recent focus on life extension programs for aging aircraft fleets has facilitated the push for improvements in the holistic life assessment process. Age degradation effects do not have to place an undue burden on the system and can be a vital part of the total design and maintenance process. In conjunction with other aspects of the aircraft system such as structural criticality, tactical importance, component replacement cost, and others, a screening of aircraft components from an 'age degradation susceptibility' point of view can potentially result in a more life cycle cost effective design.

The focused holistic process capitalizes on 'lessons learned' and successes of present design processes, while supplementing these design processes with easy-to-use and potentially very effective computational tools. A computer code, Environmental Cyclic Life Interaction Prediction Software (ECLIPSE), has been devised that implements most aspects of the entire process to provide a sound platform and framework. The software models the interaction of age degradation and cyclic damage modes and mechanisms using science and engineering principles, then simulates the progression of damage while considering both the independencies and interdependencies of environmental and cyclic behavior. The software already has been used to support several aircraft programs. Exercise of the models in the software has provided insight into difficult cracking problems caused by corrosion pitting and into corrosion problems in pressurized aircraft skins. This process integrates well into the current structural integrity design processes while addressing the age degradation challenges of the currently aging aircraft fleet. Experience gained by application of the holistic process to several aircraft problems has shown how the outputs of the predictive tools can assist a number of engineering disciplines with design, production, and maintenance of aircraft while maintaining focus on structural safety, maximum readiness, and minimal maintenance.

9.2.4 Metallic Materials Properties Development and Standardization (MMPDS)

John Bakuckas, FAA

The Military Handbook, "Metallic Materials and Elements for Aerospace Vehicle Structures," (MIL-HDBK-5), is a source of material strength properties and design values that are generally accepted as meeting the FAA 14 CFR Parts 23/25/27/ 29.613 requirements because of its rigorous standards. It also contains extensive information and data for other material properties and characteristics, such as fracture toughness strength, fatigue strength, creep strength, rupture strength, fatigue-crack propagation rate, and resistance to stress corrosion cracking.

MIL-HDBK-5 has evolved significantly over the years. Its predecessor was first published in 1937 as Army-Navy-Commerce Handbook 5 (ANC5). The United States Air Force (USAF) assumed the primary responsibility of continuing development in 1954 and, subsequently, the name of the book was changed to MIL-HDBK-5 in 1956. MIL-HDBK-5 has been continuously updated to incorporate new methodologies, add new material properties, and update existing ones. This continuing effort has enabled the Handbook to keep up with technology development and maintain up-to-date information for materials used by industry.

Detailed guidelines for statistical analysis of data were incorporated into the Handbook in 1971, which established standardized procedures for data requirements and analyses based on available statistical methods. The statistical procedures were further developed in 1984 to allow proper treatment of skewed data. As part of its continuing development, a major update of fracture toughness was completed in 1987. As digital information technology has become available and increasingly simple to use, the Handbook was distributed on CD-ROM in 1997.

In the past, the USAF had taken the lead in managing this effort and maintained a contract with Battelle Columbus Laboratory for specific technical and managerial functions, with 80% of the funds from the USAF and 20% from the FAA. However, due to recent USAF policy not to invoke or maintain military specifications or standards, USAF funding for the support of the handbook development ended in 1999. The FAA felt that the continuation of MIL-HDBK-5 was critical for certification and continued airworthiness of commercial aircraft and took the lead in supporting this effort.

As core research requirement within the FAA, the Metallic Material Properties Development and Standardization (MMPDS) document is the continuation of and replacement for MIL-HDBK-5. During fiscal year 2002, the FAA and USAF underwent a transition, which will insure the integrity MIL-HDBK-5 is maintained in the MMPDS. An interagency agreement between the FAA and the USAF has transferred the historical archives to the FAA and the MIL-HDBK-5 has been completely transitioned to the MMPDS document. On April 22-25, 2002, the FAA William J. Hughes Technical Center hosted the First Metallic Materials Properties Development Standards (MMPDS) and the 101st MIL-HDBK-5 Coordination Meetings. The meeting was well attended with over 50 participants.

The FAA considers the Handbook critically important to the FAA mission in certification and continued airworthiness and will continue to fund the core activities as required to maintain the Handbook's continued existence. The FAA will continue the process working closely with the industry and other government agencies to develop the MMPDS, continuing to provide periodic updates. The MMPDS will replace the MIL-HDBK-5 as the standard for static properties of metallic materials for the aviation industry.

9.2.5 Use of Software Service History in Certification

Charles Kilgore, FAA

The Flight Safety Research Branch published a handbook and a report on how the method of product service history may be used to gain certification credit for airborne software applications. These are applications that (1) were developed in the past and could have been developed for other domains, (2) have been previously certified for use in lower criticality aviation applications, or (3) have been certified to earlier versions or different standards than those currently used. This research effort collected and analyzed what is known and understood about applying product service history and then synthesized the data into a handbook for use in the aircraft certification process. Refer to Figure 9.2.5.1 for a description of the overall research effort design. The handbook was published as DOT/FAA/AR-01/116, "Software Service History Handbook." The report, DOT/FAA/ AR-01/125, "Software Service History Report," made recommendations to close the gaps in the existing guidance of DO-178B and Title 14 of the Code of Federal Regulations and made several recommendations for new guidance. The most important recommendation was to eliminate the inconsistencies in DO-178B between the use of service history and the prohibition of software reliability use in the assessment of system safety. These recommendations will be used as policy and guidance in the aircraft certification service. These documents should place more consistent expectations on applicants, something that has generally been shown to help control costs associated with certification.

9.2.6 Use of COTS Software and Hardware in Airborne Systems

Charles Kilgore, FAA

Using commercial off-the-shelf (COTS) software and hardware in airborne systems has the potential to (1) offer significant cost savings for small aircraft and rotorcraft, (2) reduce project development time and the associated cost, and (3) increase aircraft safety if lower cost systems could be shown to be safe and would allow the replacement of older, less capable systems. However, there is substantial concern in the aerospace industry whether methods are available or could be found for evaluating COTS used in airborne systems. Moving maps, graphical weather, situational awareness, and cockpit display of traffic information could be used in general aviation applications if efficient methods of assessing COTS were available. To address these concerns, the Flight Safety Research Branch published a report that provided significant information for use in the development of regulatory guidance on COTS software and hardware employed in flight controls and avionics systems. The report, prepared under contract with United Technologies Research Center, is titled "Study of Commercial Off-The-Shelf (COTS) Real-Time Operating Systems (RTOS) in Aviation Applications," DOT/FAA/AR-02/118.

COTS RTOS provides a variety of services to application software within a system. As RTOS services and capabilities grow in complexity, it is clear that they have an increased influence on the overall system performance and, as such, should have consideration in the overall System Safety Assessment.

The report takes a detailed look into the safety and certification issues of using a COTS RTOS in aviation applications. RTOS attributes are detailed and their safety-related properties are discussed along with considerations to address when integrating a COTS RTOS with an application in an aviation system.

Certain characteristics of RTOSs used in aviation applications are detailed in this report. Historically, aviation-based computing systems have used a federated design approach that can effectively isolate functions with respect to system criticality. However, in more recent years, manufacturers are integrating many of these functions into single computing systems with possibly different levels of criticality. RTOSs have become the central computing resource to manage these functions, and for this reason, RTOSs in integrated modular avionics (IMA) require a high level of scrutiny. The RTOS and the

associated partitioning, both spatially and temporally, of such IMA systems is important to maintain effective software level separation. The challenge is to design a partitioning solution that enables the exchange of information between partitioned functions and controlled access to other shared resources (such as I/O devices), while keeping the partitioned functions largely autonomous and unaffected by other functions.

Typical COTS software components are used in low-risk applications and many have been developed without considering the safety aspects of the software. However, if this software is to be used in airborne systems, the COTS product must be scrutinized to determine its ability to meet the intent of objectives found within RTCA/DO-178B, Software Considerations in Airborne Systems and Equipment Certification. It is difficult to access a COTS product's development and verification documentation, if any were produced, to substantiate compliance with DO-178B. However, some products are being developed specifically for the airborne market, albeit the selection is limited, it is growing. Additionally, there are other methods of compliance; however, they are difficult and rely on the regulator's ability to understand the alternate method and to apply some amount of subjective evaluation that the methods meet the intent of DO-178B objectives or provide equivalent levels of confidence.

9.2.7 Holistic Structural Integrity

David W. Hoeppner, University of Utah-QIDEC Laboratories

David W. Hoeppner, P.E., Ph.D was the chair and host for the first international conference on Holistic Structural Integrity held at Park City, UT in March, 2002. Sixteen leaders of the aircraft structural integrity community attended the conference for intensive discussions on structural integrity and related issues. Dr. Hoeppner attended the second international conference on Holistic Structural Integrity held in Fernie, B.C., Canada in March, 2003. The meeting was hosted by Jerzy Komorowski and Nick Bellinger of NRC and had numerous stimulating technical presentations.

9.3. LOADS

9.3.1 Statistical Loads Data for the Airbus A-320 Aircraft

Thomas DeFiore, FAA

University of Dayton, under contract to the FAA, completed the collection and analysis of over 10,000 flights of A-320 aircraft in commercial operation. The data, representing 30,817 hours of aircraft operation by a single U.S. operator, include flight and ground loads and operational data including accelerations, speeds, altitudes, flight duration and distance, gross weights, speed brake/spoiler cycles, thrust reverser usage, and gust velocities.

The Airbus A-320 is the first subsonic commercial aircraft equipped with fly-by-wire control throughout the entire flight envelope, and the first aircraft to have sidestick controls instead of the standard control column and aileron wheel. The fly-by-wire system controls ailerons, elevators, spoilers, flaps, leading-edge devices, engine thrust, and rudder and tail surface trim. The flight control system incorporates features that will not allow the aircraft's structural limits to be exceeded regardless of pilot input.

The airline data collection and editing system consists of two major components: (1) the data collection system installed onboard the aircraft and (2) the ground data editing station. The onboard collection system consists of a Digital Flight Data Recorder and Optical Quick Access Recorder (OQAR). The OQAR is equipped with an optical disk that can store up to 300 hours of flight data. The ground editing consists of a data integrity check and routine removal of any nonessential information deemed sensitive by the airline.

The 118 statistical data formats presented in the final report "Statistical Loads Data for the Airbus A-320 Aircraft in Commercial Operations," DOT/FAA/AR-02/35, published in April 2002, provides the FAA, airlines, and aircraft manufacturers with a detailed characterization of the A-320s in-service usage. The statistical data presented in the report demonstrated that the operational ground and airborne usage of the A-320 aircraft is similar to other large transports such as the Boeing 767, 737, and the MD-82/83 aircraft. However, there were instances, such as shown in Figure 9.3.1.1, where the A-320 appeared to be operating very close to or slightly in excess of its structural and operational limits.

9.3.2 Airborne Data Monitoring Systems

Thomas DeFiore, FAA

The Federal Aviation Administration (FAA) has re-established an Operational Loads Monitoring Research Project, which encompasses the collection, reduction, and analysis of flight and landing loads data on civil transports.

The Code of Federal Regulations, Aeronautics and Space, Airworthiness Standards are replete with loads criteria, much of which were generated prior to deregulation and in some cases prior to the design of wide-body and fly-by-wire civil aircraft. With the existence of (1) new technology, (2) newer operating rules and practices, and (3) the anticipated doubling of the air traffic within 10 years, operational flight and ground loads will be used to develop and validate airworthiness certification standards based on actual measured usage.

The output from the Operational Loads Monitoring research, which is primarily documented in FAA Technical Reports, provides substantiation of the technical basis for FAA airframe regulations and advisories. This research independently assesses the original equipment manufacturers' (OEM) design assumptions and aircraft usage analysis.
The FAA published its initial multiparameter general aviation airplane operational loads monitoring report, DOT/FAA/AR-01/44, Statistical Loads Data for Cessna-172 Aircraft Using the Aircraft

Cumulative Fatigue System (ACFS) in FY-01. The report describes a light-weight low-cost ACFS and the analyses and statistical summaries of data collected and processed from 1000 flights representing 1168 hours of Cessna-172 aircraft operational data from a major flight training university. The end product from the data acquisition effort includes statistical information on acceleration, speeds, altitudes, and flight duration and distance.

The report "A Methodology to Predict the Empennage In-Flight Loads of a General Aviation Aircraft Using Back Propagation Neural Networks, DOT/FAA/AR-00/50, provides a methodology for determining in-flight empennage loads using a neural network approach that does not require the installation of strain sensors on operational airplanes. The report describes the features of an inexpensive and effective technique for collecting empennage load spectra data for small airplanes already in service where installation of strain gauges is impractical.

The data report on the Video Landing Parameter Survey – Honolulu International Airport (HNL), DOT/FAA/AR-00/72, was published in FY-01. This is the third in a series of landing parameter surveys, which compiled typical usage information to compare with an aircraft manufacturer's sink speed design and fatigue load spectra. Four video cameras were temporarily installed along the south side of Runway 8L at HNL, and video images of 332 heavy wide-body transports were recorded, analyzed, and the results presented. Landing parameters presented included sink speed, approach speed, touchdown pitch, roll and yaw angles, off-center distance, and runway distance from the threshold. Wind and weather conditions were monitored and landing weights were available for most landings. This survey reinforced the findings of the previous FAA surveys at JFK and DCA, which demonstrated that current transport airplane sink speed distributions are substantially higher than those corresponding sink speed distributions reported 35 years ago during prior NASA surveys. Results of these surveys, which indicate that landing descent velocity increases with airplane size and/or weight, are being used to determine the possible need to increase the design descent velocities for the new Airbus A-380. The goal is to retain the same level of safety as currently certified designs.

The FAA recently built a Video Landing Parameter Survey Facility (Figure 9.3.2.1) on Runway 13 at the Atlantic City International Airport (ACY) where high-resolution video images of typical landings are recorded. This facility enables the FAA to collect operational landing impact parameters year round under a wide variety of weather conditions. In addition to obtaining landing data from regularly scheduled commercial arrivals at ACY, video image data are also recorded from frequent US Air Force and other civil and military operators who frequently conduct landing training exercises at the airport. Inclement weather data collected at this facility supplement regular survey data collected during prior surveys.

The FAA conducted two Gust Specialists Workshops that brought together over 40 international specialists to finalize the results of recently completed research studies on Statistical Discrete Gust (SDG). The SDG analysis method is designed to handle the significant non-linearity anticipated in future gust-alleviation systems. Final documentation of the SDG process is planned for FY02. Current and proposed joint FAA, NASA, and Boeing research on turbulence mitigation were also presented and evaluated.

Further details on the research is available at: http://aar400.tc.faa.gov/aar-430/airborne-data/

9.3.3 Rotorcraft Usage Monitoring and Validation of HUMS Advisory Circular

Dy Le, FAA

To conduct a Functional Hazard Assessment of a Health and Usage Monitoring System (HUMS), Bell Helicopter, Inc., under FAA funding, performed a fault tree analysis of the commercial off-the-shelf (COTS) HUMS installed on a Bell Model 412 helicopter. The FAA Rotorcraft Directorate will use the analysis results to support the Draft HUMS Advisory Circular (AC) issued by the FAA in 1999. The draft AC provides industry guidance to obtain airworthiness approval for HUMS installation, credit validation, and instructions for continued airworthiness for the full range of HUMS applications on rotorcraft.

Using HUMS, operators can monitor onboard critical helicopter components such as engines, rotor, rotor controls, drive train, and fatigue life-limited structures. HUMS offers potential benefits in enhanced safety, reduced maintenance costs, and improved operating efficiency. HUMS can be used for health monitoring to track rotor balance, assess engine performance, and aid in performing mechanical diagnostics. HUMS can be used for usage monitoring to monitor exceedance and operation and structural usages. HUMS can also be used for logistic interface and information management.

A HUMS can consist of a variety of onboard sensors and data acquisition systems. The acquired data may be processed onboard the rotorcraft or on a ground station (or a combination of both), providing the means to measure against defined criteria and general instructions for the maintenance staff and/or flight crew for intervention. Currently, the FAA has not certified or approved any HUMS for use in commercial operation.

The basic COTS HUMS used in this research project for usage monitoring consisted of:

- A centralized data acquisition and a processing unit called the HUMS Processing Unit (HPU). The HPU acquires data; converts analog, digital bus, and discrete inputs into digital form; preprocesses the data; provides display output to the HUMS Display Panel (HDP); provides continuous usage parameter data to the personal computer (PC) memory card interface for storage; and provides data access for the ground support equipment Data Retrieval Unit. HPU performs continuous built-in-testing (BIT) on the system elements.

- A set of sensors and transducers to provide signals to the HPU through wiring harnesses. Many signals are provided to the HPU by connecting existing aircraft systems via harnesses to the aircraft.

- A HUMS Display Panel mounted in the cockpit that displays operational information to the pilots. Inside the HDP, there are two PCMCIA type II card slots that can accommodate FLASH memory cards for continuous usage parameter data. The HDP contains the BIT and sends the results to the HPU.

The ground station used in this project consisted of a COTS PC with a tape backup system, a PCMCIA card slot, and a printer.

The certification process begins with the declared application intent and a determination of the resultant criticality. The declared intent should specify whether this application is for credit and if it adds to, replaces, or intervenes in maintenance practices or flight operations. When the declared intent is for credit, the end-to-end criticality for such an application should be determined and used as an input to establish the integrity criteria. If the declared intent is for noncredit, it may be certified as long as it can

be shown that the installation of the equipment will not result in a hazard to the aircraft. Therefore, the criticality describes the severity of the result of a HUMS application failure or malfunction. A functional hazard assessment (FHA) defines the criticality by considering the effect that the HUMS application can have on the safety of the aircraft. Compliance with the criticality level established by the FHA in the HUMS AC must be demonstrated.

The fault tree, as shown in Figure 9.3.3.1, was developed to support the functional hazard analysis and focused on the usage monitoring aspect of the HUMS. The fault tree presents a top-down analysis of the usage monitoring system. The analysis starts with the worst-case condition, i.e., a fatigue life-limited part being left in service too long. This is considered a potential catastrophic failure condition. The fault tree analysis shows the potential faults, which could be the cause(s) of the catastrophic failure condition, and how to prevent or compensate for each cause.

9.3.4 Mini-Health and Usage Monitoring Systems Concepts in Collecting Usage Spectrum for Fatigue Life Determination

Dy Le, FAA

A research task was undertaken to study the effectiveness of a mini-health and usage monitoring systems (HUMS) concept, compared to a complete HUMS, in collecting rotorcraft usage spectrums for determining the fatigue life of rotorcraft components. In this task, four previously developed usage spectra: the certification spectrum, the Utility Mission in Morgan City (UMMC) spectrum, the Atlanta Short Haul Mission (ASHM) spectrum, and the Gulf Coast Mission (GCM) spectrum, were used. The four spectra were originally developed using a complete HUMS. The certification mission spectrum was used as the base line spectrum for all comparisons.

Three simplified or mini-HUMS concepts were investigated. Each concept reduced the number of sensors and therefore reduced the complexity and the cost of the system by recording selected conditions and parameters (e.g., altitude, normal acceleration, airspeed, vertical velocity, and roll angle).

- Concept 1 records altitude only and applies an altitude breakdown to the certification spectrum. Thus, concept 1 was essentially an altimeter recorder. This would be equivalent to producing two certification data sets, one for below 3000 ft and another for at or above 3000 ft to account for the altitude effects on fatigue lives. The fatigue life calculations were reprocessed with the above altitude assumptions for all three mini-HUMS concepts.

- Concept 2 records altitude, normal acceleration, airspeed, and vertical velocity. Using these parameters, the amount of time the aircraft is in level flight is determined. The time in level flight was compared to the time in level flight for the certification spectrum at various air speeds. The remaining percentage time from the certification mission was factored to account for the difference in level flight time between the certification spectrum and the actual spectrum as recorded by the HUMS unit. The factored certification spectrum would then be used for the percentage time for all conditions other than level flight. Concept 2 assumes the helicopter is flown at the certification gross weight breakdown. As with concept 1, the actual altitude breakdown recorded by the HUMS unit is used.

- Concept 3 records altitude, normal acceleration, airspeed, vertical velocity, and roll angle. Using these parameters, it can be determined if the aircraft is in level flight, turning, or pulling up; the amount of time in these conditions is calculated. The percentage of time in level flight, turns, and pullups at various airspeeds is compared to the time in level flight, turns, and pullups at various airspeeds for the certification spectrum.

In the table below, the fatigue lives for the selected principal structural elements (PSEs) are shown. Shown first is the currently recommended fatigue lives with no altitude breakdown, then the fatigue lives using the three different mini-HUMS concepts along with fatigue lives using the complete HUMS package.

The mini-HUMS and the complete HUMS all use the mission altitude breakdown. Compared to the currently recommended fatigue lives with no altitude breakdown using the certification spectrum, the fatigue lives using the three mini-HUMS concepts are, in general, significantly greater. The only PSE where this is not the case is the main rotor yoke using the ASHM mission.

Table 9.3.4.1 shows that for the collective lever, main rotor spindle, and main rotor yoke, in general, the mini-HUMS fatigue lives are reasonably close to or substantially lower than the complete HUMS fatigue lives for the ASHM and GCM spectrums. For the UMMC spectrum, the mini-HUMS gives lives that are higher than the lives using the complete HUMS package for the rephase lever, the collective lever, and the main rotor spindle. However, for the main rotor yoke, the mini-HUMS lives are lower than those for the complete HUMS. For the rephase lever with the ASHM spectrum, the mini-HUMS gives fatigue lives that are substantially higher compared to the complete HUMS package. This is also true for the GCM when comparing mini-HUMS concept 3 to the complete HUMS package.

These results show that a mini-HUMS system can, in some instances, generate fatigue lives that are significantly higher than those generated by the more accurate complete HUMS package. To account for this, it may be necessary to assign a life extension limit to the part if a mini-HUMS system is to be used. For example, with a mini-HUMS system, the fatigue life of the part could not be extended beyond 200% of the recommended fatigue life using the certification spectrum, as published in the manufacturers fatigue life report. Further work is needed to establish such guidelines.

9.3.5 Effect of Ground Wind on Space Shuttle

Judith Goldish, The Boeing Company

A method was developed to assess the effect on Space Shuttle structure life due to exposure to high wind events while the vehicle is on the ground before launch. Mean wind speeds ranging from 10 knots (5.1 m/s) to 63 knots (32 m/s), which is just below a level 1 hurricane, were analyzed. Types of wind events that can be assessed include tropical storms, tropical depressions, thunderstorms, weather fronts, storms, and other occurrences of high wind speeds.

Because of the great variability in wind, it was not practical to develop a set of typical storms and events. Instead, the approach was to develop a set of standard one-hour-long wind blocks that could be combined to reconstruct any wind event. Each wind block represents a combination of wind speed and direction. Either three or four wind directions were assessed for each critical part. The one-hour length of the blocks was long enough to contain a reasonable distribution of frequency content, but short enough to be processed on existing computer equipment.

Fatigue loads spectra for the standard wind blocks were developed for locations on the Orbiter and Solid Rocket Booster (SRB) that were sensitive to ground wind. Orbiter locations included wing, tail, elevons, and payload bay door attachments. SRB locations included the forward attachment to the External Tank and the aft skirt near the attachment to the launch pad.
To assess an actual wind event, the event is reconstructed using the standard wind blocks and the effect of the wind blocks on the residual life (life above the structure certification requirement) is added up to get the total effect of the event. This method can be carried out very quickly because residual life capability

for each block has been calculated in advance. If the event shows a significant effect on the structure, then it can be analyzed in more detail.

The results showed that if the vehicle were exposed to multiple hours of mean wind speeds above 40 knots, there would be a potential for structural damage. Whenever possible, such exposure is prevented by moving the vehicle into the Vehicle Assembly Building if a large storm is found to be approaching the Kennedy Space Center.

Cumulative high wind exposure is being tracked for each Space Shuttle Orbiter vehicle.

9.3.6 A Study of Aerodynamic Effects of Ice Accretions on Aircraft Wings

James Riley, FAA

The aerodynamic efficiency of an aircraft wing can be seriously affected by ice accretions. This accretion disrupts the normal smooth airflow over the wing. The severity of these aerodynamic effects (loss of lift, increase in drag) from the ice accretions depend on the characteristics of the ice accretion. Glaze ice accretions form at temperatures near the freezing point and often have protrusions of ice, or horns, whose size, shape, and location determine their aerodynamic effect. Ridge ice accretions may form aft of a deicing system in supercooled large droplet (SLD) conditions and the size and location of the ridge also determine its aerodynamic effect. Intercylce ice forms between cycles of a deicing system, where the thickness, roughness, and extent determine its aerodynamic effect. Recent accidents and incidents in icing conditions have highlighted the need for a systematic study of the effects of different classes of ice accretions. As part of the certification process, aircraft fly with simulated ice shapes affixed to their wings to determine if the aircraft can fly safely with ice that may accrete during actual operations.

Thus, it is also necessary to determine the best ways to make and use sumulated ice shapes to produce effects as close as possible to those of real ice accretions.

In response to these concerns, the Federal Aviation Administration has sponsored a long-term research investigation at the University of Illinois at Urbana-Champaign (UIUC). The program has included icing testing the B. F. Goodrich Icing Wind Tunnel (IWT) in 1999 and 2000, aerodynamic testing at the UIUC tunnel, and at the Low Pressure Turbulence Tunnel (LTPT) at NASA Langley in Hampton, Virginia.

An important conclusion of the investigation of the effects of simulated ice horns is that the horn location may have the most determinant of the aerodynamic efficiency, if the horn size exceeds a certain threshold. Beyond this threshold, the study suggests that size plays a lesser role, and that the effect of the shape of the horn is least important of the characteristics studied. It was concluded that the location of ridge ice aft of an ice protection system was a key factor in the large loss in lift that can result from this type of ice.

Another major finding of the investigation was that the aerodynamic effect of the ice varies greatly with the type of airfoil. For example, the most adverse location for a protuberance on a National Advisory Committee for Aeronautics (NACA) 23012 airfoil is well forward of that for a natural laminar flow (NLF) 0414 airfoil. The loss of lift was also more severe for the first of these airfoils.

Another significant result was that the lift loss due to coarse sandpaper might be substantially smaller than that due to actual intercyle ice. Sandpaper has sometimes been used to simulated intercyle or thin ice in the evaluation of the operational characteristics of aircraft with ice accretions.

9.3.7 Freezing Precipitation in Flight

Richard Jeck, FAA

Freezing drizzle aloft has been suspected of causing several in-flight icing accidents and incidents over the past few decades. Most notable is the fatal Roselawn accident of October 1994 when a commuter airplane crashed near Chicago after holding in suspected freezing drizzle in clouds at an altitude of about 10,000 feet.

To learn more about the occurrences and characteristics of freezing drizzle and freezing rain aloft, (such that appropriate aircraft ice protection systems can be designed) the FAA has undertaken the task of developing a centralized database of fine-scale measurements in these kinds of icing conditions.

Specially equipped research airplanes operated by NASA Glenn Research Center, the Universities of Wyoming and North Dakota, and the Canadian Meteorological Service have obtained in-flight measurements in freezing precipitation for the past 20 years. The research flights were in the Great Lakes area, the mid-continent, the central California mountains, and the Juneau, Alaska area of the United States. Other data has come from parts of Europe and southern Argentina.

Relevant data from these flights are being collected and combined into a computerized database at the FAA William J. Hughes Technical Center. Presently, about 4000 miles of in-flight measurements in freezing drizzle and freezing rain have been compiled into the database.

An analysis of the data will indicate the average and extreme amounts of freezable water that are in these icing conditions and the range of temperatures and altitudes over which freezing precipitation has been recorded. Droplet sizes are also recorded for use in computing where the resulting ice will form on wing and tail surfaces during flight.

The data will also be used to develop representative and extreme freezing drizzle and freezing rain situations for (a) simulating freezing precipitation in icing wind tunnels or for estimating its effects on an aircraft by computer modeling and (b) any new rulemaking relative to flight in these conditions.

The latter consideration has been assigned to an international working group called the Ice Protection Harmonization Working Group (IPHWG) that was recently established under the Aviation Rulemaking Advisory Committee (ARAC) system. One task of the IPHWG is to "…define an icing environment including (freezing precipitation)…and revise the regulations, if necessary." This task will depend directly on the results of the database presently in development.

9.3.8 Dependence of Aerodynamic Effects of Ice on Aircraft Wing Geometry

James Riley, FAA

The aerodynamic efficiency of an aircraft wing can be seriously affected by ice accretions, which disrupt the normal smooth airflow over the wing. The severity of these aerodynamic effects (loss of lift, increase in drag) depends not only on the ice accretion, but on the aerodynamic characterisitics of the wing cross section (airfoil). Furthermore, the importance of the size and location of the accretion varies with the characteristics of the airfoil. Recent accidents and incidents in icing conditions have underscored the need for a systematic study of the sensitivity of different airfoil types to ice accretion and of the most critical ice shape locations for different types of airfoils. As part of the certification process, aircraft are flown with simulated ice shapes affixed to their wings to determine if the aircraft can fly safely with ice that may accrete during actual operations.

In response to these and related concerns, the FAA has sponsored a long-term research investigation at the University of Illinois at Urbana-Champaign (UIUC). The program includes aerodynamic testing in the UIUC tunnel and in the low-pressure turbulence tunnel (LTPT) at the NASA Langley Research Center in Hampton, Virginia, as well as extensive computational fluid dynamics investigations.

An important conclusion of the investigation is that the severity of the aerodynamic penalty of the ice is strongly dependent on the geometry of the airfoil as reflected in its pressure distribution and lifting characteristics. The NACA 23012 is an airfoil of a type widely used on piston and turbopropeller airplanes.[1] Much of the lift on the NACA 23012 is generated on the forward portion of the airfoil, which tends to be very sensitive to ice and experiences the greatest lift penalties when the ice is located close to, but downstream of, the point of minimum pressure on the upper surface. The NLF 0414, a natural laminar flow airfoil for which the lift is more evenly distributed over the airfoil, experiences less severe, though still very significant, penalties due to ice. The most critical ice location is aft of that for the NACA 23012, and the sensitivity to the location of the ice is much less pronounced. An airfoil with intermediate characteristics, such as the NACA 3415, exhibits intermediate characteristics with the simulation supercooled large droplet ridge-type accretion. Figure 1 compares the geometries of the three airfoils. Figure 2 shows the maximum lift coefficient ($C_{l,\,max}$) for the three airfoils without simulated ice (the straight lines at the top) and with simulated ice at locations specified by x/c, where x is the location of the simulated ice and c is the chord (the line from the leading to the trailing edge) of the airfoil. (Thus, $x/c = 0.20$ means that the simulated ice covers about 20% of the wing from the leading edge back.) The NACA 23012 suffers the largest penalty at $x/c = 0.12$, where the maximum lift coefficient is less than 0.3 (a penalty of well over 75%). However, the the maximum lift coefficient then increases for simulated ice shapes closer to the leading edge. For the other two airfoils, the penalty is not as severe, around $x/c = 0.12$, but then the maxium lift steadily declines as the ice shape is moved back.

REFERENCE

[1] Abbott, I.H. and von Doenhoff, A.E., Theory of Wing Sections, Dover Press, 1959

9.3.9 Aircraft Ice Detector Performance Specification

Edward Pugacz, FAA

Aircraft ice detection equipment for in-flight use has been available for many years. However, until recently, there has been no such equipment for use while the aircraft is on the ground. The detection of ice accretions in flight is relatively simple compared to the situation during ground operations. In flight, the ice detector only has to detect the onset of conditions suitable for ice accretion. This is usually accomplished by using a small vibrating probe whose vibrational frequency changes as ice accretes on it. The in-flight ice detector's design, placement, and detection threshold are such that ice usually accretes on the detector before it begins accreting on the aircraft, thereby giving the flight crew advance notice that action must be taken. During ground operations, an ice detector must detect ice, snow, frost, and all other types of frozen contamination on large areas of the critical aircraft surfaces that are made of different materials and coatings. In addition, these ice detectors must be able to detect frozen contamination in aircraft deicing fluids, indicating that the fluid has failed. This is a formidable technical challenge. In the past 5 years, a number of manufacturers have introduced ice detection equipment to use during aircraft ground operations. While this equipment has only been used experimentally, there has been no uniform standard by which to test this equipment. This lack of testing has prevented the certification of this equipment as a primary means to detect unsafe levels of frozen contamination on aircraft during ground operations.

Over a 3-year period, AAR-440 participated in the development of a Minimum Operational Performance (MOP) Specification for ground ice detection equipment. This specification was developed under the auspices of the European Organization For Civil Aviation Equipment (EUROCAE) Working Group 54 (WG54.) This working group consisted of representatives from regulatory agencies, equipment manufacturers, end users, and aircraft manufacturers from Europe and North America. This specification provides design as well as laboratory and installed testing guidance. The task of developing this specification was greatly complicated by the fact that there are currently three major types of ground ice detection equipment (spot sensors, local area sensors, and wide area sensors).

In addition, there are two general methodologies for using of ground ice detection systems (onboard or remote from the aircraft). The completed EUROCAE document (ED104) was subsequently coordinated with the Society of Automotive Engineers (SAE) Committee, G-12 Ice Detection Sub-Committee. AAR-440 personnel co-chaired two of the G-12 subcommittees, including ice detection. The specification will be published jointly and will as SAE Aerospace Standard AS5116a.

9.4. FATIGUE AND FRACTURE

9.4.1 Development of Residual Strength Prediction Methodology for Monolithic Structures – An Overview

B.R. Seshadri, Old Dominion University; M.A. James, National Institute of Aerospace; W.M. Johnston, Jr., Lockheed Martin Engineering and Sciences Corporation; R.D. Young, NASA Langley Research Center; and J.C. Newman, Jr., Mississippi State University

The aircraft industry is exploring the prospect of replacing built-up structures with integrally stiffened structures for aircraft applications. With the emergence of high speed machining and improvements in other manufacturing technologies, there is a great promise to significantly reduce part count and manufacturing cost, but methods need to be developed to predict the residual strength of these structures. As part of the NASA Airframe Structural Integrity Program, a fracture simulation methodology based on the critical-crack-tip-opening angle (CTOA) was developed to predict the residual strength of damaged aircraft structures. The methodology has been experimentally verified for structures ranging from laboratory coupons up to full-scale built-up structural components with single and multiple-site cracks. Efforts are under way at NASA Langley Research Center to extend this methodology to these new integrally stiffened structures. These extensions include modifications that account for crack branching into integral stiffeners as well as thickness variations in the panel. To validate these modifications, a series of flat integrally stiffened panels were designed, fabricated, tested and analyzed for their residual strength at the NASA Langley Research Center. This review summarizes some of the results determined from the residual strength prediction methodology development program for integrally stiffened panels at NASA Langley Research (refs. 1-5).

The analysis methodology used to characterize the critical CTOA value (ψ_c) for each material thickness was to match the maximum load from the analysis with the average maximum load from the tests. Three-dimensional finite element analyses were used to find the critical CTOA values. By using these CTOA values in a finite element analyses, the plane-strain core heights were estimated. Once the required plane-strain core heights were determined for various thicknesses, the residual strength analysis of 40-inch-wide integral panel was performed using STAGS finite element code. The integrally stiffened panel tested had a 5.9-inch-long lead crack located between the second and third integral stiffeners as shown in Figure 9.4.1.1. Schematic representation of crack branching for an integrally stiffened panel is shown in Figure 9.4.1.2. The test results (open symbols) and analytical prediction (solid line) corresponding to the right crack tip are shown in Figure 9.4.1.3. The inset shows the relative location of the integral stiffener close to the right crack tip. The test results indicate that failure occurred when the right crack tip reached the edge of the integral stiffener (solid symbol). The analysis results predict similar behavior and the crack growth became unstable when the crack tip entered the integral stiffener. The load-crack extension data from the analysis compares well with the test results, and the failure load predicted from the STAGS analysis is within 3% of the test failure load. Analysis results were also compared with strain gage readings in Figure 9.4.1.4. The integrally stiffened panel had strain gages mounted at several distinct locations on the sheet and on the stiffener flanges (front and back). One set of strain gages was located on the sheet surface 2 inches above the initial crack symmetry plane. Symbols and lines represent the test and analysis results, respectively. As applied load increases, the right crack tip continues to grow and the strains increase as indicated by the front and back right strain gages (solid symbols). The left crack tip has already grown past the strain gages, which do not indicate any increase in strains. This observation is indicated by the front and back left strain gage data (open symbols). The analysis results represented by the lines represent this behavior, and the results compare well with the strain gage measurements.

An additional 20-inch-wide integrally stiffened panel was analyzed for residual strength evaluation using the ZIP3D and the STAGS codes. The growth of secondary cracks is controlled by independent critical

crack tip opening angles. The panel was made up of 2024-T351 aluminum alloy material. Alcoa tested a series of 16-inch-wide, 0.25-inch-thick M(T) specimens, and the corresponding test results were used in calibrating critical crack tip opening angles and plane-strain core heights. These calibrated parameters were used in the residual strength predictions of for these panels. These panels were analyzed with a combination of solid and shell elements by using new capabilities in STAGS. For this purpose, a finite element model with solid and shell elements was generated. A typical schematic representation of such a model is shown in Figure 9.4.1.5. Rigid links were used to maintain displacement compatibility across solid and shell element transition regions. By using solid elements along the crack symmetry plane, the three-dimensional constraint condition around the crack tip region is automatically imposed in the model. Only the CTOA needs to be calibrated from laboratory specimens. With this new feature, one can represent the out-of-plane deformations of the structure with nonlinear shell elements while simultaneously modeling the crack tip region with solid elements. Comparison of load-crack extension results for a 20-inch-wide integrally stiffened panel is shown in Figure 9.4.1.6. Since experimental load-crack extension data were not available for comparison, a horizontal dashed line indicates the maximum load. Solid, dash-dot-dot and dash-dot lines indicate the ZIP3D, STAGS and STAGS3D analysis results respectively. The vertical bar indicates the location of the intact integral stiffener. STAGS analysis results with solid and shell elements represented by the dash-dot line compare well with other analyses results. ZIP3D, STAGS and STAGS3D analysis results compare well with the maximum test load, and are within 2% of the maximum test load. All of the analyses have similar characteristics, and once the lead crack passes the integral stiffener, the crack growth becomes unstable.

REFERENCES

[1] Newman, J. C., Jr., Seshadri, B. R., and Dawicke, D. S., " Residual Strength Analyses of Stiffened and Unstiffened Panels – Part I: Laboratory Specimens," *Engineering Fracture Mechanics*, 70, 3-4, 2003, pp. 493-508.

[2] Seshadri, B. R., Newman, J. C., Jr., and Dawicke, D. S., " Residual Strength Analyses of Stiffened and Unstiffened Panels – Part II: Wide Panels," *Engineering Fracture Mechanics*, 70, 3-4, 2003, pp. 509-524.

[3] Seshadri, B. R., James, M.A., Johnston, W. M. Jr., Young, R.D., and Newman, J. C., Jr., "Recent Developments in the Analysis of Monolithic Structures at NASA Langley," 6th *Joint FAA/DoD/NASA Conference on Aging Aircraft*, San Francisco, CA, September 2002.

[4] Seshadri, B. R., James, M.A., Johnston, W. M. Jr., and Newman, J. C., Jr., "Finite Element Fracture Simulation of Integrally-Stiffened Panels," 5th *Joint NASA/FAA/DoD Conference on Aging Aircraft*, Orlando, FL, September 2001.

[5] Seshadri, B. R., Newman, J.C., Jr., Young, R.D., and Bucci, R. J., "Residual Strength Analyses of Cracked Integrally-Stiffened Panels," *2001 USAF Aircraft Structural Integrity Program Conference*, Williamsburg, VA, December 2001.

9.4.2 Crack Growth and Stress Intensity Prediction Techniques

Jim Harter, AFRL/VASM, USAF Research Laboratories/Air Vehicles
Contractor: Analytical Processes/Engineered Solutions, APES, Inc., St. Louis, MO

The primary objectives of this program were:

- Determine the feasibility of the direct interaction of AFGROW with external “K-Solvers” to provide analysis of off-menu crack scenarios, and
- Develop a detailed integration plan for the automation of stress intensity factor generation for specific geometry via commercially available structural analysis programs and crack growth code, AFGROW.

This project demonstrated in 2002 that, by taking advantage of advances in computing technology that facilitate development of tools that integrate crack growth and K-solver software, vast improvements in next generation life prediction and assessment methods are possible today. The interaction of a structural finite element code, having crack tip Mode I Stress Intensity Factor (SIF) capabilities (referred to as a "K-solver"), with a crack growth analysis code (such as AFGROW) can provide more efficient life assessment and prediction techniques to the structures community. The program demonstrated the interactive capability by integration of a "K-solver" developed by Engineering Software Research and Development's (ESRD, Inc., St. Louis, Missouri, USA), a *p*-version finite element code called "StressCheck", with the USAF/AFRL crack growth code AFGROW. The resulting customized software demonstrated the proposed approach and serves as a benchmark of the required capability that would qualify other candidate K-solvers such as other FEM or boundary element software for integration. The StressCheck software was able to efficiently communicate via an Application Programming Interface (API) with AFGROW. AFGROW itself is one of the only crack growth codes offering an API suitable for interactive programming.

The Integration Plan describes the infrastructure and guidelines for evolving the technology, outlines plans and prioritizes activities, with the goal of ensuring that the USAF and industry are able to capture the benefits of this technology. The virtually infinite number of structural geometries, loading and cracking configurations and solutions that could be improved were classified into eleven Problem Classes (see Figure 9.4.2.1). A Complexity Rating Matrix was established to aid in setting priorities and evaluating the level of technical skill needed to construct integrated solutions. For each Problem Class; the specific solution needs were identified, problem complexity was defined, relative priorities within the aerospace industry were documented, and technical, business and integration cases for each Class were addressed. Demonstration software illustrated (see Figure 9.4.2.2) that software technology such as Microsoft COM (Component Object Model) enables construction of customized software for many Problem Classes, while for other Problem Classes the current software technology still lacks maturity and would require interactive solutions that would be unwieldy except where commitment of resources to develop full interactive solutions is justified by internal requirements. For some complex problem classes, interactive solutions are simply not feasible or practical in the near term.

A system specification was defined in sufficient detail to allow the integration with AFGROW with any K-solver, provided that the K-solver meets the system specification. The system specification includes requirements for the end integrator of the K-solver and AFGROW product; i.e., what the integrator must be capable of, what criteria must be defined, etc. Several representative examples were demonstrated. Recommendations for near- and long-term objectives were made and a road map for capturing other important structural problems that currently are difficult to solve without interactive methods was defined.

9.4.3 Accelerated Threshold Fatigue Crack Growth Rate Confidence Intervals for Small Fatigue Cracks

R.S. Piascik, NASA Langley Research Center and J.A. Newman, U.S. Army Research Laboratory

Fatigue crack growth (FCG) research conducted in the near threshold regime has identified a room temperature creep crack growth damage mechanism for powder metallurgy (PM) aluminum alloy 8009. The unusual room temperature near-threshold FCG behavior observed during constant-K_{max} testing (5.5 and 11 MPa$\sqrt{m}$) of alloy 8009 is plotted in Figure 9.4.3.1a [1, 2]. Transitions to accelerated FCG rates (dramatic slope changes in the d*a*/dN versus ΔK data identified with arrows) occur and are correlated with changes in crack surface morphology. For both K_{max} levels, a flat crack surface morphology (micrographs shown in Figures 9.4.3.1c and 9.4.3.1e) was observed at higher levels of ΔK. As ΔK was reduced, an accelerated d*a*/dN was observed, and the crack surface abruptly changed to a micro-void morphology (shown in Figures 9.4.3.1b and 9.4.3.1d) similar to that observed during elevated

temperature creep crack growth. Additional testing has shown that the post-transition FCG is time dependent, rather than cycle dependent, such that d*a*/dt depends only on the value of K_{max}.

To investigate the behavior shown in Figure 9.4.3.1, constant-K_{max} = 7.7 MPa?m tests were conducted in ultra-high vacuum (< 10^{-7} Pa) (UHV) and at temperatures of 297 K, 339 K, and 366 K. These data (see Figure 9.4.3.2) reveal that the FCG transition behavior shown in laboratory air (recall Figure 9.4.3.1a) persists in UHV and is dependent on temperature. Therefore, the anomalous FCG behavior of alloy 8009 is not dependent on environment and is likely the result of a creep mechanism. A series of static load tests were conducted to show that the near threshold micro-void crack growth phenomenon is the result of room temperature creep. Here, FCG specimens were held at a constant load that corresponded to a K = 11.0 MPa√m. Specimens were held at this load for a specified time and were cycled at K_{max} = 11.0 MPa√m and R = 0.5 to mark the crack surface. The crack surfaces produced during two of the constant load tests are shown in Figures 9.4.3.2b and 9.4.3.2c. The crack surface morphology is nearly identical to the post-transition crack surface at the same K_{max} level (recall Figure 9.4.3.1b). The centerline crack growth increments, Δ*a*, for each constant-load tests are plotted against the time held at constant load in Figure 9.4.3.2d. The solid line fitted through the first four data points (before crack tunneling effects significantly affect the crack driving force) nearly corresponds to the time-dependent crack growth rate at the "b/c" transition of Figure 9.4.3.1a, d*a*/dt = 2.05×10^{-8} m/s (dashed line).

Results show that the near-threshold accelerated fatigue crack growth observed in aluminum alloy 8009 is the result of a creep dominated damage mechanism. The micro-void crack growth mechanism requires a high local triaxial state of stress (plane-strain specimen interior) and elevated K_{max} levels ($K_{max} > 0.4\ K_{IC}$) during fatigue loading.

REFERENCES

[1] J.A. Newman, W.T. Riddell, R.S. Piascik, *ASTM STP 1372*, ASTM, 2000, p. 63-77.

[2] R.S. Piascik and J.A. Newman, NASA/TM-2002-211676.

9.4.4 An Extrapolation Method for Estimating Crack Growth Rate Confidence Intervals for Small Fatigue Cracks

R.L. Carlson, Georgia Institute of Technology, USA, and M.D. Halliday, University of Birmingham, United Kingdom

The objective of the research described in Reference [1] was to perform a statistical analysis of scatter observed in small fatigue crack growth experiments. The results were used to obtain confidence intervals for crack growth rate as a function of crack length, and to examine the use of a method for extrapolating crack growth rates back to an early stage of crack growth. The data used in the procedure presented here were obtained from fatigue tests on small corner cracks in 6061-T651 aluminum specimens. The average transverse grain size was 200 μm. Crack length measurements were obtained by use of a telemicroscope. Each of the test data cracks emerged from a 150 μm notch, and a cubic regression analysis was performed for each test specimen. Each regression equation was differentiated with respect to load cycle, N, and a Student's *t* analysis of growth rates was performed for 95% confidence intervals. The results are shown in Figure 9.4.4.1. The range of the variables is small, so a Cartesian coordinate plot, rather than a log-log plot, was used.

The basis for the extrapolation procedure used was the expectation that as extensions of the 95% bound curves move to the left, they should terminate in the vicinity of the d*a*/d*N* versus *a* origin in Figure 9.4.4.1. The resulting extensions could represent either growth of a primary crack from micro-multisite cracking on a smooth surface, or growth from a notch-like flaw. For the exploratory studies described the extrapolation function selected had the form

$$\frac{da}{dN} = pa^3 + qa^2 . \qquad (1)$$

This function is zero at the origin, and it has zero slope at the origin. The values of the constant p and q were determined to provide continuity of the function, and its first derivative at the juncture points with the 95% bounds. The resulting, solid extrapolation curves are shown in Figure 9.4.4.2. The plotted points represent test results. Equations for load cycle as a function of crack length were obtained by integration of Equation (1) to obtain the solid curves shown. The plotted points were obtained by numerical integration of test points of Figure 9.4.4.1.

For the analysis presented, an initial value of a = 200μm was chosen for N = 0. This value of crack length is of the order of the given grain size. The results are plotted in Figure 9.4.4.3 with N as the ordinate. An examination of Figure 9.4.4.3 reveals that at a crack length of 1000μm, the values for N are about 250000 and 1000000. These values could be added to the number of cycles between 1000μm and the critical 'long' crack length to obtain the fatigue life.

REFERENCE

[1] Carlson, R. L. and Halliday, M. D., "An Extrapolation Method for Estimating Crack Growth Rate Confidence Intervals from Small Fatigue Crack Data," Journal of Testing and Evaluation of the ASTM, May 2002, pp. 179-185.

9.4.5 Crack Growth Modeling for Rotorcraft

Dy Lee, FAA

The FAA, under joint funding with the U.S. Air Force. U.S. Army, and NASA, is sponsoring a new fatigue crack growth model for rotorcraft being developed at the Cranfield University, United Kingdom. This model defines an effective stress-intensity factor that accounts for crack closure, residual compressive stresses, and material crack growth threshold.

The difference between the model being developed and other models is the central parameter for this model is the crack propagation stress-intensity factor, K_{PR}. K_{PR} is defined as the stress-intensity factor when the crack starts to propagate during the loading phase of a cycle.

Recent research indicates non-conservative life predictions are obtained using traditional models for fatigue crack growth when considering helicopter load spectra. The research at Cranfield compares the accuracy model the K_{PR} model with that of well-established models (Fastran and AFGROW) at both short- and long-crack lengths. The predictions will be validated against experimental data obtained by subjecting crack growth samples to actual helicopter service load histories.

A general description of the relatively simple loading sequences in terms of K_{PR} leads to a scheme that is denoted as the Fatigue Crack Growth (FCG) Map. The FCG map defines all possible crack growth conditions and is the heart of the crack growth prediction method.

The FCG Map will be generated for different alloys of different temperatures and strengths, such as 7010 aluminum and a high-strength quenched and tempered steel.

9.4.6 Characterization of Crack Length Measurement Methods for Flat Fracture with Tunneling

Mark A. James, National Institute of Aerospace, and James C. Newman, Jr., Mississippi State University

Recently, a wide variety of fracture tests were conducted on 6.35 mm thick 2024-T351 aluminum alloy in the LT orientation [1]. A consistent observation made of the load-crack extension curves (and similar curves for many other thin sheet and plate materials) is that the straight crack-front analysis generally over-predicts crack extension, before and after maximum load. However, the analysis matches the δ_5 behavior of the tests very well (δ_5 is the displacement measured across the original crack tip location using a 5 mm gauge length). The results compared very well, both before and after maximum load, corresponding respectively to the local and remote stages of crack extension. The results strongly suggest that the flat, straight crack-front in the 3D analysis represents the "average" crack length at any given load. A more appropriate comparison metric may be to use an average crack length measure, such as unloading compliance or area average. A new compliance-based measurement method using the δ_5 displacement was developed to take advantage of its increased sensitivity.

Experiments and analyses were performed [2] to characterize the crack tunneling for the 6.35 mm thick 2024-T351 aluminum alloy. Compact tension specimens (W = 152 mm) were fatigue pre-cracked at low stress-intensity factor levels (8 MPa $\sqrt{m}$) to an a/W ratio of 0.4. Each specimen was loaded in displacement control just enough to cause a predetermined amount of surface-crack extension. The fracture crack-front was marked using fatigue crack growth at a high stress ratio (R = 0.75 or 0.8) and a relatively high load (80% of the current fracture load). Figure 9.4.6.1 shows a typical measured fatigue pre-crack shape and fracture surface crack shape and compares several other crack length measures with the crack profile shape. The experimentally measured CMOD unloading compliance crack length is nearly the same as the visual crack length. The experimentally measured δ_5 compliance value nearly matches the area average. Figure 9.4.6.2 compares tunneling data with surface crack extension and analysis results. The open symbols show the "original" surface measured data from Reference 1. The closed symbols show the new data from the tunneling test. Surface crack measurements are significantly different from the maximum tunneling on the interior. Figures 9.4.6.1 and 9.4.6.2 show that the analysis results fall within the tunneling range for the full extent of crack extension. The load versus crack-extension results show significantly improved correlation between the area-average test data and the analysis results compared to the original load-surface crack extension.

Since tunneling does occur in many cases, it is desirable to account for the tunneling either in the analysis or in the test data. The most desirable approach is to modify the analysis to include crack-front shapes that match the experimental results [3] or use a modeling methodology that allows the tunneling to evolve naturally as part of the analysis. The δ_5 compliance approach is the overall best here because it is sensitive to tunneling, approaches the area average measurements, and is relatively easy to implement using digital imaging systems.

REFERENCES

[1] James, M. A. and Newman, J. C., Jr., "Three Dimensional Analysis of Crack-Tip-Opening Angles and δ_5-Resistance Curves for 2024-T351 Aluminum Alloy," *Fatigue and Fracture Mechanics: 32nd Volume, ASTM STP 1406*, Ravinder Chona, Ed., American Society for Testing and Materials, West Conshohocken, PA, 2000, pp 279-297.

[2] James, M. A. and Newman, J. C., Jr., "Characterization of Crack Length Measurement Methods for Flat Fracture with Tunneling," *Fatigue and Fracture Mechanics: 33rd Volume, ASTM STP 1417*, W. G. Reuter and R. S. Piascik, Eds., American Society for Testing and Materials, West Conshohocken, PA, 2003 (in press).

[3] Dawicke, D. S., J. C. Newman, Jr., and C. A. Bigelow, "Three-dimensional CTOA and Constraint Effects during Stable Tearing in Thin Sheet Material," *ASTM STP 1256*, W. G. Reuter, J. H. Underwood and J. C. Newman, Jr., Editors, American Society for Testing and Materials, pp. 223-242, 1995.

9.4.7 2nd Generation Crack Growth Prediction Methodology for Cold Worked Holes

W.T. Fujimoto, Advanced Structural Technology, Inc. and E.J. Tuegel, US Air Force Research Laboratory

An advanced joint analysis tool is being developed to: (1) exploit the life enhancement potential of coldworked holes and/or interference fit bushings, and (2) to develop members with increased resistance to structural life degradation. The tool will serve as the foundation for an analytical certification capability for joints with coldworked holes, minimizing or eliminating the testing presently required to certify such joints. In Phase I, ASTI demonstrated the feasibility of a physics-based approach for predicting the crack formation and crack growth lives for complex multi-layer joints with cold worked holes. The physics-based approach models the mechanisms by which residual stresses are induced during the coldworking process and the mechanisms by which a crack (or system of cracks) grows through this residual stress field. This approach combines closed-form elastoplastic analyses of the coldworking process, 3D elastoplastic finite element analyses (for developing correction factors for accounting for through-the-thickness variations), 3D elastoplastic analysis of the growing crack, multi-layer joint analyses using virtual fasteners, probabilistic fatigue analyses of the net section, and a novel virtual crack approach for determining stress intensity factors, into a CAD-based system capable of tracking the multi-stage growth of a crack in a cold worked joint.

Use of a physics-based approach, rather than a phenomenological approach, allows the residual stress field and the crack driving stress field to be obtained from basic material and geometric properties, and minimizes the need for empirical correction factors. Furthermore, because the approach treats the coldworked hole as part of a complex interacting structural system comprised of the adjoining layers and fasteners, rather than as an isolated hole, it accounts for the influence of secondary bending and fastener deformation on life.

Factors not handled by existing analysis methods that are explicitly handled by the physics-based approach include the following:

- Crack formation and growth in the residual tension zone away from the hole, and the resulting multi-stage crack growth pattern (Figure 9.4.7.1).
- Variation of the residual stress through the thickness of a cold worked member.
- Relaxation of the residual stress field due to clean-up reaming of the hole.
- Relaxation of the residual stress field due to overloads or underloads.
- Relaxation of the residual stress field due to crack growth into the residual tension zone.
- Relaxation of the residual stress field due to cyclic reyielding of the residual tension zone.
- Interaction of the hole with a fastener (and with the adjacent elements in a multi-layer joint)
- Secondary bending
- Fastener clearance/interference

A key to the approach is the use of probabilistic fatigue analyses to determine the most probable initial cracking location on the crack face. The probabilistic analyses account for the influence of joint design, interference level, fastener type, material properties, and loading in determining whether the crack initially forms at the edge of the hole or away from the hole in the residual tension zone. If the crack

initiates away from the hole in the residual tension zone, a multi-stage model of the crack growth process tracks the relaxation of the residual stress field as the initial crack grows through the residual tension zone, while simultaneously tracking the fatigue damage at the hole edge. Upon initiating a secondary fatigue crack at the hole edge, a secondary crack is "inserted" at the hole edge and the system of cracks are tracked as the cracks coalesce into a single macro-crack. If the crack initiates at the edge of the hole, the cyclic relaxation that occurs as the crack advances into the residual tension zone is tracked.

To facilitate the use of the software system by structural engineers, a prototype of a novel CAD-based system for performing fatigue and damage tolerance analyses of complex joints was developed. The system features a graphical object-oriented modeler that allows the rapid "click-and-drag" synthesis and modification of complex multi-layer joints from parametric objects. An automated mesh routine automatically meshes the model into a finite element model, eliminating the need for explicitly meshing the model. A unique feature planned for the CAD-based system is the ability to create custom damage progression scenarios using "click, drag-and-drop" modeling. These custom damage progression scenarios will allow the user to model the progressive spread of damage between holes, while accounting for load shedding and load redistribution as the crack system grows. Examples of the complex crack growth scenarios for which this approach is intended are shown in Figure 9.4.7.2.

9.4.8 Bulging Effects on Longitudinal Cracks in Lap Joints of Pressurized Aircraft Fuselage

John Bakuckas, FAA

Longitudinal cracks in pressurized aircraft fuselage structures are subjected to complex stress and displacement fields resulting in nonlinear out-of-plane deformations. The response of such cracks is characterized by large out-of-plane deformations or bulging of the surfaces of the crack, as illustrated in Figure 9.4.8.1. The so-called bulging effect can significantly elevate the stress-intensity factor (SIF) at the crack tip and reduce the residual strength. One way to measure the bulging effect is by the bulging factor, which is the ratio of the SIF of a longitudinal crack in the curved fuselage to the SIF for the same crack in a flat panel. The damage tolerance design philosophy requires determination of realistic stress state in the vicinity of cracks in airframe fuselage structure. However, most studies of bulging effects are for idealized unstiffened shells. Few studies have been conducted to study the significance of bulging effects on cracks in lap joints of aircraft fuselage structure and the consequence of not including these effects in the stress predictions and subsequent damage tolerance analysis. An area of particular concern is the critical rivet row in a longitudinal lap splice joint, 1 of the 16 critical areas identified by the Airworthiness Assurance Working Group as having the potential for multiple-site fatigue crack initiation.

A study was undertaken to examine the effects of bulging of a mid-bay crack in the critical row of a longitudinal lap splice joint. A typical three-rivet row lap joint configuration, which contained a mid-bay crack in the critical rivet row, was analyzed. The bulging factors were calculated using a nonlinear finite element analysis. The SIF at the crack tip was calculated using the Modified Closure Integral method. Parametric studies were done to examine the effects of crack length, applied pressure, and stiffening elements (stringers and frames) on the bulging factor.

In general, results show that the bulging phenomenon occurred in the typical longitudinal lap joint considered, even with stiffening elements. Figure 9.4.8.2 shows representative results from the study. For the configurations analyzed, bulging factors were the highest for the unstiffened case and were reduced with each additional stiffening element. In all cases, the lap joint provided some stiffening effect, reducing the bulging factor compared to the baseline case.

For short cracks (cracks much smaller than the stringer spacing), a near-constant response was obtained for the bulging factor as a function of the applied pressure. The presence of the stiffeners only slightly

reduced the bulging factor for the shorter cracks. The cracks were too small and too far from the stringers to be affected by the stiffening elements. For longer cracks, the bulging factor varied nonlinearly as a function of the applied pressure, and the presence of the stiffeners significantly reduced the bulging factor.

9.4.9 Stress Intensity Factor Solutions for Multiple Through Cracks Growing To and From Holes in Finite Width Plates

J.A. Harter, Structural Mechanics Branch, US Air Force Research Laboratory

Stress intensity solutions for multiple through cracks growing to and from holes may be found in the literature for infinite plates. However, for practical applications, solutions are required for finite width plates. A project to develop solutions for two, independent through cracks (with holes) in finite width plates (see **Error! Reference source not found.**) was initiated to address this shortcoming [1]. The solutions were developed using the p-version finite element code, StressCheck. An example of one of the finite element models is shown in **Error! Reference source not found.**. As would be expected, the solutions were extremely dependent on the relative proximity of the cracks and holes. In addition, the solutions were affected, in a very complex manner, by the location of the cracks relative to the free edges of the plate.

The infinite width case was approximated using a plate width of 101.6 cm with two cracks of various lengths and a 6.35 mm hole where both the cracks and the hole were located in the central area of the plate (relatively far from either free edge). Finite width cases were modeled using the following plate widths: 50.8, 40.64, 20.32, 10.16, 5.08, 2.54, 1.905, and 1.27 cm. The standard solution for each crack tip was developed based on the standard single crack solution and a correction factor(s) determined from the appropriate finite element model. The correction factors (see **Error! Reference source not found.**) were curve fit from the finite element results where possible. In cases that were not suitable for curve fitting, tabular corrections were applied.

Numerous geometric combinations were considered:

Two, unequal cracks growing from a single hole
Single crack at a hole and a second crack growing to a hole
Two, unequal internal cracks growing to a hole
Two, unequal edge cracks growing to a hole
Single internal and a single edge crack growing to a hole
Single internal crack growing to a hole
Single edge crack growing to a hole

Solution error was within approximately 3 percent (based on the finite element results) for the vast majority of cases. Larger errors exist for some extreme geometric cases (i.e. crack tip very close to a free edge). The solutions have been incorporated in the U.S. Air Force crack growth life prediction program, AFGROW, and are being documented in an Air Force technical report.

REFERENCE

[1] Harter, J.A., Taluk, D., and Honeycutt, K., “Damage Tolerance Application of Multiple Cracks and Time Dependence,” to be published as a U.S. Air Force TR

9.4.10 Test and Analysis Based Stress Intensity Factors for Interference-Fit (Taper-Lok ®) Fasteners

S. Shah, K. Duffié, S. Ramachandran, Structural Integrity Department, Lockheed Martin Aeronautics Co. and Thomas Lamb, C-141 System Program Office, Warner Robins Air Force Base

An analysis procedure has been developed to compute Stress Intensity Factors (SIF) for a single radial crack emanating from a no load transfer interference-fit fastener (Taper-Look ®) hole. The details considered are those found on C-141 and B-1 aircraft. Steel and titanium fasteners in aluminum plate are analyzed. Then, analytically derived SIF are used to compute crack growth for Constant Amplitude (CA) spectra. The analytical crack growth is correlated with test data for coupons subjected to constant amplitude (CA) spectrum. Further analysis is necessary to verify the validity of the procedure for variable amplitude spectra. Also additional analysis and testing is needed to develop and verify procedure for other plate/fastener material combinations and load transfer cases.

Approach

The Green's function approach is used to obtain the SIF for a single radial crack emanating from an interference-fit fastener hole. V. Shivakumar and Forman [1] obtained Stress Intensity Factors K_I and K_{II} for a point-loaded crack emanating from a circular hole in an infinite plate. A series approach and the Muskhelishvili formulation in the two-dimensional theory of elasticity were used to derive the solution. The solutions developed in [1] were for a through the thickness crack. Ball [2] developed a solution for corner crack.

The Green's function approach requires, for a given loading, the stress distribution in an unflawed (uncracked) structure. This stress distribution, along with the appropriate Green's function, is integrated to obtain SIF solutions.

Finite Element Model (FEM) Description

The stress distribution in the vicinity of the hole is elastic-plastic. 2D Finite Element Model (FEM) using a 4-node quadrilateral bilinear plane stress element CPS4I [5] was developed. In the model, the fastener was explicitly modeled, but the taper of shank and countersunk of the fastener were not modeled.

The contact surface was defined between the fastener and hole. The level of interference was modeled using the initial clearance feature available in ABAQUS code. The material non-linearity was incorporated using stress-strain data from Mil-Handbook-5 [4]. The isotropic hardening rule was used. The three-step loading was run consecutively. The three steps are:

- Interference only
- Interference with far-field loading applied
- Interference with far-field loading removed

Figure 9.4.10.1 shows the stress distribution for specimen configuration 'A' for the average (0.00300 in.) interference respectively. Configuration 'A' has 1/4-in. diameter steel Taper-Lok® installed in 7075-T6 0.160 in. thick plate. The applied far-field stress is 18 KSI.

Stress Intensity Factor Solutions

The unflawed stress distribution along with Green's function derived in [2] is used to obtain SIF for a through the thickness crack. The computer program by Ball [3] was used to perform integration. The computer program uses 10-point Gauss-Legandre Quadrature discussed in [7].

The SIF for specimen "A" configuration for an applied far field stress of 18 Ksi and subsequent unloading are shown in Figure 9.4.10.2. The results (not Shown here) also show that stress intensity range, ΔK, for a given configuration and stress range ($\Delta\sigma$), are independent of interference levels considered; however,

the effective stress ratio, R_{eff} = Kmin / Kmax is not. This effect needs to be included in the crack growth analysis. These results are used to correlate Constant Amplitude (CA) coupon fatigue tests.

Correlation of Analytical Results to Test Results

The SIFs computed using the above procedure are used to correlate the test crack growth data for specimens A6 and A7. The specimens A6 and A7 were tested for a constant amplitude spectrum of σ_{max} = 18 KSI and R=0.10. The correlation is shown in Figure 9.4.10.3.

KEYWORDS

Stress-Intensity Factor, Green's Function, Interference-fit, Taper-Lok®, Residual Stress, Effective Stress Ratio.

REFERENCES

[1] V. Shivakumar and R. G. Forman (August 1980), Green's Function for a Crack Emanating From a Circular Hole in an Infinite Sheet, International Journal of Fracture, Volume 16, No. 4.

[2] D. L. Ball (December 1994), Service Life Enhancement Modeling and Evaluation: Fracture Analysis of Cold Expanded Holes, ERR-FW-4315, Lockheed Fort Worth Company, Fort Worth, Texas, 76101.

[3] D. L. Ball (September 2000), Metallic Life Analysis Program: Metlife V1.3 Technical Approach, MR (FF)-1022, Revision C, Volume 2, Lockheed Martin Tactical Aircraft Systems, Fort Worth, Texas 76101 (unreleased).

[4] MIL-HDBK-5H, Military Handbook, Metallic Materials and Elements for Aerospace Vehicle Structures, December 1998.

[5] ABAQUS/Standard User's Manual Version 5.8, Hibbitt, Karlsson and Sorenson, Inc., Providence, RI 1998.

9.5. DAMAGE TOLERANCE

9.5.1 USAF Damage Tolerant Design Handbook: Guidelines for the Analysis and Design of Damage Tolerant Aircraft Structures

Peggy C. Miedlar, Alan P. Berens, Allan W. Gunderson, Joseph P. Gallagher, University of Dayton Research Institute

In the early 1970's, the United States Air Force (USAF) developed a damage tolerance philosophy to help eliminate the type of structural failures and cracking problems that had been encountered on various military aircraft. Air Force review of structural failures had revealed that the safe life philosophy did not protect against designs that were intolerant to defects that could be introduced during manufacturing or during in-service use. From the standpoint of flight safety, it was found prudent to assume that new airframe structures could contain initial damage (e.g. scratches, flaws, burrs, cracks, etc) and that not all cracks would be found during inspections of older airframes. Accordingly, a damage tolerance philosophy was formulated using the assumption that pre-existing damage would be present at critical locations of all structurally significant details. The intent was to ensure that the maximum possible initial damage would not grow to a size that would endanger flight safety during two service lives of the aircraft. Damage tolerance was formally adopted by the Air Force as part of the Airplane Structural Integrity Program (ASIP) [MIL-STD-1530, 1972] and was implemented originally through MIL-A-83444, Airplane Damage Tolerance Requirements. The Air Force now implements damage tolerant design through the recommended practices of the Department of Defense Joint Services Specification Guide, JSSG-2006 [1998].

The primary purpose of the Damage Tolerant Design Handbook is to provide guidelines and state-of-the-art analysis methods that should aid engineering personnel in complying with the intent of the USAF Airplane Damage Tolerant Guidelines for metallic structures. A secondary purpose is to provide specific background data and justification for the detailed guidelines. The handbook has been structured to provide a clear and concise summary of the Damage Tolerant Requirements and the supporting data and rationale behind the critical assumptions. Where appropriate, analysis methods, test techniques, and NDI methods are provided with suggested and/or recommended practices, limitations, etc. so stated. In the Handbook, pertinent paragraphs of JSSG-2006 are referenced.

The newest version of the Handbook is presented as a web-based document, allowing easy access for all users from any location. The web document format allows timely updates as new methodologies emerge and technologies advance. Finding information will be easier with the search capabilities available in electronic documents. Hyperlinks are provided for sub-sections, figures, tables, and references within the handbook, as well as to other related web sites. Links are provided to websites where referenced papers can be found, software can be downloaded, and additional in-depth information is provided. Advantages of this are to give the user the most accurate, up-to-date information without reprinting the Handbook.

In addition to the web pages, each Section of the Handbook, as well as the Sample Problems, is available as a .pdf file that can be downloaded and printed.

REFERENCE

[1] P. C. Miedlar, A. P. Berens, A.W. Gunderson, J.P. Gallagher. (2003). "USAF Damage Tolerant Design Handbook: Guidelines for the Analysis And Design Of Damage Tolerant Aircraft Structures." AFRL-VA-WP-TR2003-3002. http://www.dtdesh.wpafb.af.mil

9.5.2 Probability of Failure Analysis for Fracture Critical F-22 Titanium Castings

T.R. Brussat and P.J. Caruso, Lockheed Martin Aeronautics Company

Flaws inherent in the casting process present a unique challenge for maintaining damage tolerance of Titanium cast parts used in fracture critical F-22 airframe structure. Shell inclusions, in particular, are crack-like, can be difficult to detect, and occur frequently. Flaw size can occasionally approach 0.50 inch. Based on demonstrated radiographic non-destructive inspection (NDI), the conventional 0.05-inch assumed initial flaw size for damage tolerance was increased significantly for shell flaws. Even so, the 2-lifetime analysis with these increased initial flaw size assumptions was not, by itself, considered adequate to ensure the required minimum probability of failure (PoF).

Shell inclusion flaws in castings are significantly more commonplace than is the norm for other aerospace metallic materials approved for Fracture Critical use. A shell flaw is a fragment of the mold that, typically, spalls off during the pour and remains suspended in the molten Titanium during solidification. Because it is thin and very brittle, this flaw behaves like an initial crack in the final part. Before final heat treatment, castings are x-ray inspected; any flaws found are removed; and the area is weld-repaired. Once heat-treated, all properties, whether previously weld repaired or not, are homogeneous. Because radiographic inspection is imperfect, there is a small but finite probability that the flaw may not be detected and may grow to cause catastrophic failure within the design lifetime of the aircraft.

A detailed PoF analysis is conducted to establish shell flaw frequency limits and thereby assure that the assumed initial flaws are infrequent enough to be considered ‘rogue” flaws. The analysis provides an estimate of the number of shell defects for all castings that would result in a per-flight PoF less than 10^{-7}, the criterion for acceptability (See Figure 9.5.2.1).

The PoF calculation process is summarized in Figure 9.5.2.2. The potentially critical details are identified and characterized for each Fracture Critical casting, and each such detail in the each casting is considered separately. Each possible random flaw for the detail can be described in terms of its size, orientation for radiographic inspection, and edge distance. These characteristics correspond to a probability of occurrence for that flaw and a probability that the flaw will not be detected. The size, edge distance, and orientation to the maximum principal stress, together with the damage tolerance margin or life at the critical detail for the design initial flaw, enables estimation of the predicted life for the random flaw. Its actual life may differ from prediction; thus, the probability of actual failure in less than 1 lifetime due to the random initial flaw is calculated. This PoF is summed over all possible flaws near the detail, then over all critical details in the casting, and finally over all Fracture Critical castings on the aircraft. The total, multiplied by the number of flaws per casting, is an estimate of the PoF of the aircraft due to shell inclusions in castings.

Based on a variety of data and supported by Fracture Mechanics theory, all the necessary relationships are derived to perform this calculation. F-22 used this PoF method to establish acceptance limits based on the number of shell inclusions in a casting. These limits are in the F-22 process specification for Titanium investment castings. Periodic reviews of shell occurrence data are conducted to assure that the assumptions of this analysis are not violated.

Thus, Structural integrity of F-22 fracture critical Titanium cast parts is assured by a combination of damage tolerance design and analysis plus process controls. This probability analysis has been used to provide a quantitative measure of the acceptability of ongoing process controls to minimize shell inclusions.

REFERENCE

[1] T. R. Brussat and P. J. Caruso; "Probability of Failure Analysis for Fracture Critical F-22 Titanium Castings" Proceedings of 2001 USAF ASIP Conference, December 2001.

9.5.3 Significance of Local Multiple Crack Growth Consideration on Aging Aircraft Structural Damage Tolerance Analysis

Jason Dai, Matt Creager, Kirk Odian, Structural Integrity Engineering Co. and Patrick Safarian*, FAA

There are increasing requirements from Airworthiness Authorities to perform damage tolerance analyses of aircraft primary structure to support aging aircraft structural Repair Assessment Programs (RAPs) and Supplementary Type Certificate (STC) Supplementary Structural Inspection Programs (SSIPs). It has been common practice in many aircraft Type Certification (TC) programs, that the Structural Inspection Threshold and Repeat Intervals for given structural details are based on damage tolerance analyses that start with an assumption of a single primary rogue flaw (typically 0.05 inch) in the worst location and orientation. This rogue flaw has been used to account for anomalous defects during manufacture. Lately, some manufacturers have included the consideration of simultaneously occurring secondary flaws. As for the aging airplane structures that are affected by repairs or STC installations, currently there is no uniform procedure for determining the initial flaw size configuration. Recently, the increasing awareness of Widespread Fatigue Damage (WFD) and corrosion in the aging aircraft structure has prompted some structural analysts to apply more stringent criteria for the aging aircraft structure's damage tolerance analyses. For instance, rather than using a single 0.05 inch initial corner crack at the edge of a hole, an additional typical secondary crack at the opposite side of the same hole has been assumed. This is based on the following considerations. For existing fastener holes in an aging aircraft's structural detail, potential Multiple Site Damage (MSD) type cracks may have pre-existed a repair or STC modification, and for freshly drilled holes in the aging structural parts, potential corrosion pitting, workmanship and other types of surface degradations may cause multiple cracks to occur in the hole.

Based on a current repair assessment program and experience on development of SSIP for 727/737 Freighter Conversion STCs, the influence of initial crack configurations (single flaw case vs. local MSD consideration) at a fastener hole on the analytical repeat inspection intervals are studied through typical skin repair assessment examples. In those skin repairs, the OEM skins of 0.040 inch thick have been repaired with 0.05 inch thick doublers of various sizes. The repeat inspection pertaining to different inspection methods are calculated with consideration of MSD crack "patching" for larger repair sizes. For the lead fastener rows, there are similarities between skin repairs and the skin lap splice joints. From lap splice MSD analysis experience it is normally assumed that crack growth starts from a fastener hole under the compounding influence of adjacent cracks and grows to ~1.0 inch, whereupon the MSD "patching process" links the crack length to form a 5 inch long skin crack. The 5 inch patching was established by Boeing for the 727/737 lap joints[1] which extend to the length of the aircraft. However for most skin repairs, the repair size is smaller than one frame bay and the actual patching size would therefore be smaller than 5 inches. Therefore to be conservative herein, it is assumed that the OEM skin patching size for 20 inch wide repairs is 5 inches (i.e. after the crack grows to 1" inch long, it will jump to form a 5" long crack). The patching size is assumed to reduce or increase linearly as the repair size gets smaller or bigger respectively. As a cut-off point, when repair widths are less than 12 inches, no crack patching is assumed. For the local MSD case, the initial cracks at a hole in the leading row is considered where two diametrically opposed, non-symmetrical corner cracks exist. One crack is 0.05 inch long and is referred to as the lead crack, while the other is 0.015 inch long (for existing holes with local MSD consideration [1]) or 0.005 inch long (for newly drilled holes in an aging structural material) and is referred to as a secondary crack. Ref. to Figure 9.5.3.1 and 9.5.3.2. Here the size 0.015 inch is statistically based on tear down inspection [1] and size 0.005 is a typical secondary crack size being used by the industry [2]. The

compounding interaction between the two cracks is considered. Without involving any changes in existing NASGRO code, a computer program utilizing Visual Basic in the popular MS Excel Spreadsheet was developed (as shown in Figure 9.5.3.6) so that the analysis can be performed using standard NASGRO cracked hole models (e.g.TC03, CC02). The interaction terms of the cracks are calculated and updated during specified crack propagation calculation cycle increments.

It is found that the proposed multiple local initial crack configuration (Case 2) will result in more stringent inspection threshold and repeat intervals for a given structural detail. This is especially true for a fastener hole with high load transfer. As shown in Figure 9.5.3.3 for the skin repairs, the calculated inspection intervals with conventional single 0.05 inch rogue flaw (Case 1) produce much higher (less conservative) inspection intervals for the NDI inspections (HFEC and LFEC) than that calculated based on a local MSD initial crack consideration. As expected, there is no impact on the detailed visual inspection intervals with regard to the choice of the initial crack configurations. It is believed that Case 2 approach is more prudent for the modified aging aircraft structures. The resulting inspection data for typical skin repair in 727 Freighter Conversion STC affected area is shown in Figure 9.5.3.4, which can then be used by the operators to setup inspection job cards based on repair size and inspection techniques available. Furthermore, a study on the sensitivity of secondary crack initial size is also performed. As shown in Figure 9.5.3.5, the impact by choosing 0.005 inch or 0.015 inch secondary crack size is not significant. It only slightly affects HFEC inspection intervals. Combining with fleet inspection and operation experience for the freighter conversions, it is believed that applying local MSD consideration in deriving inspection program balances well the need for a more stringent analysis regarding to aging aircraft structures and the economics for the operators.

* The view expressed in the article are those of the author and not necessarily represent the views of the agency.

REFERENCE

[1] U. G. Goranson, "Damage Tolerance – Facts and Fiction", 17th ICAF, June 1993.

[2] T. Swift, "Verification of Methods for Damage Tolerance Evaluation of Aircraft Structures to FAA Requirements", 12th ICAF, France, 1983.

9.5.4 Damage Tolerance of High Cycle Fatigue Structures

Scott C. Forth, NASA Langley Research Center

Damage-tolerance methodology is positioned to replace safe-life methodologies for designing aerospace structures. The argument for implementing a damage-tolerance method comes from the fundamental fact that aerospace structures typically fail by fatigue cracking. Therefore, if technology permits prediction of fatigue-crack growth in structures, a damage-tolerance method should deliver the most accurate prediction of component life. Implementing damage-tolerance (DT) into high-cycle-fatigue (HCF) components will require a shift from traditional DT methods that rely on detecting an initial flaw with nondestructive inspection (NDI) methods. The rapid accumulation of cycles in a HCF component will result in a design based on a traditional DT method that is either impractical because of frequent inspections, or because the design will be too heavy to operate efficiently. Furthermore, once a HCF component develops a detectable propagating crack, the remaining fatigue life is short, sometimes less than one flight hour, which does not leave sufficient time for inspection. Therefore, designing a HCF component will require basing the life analysis on an initial flaw that is undetectable with current NDI technology.

Inspecting for cracks that are 0.10 to 0.30 mm long is not practical with current technology, and designing heavier parts to provide adequate time to identify detectable cracks is unacceptable. Therefore, DT design of HCF components necessitates an improvement in NDI technology or an alternative to inspecting for cracks. Most fatigue failures are a result of surface damage, such as corrosion and foreign object damage (FOD), which can be detected through visual inspection. Understanding the impact this damage has on component life, one can safely maintain structural integrity through damage tolerance without directly inspecting for cracks. Contrary to classic damage tolerance, an operator would be required to inspect for FOD and corrosion damage – precursors to fatigue cracking – instead of actual cracks. It behooves industry to address HCF issues that obstruct the adoption of damage tolerance. The companies that develop this technology will realize significant improvements in safety and operating cost. Replacing parts without cause is no longer economically viable for fleet management.

The transition from stress-life management of aerospace structures to that based on damage-tolerance will not by easy. There is significant history clearly illustrating stress-life methods as safe and reliable. However, aerospace manufacturers must still rely upon damage-tolerance methods to explain service failures and further maintain the safety of the fleet. It is logical that the adoption of damage-tolerance principles into the design will save the company development funds, and additional costs when a component unexpectedly fails. Furthermore, as illustrated by the spindle lug example presented in Figures 9.5.4.1-9.5.4.3 and Table 9.5.4.1, the cost of operating a damage-tolerance designed part is significantly less in the long term, even with changes in the usage environment (see Refs. [1]-[2] for details). Furthermore, the continued zeal for stress-life methods, such as flaw-tolerance methods, will cost operators and manufacturers both profit and safety. This fact will be replayed every time a manufacturer is required to develop damage-tolerance data to manage a field issue, and an operator is hindered by unmanageable inspections. Implementation of damage-tolerance design and management methods for aerospace structures is possible. Aerospace companies prepared to adopt damage-tolerance methods will manufacture better, safer products and increase profits for themselves and their operators.

REFERENCES

[1] Forth, S.C., "Implementation of Damage Tolerance in High Cycle Fatigue Systems," *Proc. of the 14th European Conference on Fracture*, 2002.

[2] Forth, S.C., R.A. Everett and J.A. Newman, "A Novel Approach to Rotorcraft Damage Tolerance," *Proc. of 6th Aging Aircraft Conference*, 2002.

9.5.5 Development of a Robust Fracture Mechanics Methodology for Rotorcraft Damage Tolerance Analysis

Dy Le, FAA

Under FAA funding, the University of California, Los Angeles, in collaboration with the Rotorcraft Industry Technology Association (RITA), is developing a robust fracture mechanics methodology. There is a need for an accurate and efficient assessment of stress-intensity factors in rotorcraft parts with complex geometries and load paths. Accordingly, this effort was undertaken to address arbitrarily shaped and warped fabrication and service-induced cracks that can initiate fatigue crack growth in rotorcraft components. The resulting methodology is based on an innovative approach in which the Symmetric Galerkin Boundary Element Method (SGBEM) alternates with the finite element method (FEM). The method can calculate stress-intensity factors (and, when appropriate, elastic-plastic crack-tip criteria) to accurately predict fatigue crack growth for rotorcraft applications.

Analysis of complicated rotorcraft structures can be efficiently performed using a multistage hierarchical analysis strategy. The hierarchical analysis consists of a series of multiple analyses of different scales (global, intermediate, and local). Boundary condition (BC) transfer is performed at each stage except the global one. The unknown BC along the subregion boundary of the current model is extracted from the output of the previous model through a BC transfer process (Figure 9.5.5.1).

Automated Global, Intermediate, and Local Evaluation (AGILE) is a suite of software tools that was developed for the automation of hierarchical analysis of complex structures. AGILE-2D/3D supports the calculation of fracture mechanics parameters for cracks in rotorcraft structural components, parameters such as stress-intensity factor and J-integral. AGILE-2D handles beam and shell structures. AGILE-3D handles a bulk solid structure, where the crack may be a nonplanar surface crack or an embedded crack. AGILE software consists of boundary condition (BC) transfer tools for local fracture mechanics analysis. General-purpose finite element codes (NASTRAN and ANSYS) are used for global and intermediate stress analyses (Figure 9.5.5.2).

SGBEM-FEM Alternating Method: An efficient and highly accurate method, Symmetric Galerkin Boundary Element Method-Finite Element Method (SGBEM-FEM), for the analysis of 3D nonplanar cracks and their growth in structural components of complicated geometries has been developed. The crack is modeled by the Symmetric Galerkin Boundary Element Method as a distribution of displacement discontinuities as if in an infinite medium. The finite element method is used to perform the stress analysis for the uncracked body only. The solution for the structural component which contains the crack is obtained in an iteration procedure that alternates between the FEM solution for the uncracked body and the SGBEM solution for the crack in an infinite body. Both elastic and elastic-plastic variants of the alternating method are implemented.

The SGBEM is a way of satisfying the boundary integral equations of elasticity in a Galerkin weak form, as opposed to the method of collocations that is generally used to satisfy the integral equations in the traditional BEM. SGBEM is characterized by weakly singular kernels. After a special transformation that removes the singularity from the kernels, the boundary element matrices can be integrated with the use of conventional Gaussian quadrature. A crack is modeled as a distribution of displacement discontinuities with the crack surface discretized by quadratic eight-node boundary elements. Quarter-point singular elements are placed near the crack front. With the use of the SGBEM/FEM alternating procedure, the crack tip parameters for planar and nonplanar cracks in infinite media, and for embedded and surface cracks in finite bodies, can be calculated.

More specifically, for an infinite 3D body containing a nonplanar crack of arbitrary geometry, a distributed load is applied at the crack surface. The crack can then be described by a distribution of displacement discontinuity for which the following weakly singular boundary integral equation is valid for the crack.

9.6. FRETTING FATIGUE

9.6.1 Fretting Fatigue of Advanced Aircraft Materials

T.N. Farris and A.F. Grandt, Jr., Purdue University

The objective of this research is to determine conditions that cause fretting induced cracks to form in advanced aircraft materials. Fretting is associated with sliding contact between two tightly clamped surfaces, such as the turbine blade/disk interface, and can lead to early crack formation and unacceptably short fatigue lives. Attachment fatigue (fretting) has been identified as one of the key sources for high cycle fatigue (HCF) engine failures that has led to the grounding of many military aircraft. The current research is directed at developing analysis methods that enable design of turbine engine components and other mechanical joints in aircraft structures that are resistant to attachment fatigue failures.

The Purdue HCF program is part of a large collaborative effort that involves other researchers from the Air Force Research Laboratory, General Electric Aircraft Engines, Pratt & Whitney, Allison Engine Company, Honeywell, Southwest Research Institute, and the University of Dayton Research Institute. Purdue contributions to this interdisciplinary team have focused on attachment (fretting) fatigue. Purdue has, for example, developed an integral equation approach to calculate detailed edge-of-contact stress distributions caused by the fretting action. These stress analyses are combined with data from tribology and baseline fatigue experiments, along with detailed analysis of the fretting induced cracks to develop a total life prediction methodology for attachment fatigue failure.

A comprehensive test program has been conducted to evaluate the attachment fatigue life analysis scheme. These experiments involve both room and elevated temperature fatigue tests of specimens that are clamped between two contact pads and then subjected to a remote cyclic force as shown in Figure 9.6.1.1. The number of cycles required to develop and propagate fretting cracks at the specimen/pad interface is measured and compared with the predictions, and in general show excellent agreement between analysis and experiment as shown in Figure 9.6.1.2. The fracture surfaces are also examined with a scanning electron microscope to provide details about the growth of the fretting induced cracks. Various combinations of specimen/contact pad materials have been studied, including aluminum alloys and advanced turbine engine alloys such as Titanium 6-4, IN-100, Inco 718, and single crystal nickel alloys. The excellent agreement between analysis and experiment has resulted in transfer of the life prediction codes to the engine companies, who are using them to assess hardware that has been prone to attachment fatigue. The Purdue integral equation tools have led to increased accuracy and reduced computational time when compared to existing industry analysis methods and have been applied to at least 15 products by one of the engine companies.

REFERENCES

[1] Murthy, H., Farris, T.N., and Slavik, D.C. "Fretting Fatigue of Ti-6Al-4V Subjected to Blade/Disk Contact Loading," *Developments in Fracture Mechanics for the New Century*, 50th Anniversary of Japan Society of Materials Science, Osaka, May 2001, pp 41-48.

[2] Rajeev, P.T., Murthy, H. and Farris, T.N., "Load History Effects on Fretting Contacts of Isotropic Materials," *Proc of ASME Turbo Expo 2002,* Amsterdam, June 2002, GT 2002-30297.

[3] Murthy, H., Farris, T.N. and Okane, M. "Investigation of Fretting Characteristics of Turbine Materials at Higher Temperatures," in *Proceedings of 42nd AIAA/ASME/ASCE/AHS/ASC Structures, Structural Dynamics and Materials Conference*, Denver, CO, April 2002.

[4] P. J. Golden and A. F. Grandt, Jr., "Crack Growth Predictions of Ti-6Al-4V Fretting Fatigue Tests," 7th National Turbine Engine High Cycle Fatigue (HCF) Conference, Palm Beach Gardens, Florida, 14-17 May, 2002.

[5] D. B. Garcia and A. F. Grandt, Jr., "Fractographic Examination of Fretting Induced Cracks in Ti-6Al-4-V, 7th National Turbine Engine High Cycle Fatigue (HCF) Conference, Palm Beach Gardens, Florida, 14-17 May, 2002.

[6] Goryacheva, I.G., Murthy, H. and Farris, T.N., "Contact Problem with Partial Slip for the Inclined Punch with Rounded Edges," *International Journal of Fatigue,* **24**, pp 1191-1201 (2002).

[7[Rajeev, P.T. and Farris, T.N., "Numerical Analysis of Fretting Contacts of Dissimilar Isotropic and Anisotropic Materials," *Journal of Strain Analysis*, **37**(6), pp 503-517, (2002).

9.6.2 Polycrystal Plasticity Analyses of Fretting Fatigue

R.W. Neu, D.L. McDowell, C-H Goh, D.R. Swalla, J.R. Mayeur, Georgia Institute of Technology

Fretting fatigue is often the root cause of the nucleation of high cycle fatigue cracks at attachments of structural components. In fretting, cyclic plastic deformation, cumulative deformation and damage occur within depths comparable to the grain size. Therefore, a more physically realistic constitutive model is required to take into account the discrete grains and their crystallographic orientation distribution in this region to better capture the heterogeneity of the dislocation slip in the fretting damage process volume. This is accomplished by using a state-of-the-art computational continuum crystal plasticity material model developed to represent these effects in Ti-6Al-4V. A two-dimensional finite element model shown in Figure 9.6.2.1 is used to simulate an ideal fretting condition. A similar finite element model is used to simulation fretting fatigue. The simulation results are compared with carefully controlled and monitored fretting and fretting fatigue experiments. Studies examine how the characteristics of the plasticity produced by fretting changes with key fretting parameters including the normal contact force (P), the tangential force amplitude (Q), and the coefficient of friction (μ) at the contact.

Polycrystal plasticity simulations of fretting exhibit several significant features that are not manifested by simulations using homogeneous J_2 plasticity with nonlinear kinematic hardening, typical of what is used in conventional elastic-plastic simulations. First, as shown in Figure 9.6.2.2, the distribution of cumulative plastic strain using crystal plasticity is considerably more heterogeneous and extends deeper than the distribution obtained using the homogeneous model. In addition, the nature of the plastic strain accumulation predicted by crystal plasticity is a progressive cyclic ratchetting of the plastic shear strain whereas the homogeneous theory predicts that reversed cyclic plasticity dominates. The crystal plasticity simulations help explain the deformation and cracking phenomena observed in fretting experiments on Ti-6Al-4V that cannot be explained using a homogeneous elastic-plastic model.

Current work is focused on extending the crystal plasticity model for Ti-6Al-4V to three-dimensions, examining the effects of the alpha and beta phases in Ti-6Al-4V, and studying the influence of texture. In addition, the deformation fields developed in fretting experiments are being studied using orientation imaging microscopy (OIM) to determine how fretting changes the microstructure and its relationship to crack formation.

REFERENCES

[1] Goh, C.-H., Neu, R.W., and McDowell, D.L., "Crystallographic Plasticity in Fretting of Ti-6Al-4V," *International Journal of Plasticity*, 2003 (in press).

[2] Wallace, J.M. and Neu, R.W., "Fretting Fatigue Crack Nucleation in Ti-6Al-4V," *Fatigue and Fracture of Engineering Materials and Structures*, 2003 (in press).

[3] Goh, C.-H., Neu, R.W., and McDowell, D.L., "Influence of Nonhomogeneous Material in Fretting Fatigue," *Fretting Fatigue: Advances in Basic Understanding and Applications, ASTM STP 1425*, 2003 (in press).

[4] Goh, C.-H., Neu, R.W., and McDowell, D.L., "Role of Heterogeneity of Material in the Nucleation of Fretting Fatigue Cracks," proc. 7th National Turbine Engine High Cycle Fatigue Conference (HCF '02), Palm Beach Gardens, FL, 14-17 May 2002. (on CD)

[5] Goh, C.-H., Wallace, J.M., Neu, R.W., and McDowell, D.L., "Polycrystal Plasticity Simulations of Fretting Fatigue," *International Journal of Fatigue*, Vol. 23, Supplement 1, 2001, pp. S423-S435.

[6] Goh, C.-H., Neu, R.W., and McDowell, D.L., "Shakedown, Ratchetting, and Reversed Cyclic Plasticity in Fretting Fatigue of Ti-6Al-4V Based on Polycrystal Plasticity Simulations," proc. 6th National Turbine Engine High Cycle Fatigue Conference (HCF '01), Jacksonville, FL, 5-8 March 2001. (on CD)

9.6.3 Fretting Fatigue Model in Support for Condition Based Monitoring

Scott Prost-Domasky and Craig Brooks, APES, Inc. and Eric Tuegel, AFRL/VASM

The principal objectives of this 3-year program are:
1) Research the role and effects of fretting on the structural life of components,
2) Develop and demonstrate fretting fatigue prediction algorithms, and
3) Integrate the analysis into structural integrity methods.

The 2002 efforts focused on identifying potential analysis methods for fretting fatigue. Criteria for selecting analytical models for further investigation included: (1) physics-based, (2) demonstration of some accuracy in predicting experimental results, and (3) ease of integration with existing structural integrity analysis algorithms. Based upon these criteria, fracture mechanics-based approaches were chosen for further development (Figure 9.6.3.1). The analytical model being developed uses elements from the analytical and experimental work of Dr T. Hattori [1] at Hitachi; the 'Crack Analogue' approach, relating the stress field at the corners of fretting pads to that at the tip of a crack in an infinite plate under different loadings, developed at the Massachusetts Institute of Technology [2]; and the "fretting map" approach introduced at the University of Lyon in France [3]. The Initial Discontinuity State (IDS) is the distribution of initial "cracks" to begin the fracture mechanics analysis of fretting.

Efforts for 2003 and 2004 will focus on developing and verifying the stress intensity solutions needed for fretting fatigue scenarios, developing the experimental data needed to verify the analysis, and integrating the technology into a robust application. Stress intensity solutions will be developed with finite element analysis software that enables extraction of high quality crack tip singularity measures. The experimental program for verification of the analysis will proceed in a building block manner beginning with the simple pad on bar fretting tests and culminating with tests of single fastener lap joint specimens.

Analytical predictions will be compared to the experimental results after each series of tests to determine if refinements in the model are needed before proceeding to the next level of complexity (Figure 9.6.3.2). The analysis model will be integrated into structural analysis software that uses AFGROW to perform the crack growth analysis. Future development will incorporate the fretting fatigue analysis with ECLIPSE (Environmental Cyclic Life Prediction Software) and AFGROW to form a "Holistic Structural Assessment Method" that model damage development from many sources, i.e., fatigue, fretting, and corrosion [4].

REFERENCES

[1] Hattori, T., Nakamura, M., Sakata, H., and Watanabe, T. (1988) "Fretting Fatigue Analysis using Fracture Mechanics", *Japan Society of Mechanical Engineers International Journal—Series 1,* **31**, 100-107.

[2] Giannakopoulos, A.E., Lindley, T.C., and Suresh, S. (1998) "Aspects of Equivalence Between Contact Mechanics and Fracture Mechanics: Theoretical Connections and a Life-Prediction Methodology for Fretting-Fatigue", *Acta Materialia*, **46**, No. 9, 2955-2968.

[3] Vincent, L., Godet, M., and Berthier, Y. (1994) Rapport final, Contract "Programme Fretting—Fatigue", No. 9196030004717586, 178 pages.

[4] Brooks, C.L. and Simpson, D. (1998) "Integrating Real Time Age Degradation into the Structural Integrity Process" *Proceedings of NATO RTO's Workshop 2 on Fatigue in the Presence of Corrosion*, Corfu, Greece.

9.6.4 Application of Low Plasticity Burnishing to Increase Fretting Fatigue Strength of Ti-6Al-4V

Ravi A. Ravindranath, Naval Air System Command and Paul S. Prevey, Lambda Research

Dovetail fretting is second only to foreign object damage (FOD) in limiting the fatigue performance of turbine engine fan and compressor stages. A great deal of research effort has been devoted to the understanding and control of fretting in titanium alloys.[1] Current means of fretting damage mitigation are limited to the use of anti-fretting coatings to reduce the frictional shear stresses and shot peening to retard crack growth. Neither treatment has been effective, except for short period of engine life. The deep compression and improved surface finish produced by low plasticity burnishing (LPB), has been shown to completely mitigate fretting fatigue damage in Ti-6Al-4V by arresting the development and growth of the shear micro-cracks.[2] A means of mitigating fretting fatigue damage would offer even greater benefit in terms of cost savings and fleet readiness. The fretting fatigue performance of LPB on Ti-6Al-4V was compared to conventional shot peening (SP) and electropolished (ELP). The deep compressive layer generated by LPB provided mitigation of fatigue damage and improved damage tolerance.

LPB produced a depth of compression nominally 0.040 in. with maximum compressive stress on the order of –100 ksi, which was stable after thermal exposure at 375°C for 10 hrs. In contrast, the compression on the highly cold worked SP surface was dramatically reduced by the same thermal exposure as shown in Figure 9.6.4.1.

High cycle fretting fatigue results shown in Figure 9.6.4.2 indicate a substantial debit in fatigue life from fretting for both SP and ELP conditions, with little or no effect on LPB treated specimens. Fretting damage of both SP and ELP surfaces reduced the fatigue life by over an order of magnitude and fatigue

strength by more than a factor of two. This difference in fretting behavior is attributed to deep compression from LPB inhibiting crack initiation and propagation from the fretting scars. Although fretting scar size was much smaller in the case of ELP specimens as compared to the LPB specimens, the latter outperformed the former in fretting fatigue. Fractographic evidence indicated fretting damage in the form of near surface cracks are affected by the combined stress state. LPB specimens showed superior fretting fatigue performance due to the deep, thermally stable compressive residual stress introduced on the surface, while the ELP specimens had practically no residual stresses and the SP specimens had a shallow region of compressive residual stresses.

REFERENCES

[1] Proceedings of the “National Turbine Engine HCF Conference”, 1 throught VI

[2] Lambda Research report “Application of Low Plasticity Burnishing (LPB) to Increase Fretting Fatigue Strength of Ti-6Al-4V,” Project 674-10201, Nov. 2002 for WPAFB Air Force Research Laboratory

9.6.5 Fretting Fatigue

David W. Hoeppner, Univerity of Utah-QIDEC Laboratories

David W. Hoeppner attended the third international symposium on Fretting Fatigue held in Nagoaka, Japan in May, 2001. He also served on the planning committee for the meeting. QIDEC personnel presented three papers at the meeting. Two of the papers were intended for publication and are listed below. David W. Hoeppner also served as the co-editor of the proceedings of the meeting which have just recently been published by ASTM. The publication is **Fretting Fatigue, Advances in Basic Understanding and Applications**, ASTM STP 1425, Editors, Steven E. Kinyon, David W. Hoeppner, Yoshiharu Mutoh, ASTM International, West Conshohocken, PA, 2003.

REFERENCES

[1] Clark, P. N., Hoeppner, D.W., "Fretting Fatigue Initial Damage State to Cracking State: Observations and Analysis", Fretting Fatigue: Advances in the Basic Understanding and Applications, STP 1425, S.E. Kinyon, D.W. Hoeppner, and Y. Mutoh, Eds., American Society for Testing and Materials International, West Conshohocken, PA, pp 44-58, 2003.

[2] Hoeppner, D.W., Taylor, Amy M.H., Venkatesan, Chandrasekaran, "Fretting Fatigue Behavior of Titanium Alloys", Fretting Fatigue: Advances in the Basic Understanding and Applications, STP 1425, S.E. Kinyon, D.W. Hoeppner, and Y. Mutoh, Eds., American Society for Testing and Materials International, West Conshohocken, PA, pp 291-306, 2003.

9.6.6 Fretting Fatigue

David W. Hoeppner, University of Utah-QIDEC Laboratories

David W. Hoeppner served on the Planning Committee for the Fourth International Symposium on Fretting Fatigue to be held in Lyon, France May 26-28, 2004.

9.7. WIDESPREAD FATIGUE DAMAGE

9.7.1 Widespread Fatigue Damage Assessment Approach

John G. Bakuckas, FAA

A methodology to assess the development of widespread fatigue damage (WFD) and its effect on the residual strength of aircraft structure has been developed. WFD in a structure is characterized by the simultaneous presence of cracks in multiple structural components where the cracks are of sufficient size and density that the structure will no longer meet its damage tolerance requirement

WFD is a complex phenomena that is extremely difficult to analyze using standard methods developed from first principles of linear elastic fracture mechanics (LEFM). Because of limitations on LEFM applications, more advanced methods have been explored and developed over the past decade with the support and sponsorship of the Federal Aviation Administration (FAA) and the National Aeronautics and Space Administration (NASA). The methods include analytical tools to determine parameters governing the initiation and growth of cracks and elastic-plastic fracture criterion for residual strength determinations. The tools include (1) the finite element alternating method (FEAM, a computationally efficient yet rigorous approach to calculate two- and three-dimensional stress-intensity factor (SIF) solutions governing crack formation and growth; (2) FASTRAN, a fatigue crack growth analysis program using a crack closure model; and (3) STAGS, an advanced finite element program implemented with fracture mechanics and stable tearing analysis capabilities for generalized shell structures. Elastic-plastic failure criterion include the plastic zone touch (PZT), crack-tip opening angle (CTOA), and the T* integral. With these tools and criterion, analyzing different stages of multiple-site crack initiation, growth, linkup, and catastrophic fracture can be analyzed. Such analyses can also provide a framework for WFD assessment.

In this study, WFD was addressed on two fronts: (1) characterizing MSD by studying the initiation and growth of cracks in the evolution of multiple-site cracks and (2) determining the effects of MSD on the residual strength.

In characterizing crack initiation, experimentally generated equivalent initial flaw size (EIFS) data and an analytical closure model in FASTRAN were used to determine initial flaw sizes and distribution for multiple-site cracking for four joint configurations as shown in Figure 9.7.1.1.

A thorough residual strength assessment approach has been developed for aircraft structure containing MSD. The approach, based on nonlinear finite element analysis and the PZT, CTOA, and T* integral criterion, was applied and verified for three cases outlined below.

1. MSD in Flat Panels: The effect of small MSD on residual strength was determined and the elastic-plastic criterion of T* integral, CTOA, and PZT fracture criteria were evaluated. These criteria correlated well with the experimental results.

2. MSD in Curved Panels: The effects of MSD on the fatigue crack growth and residual strength of curved fuselage panels was studied using the FASTER facility. Four panels were tested, two panels with a longitudinal lap splice and two with a circumferential butt joint. For each joint configuration, one panel contained only a lead crack and the other contained a lead crack with multiple cracks located along the outer critical rivet row of the joints. Geometric nonlinear finite element analyses, using STAGS and the CTOA criteria, were used to predict the residual strength. Comparisons with strain gage data verified the finite element models. In general, the small multiple cracks did not have an effect on the overall global strain response. However, the small multiple cracks reduced the number of cycles to grow a fatigue crack

to a predetermined length by 37% for the longitudinal lap joint, as shown in Figure 9.7.1.2, and by 27% for the circumferential butt joint panels. In addition, the presence of multiple cracks reduced the residual strength of the panels with a longitudinal lap joint by approximately 20%. The measured and predicted residual strength were in good agreement.

3. MSD in Aft Pressure Bulkhead: The purpose of this test was to verify the generality of the approach validated for the flat- and curved-panel cases by applying it to a different large-scale airframe structure, that is, to an aft pressure bulkhead. Geometric nonlinear finite element analyses, using STAGS and the CTOA criteria, predicted the residual strength. The measured and predicted residual strength were in good agreement, as shown in Figure 9.7.1.3.

9.7.2 Three-Dimensional Stress-Intensity Factors for Cracks at Fastener Holes

John G. Bakuckas, FAA

To predict crack growth and residual strength of riveted joints subjected to widespread fatigue damage (WFD), accurate stress and fracture analyses of corner and surface cracks emanating from a rivet hole are needed. To address this need, the existing database of three-dimensional stress-intensity factor solutions has been expanded.

The solutions were obtained using the finite element method and by applying a global-intermediate-local hierarchical approach. The stress-intensity factors were determined at different locations along the countersunk rivet hole. A very refined mesh was used along the crack front to obtain accurate solutions. A wide range of crack sizes and shapes, which represent typical damage scenarios in an aircraft fuselage were considered.

Two groups of problems were addressed. In the first group, small cracks at different locations along the countersunk rivet hole were considered. (Figure 9.7.2.1)

In the second group, corner cracks growing out of the faying surface were considered. (Figure 9.7.2.2) The stress-intensity factors are normalized and shown as boundary correction factors. Three different loading scenarios were considered: far-field tension, far-field bending, and wedge loading. Parametric studies are conducted by varying *a/t*, *a/c, and h/t* ratios, where *a* is crack length and depth direction, *c* is surface crack length, and *t* is thickness.

In general, the relative magnitude of the boundary correction factor at a point in the crack front is proportional to its distance from the hole boundary. (Figure 9.7.2.3) However, this is locally influenced by the presence of stress-raisers such as points along the countersunk hole where the geometry changes abruptly and the relative magnitude of the load transferred in the vicinity of the point on the crack front. All these local effects tend to increase the boundary correction factor.
A typical result for a corner crack under tension is shown in Figure 9.7.2.4. Here the boundary correction factors are plotted as a function of physical angle. The physical angle is zero at the faying surface and increases to 90° at the hole boundary. In the case shown, *a/t* and *h/t* ratios are both 0.5. The values are plotted for cracks with three different *a/c* ratios. Results show that at the faying surface the crack front that is farthest from the corner has the lowest value of boundary correction factor. As one moves along the crack front, the boundary correction factor increases monotonically for all three crack fronts and as the three crack fronts merge at the knee, so does the boundary correction factors.

Another typical result for a crack at the knee of the countersunk hole is shown in Figure 9.7.2.5. All the cracks have an a/c ratio of 0.4. In this case, the physical angle is measured along the crack front from the straight shank of the hole to the inclined section of the hole. Three cracks with different *a/t* ratios are considered. For each crack the boundary correction factor decreases as one moves away from the hole

boundary, as is minimum when one is furthest away from the hole (at $\theta = 90°$). Thus, a crack at the knee has the potential to grow along its two edges, therefore becoming shallower until it becomes a break-through crack. In general, the closer a crack front is to the knee, the higher the boundary correction factor. An exception is the deepest crack with $a/t = 0.4$. At $\theta < 45°$ the crack front comes very close to the corner of the rivet hole and is influenced by it, thereby showing a higher value for the boundary correction factor.

9.7.3 Initiation and Distribution of Fatigue Cracks in a Fuselage Lap Joint Curved Panel

John G. Bakuckus, FAA

A study was conducted on the formation and evolution of multiple-site damage (MSD) emanating from the rivet holes in the lap joint of an initially undamaged full-scale fuselage curved panel subjected to fatigue loading. The experimental work was conducted at the Full-Scale Aircraft Structural Test Evaluation and Research (FASTER) facility located at the Federal Aviation Administration William J. Hughes Technical Center, Atlantic City International Airport, New Jersey. The objective of this test was to characterize initiation, distribution, and linkup of MSD cracks. Quasi-static tests were conducted first to ensure a proper load introduction to the panel. Test results showed a large bending deformation locally along the critical outer rivet row in the lap joint area. The experimental data were compared to predictors made using geometrically nonlinear finite element analyses.

The curved panel was subjected to a fatigue loading with a marker band spectrum. During the fatigue test, rivets in the panel were periodically inspected for cracks using a nondestructive eddy-current system and by visual inspection. High eddy-current signals were recorded at rivets along the critical outer rivet row of the lap joint prior to visual detection of skin cracks. The typical damage development in the outer row of the lap joint is illustrated in Figure 9.7.3.1 with a series of photographic images. The full-load cycle number at which each image was taken is also shown in the figure. Damage in the rivet was first observed in the form of a rivet head crack.

Subsequently, the crack grew along a curved path that seemed to follow the perimeter of the rivet stem, Figure 9.7.3.1(a). Water leakage from this crack indicates that it was a through-the-thickness crack. It is noted that the loading used in this study is much higher than what a fuselage would experience during normal service conditions. The rivets are not designed to sustain such high fatigue loads. Thus, it is believed that the rivet head crack initiated at the rivet shank-countersink interface due to the stress concentration in that area and propagated upwards to the surface. As the fatigue test continued, a through-the- thickness crack appeared on the right side of the rivet. The through crack grew in both directions and eventually linked up with the rivet hole, Figure 9.7.3.1(c).

At a later stage, another through-the-thickness crack appeared on the left side of the rivet, Figure 9.7.3.1(d). This crack also grew in both directions and linked up with the rivet hole, Figure 9.7.3.1(e). Finally, the rivet head crack propagated to the edge of the rivet hole and joined the other two cracks to form a major crack that cuts through the rivet itself, Figure 9.7.3.1(f). A similar damage evolution process was observed at the rivets in the outer row. Other MSD cracks were observed at rivets holding the shear clips to the skin at the shear clip cutouts located at the frame stringer intersections.

Crack growth rates were calculated for two sets of msd cracks, results agreed very well with those from other similar studies. Results obtained in this study, although for longer crack lengths and different joint and panel configurations, follow the trend of the data very well, as shown in Figure 9.7.3.2. This indicates that the fatigue cracks from the three different studies grew at similar rates.

These msd cracks eventually linked up to form a large lead crack as shown in Figure 9.7.3.3. In the figure, a schematic is provided of the crack path along the outer rivet row between frames 2 and 3. The first crack linkup occurred between rivets designated a22 and a23 after 106,217 cycles. The lead crack then grew very rapidly. After 107,448 pressurization cycles, the msd evolved into a 16″ two-bay crack through rivets designated a17 and a27.

The panel was then subjected to quasi-static pressurization up to failure to measure the residual strength. The panel failed catastrophically at 17.8 psi pressure along the outer rivet row exhibiting no crack turning (flapping) or arrest capability. As shown in Figure 9.7.3.4, the crack grew across five frames designated F2 through F6. In addition, frames 3, 4, and 5 were fractured. Data from this test will be used to calibrate and validate methodologies to assess widespread fatigue damage (WFD). Posttest fractographic studies will be conducted to reconstruct and map the crack growth histories.

9.8. CORROSION/FATIGUE

9.8.1 Corrosion Fatigue Structural Demonstration (CFSD) Program

R.P. Bell and J.T. Huang, Lockheed Martin Aeronautics Company

The CFSD program is funded by the U.S.A.F. Research Lab (AFRL) with contribution from the U. S. Navy. The AFRL program manager is Mr. Michael Falugi; technical advisor is Dr. Eric Tuegel. The prime contractor is Lockheed Martin (LM) Aeronautics Company - Marietta, GA; the subcontractors include Analytical Processes/Engineering Solutions (APES) Inc., National Research Council of Canada (NRCC), University of Utah (UofU), Science Applications International Corporation (SAIC), Northrop Grumman Corporation (NGC), Southwest Research Institute (SwRI), and NCI (NCI) Information Systems, Inc. The program began in March 2000 and is scheduled for completion by May 2003.

The overall objective is to develop, enhance, verify, and demonstrate a modified aircraft structural integrity program (ASIP) corrosion fatigue methodology and the associated corrosion fatigue methods, models, technologies, and software for more accurate prediction of the fatigue, corrosion, and corrosion fatigue in aircraft. The intent is to reduce the cost of maintaining aging aircraft while ensuring reliability. The cost reduction benefits can be derived from reduced unscheduled high cost maintenance on aircraft and planning for lower cost aircraft logistics center (ALC) inspection and maintenance.

In order to ensure that the needs of the ALCs are met, frequent consultations with the ALCs were made. In addition, the team has compiled several lists of corrosion fatigue hot spots on C-141 and C-130 aircraft and a list of candidate corrosion fatigue problem areas on B707, E-8, and KC-135 aircraft. As a result, the team has also developed corrosion metrics for CFSD.

Derivation of Corrosion Thinning Growth Rates (LM)

An extensive review and statistical analyses of C-141 fleet repair data was conducted. For this task, about 16,000 C-141 "202 forms," gathered during 1990 through 2000, were reviewed, from which about 800 cases of "corrosion without cracking" (grind-out and repair) were identified. A total of 308 cases were then selected for estimating corrosion growth rates. Using the environmental severity indices (ESI) data in a 1998 report by NCI to AFRL, statistical analyses were made of the corrosion grind-out data in terms of the time in service, time since paint, time of wetness since paint, and time weighted by environmental severity index (TWESI) since paint, where the parameters were in order of goodness-of-fit. The best fit was obtained using TWESI since paint, which gives the C-141 corrosion thinning growth rates for application. Because the data came from C-141 repair records, and derivation process is rigorous, the resulting growth rates are considered to have been validated on C-141.

Separately, NGC has compiled grind-out depth data for the lower wing of two Boeing 707 aircraft after 24 years in service. For each of these two aircraft, the cumulative distribution of the number of occurrence as a function of grind-out depth correlates well with the predicted distribution using Lap Joint Corrosion Prediction Model (LJCPM).

The two studies mentioned above demonstrate that corrosion thinning growth rates can be derived from grind-out data for prediction purposes, even though the resulting rates may be somewhat aircraft dependent and may exhibit a significant amount of scatter.

Application and Validation of ESI and TOW Indices (LM/NGC)

Under CFSD, two indices were used to rank the relative environmental severities of the outdoor atmosphere at various U. S. Air Force bases. These are the Environmental Severity Indices (ESI) established by NCI for AFRL and time of wetness (TOW) indices obtained by running the Lap Joint

Corrosion Prediction Model (LJCPM) program, where a wet index is the percent of days with rain or very high humidity at the base. Although the ranking of air bases according to the ESI data deviates somewhat from that of TOW indices, it is concluded that the two indices are both good data to use as a start because of three reasons: the corrosion process of aluminum alloys is strongly driven by chloride and moisture contents, the derivation of ESI uses TOW as an independent variable, and there is a good overall correlation of the two indices although there are some exceptions.

The results of statistical analyses of the C-141 corrosion grind-out data indirectly validated that both ESI and TOW data sets are good indicators of the chloride and moisture containing outdoor environments that cause corrosion in aircraft. In a separate study, NGC has established a reasonable good correlation between skin replacement during Joint STARS refurbishment and relative environmental severity ranking for five of seven aircraft evaluated.

Stress Intensity Solutions for Pits CSK Holes and Lap Joints (APES/LM)
To enhance the analytical capabilities, finite element analyses were made of pits of various shapes and sizes to determine their K_t values and then beta correction factors were developed for typical CSK holes. In addition, finite element analyses of lap joints were also made to simulate the effects of pressure due to corrosion products at the faying surfaces and to determine the stress intensities for cracks emanating from the CSK holes.

Refinements and validation of Corrosion Fatigue Models (APES/LM/NRCC)
The corrosion models targeted for development or refinement include the corrosion thinning growth model or rates, power law pit growth models, effect of surface topography due to pitting on short crack growth, and pillowing resulting from built-up corrosion products around fastener holes within lap splices. The validation of modeling techniques for pits is being achieved by correlating the predicted and tested fatigue lives of various coupons having corrosion pits.

Implementation of Corrosion Fatigue Capabilities into C-141 Fleet Tracking Codes (LM)
New capabilities to account for corrosion effects have been implemented in Lockheed Martin's C-141 aircraft tracking programs. The new capabilities include the use of environmentally assisted fatigue crack growth (FCG) rate data and general corrosion thinning. To account for other corrosion effects, the tracking programs also can utilize Beta correction factors as input with correction having been made using data from external sources such as ECLIPSE developed by APES.

The C-141 tracking codes predict the growth of cracks, in one solution run, at the critical locations in all twenty-one structural zones on each aircraft for the entire C-141 fleet. The predictions are based on the aircraft mission mixes which are referenced to the bases by quarter. The codes make four predictions for each crack, two of which are for bracketed life predictions and the other two for fail-safety evaluation. One of the four crack lengths can be reset based on NDI inspections.

The basic program package has been checked out and is in operation on the IBM VM/CMS system. Crack growth analyses have been completed using C-141 individual aircraft usage data from 1991 through 2002. Analysis was conducted for all twenty-one tracking zones using both environmental FCG data referenced to aircraft basing and 90% RH air FCG data, respectively.

Separately, a PC version of another FCG prediction program (P6050) has been developed and revised to include similar corrosion capabilities mentioned above. This program is also in operation.

Validation of ECLIPSE/AFGROW on Boeing Aircraft (NGC)
NGC has performed an assessment of the ability of ECLIPSE/AFGROW to predict cracking on Boeing 707 aircraft. The assessment included life predictions and sensitivity studies for three structural locations including a fuselage lap joint, cockpit window post, and lower wing stringers, all of which seemed to have corrosion problems. The predicted lives were compared to actual aircraft corrosion fatigue cracking data. The sensitivity studies included variations in FCG data, initial discontinuity state (IDS), and age degradation mechanisms. It was found that the assumption of no-corrosion resulted in very unconservative predictions; while the use of high humidity air FCG data and corrosion options (such as pillowing and surface topography) resulted in more realistic and accurate predictions.

Investigation of Aircraft Panels and Naturally Corroded Sheets (UofU/NRCC/LM)
In order to better understand the corrosion problems that occurred in aircraft and outdoor environments, several efforts were undertaken. (1) An extensive investigation was made for an aircraft panel having cracking, pitting, and inter-granular attack in many of its 2,600 fastener holes. This work involved in-screening inspection, detailed inspections, metallurgical microscope and SEM inspections, and fatigue testing of coupons cut from the panel. (2) Pitting damage study and fatigue coupon testing for C-130 MLG wheel panels having pitting due to exposure in out-door environment for different time intervals. (3) Investigated ion of a C-141 fuselage skin panel holes having circumferential cracks, corrosion pits, and inter-granular attack. (4) SEM study of a fractured fatigue tested ESI sample from Battelle. (5) Characterization of two ESI samples from Battelle having pitting and inter-granular attack due to exposure in outdoor environment.

Pit Growth, Pit-to-Crack and Short Crack Tests (UofU)
Tests on artificially corroded 2024-T3 and 7075-T6 coupons were conducted to develop data for pit growth, pit-to-crack, and short crack. For the pitting test coupons, extensive efforts were made to collect data for pit size, shape, and densities. Fatigue testing to failure and fractography were also conducted for the pitting test coupons to determine their fatigue lives and failure mechanisms including the sizes of pits or discontinuities at the fatigue origins.

The results show that the ranges of fatigue life are high, that pits may not necessarily lead to cracking, and that crack nucleation sites depend on pit size, shapes, and other factors. Currently, the pit data and fatigue test results are being used for analytical predictions and correlations. Pending further evaluation, the data nevertheless suggests that if a consistent prediction scheme (which assumes that the initial crack size is a certain combination of the IDS value and pit depth) is used, the ratio of tested life to predicted life would likely fall within a wide range.

IDS Tests (NRCC)
Particles or initial discontinuity states (IDS) in 2024-T3 and 7075-T6 sheets were identified to determine their size, shape and distributions. Fatigue testing and fractography were conducted for new, flat, non-clad and used, apparently uncorroded, both sides clad 2024-T3 sheets, new, flat, non-clad 7075-T6 sheets, and old unused 7075-T6 extrusions, respectively.

The effects of various parameters on fatigue lives were evaluated. In addition, it was determined that, for the new bare 2024-T3 sheets, the constituent particles at the fatigue origins caused the crack nucleation; the sizes of these particles are at the high end of the general IDS distribution, and there was almost no evidence of multiple crack nucleation sites in the bare sheets. For the used clad 2024-T3 sheets, however, the fatigue origins were located at the clad surfaces where multiple nucleation sites were observed yet no constituent particles were found. For the 7075-T6 alloy, not much particle involvement was observed. In the 7075-T6 cases and 2024-T3 clad cases, the surface irregularities, orientation and size of grains, and

persistent slip bands, were judged to have caused crack nucleation. For the clad 2024-T3, the weakness of clad may have played a role.

MDS Tests (NRCC)
The discontinuity state (DS) at a particular time is referred to as a modified discontinuity state (MDS). Fatigue tests to failure on coupons fabricated from naturally corroded lap joints taken from two aircraft were carried out to determine the MDS values that can cause fatigue cracks to nucleate in corroded lap joints. Two material systems were examined, 2024-T3 and 7079-T6.

The tests have been completed and results are being evaluated. Although corrosion was present along the faying surface of the lap joints, a number of the coupons failed due to cracks nucleating at the non-corroded clad layer (outer surface of the lap joint). This failure location suggests that the MDS present along the corroded gauge length in some of the coupons was evolving slower than the DS associated with the cladding.

MSD Tests (NRCC)
Fatigue tests have been performed on multi-row and multi-column single lap splice elements made of clad 2024-T3 sheets and 7079-T6 sheets. Several splice elements were pre-corroded in the laboratory and then fatigue tested; a few uncorroded splice elements were also fatigue tested. The test program is being used to define the fatigue and corrosion fatigue behavior and failure mechanisms in fuselage splices for modeling purposes and to provide an element-level validation of the multi-site damage (MSD) modeling strategy.

The post-test examination included the identification of associations between crack nucleation and discontinuities such as pitting, inter-granular corrosion, fretting damage, cladding, and constituent particles. Differences in the nominal stress distributions, failure mechanisms, and crack growth patterns between corroded and non-corroded splice elements were observed.

NDI Efforts (SAIC)
In order to achieve the NDI objectives, SAIC has optimized the mature NDI techniques and performed inspections on naturally and artificially corroded specimens. The eddy current methods employed were of conventional fixed, single or dual frequency technique using a commercially available eddy current instrument and probe. The ultrasonic method employed is a conventional pulse-echo immersion technique using a high frequency, broadband, focused probe. Special techniques were fine tuned to handle the effects of aluminum clad layer thickness on eddy current imaging and dual frequency eddy current approach to mitigate the panel gap effects. Other than the use of pulse-echo ultrasound and conventional eddy current (EC) techniques, field applicable technologies such as pulsed eddy current (PEC), thermal imaging and phased array have been researched.
SAIC has applied the mature NDI techniques to obtain data from corroded aircraft components including Boeing 747 and 727 fuselage lap joint panels at NRCC, as well as a P-3 wing skin joint, a C-141 fuselage splice joint, and a C-141 crown splice (wing station 77) at LM Aero -Marietta. All acquired NDI data from NRCC specimens has been supplied to NRCC to investigate relations between the thickness loss and RMS surface roughness. SAIC has also applied the same NDI techniques to obtain data from engineered corrosion specimens including the Multi-Site Damage (MSD) specimens at NRCC, round robin experiment at UDRI with a combination of engineered and naturally corroded specimens for POD studies. In addition, SAIC has participated in a Corrosion Round Robin Experiment at Sandia / AANC Validation Center. Engineered corrosion specimens and examples of actual exfoliation were included.

NDI Efforts (NRCC)
This work started with corrosion characterizations of a corroded 2024-T3 fuselage lap splice using several NDI techniques. After the NDI inspections, the splice was disassembled and the corrosion damage topography at the faying surfaces was measured using different methods, such as digitized X-ray (DXR) thickness mapping, confocal microscopy, optical and scanning electron microscopy (SEM), and metallographic sectioning. In addition, the 3-D digitized maps for many corroded regions within the lap splice obtained using the X-ray method were analyzed in order to examine the relationships between the RMS surface roughness and NDI measured thickness loss. It was shown that this relationship is somewhat affected by the areas of interrogation spots, which suggests a need to consider area as the third variable in that relationship.

Open and Filled Holes Coupon Tests (SwRI)
Fatigue tests were performed to determine the effects mild, prior artificially generated corrosion has on the fatigue life of open and filled holes in 7075-T6 sheets. The initial crack size during fatigue testing was generally less than 0.010 inch. It does not appear that there is any definitive fatigue life difference between the uncorroded and corroded specimens for the mild corrosion examined. Nor was there any difference observed whether the corrosion was localized on the faces of the specimen or on the faces and in the bore of the hole. This study confirms that a mild corroded surface has little effect on the growth of long cracks which are cyclic load driven.

Fail-Safety Analyses by Risk Approach (LM)
The high scatters and ranges that are evident in the C-141 corrosion grind-out data, back-calculated IDS values, and fatigue lives of test coupons having pits, as presented above, underscore a need to approach crack growth prediction and fail-safety evaluation from statistical perspectives.

To demonstrate this concept, two C-141 splices were analyzed: the FS678 forward fuselage longitudinal splice along the WL255 longeron and the zone 17 FS1178E aft fuselage circumferential splice. The forward longitudinal splice has to sustain pressure cycles only; the aft circumferential splice has to sustain the pressure loads, gust loads, and flight loads.

It is assumed that the aircraft was fail-safe when it came out of the factory; the question is whether it is still fail-safe with cracks and corrosion. Listed below are the scenario, fail-safety criterion, and risk approaches. Assume a 12-inch 2-bay lead crack, a major member in between having been severed, and the nearest fastener hole (along the path of the lead crack) having a certain flaw size distribution, which can be an IDS distribution or a modification of that.

Under the MSD scenario, the Beta factors for both the lead crack and small crack at the adjacent hole affect each other. To account for this effect, the Kamei Yokuburi method is applied. As both flaws grow, the residual strength decreases. At some stage, the flaws become so large that the fail-safety criterion (the probability of failure being no greater than 1×10^{-4}) is no longer satisfied. Note that this criterion is stricter than the one used in the original design evaluation.
The probability of failure was calculated using PROF.

The results show that the forward longitudinal splice is more damage tolerant than the aft circumferential splice, and the assumption of corrosion leads to shorter fail-safety life. Note that for demonstration purposes, corrosion is assumed to occur. This was handled by using data from ECLIPSE for a “moderate corrosion” condition to account for the effect of topography due to pitting to make adjustment for the beta corrections factors. This ECLIPSE data is used even though its corrections for topography need to be justified.

The analytical steps taken here are first cut, and efforts shall be continued to evaluate and refine this analytical approach.

9.8.2 Corrosion and Fatigue in High Strength Aluminum Alloys: Life Prediction Issues

Basir Shafiq, University of Puerto Rico and Vinod S. Agarwala, Naval Air Systems Command

Studies have shown that all fatigue testing must be performed in the presence of corrosive environments and at frequencies realistic to the service environment to determine meaningful crack initiation and growth parameters before they can be used in life prediction models, if corrosion is anticipated.

Fatigue experiments performed on 7075-T6 Al alloy at various frequencies, stress levels and under alternating wet and dry environments indicate that simultaneous action of corrosion and fatigue substantially accelerates crack initiation and growth rates as compared to pure fatigue (dry air) condition. Fig. 1 shows the dramatic difference in FCG rates of specimens tested in dry air (ICT) and in the presence of electrolyte (ACT) subjected to various frequencies. Specimen in the presence of electrolyte exhibited an up to five fold increase in the CGR at all frequencies leading to significantly reduced lifetime in the crack propagation stage as compared to specimens tested in dry air conditions. Increase in the CFCG at a lower frequency is associated with longer time available per cycle for electrochemical reactions to occur such as ionic transport, anodic dissolution, and hydrogen diffusion and embrittlement [1]. Figure 9.8.2.1 also indicates that CFCG rate decreases as the frequency is increased, however, it never approaches the CGR of dry air specimens, showing the effects of corrosion even at very high frequencies (or short times).

It was also found that lowering the frequency or increasing the stress level substantially reduces crack initiation time and overall fatigue life. S-N tests (performed between 7% and 18% of the static fracture strength) have shown a continuous downward trend without reaching a plateau or threshold value. Up to an order of magnitude reduction in lifetime (of 0.25-mm) was observed in specimen tested in the presence of electrolyte as compared to dry air test condition.

In experiments performed under alternating wet and dry test conditions, i.e. mildly corrosive (salt solution) to non-corrosive dry air, the fatigue process (crack growth rate) seem to adapt rapidly to the changing environment. Sudden reduction in crack growth rates were observed at transition points between dry and wet cycles, especially at lower stress levels and ratios. However, at every transition point, crack growth rate reduction was followed by a rapid increase to the velocity of respective dry or wet environment as shown in Figure 9.8.2.2. This refers to a simulation of real service condition for carrier-based aircraft.

These observations conclude that when cracks are present, aircraft structural integrity will be compromised even under mildly aggressive environments and at sub-critical stresses regardless of changing of environments and/or test frequency or stress level [1].

REFERENCE

[1] B. Shafiq and V. S. Agarwala: Corrosion and Fatigue in High Strength 7075-T6 Aluminum: Life Prediction Issues, submitted for publication at AIAA.

9.8.3 Corrosion Fatigue

David W. Hoeppner, University of Utah-QIDEC Laboratories

Over the past two years at the University of Utah, significant amounts of research have been accomplished. This research has been performed under contract from Lockheed Martin Aeronautical

Company with the prime contractor being the United States Air Force through the Corrosion Fatigue Structural Demonstration (CFSD) program. David W. Hoeppner, P.E., Ph.D. was the Principal Investigator of the program and Dr. Paul Clark and Dr. Charles Elliott were the co-principal investigators. Ms. Amy Taylor assisted no part of the research. Students involved in the research were Ms. Kimberli Jones, Mr. Sergio Limon, Mr. Larry Smiltneek, Mr. Michael and Risik. Areas studied include pit growth, pit-to-crack transition, short crack growth, and inspection of a naturally aged 7075-T6 aluminum fuselage panel.

As aircraft age there is an increased probability that the structure will experience pitting through corrosion. The structure also experiences a range of loading conditions such as cyclic, sustained or no load and environmental conditions ranging from cold to hot and wet to dry. Issues related to pitting growth behavior, pit-to-crack transition and short crack growth are of paramount importance in order to predict and manage corrosion on structures of aircraft. The studies performed during the CFSD program investigated concomitant corrosion fatigue where a specimen is exposed to cyclic loading and a corrosive chemical environment (3.5% NaCl aerated solution) simultaneously, the effects of prior corrosion on specimens subjected to laboratory induced corrosion and naturally corroded specimens machined from an aged fuselage panel that had been removed from service. The materials examined in this study included 2024-T3 and 7075-T6. The 2024-T3 and 7075-T6 were each examined in two sheet thicknesses 0.063" and 0.160". Additionally, the 7075-T6 was examined in extruded form (0.155") with specimens cut from a pristine C-141 upper wing structure. The fuselage panel material was determined to be 7075-T6.

The pitting growth specimens were subjected to a 3.5% NaCl solution and to one of four different loading conditions (cyclic load, sustained load, no load or no load at 160ºF), then cycled to fracture while concomitantly subjected to the saline environment. The various room temperature loading conditions had no significant effect on the pitting behavior of the different materials under the stated experimental conditions. The elevated temperature increased the pit density on the 2024-T3 materials and decreased the number and size of pits on the 7075-T6 materials. The elevated temperature condition did not significantly influence the residual fatigue life of any of the materials examined within this study.

The pit-to-crack transition study focused on observing the pit-to-crack transition of pitting corrosion to fatigue cracking and documenting the primary contributing factors that influence that transition.

Three modified discontinuity states (MDS) were studied. All prior laboratory induced corrosion specimens in the study fractured from cracks associated with pitting. Pit-to-crack transition was successfully captured visually for these specimens. An example of this is shown in Figure 9.8.3.1. Most of these critical pits were not the deepest present on the specimen. Results from the pit-to-crack transition experimentation revealed that there were dramatic effects on the fatigue life between the various materials, thicknesses, and laboratory induced corrosion states. The results indicated that quantities such as pit surface area and surrounding pit proximity played just as important roles as pit depth in determining when and where a fatigue crack would form.

The short crack growth experiments proved to be the most challenging of the experimental programs undertaken through the CFSD program. Dozens upon dozens of pilot experiments were performed in an attempt to develop a precise and executable experimental protocol. The effect of corrosion was documented to have a pronounced effect on the short crack growth rate of all materials investigated.

An aged 7075-T6 aluminum fuselage panel was inspected for evidence of cyclic and time-dependent degradation. While corrosion pitting and intergranular attack (IGA) were the focus of the investigation, evidence of cracking, general corrosion, exfoliation and fretting were documented as well. Significant levels of corrosion or cracking damage were discovered at these relatively low magnification levels in

approximately 44% of the rivet holes. It is judged that none of this was predicted by the structural design. Figure 9.8.3.2 illustrates the type of damage found in the rivet holes.

Along with the investigation for time-based degradation, a series of fatigue experiments were performed on double edge notch tensile (DENT) specimens. The DENT specimens were manufactured from both the naturally corroded panel and from a pristine sheet of 7075-T6 aluminum. The pristine DENT specimens were used as a baseline of comparison against naturally corroded DENT specimens and laboratory induced corrosion on previously pristine DENT specimens.

Sectioned specimens were examined with metallurgical microscopes. This investigation revealed tunneling pits, pitting in the countersink region, intergranular attack (IGA), cracking, pitting away from the rivet holes and fretting.

A paper, "Pitting Behavior and Residual Fatigue Life of 2024-T3 Aluminum Considering Loading and Sheet Thickness", was published in the Journal of the Mechanical Behaviour of Materials in 2002. This paper details the pit growth work completed for 2024-T3. The authors for this paper are Paul N. Clark and David W. Hoeppner.

A paper was presented at the USAF Aircraft Structural Integrity Program (ASIP) in December 2002 entitled "Observations From the Inspection and Sectioning of an Aged Fuselage Panel." This paper presents the work performed on the aged panel from the CFSD program. Authors for this paper were Paul N. Clark, Kimberli Jones, J.T. Huang, and David W. Hoeppner.

A poster/paper focusing on the 7075-T6 extruded pit growth specimens from the CFSD program was presented at the International Committee on Aeronautical Fatigue (ICAF) 2003 meeting. The title of the paper is "Pitting Behavior and Residual Fatigue Life of 7075-T6 Aluminum Extruded C-141 Wing" authored by Paul N. Clark, Kimberli Jones, and David W. Hoeppner.

9.9. TESTING

9.9.1 S-3B Viking Service Life Extension Testing

Nicholas Mitchell, Lockheed Martin Aeronautics Company

The United States Navy (USN) has operated the S-3 carrier-based aircraft in multi-mission roles including anti-submarine warfare, tactical support, and fleet tanking operations. The USN Naval Air Systems Command has expressed the need to extend the aircraft service life and operate its fleet of S-3B aircraft to the year 2015. To meet the requirement of maintaining the operational capability of the S-3B aircraft fleet through the target date, a Full-Scale Fatigue Test Program (FSFT), the culminating phase of a detailed S-3B airframe Service Life Assessment Program (SLAP), is underway.

A total of 187 S-3 aircraft were built, first entering fleet operational service in 1971. As of January 2002, 109 S-3B configured aircraft remained operationally active, with a fleet average of 9,800 flights hours and 2,000 catapult launches and arrestments per aircraft. Several aircraft are now close to exceeding the certified structural life associated with 13,000 flights hours and 3,000 catapult launches and arrestments. Testing will assess the ability of the current airframe structure to operate for 17,750 flight hours and 4,331 catapults and arrestments, an approximate thirty-percent increase to the airframe certified structural life.

Lockheed Martin Aeronautics Company, under contract with the USN has planned, designed, and is conducting the Full-Scale Fatigue Test program. When completed, the test program will substantiate the installation of structural Service Life Extension Program (SLEP) kits in the USN's fleet of S-3B aircraft, then will verify that the airframe can successfully achieve the desired extended structural life, and will provide input data to modify the existing S-3B aircraft operational inspection and maintenance program. The test data generated also can serve to refine the S-3B analytical model. Significantly, the test and the resulting data will provide valuable input for refinement of aging aircraft technologies used for structural fatigue life prediction across other aircraft platforms.

The S-3B Full-Scale Fatigue Test program includes the simultaneous and independent fatigue cyclic loading on two full-scale S-3B test articles. Taken together, the two test airframes represent a complete S-3B airframe. The airframes under test were previously retired, one being resurrected from decommissioned storage status at a desert storage facility and the other from previous use as a flight test aircraft. At the conclusion of testing a comprehensive teardown inspection effort, including NDI and SEM investigations, will be conducted to verify the analytically predicted structural damage and to investigate any additional resulting damage not predicted by the analytical models.

The testing phase of the program includes fatigue cyclic loading (application of initial, or "aging" cycles) of the test articles, installation of the SLEP kits - correlated with the planned installation of the kits in the fleet, further cyclic loading with detailed visual and NDI inspections performed at scheduled intervals, repairs of any structural anomalies found, post-test teardown, and analysis. A fatigue test spectrum representative of S-3B fleet aircraft usage is applied. This complete effort will verify that the installation of SLEP kits, in identified critical areas, would extend the structural life of the S-3B airframe to the desired service life goals. See Figure 9.9.1.1 and Figure 9.9.1.2.

9.9.2 The P-3C Service Life Assessment Program – Full Scale Fatigue Test

Jorge Lamas, Lockheed Martin Aeronautics Company and Michael L. Edwards, Naval Aviation Systems

The United States Navy (USN) and its three international partners, Canadian Forces, Royal Australian Air Force, and Royal Netherlands Navy, have identified a need to conduct a series of programs to assess and extend the operational service life of the P-3C aircraft. The P-3C has been the U.S. Navy's primary

maritime surveillance aircraft for nearly 40 years, and has served the partnering forces for several decades.

The P-3C Service Life Assessment Program (SLAP) is tailored to evaluate, through full scale testing, the fatigue life and damage tolerance characteristics of the P-3C airframe. The program also will design and validate structural modifications and repair solutions, some using newly qualified materials, required to attain a Year 2015 service life goal. To that end, the fatigue test program, comprising four separate tests, namely, Wing/Fuselage; Empennage; Main Landing Gear; and Nose Landing Gear, is being conducted by or under the direction of the Lockheed Martin Aeronautics Company Structural Test Laboratory.

The test article used entered service with the USN on June 12, 1969, and accumulated 10,987 flight hours and 16,543 landings during its service life. Prior to delivery for test on June 9, 1999, the aircraft underwent a major material improvement program, as part of the USN's P-3C Sustained Readiness Program (SRP), consisting of removing and replacing several airframe structural items that had experienced considerable corrosion. To accommodate the international partners, whose aircraft have not undergone SRP, the right hand wing of the test article was not retrofitted with new parts.

The four tests comprise 160 control channels and over 1600 channels of data. The largest test, the Wing/Fuselage, employs 117 control channels for 125 hydraulic actuators, moves flaps under load, and pressurizes the cabin and five fuel tanks. The Wing/Fuselage test also has 1050 channels of strain gage and deflection data that is recorded at each of the 2.4 million load points and during regularly scheduled strain surveys.

The need for extremely refined loading of the test articles presented many test fixture design challenges. These challenges included independent external load applications to control surfaces during surface rotations, pressurization changes to the cabin and fuel tanks during concurrent load cycling, and the use of aircraft sections as backup structures for the separate landing gear tests, rather than the commonly used steel bulkheads.

The P-3C SLAP test plan called for the application of 2.4 million load points as noted, representing 38,000 flight hours; 11,149 flights; and 59,728 landings. Regularly scheduled inspections are conducted, with significant non-destructive inspection (NDI) effort concentrated on fatigue critical areas (FCAs). The pre-test definition of the FCAs, allowing for tailored inspection intervals and efficient use of manpower, was one of the risk mitigations used to control the test schedule and budget. See Figure 9.9.2.1 and Figure 9.9.2.2.

9.9.3 The F/A-18E/F Full-Scale Static and Fatigue Test Programs – An Overview

R. Perez, Boeing

The structural certification of F/A-18E/F airframe included full-scale fatigue and static test programs. This paper outlines the test programs, discusses test objectives, discusses test results, highlights some significant advancements in the state-of-the-art developed to support this test program, and offers recommendations for future full-scale certification test programs.
The method used to correlate static test measured strains to finite element model predictions is discussed. The method used to certify redesigned structural components without the benefit of a full-duration fatigue test is discussed. Innovations involving real-time data monitoring, rapid post-test analysis of results, characterization of measured endpoint strains during fatigue cycling, and comparison of block-to-block measured strain response are discussed.

There were many lessons learned during these test programs. These are summarized and discussed in the paper. Recommendations for future full-scale certification test programs are also discussed.

The test was completed in February 2003. See Figure 9.9.3.1 and Figure 9.9.3.2.

REFERENCE

[1] Sullentrup, M.G., "**The F/A-18E/F Full-Scale Static and Fatigue Test Programs – An Overview,"** *Fatigue Testing and Analysis Under Variable Amplitude Loading Conditions, ASTM STP 1439*, P. C. McKeighan and N. Ranganathan Eds., ASTM International, West Conshohocken, PA, 2003.

9.9.4 Vertical Drop Test of a Narrow-Body Transport Fuselage Section with Overhead Stowage Bins Onboard

Gary Frings, FAA

The FAA technical report "Vertical Drop Test of a Narrow-Body Transport Fuselage Section With Overhead Stowage Bins Onboard," DOT/FAA/AR-01/100, describes the vertical drop test of a B737-100 fuselage section at the FAA William J. Hughes Technical Center. The objective of the test was to evaluate the response behavior of the overhead stowage bin installations when subjected to a severe, but survivable, impact condition. Of particular interest is a comparison of the pretest static, steady-state forces to which the bins were subjected during their calibration versus the dynamic forces generated during the impact test.

The 10-foot-long airframe section was dropped from a height of 14 feet, thereby generating a final impact velocity of 30 feet per second. The airframe section was configured to simulate the load density at the maximum takeoff condition. The final weight of 8870 pounds included cabin seats, dummy occupants, overhead stowage bins with contents, and cargo compartment luggage. The test article was fully instrumented with strain gages, accelerometers, and onboard, as well as ground-based, IRIG-capable high-speed cameras. See Figure 9.9.4.1 and Figure 9.9.4.2.

The fuselage test section sustained severe deformation of the cargo compartment, crushing approximately two feet. The luggage influenced the manner in which the fuselage crushed by limiting the g forces experienced at the seat tracks to approximately15 g's and increasing the pulse duration to approximately 135 milliseconds. Although numerous fuselage structural members fractured during the test, a habitable environment was maintained for the occupants, and the test was considered survivable.

Both overhead stowage bins maintained their structural integrity and remained attached to the fuselage. The bins sustained up to 14-g dynamic loading. These bins were able to support, conservatively, dynamic loads in excess of twice the static load certification requirements. Comparison of the dynamic versus static loading of the bins in the vertical direction, for each bin support, using resolved loads and calculated and expected loads, showed good correlation. However, the distribution of the loads among the bin supports was different in the dynamic versus static case. The maximum loading that the critical bin supports experienced during the test did not exceed 70% of their failure load.

9.9.5 Ground-Based Fuel Tank Inerting Proof of Concept Flight and Ground Tests

William Cavage, FAA

Since the TWA flight 800 accident in July 1996, significant emphasis has been placed on fuel tank safety. One proposed method of reducing the flammability of fuel tanks is fuel tank inerting, which is commonly

used by the military. However, the systems weight, resource requirements, and low-dispatch reliability have indicated that military fuel tank inerting systems would not be practical for application in transport airplanes. The Aviation Rulemaking Advisory Committee (ARAC) Fuel Tank Harmonization Working Group, commissioned by the FAA to evaluate various concepts for preventing fuel tank explosions in commercial transport aircraft, concluded that the most potentially cost-effective method of fuel tank flammability reduction is ground-based inerting (GBI). Ground-based inerting is defined by inerting fuel tanks during ground operations, when the threat of explosion is perceived to be the greatest. Theoretically, the benefit of an inert ullage would extend into ground operations, takeoff, and the first stages of the flight depending on fuel load, turn time, and ground conditions. Although significant research has been performed to quantify the ability of nitrogen or nitrogen-enriched air (NEA) to inert a commercial transport fuel tank, ground-based inerting had never been attempted in an operational aircraft.

A series of aircraft flight and ground tests were performed by the Federal Aviation Administration (FAA) and the Boeing Company to evaluate the effectiveness of GBI as a means of reducing the flammability of fuel tanks in the commercial transport fleet. Boeing provided a 737-700 for modification and testing. A nitrogen-enriched air distribution manifold (designed, built, and installed by Boeing) deposited the ground-based NEA into the center wing tank (CWT). The fuel tank was instrumented with gas-sample tubing and thermocouples to measure the fuel tank inerting and heating during testing. The FAA developed an in-flight gas-sampling system, integrated with eight oxygen analyzers, to continuously monitor the ullage oxygen concentration at eight different locations (Figure 9.9.5.1). Other data such as fuel load, air speed, altitude, and similar flight parameters were made available from the aircraft data bus. A series of ten tests were performed (five flight, five ground) under different ground and flight conditions demonstrating GBI's ability to reduce fuel tank flammability.

The CWT was inerted with NEA, produced by an industrial gas generator, to approximately 8% oxygen concentration by volume for each test. The aircraft condition was then set (fuel load, wind condition, flight condition) and the oxygen concentration in the CWT was continuously monitored. The tank was inerted in approximately 1.8 volume tank exchanges, which is slightly greater then the exact solution predicted. Results with low fuel loads showed that, under quiescent conditions, the oxygen concentration in the fuel tank remained somewhat constant, keeping the CWT inert (below 10% to 12% oxygen by volume) for relatively long periods of time. However, due to the cross-venting configuration of certain Boeing aircraft, some wind conditions created cross flows within the CWT, which caused a loss of nitrogen inerting gas and allowed for significant increases in the oxygen concentration. Some flight conditions also contributed to cross-venting and created high oxygen concentrations within the fuel tank. A modification to the vent system prevented cross flow within the CWT and created a significant increase in the time that the oxygen concentration remained below 10%, even at low to moderate fuel loads (Figure 9.9.5.2). High fuel load tests quickly became noninert, since the consumption of fuel induces airflow into the tank vent, increasing the ullage oxygen concentration.

9.9.6 Completion of Full-Scale Traffic Testing on Initial NAPTF Test Pavements

Gordon Hayhoe, FAA

Traffic testing of the initial nine test pavements (test items) at the National Airport Pavement Test Facility (NAPTF) was completed in early FY02. Loads were applied to test items with low-strength subgrade flexible stabilized base construction (LFS), low-strength subgrade flexible conventional construction (LFC), high-strength subgrade flexible stabilized base construction (HFS), and high-strength subgrade flexible conventional construction (HFC). Results of NAPTF traffic tests are significant, since they will be incorporated by the FAA into the new airport pavement design standards that will be applicable to next-generation heavy commercial aircraft, including the Boeing 777 and Airbus A-380.

The NAPTF was completed in 1999 and dedicated in April of that year. Traffic testing of the six flexible (asphalt) and three rigid (concrete) test items began in February 2000. The primary objective of the tests was to subject the test pavements to simulated heavy multiaxle aircraft traffic and to observe the number of vehicle passes before structural failure of the pavements. The two carriages of the NAPTF test vehicle (Figure 9.9.6.1) were configured to simulate taxi loads from a six-wheel B-777 main gear (carriage on the left side of the photograph) and a four-wheel B-747 main gear (carriage on the right side), respectively. In this way, the relative performance of the various pavements under these gear configurations could be compared. A secondary objective was to collect data from the approximately 1000 sensors embedded in the pavements for use in analysis.

The two test items constructed on a medium-strength subgrade (designated MFS and MFC) exhibited clear structural failures after repeated passes of the load vehicles. For these test items, the ultimate failure was characterized by deep rutting (approximately 6 inches) in the center of the load path, along with visible upheaval of the pavement structure at the fringes of the load path (Figure 9.9.6.2). This type of failure is indicative of shear flow in the subgrade, a conclusion that was supported by posttraffic investigations. Two other flexible pavement test items constructed on low-strength material (LFS and LFC) exhibited incomplete failures (i.e., the pavement structure showed significant damage after repeated traffic loading, although ultimate shear failure of the subgrade did not occur). Flexible test items constructed on high-strength subgrade material (HFS and HFC) showed no signs of failure after repeated traffic.

For the three rigid (concrete) pavement test items, failure was defined as a shattered slab condition, i.e., the concrete slabs are broken into multiple pieces. Although this final condition was attained in traffic loading for all three test items (LRS, MRS, and HRS), posttraffic investigations revealed that, in most cases, the cracks were due to the curling up of the slab corners that occurred before the tests began. When the traffic testing started, breaks occurred in the corners because of the pretest deformation rather than from the fatigue damage. This damage mechanism needs to be considered in analyzing the rigid pavement results.

Throughout the tests, the pavements were continuously monitored at regular intervals using visual surveys, nondestructive testing methods, and pavement profiling. After the traffic was stopped, posttraffic investigations were performed. Trenches were dug to expose the layers of pavement for direct visual inspection of the damaged structure. Monitoring and posttraffic testing provided extensive documentation that will be valuable in the analysis of the tests.

Data from the traffic testing at the NAPTF is available via the Internet in a searchable database. For additional details see the next article, National Airport Pavement Test Facility Database.

9.9.7 National Airport Pavement Test Facility Database

David Brill, FAA

Traffic testing at the NAPTF resulted in the accumulation of a vast quantity of test data. These data were primarily collected from approximately 1000 sensors embedded in the test pavements but also included pavement profiles and nondestructive pavement test (falling-weight deflectometer (FWD)) results. To store and retrieve the data reliably, the Airport Technology R&D Branch designed and built a relational database using the Structured Query Language (SQL) Server 7.0 system. The database is searchable over the Internet, providing convenient access to the NAPTF data (see at right).

Some sections of the database have been accessible over the Internet for about a year, but the full database, including dynamic sensor data from flexible (asphalt) test pavements, came on-line starting in June 2002. (Figure 9.9.7.1) Searchable records are grouped into three main categories:

- Static data. Static sensor readings are taken at regular hourly intervals. This category includes environmental sensors such as temperature and moisture gages.
- Dynamic data. Dynamic sensor readings are triggered by the movement of the vehicle and record the pavement's response to dynamic loads. This category includes the embedded strain gages, deflection sensors, and pressure cells.

- Other data. This category covers FWD results, pavement profile data, and pavement condition reports.

Using SQL commands, it is possible for an Internet user to retrieve specific subsets of data, e.g., concentrating on a particular test pavement, sensor, or range of dates. For less experienced database users, the most frequently used searches have been implemented on web forms.

In addition to the standard static, dynamic, and custom data search forms, background information on the NAPTF testing and instructions on how to use the database are available on the web site. These web-based materials include maps of the database showing the tabular structure of the database and the fields and data types associated with each table. A Daily Traffic Repetition table was created that summarizes the month-by-month and day-by-day testing schedule for each test pavement. By referring to this table, users can find the particular dynamic data they are looking for.

The NAPTF database has been completely populated, and its current statistics are as follows:

Static Data Records: 2,478,550
Dynamic Data Records: 11,018,340
Total Size of Database: 25 Gigabytes

Between April 12 and July 16, 2002, the NAPTF database was visited 58,136 times. The URL is: http://www.airporttech.tc.faa.gov/NAPTF/.

9.9.8 Consolidated Aerospace Structures Research Laboratory

Ken Leger, AFRL/VASV

The Air Force Research Laboratory (AFRL) is creating a new Consolidated Aerospace Structures Research Laboratory (CASRL) at Wright-Patterson AFB by combining and upgrading two existing Air Vehicles Directorate test facilities. According to Ken Leger, Chief of the Experimental Validation Branch in the directorate's Structures Division, Butt Construction of Dayton, Ohio is performing modifications to place all research efforts in a common building, under an $19.4 million US Army Corps of Engineers military construction contract awarded in the fall of 2000.

"Directorate scientists and engineers now perform acoustic, vibration and heat tests on small aerospace structures in one building, while doing flight loads and heat test on larger structures, such as wings and fuslages, in another building," Leger said. "The new lab, to be completed in the summer of 2003, will permit simultaneous flight load, heat and acoustic tests for aerospace structures as large as 4 ft by 4 ft with a planned upgrade to 10 ft by 10 ft in the near future." Using the CASRL, researchers in the directorate's Structures Division can test futuristic aerospace items, such as 'skins' for next-generation,

reusable, space-launch vehicles, for example," Leger explained. "When completed, the CASRL will offer scientists pioneering tomorrow's technologies more than 36,000 square feet of test space."

Figure 9.9.8.1 pictorially illustrates some of the existing and potential future military vehicles that guide the Air Vehicles Directorate technology programs. Figure 9.9.8.2 illustrates an artist's conception of the CASRL and some of the test capabilities of the CASRL.

9.10. COMPOSITES

9.10.1 Composite Material Control and Standardization

Curtis Davies, FAA

The material properties of composite structures are manufactured into the structure during the manufacturing process. Material procurement and processing specifications used to produce composite materials must contain sufficient information to ensure that critical process parameters are identified. This will assure production reliability of composite materials and adherence to expected part performance standards. Due to the wide variety of composite structures now emerging for certification, control of the materials is rapidly becoming a vital issue with respect to the overall assurance of safety.

In recent years, NASA, the FAA, and industry have worked together to develop a cost-effective method of qualifying composite material systems by sharing central material qualification databases such as MIL-HDBK-17 and the Advanced General Aviation Transport Experiment (AGATE). Through these shared databases, a manufacturer can select an approved composite material system to fabricate parts and perform a smaller subset of testing to a specific application (see FAA technical report "Material Qualification and Equivalency for Polymer Matrix Composite Material Systems," DOT/FAA/AR-00/47).

For materials to be accepted into these shared databases, all materials are required to be:

- Manufactured in accordance with a material specification that imposes control of the key physical, chemical, and mechanical properties.

- Processed in accordance with a process specification that controls key processing parameters.

Currently, the guidelines for creating the material and process specifications are not available as a single reference source. The information is spread between numerous technical reports, general industry knowledge, and lessons learned on individual programs.

To assist the effort to standardize engineering protocol, the FAA has identified the essential information required for the development of composite material procurement and processing specifications. The current focus is on polymer matrix prepreg composite materials such as carbon/graphite and glass. This will be expanded as other material and process combinations emerge.

The research is focused towards promotion of standardized material procurement and processing specifications. The objective of this project is to develop standard specification requirements that will meet the FAA's needs for accepting material procurement and processing specifications as part of a certification program. The research will establish a set of controls and tests on the production and fabrication process of composite materials to assure that a consistent and reliable product is produced and accepted for use in aviation applications. The project goals are:

- To greatly reduce the number of material and process specifications for identical composite material systems by using shared databases.

- To enhance the safety of composite structures by establishing guidelines for material and process specifications that will control key characteristics and produce stable properties.

- To eliminate the extra design costs associated with duplicative composite material testing and producing material and processing documentation requirements.

All criteria for materials procurement specifications and material fabrication specifications were identified based on known quality assurance methodology. Advanced technology areas were recognized that require quality assurance method development. These include additional manufacturing and fabrication process controls, and advanced inspection methodologies to consistently and reliably control composite products.

Material specification information includes recommendations and guidelines for basic fiber, matrix, and cured component characteristics; chemical, mechanical, and physical properties; safety and health information; transportation, storage, and handling; and testing including type, number, and frequency of tests. Processing information includes recommendations for fabrication method control and environmental conditions, inspection criteria at each operation, storage and handling throughout the process, process controls, materials, test specimen construction and processing, personnel qualifications, and tool proofing control.

Two draft documents with the recommended information and criteria for inclusion in composite materials procurement and processing documents were generated this year. These documents were a collection of the experiences of a group of industry composite professionals and FAA composite specialists. The two drafts were developed through the efforts of AAR-450 under a contract to Wichita State University.

A workshop to solicit industry comments from material suppliers and original equipment manufacturers was held in August 2002. The workshop was the first step towards creating a proposed policy and rulemaking by the Small Airplane Directorate. The participants critiqued two drafts of recommendations and guidelines to develop material and process specifications for composite materials.

The comments on the two draft documents will be addressed before they are published as:

"Guidelines and Recommended Criteria for the Development of a Material Specification for Carbon Fiber/Epoxy Unidirectional Prepregs," DOT/FAA/AR-02/109

"Guidelines for the Development of Process Specifications, Instructions, and Controls for the Fabrication of Fiber-Reinforced Polymer Composites," DOT/FAA/AR-02/110

9.10.2 Methodology for Delamination Growth Assessment in Composite Material Aircraft Structures

Peter Shyprykevich, FAA

Delamination growth is a common failure mode in laminated composite aircraft structures. Delaminations occur in critical areas of the structure, as shown in Figure 9.10.2.1, and their presence needs to be addressed to satisfy damage tolerance requirements during certification and in service to guide inspection and repair activities. Presently, the criticality of the delaminations, by size and location, is determined by tests. An efficient analytical methodology will reduce testing and, hence, reduce the cost of certification and aircraft maintenance.

A methodology was developed at Syracuse University under an FAA grant to address this problem. An energy release rate (ERR) approach analysis, which predicts delamination growth, was developed to overcome the limitations of current, state-of-the art methodologies. In the ERR methodology two- and three-dimensional crack tip elements (CTE) were used and shown to predict the same values of energy release rate and mode mixity as two- and three-dimensional continuum finite element (FE) analyses for a wide variety of geometries, materials, lay-ups, and loading. Moreover, the crack tip element (CTE)

analyses are considerably simpler and require orders of magnitude less setup and execution time compared to typical FE analyses.

Next, it was demonstrated that the CTE analyses may also be used to decompose the total energy release rate into non-classical mode I, II, and III components. This non-singular field (NSF) decomposition may be used, along with toughness versus mode mix data obtained from standard ASTM test methods using unidirectional laminates with midplane delaminations, to predict delamination growth with considerably better accuracy than the classical, state-of-the-art approach. This is due to the fact that the near-tip damage zone is sufficiently large in polymeric matrix composites to invalidate the classical assumptions, whereas the NSF mode decomposition is constructed in a manner that is insensitive to the details of this local damage state.

This was demonstrated by applying both the classical and CTE/NSF approaches to make delamination growth predictions in four different graphite-reinforced composites. The matrices included an epoxy, a toughened epoxy, a thermoplastic interlayer-toughened epoxy, and a thermoplastic. For this portion of the study, only flat-plate geometry specimens were considered. However, these included a wide variety of in-plane and bending loading conditions applied to unidirectional and multidirectional laminates containing delaminations at arbitrary locations. For all materials, loading, and lay-ups examined, the CTE/NSF approach was demonstrated to have excellent predictive ability, whereas, in many cases, the predictive capability of the classical approach was quite poor.

The final assessment of accuracy of the 3D CTE formulation involved an evaluation of the energy release rate for a delamination in a typical skin-stringer configuration subjected to bending and tensile loads. The stiffened-skin geometry considered is presented in Figure 9.10.2.2. The geometry consists of a section of a flat sheet that is reinforced by a hat stiffener. The skin and stringer are bonded along these flanges and are co-cured. The stringer is slightly shorter than the skin, and it is assumed that a delamination exists along the final 9.53 mm of the stringer's length. The test used to analyze the comparison is shown in Figure 9.10.2.3. By comparing the predicted results to the trend lines, it is observed that the CTE predictions for delamination onset are quite good and slightly on the conservative side. The predictions for the next few increments of growth are also quite good. For subsequent predictions, the predictions for growth for the left delamination are slightly high and the predictions for the right delamination are somewhat conservative. That is, the right delamination front advanced a little more slowly than predicted.

In summary, there are two main components to this methodology. First, for the material of interest, toughness is determined experimentally as a function of mode mix for mixed mode I-II loadings. This is done using relatively standard test methods on unidirectional laminates containing midplane delaminations. Second, a crack tip element analysis is used to determine the ERR and NSF mode mix in the local region of the structure of interest. The mode mix for this problem is expressed in terms of G_S/G, where $G_S = G_{II} + G_{III}$. Delamination growth is assessed by comparing the predicted ERR to the toughness at the predicted NSF mode mix. For this process, it is assumed that the toughness versus G_S/G relation is equivalent to the toughness versus G_{II}/G relation.

The developed methodology has the potential of profoundly affecting design, analysis, and certification procedures for composite aircraft structures. First, it will allow a relatively rapid assessment at a large number of possible locations, under a wide range of loadings, where delamination growth is likely. This will provide an early identification of possible failure sites that may not be found by the current selective testing approach, resulting in improved flight safety. Second, knowledge of the critical size and location of delaminations will reduce aircraft maintenance activity, as it will serve as a guide for repair actions. Finally, this methodology may allow the implementation of a more economic certification procedure

based on a mix of analysis and testing to assure a damage tolerant structure, similar to that presently in use for metallic structures.

9.10.3 Impact Damage Characterization of Composite Sandwich Structures

Peter Shyprykevich, FAA

The damage resistance and damage tolerance of sandwich composite structures to the potential threat of impact damage were studied as it affects structural integrity in both commercial and military applications. The need for a better understanding of impact damage in sandwich structures is further accentuated in view of the increasing use of composite sandwich configurations in general aviation (GA) aircraft where thin skins of carbon/epoxy and fiberglass/epoxy are typical, as illustrated by the Raytheon Premier I, Figure 9.10.3.1.

Impact damage states in sandwich structures were characterized by tests and analyses conducted by Wichita State University under an FAA grant. Analyses consisted of developing quadratic response surfaces based on selected experiments. Using analyses, the test data was interpolated to conditions that were not tested, and in this way, expanded the usefulness of the database. The developed analytical tool is capable of estimating visible indent damage and internal delamination damage from an impact event described by projectile radius, impact energy, and velocity as a function of the geometry of the sandwich, its facesheet and thickness, and the core density and thickness.

The study's experimental portion consisted of testing sandwich panels with different skin thicknesses, honeycomb core thicknesses, and densities with damages caused by various impact events. Three different quasi-isotropic skin lay-up sequences and two different core thicknesses, resulting in six sandwich configurations, were used in this study. The impact tests were conducted at a nominal constant impact velocity of 96.6 in/sec at various energy levels. Hemispherical steel impactors with diameters of 1.00″ and 3.00″ were used. The effects of different damage states were quantified by conducting uniaxial edgewise-compressive tests on the impacted specimens. The failure mechanisms governing the sandwich panels with different damage modes were identified.

The impacted specimens were inspected for damage using nondestructive inspection (NDI) methods. Planar damage area and residual indentation depths were used to implicitly quantify the damage state. The results indicated that a larger diameter impactor produces a very benign-appearing damage state, wherein no surface fracture or cracks or visually perceptible levels of indentation exist. However, NDI did indicate a very large damaged region. A select number of specimens were subjected to destructive sectioning to study the true nature of the damage. It was observed that for specimens impacted with a larger diameter impactor, the sandwich core had undergone localized crushing close to the impacted skin over a considerable area. However, the impacted skin, which had no noticeable damage, retained most of its original stiffness and had sprung back close to its original position. This damage scenario proved to be the most elusive when the impacted specimens were inspected using a visual inspection protocol. It was conclusively shown that the visual inspection methods can be very misleading. Therefore, the residual indentation by itself cannot be used as a reliable damage metric for static ultimate strength and damage tolerance criteria of sandwich structures.

The variation of compression after impact (CAI) strength with the planar damage area for different sandwich configurations and two impactor diameters are shown in Figure 9.10.3.2. It can be seen that the CAI strengths decrease when the planar damage area increases. Figure 9.10.3.2 shows that the CAI strengths dropped by approximately 40% of the nonimpacted panel strengths. This is a significant drop and must be accounted for in the design.

The variation of the CAI strengths with the maximum residual indentation depth for the same parameters as in Figure 9.10.3.2 is summarized in Figure 9.10.3.3. The figure clearly underlines the disadvantage of using the dent depth as an indicator of severity of damage because there is no clear trend in the reduction of CAI with dent depth. The specimens with higher dent depths possessed higher CAI strengths, which corresponded to compressive failures while the specimens with significantly smaller dent depths (but had large damage areas) possessed lower CAI strengths corresponding to a local buckling-induced failure mechanism.

For a fixed set of impact parameters, response surface estimates for the planar damage size and residual facesheet indentation suggest that impact damage development is highly material and lay-up configuration dependent. Increasing the thickness of the core material and the decreasing the number of facesheet plies resulted in the greatest reduction in the estimated planar damage dimension while increasing the amount of facesheet indentation. An increase in the impactor diameter can result in a significant increase in the estimated planar damage size as well as a decrease in the residual facesheet indentation, particularly for those sandwich panels with thicker facesheets. Moreover, those combinations of material system and impact parameters, which lead to the maximum estimated internal damage, do not correspond to those that result in the greatest facesheet indentation. Hence, it may be possible to tailor sandwich composite designs in order to maximize the degree of detectable facesheet damage while minimizing the internal damage associated with expected impacts. These efforts may facilitate sandwich panel design by establishing relationships between material configuration and impact parameters that lead to improved damage resistance and damage tolerance.

The study showed that other damage metrics, such as internal planar damage size, need to be considered in addition to visual dent depth, when generating a database to support development and certification of composite sandwich structure. It is very important to understand the effects of impact damage on static ultimate strength and damage tolerance criteria crucial to safety, as well as the implications to maintenance. One method for characterizing damage that is not clearly visible could be a simple manual tap, which is well within the capability of field inspections. In summary, the results of this study may affect inspection procedures in the factory and in aircraft operation.

9.10.4 Effects of Surface Preparation on the Long-Term Durability of Composite Bonded Joints

Curtis Davies, FAA

The long-term durability of adhesively bonded composite joints is critical to modern aircraft structures, since bonding is being adopted more frequently as an alternative to mechanical fastening. The advantages of bonding over mechanical means of fastening include higher stiffness, more uniform load distribution, cleaner aerodynamic lines, part consolidation, elimination of holes in adherends (thereby reducing stress concentrations and increasing load-bearing area), and less labor. The surface preparation of the adherends is critical to bond performance and affects initial strength, long-term durability, fracture toughness, and failure modes of bonded joints.

Inadequate surface roughening, environmental effects, possible chemical contamination, and other mechanical and chemical factors can prevent adhesives from bonding properly to composites, resulting in interfacial failures. These failures can occur at loads well below those of properly bonded joints that fail cohesively. Other interfacial failures occur over time in service as joints are exposed to harsh environments, such as elevated temperature and humidity, which do not affect well-prepared adherends. FAA research is intended to provide greater insight and extensive data to support increased application and confidence in bonded structures.

This study focuses on the effects of peel plies, release films, release fabrics, grit blasting, and environmental exposure; these not only have significant mechanical and chemical effects on bond integrity but are also relevant to aviation manufacturing processes. In this study, two potential factors were evaluated, with focus on the following:

- Effects of possible chemical contamination from release fabrics, release films, and peel plies during adherend cure.

- Chemical and mechanical effects of abrasion on the fracture toughness and failure mode.

The relative importance of each of the two factors in contributing to the bond strength and durability were determined. These results can be used to provide manufacturers with bonding guidance and to assist the FAA with certification procedures.

Nondestructive testing included X-ray photography of crack fronts, energy dispersive spectroscopy (EDS), X-ray photoelectron spectroscopy (XPS), surface chemistry analyses, and scanning electron microscope (SEM) imaging of prepared surfaces. Nondestructive microscopy and spectroscopy tests revealed chemistry and morphology features that explained the destructive test results. Smooth and fluorine-contaminated surfaces were neither chemically nor mechanically acceptable, although blasting created rough, less-contaminated surfaces. Results illustrate that release agents deposited on adherend surfaces during their cure cycle prevented proper adhesion.

Among the various nondestructive test methods used to evaluate prebond surfaces, SEM and XPS provided excellent information, while EDS revealed very little. SEM images could be used for qualitative morphological assessments to provide feedback on abrasion, peel ply removal, and other morphology-modifying processes. XPS revealed accurate chemical assessments of surfaces, aiding in correlation of specific elements to bond performance, especially failure mode. Because EDS examines chemical composition deeper than XPS does, EDS did not detect differences even between grossly different surface preparations. Finally, the X-ray photography was a useful tool in understanding crack front behavior in these opaque joints, justifying the optical tick mark measurement methods used in most of the tests for the given specimens.

Strength and fracture tests were performed on paste and film adhesive joints, and microscopy and chemical analyses were conducted on sample adherends. Because there were difficulties and variations in processing the paste adhesive, film adhesive was used for the majority of the tests in this study. The film adhesive removed several possible variables such as bond thickness and adhesive distribution. Additionally, film adhesive is more typical of commercial aviation bonded structures and its use, in addition to paste, broadens and generalizes the results of the tests.

Four release materials were tested during this program. Three different versions of the same polyester cloth were used. They were a scoured and heat set (NAT), very low porosity (VLP), and super release blue (SRB). VLP is mechanically finished through calendering. In the proprietary calendering process, the cloth is passed between several pairs of heated rollers that compress the material, reducing its porosity and flattening out the cloth's fibers. The use of VLP results in less resin bleed into the peel ply during cure. This improves releasability without the chemical agents that impede secondary bonding. SRB release fabric is a version that has an inert, heat-stabilized, cross-linked siloxane polymer finish. The fourth material was a release film, fluorinated ethylene propylene (FEP).

Grit-blasted FEP samples performed the worst of the four (see Figure 9.10.4.1), preceded by blasted SRB and VLP, with blasted NAT specimens producing the highest strength, see Figure 9.10.4.2. NAT

specimen shear strength was increased only slightly from blasting. SRB surfaces were rough but contaminated heavily with silicon, indicating that chemistry is at least as important as morphology. Blasting improved SRB surfaces greatly, even though they still produced unacceptable bonds in the destructive tests. VLP and NAT surfaces were contaminant free but the VLP surfaces were not as textured as the NAT surfaces, indicating that a difference in surface morphology does lead to different bond qualities, even if the chemistry is identical. Blasted VLP and NAT surfaces had improved morphology but little chemistry change, which resulted in increased performance in all of the destructive tests, proving the benefits of surface roughening. While mechanical abrasion did improve their fracture toughness and lowered their contamination greatly, the test values did not reach the levels of samples that were not contaminated before bonding, and the interfacial modes of failure did not always change to desirable modes.

Because each combination of materials can produce different chemical and mechanical bonding conditions, it was impossible to provide a single set of bonding rules. Every adhesive and adherend's exact chemical composition is proprietary, further hindering attempts to apply specific test data to other adhesive designs. Therefore, bonded joints that use similar materials cannot be assumed to perform like their counterparts, and even minor batch-to-batch material variations can change bonding performance significantly. Therefore, not only should all joint combinations be tested before production, but all incoming materials must also be tested as part of a continuous quality assurance program for adhesive bonding fabrication for aviation applications.

The results and trends of the study can be used as bonding guidelines and to increase awareness of potential surface preparation problems. Distinctions between peel plies, release fabrics, and release films apply to any bonding application, though the exact results will certainly vary greatly based on a specific product. Release fabrics and release films left bond-inhibiting contaminants, while peel plies did not. The extremely smooth surface created by a release film provided a poor mechanical interface, while the textures from peel plies and release fabrics were better suited to bonding. Likewise, effects of grit blasting were similar but not identical between the different joints tested. Grit blasting, if performed carefully at parameters similar to those used in this research, is strongly recommended for all bonding operations for its chemical and morphological benefits.

9.10.5 AFOSR New World Vistas Task 33 Composite Materials and Structures

Larry Byrd, USAF, AFRL/VASA

This program was a 5 year effort from 1997-2001. The goal of the research initiative was to provide a fundamental knowledge base for the failure of high performance, light-weight structures for global reach vehicle technology. The primary research objectives were:

- Development of theoretical and analytical models for the prediction of nonlinear response of high temperature composites to thermal and acoustic loads.

- Development of composite structural failure definition and damage accumulation when exposed to combined thermal and acoustic loads.

To achieve these objectives, experimental and theoretical research was undertaken focusing on the sonic fatigue of a relatively new class of composites described as ceramic matrix composites. The experimental work started with small coupons tested on electromechanical shakers and transitioned to 12x18" panels which were tested in a traveling wave tube modified to apply thermal loads. A number of techniques were developed that improved the testing of these materials. The theoretical work can be categorized as

- Dynamic nonlinear response of plates to elevated temperatures and acoustic loading.
- Micro-mechanics and damage in the composite material.
- Fatigue life prediction methods.

The dynamic nonlinear response was modeled analytically for uniform, isotropic and composite plates and numerically for plates stiffened around the edges. The stiffened plates were used in the experimental work to insure the failure would occur first in the middle of the panel away from the edges. Of special interest was the behavior of the panels once snap-through occurred and the vibration was about the buckled position. For nonlinear modeling, the ABACUS® finite element code was used as well as a reduced order method using modal coordinates. These methods captured the peak broadening and shifting effects associated with nonlinear behavior but still were not as accurate as desired when used to predict fatigue life.

The micro-mechanical work transitioned from modeling crack spacing in uniaxial composites with cyclic in-plane loads to modeling cracking in orthotropic composites with cyclic transverse loading to the effect of cracking on damping. The modeling predicted changes in stiffness and temperature fluctuations as damage progressed. The temperature fluctuations were used by an innovative differential thermography system to indicate stresses at the surface. The changes in stiffness were used experimentally to indicate damage and ultimately failure. The work with the differential thermography system led to a pending patent application for the detection of corrosion under coated surfaces in FY2002. Changes in damping with damage were studied because this changes the dynamic response and as a possible method to better predict fatigue failure.

The fatigue life prediction work examined the use of the rainflow cycle counting method, the minimum record length necessary to obtain random load distribution characteristics and damage accumulation modeling. Fatigue life was also predicted using spectral density based probability distributions. Here the appropriate cycle probability density function is estimated from the moments of the response power spectral distribution (PSD) using the Dirlik technique. The PSD for a multimodal response was generated numerically using ABAQUS®.

Figure 9.10.5.1 shows a panel in a shaker ready for testing. A laser vibrometer and differential thermography system was used to indicate mode shape and track high stress regions associated with cracks. Figure 9.10.5.2. shows a panel that has failed in a room temperature test in the traveling wave tube exposed to acoustic excitation.

REFERENCES

[1] Birman, V., and Byrd, L.W., “Onset of Matrix Cracking in Angle Ply Ceramic Matrix Composites”, submitted for publication in the International Journal of Mechanical Science

[2] Birman, V., and Byrd, L.W., “Effect of Matrix Cracking in Cross Ply Ceramic Matrix Composite Beams on Their Mechanical Properties and Natural Frequencies”, submitted for publication in the International Journal of Non-Linear Mechanics

[3] Spottswood, M. S. and Mignolet, M.P, “Experimental Nonlinear Response Of Tapered Ceramic Matrix Composite Plates To Base Excitation” submitted for publication in the AIAA Journal

[4] Spottswood, M. and Wolfe, H., "Comparing Fatigue Life Estimates Using Experimental and Spectral Density Based Probability Distributions" accepted for publication in the Journal of Aircraft

9.10.6 Fracture Process Zone Modeling of Small Cracks in Structural Ceramics Under Static and Cyclic Loading

Kenneth W. White, University of Houston

All-Oxide fiber-reinforced ceramic-matrix composites (CMCs) are of great interest for use in high-temperature aerospace applications where their high oxidation resistance is required. Usually, they are designed using the weak interface concept to avoid embrittlement but a second concept accepting the formation of strong interfaces emerged: In 1996, Tu et al [1] proposed the H-Crack concept. When cracks form in the weakest fiber bundle, they extend into the matrix, which is designed to deflect the crack. So, it does not propagate to the next fiber bundle.

The Post Fracture tensile test (PFT) is a method to characterize the microstructural features responsible for the bridging tractions that strongly influence the R-Curves of CFCCs [4]. This isolates a small number of fibers (about fiber bundles) for tensile testing. After the SENB test, the specimen is partly cracked in the notch plane. After that, a back notch is machined to remove the remaining uncracked ligament and a tensile test is performed: the PFT. Figure 9.10.6.1 is a family of PFT curves. The curves corresponding to different tests on different specimen are inserted in this graph with respect to the initial CODs of the specimen tested. Two observations can be made: The maximum stress is linearly dependent of the initial COD. But of most interest is the excellent agreement between the advanced stages of the separation event for all four curves where equivalent CODs overlap. This supports the significance of the strain softening segment of the PFT curves with respect to the development of an active fracture process zone in the crack tip wake region. Therefore, the individual PFT results can be viewed as incremental representations of the crack face separation event. The bridging relation was then used to compute the full R-Curve for any testing configuration using the relationship provided by Fett et al [5].

To support this theory, we show loading/reloading results of a PFT specimen after passing the peak (Figure 9.10.6.2): The specimen was first coated with gold for SEM photography before being loaded into the strain softening region. After unloading, it was coated with carbon and a new picture was taken. On this picture, it is possible to measure the length of fiber that was only coated with carbon. This recently pulled-out fiber length can be taken as a measure of the increase in COD. After that, the specimen was loaded again and we could verify the agreement between the two curves with respect to the increase in COD measured with the SEM.

REFERENCES

[1] Concept for a Damage-Tolerant Ceramic Composite with "Strong" Interface, Wen-Chiang Tu, Fred F. Lange and Anthony G. Evans, Journal of the American Ceramic Society, 79 [2] pp.417-24 (1996)

[2] The Processing and Performance of an All-Oxide Ceramic Composite, C. G. Levi, J. Y. Yang, B. J. Dalgleisch, F. W. Zok and A. G. Evans, Journal of the American Ceramic Society, 81 [8] pp.2077-86 (1998)

[3] Mechanical Properties of Porous-Matrix Ceramic Composites, Frank W. Zok, Carlos G. Levi, Advanced Engineering Materials, 3 [1-2] pp.15-23 (2001)

[4] Charcterization of wake-zone tractions in an oxidation-inhibited carbon/carbon composite, Arthur J. Lucchesi, John C. Hay and Kenneth W. White, Composites Science and Technology, 49 pp.315-325 (1993)

[5] Edging Stress relation from a combined evaluation of the R-curve and post-fracture tensile tests, T. Fett, D. Munz, X. Dai and K. W. White, International Journal of Fracture, 104 pp.375-385 (2000)

9.11. REPAIR AND LIFE EXTENSION

9.11.1 Probabilistic Optimum-Cost Risk-Based Maintenance Analysis for Aircraft Structure Components

D.M. Ghiocel, STI Technologies and E. Tuegel, USAF, AFRL/VASM

The overall scope of this research effort is *to develop a prototype engineering computational tool for predicting aircraft component reliability, remaining life and further the life-cycle cost under corrosion-fatigue damage.* By developing physics-based stochastic models for idealizing the operating environment, pressure loading, structural behavior and material corrosion-fatigue progressive damage*, the component reliability analysis and the maintenance cost analysis are approached from an advanced physical understanding and modeling.* Using the prototype tool, aircraft component reliability and remaining life can be predicted at any time. Further, a risk-based optimal-cost maintenance analysis can be performed. The focus of this SBIR project is on crevice corrosion effects for different lap joint designs.

Using the prototype software designer or maintenance engineer can quickly perform *what-if* analyses to see how different design modifications affect a component's risk of failure, the predicted life and/or the induced maintenance costs. For an engine designer, *what-if* analyses represent a key aspect for obtaining robust, affordable and durable cost-effective designs. Through *what-if* analyses, the design engineer understands, in much more detail, the behavior of his design, so that he can make the optimal technical decision. The what-if questions can include: What is the overall effect of different maintenance strategies against corrosion-fatigue damage on the component life prediction? How much does the NDE technique accuracy influence the component reliability and maintenance cost? How much does the operator skills influence the component reliability? How much does the corrosion-fatigue crack rejection criteria influence reliability?

The prototype engineering tool developed under this project is based on a **physics-based reliability engineering approach** that bridges and integrates intimately the **structural reliability** concepts and tools with the **classical reliability engineering** concepts and tools. Component reliability is expressed in terms of the failure probabilities and reliability indices. The following statistics and reliability metrics can be computed:

1. Crack Length Statistics Evolution with No or Multiple Inspection Intervals
2. Failure Risk Evolution with No or Multiple Inspection Intervals
3. Reliability Index Evolution with No or Multiple Inspection Intervals
4. Hazard Failure Rate Evolution with No or Multiple Inspection Intervals
5. Average Hazard Failure Rates per Inspection Intervals
6. Number of Failures (Removals) per Inspection Intervals
7. PDF of the Parent Crack Length Population after Each Inspection
8. Equivalent Weibull Failure (Life) Models
9. Posterior PDF of Life Via Bayesian Updating to Incorporate Failure Data
10. Posterior PDF of Crack Size Via Bayesian Updating to Include Inspection Data

Figure 9.11.1.1 shows the failure risk evolutions for a generic aging aircraft component without and with maintenance. From these plots it can be noted that if a failure probability of 0.001 is accepted, then the component life computed for this probability level assuming a 0.50 in critical crack length criteria is about 8,000 FH with no inspection, and about 18,000 FH with three inspections. Further, it can be seen that the second inspection at 9000 FH is more efficient than the first inspection at 4000 FH. The first inspection is too early and therefore has a more reduced effect. The second inspection reduces the failure probability by a few orders of magnitude. The size of the down-jumps in failure probability evolution

after the inspection times is a measure of how efficient the inspection set at that time is. Figure 9.11.1.2 shows the computed maintenance replacement costs assuming that the unscheduled on-line replacement is ten times more expensive than scheduled off-line replacement. It can be observed that the effect of the inspections is to double the optimal-cost replacement time and to reduce the overall replacement cost to half of one third.

9.11.2 FTI Research Summary

Len Reid and Jude Restis, Fatigue Technology Inc.

Effects of Cold Expansion Processes on Damage Tolerance

Ongoing tests were performed over the past two years to evaluate the effects of FTI's cold expansion processes on the crack growth lives and damage tolerance of different configurations including; an-isotropic grain material (Aluminum Lithium), interaction of shot peening and cold expansion on lugs, and the effect of Ionized Vapor deposition (IVD) aluminum coatings. The following are summaries of these tests and reviews of two aircraft applications.

Cold-Working of materials with an-isotropic properties due to grain direction

Static cracking was discovered emanating from holes in Aluminum Lithium material in the short transverse plane after they were cold expanded. In conjunction with the OEM involved, FTI performed extensive dynamic analysis of the failure mechanism to determine the cause of cracking in this grain direction.

Aluminum Lithium has very low elongation (1.5%) and shear properties in the short transverse grain direction. Like other high strength aluminum alloys such as 7050, the low elongation properties in the short grain direction of aluminum lithium were found to initiate static cracks during cold working at the normal applied expansion of 3.5%. Unlike the radial cracks that generally initiated at the shear discontinuity at the sleeve gap in the other alloys, the cracks in the aluminum lithium were oriented along the long grain direction, often at multiple sites not associated with the sleeve gap. Reducing the applied expansion to slightly below 2% failed to eliminate the cracking phenomenon. Finite Element Analysis (FEA) determined the most likely cause of failure to be high shear stresses at the failure origins. Research and analysis is ongoing to determine if the aluminum lithium material can be processed using cold expansion and to optimize the method.

Evaluation of the Interaction of Shot-Peening and Cold Expansion in an Lug

A recent investigation evaluated the interaction of the shot-peening and cold expansion processes in a helicopter blade-attaching lug. A large radius detail at the edge of a lug bore was shot-peened prior to installation of a FTI high interference fit ForceMate bushing. During testing, the fatigue life improvement was found to be less than expected. Further examination determined that the failure origin occurred at the junction of the shot-peened radius with the straight section of the bore of the hole. A Finite Element Analysis (FEA) showed that the shot peened radius was subjected to a large deformation during installation of the ForceMate bushing at this same position and was identified as the most probable cause of failure. Crack initiation at this location could have occurred due to the superposition of the local high strains and repeated strain cycling that occurred at the surface during shot-peening with the large scale deformation that occurred during bushing installation. A detailed FEA analysis of that area of the lug showed that a change to the detail design of the radius could eliminate the coincidence of the high strain at the failure location. FEA proved very useful in investigating the effects of residual stress/strains due to surface treatment methods on detailed design features such as chamfers and radii at the edges of holes. The lug is currently in test.

Effect of IVD Surface coating on Fatigue Life of Cold Expanded Holes
FTI recently compared the fatigue life of non-cold expanded and cold expanded holes in open hole test specimens manufactured from 7075-T651 which were Ionized Vapor Deposition (IVD) Aluminum coated. IVD coating is typically used on aluminum structure, such as bulkheads, to provide corrosion protection. As part of the process to apply the coating, the parts are etched in a similar manner to the pre-surface preparation for anodizing. The concern about the use of this process is that the etching process is known to have a detrimental effect on fatigue life.

The cold expansion process plastically yields the area around a hole to provide beneficial compressive residual stresses, which are known to slow down crack growth but not necessarily affect crack initiation. This test program looked at the combined effect of material yielding due to cold expansion and the surface etching from IVD coating on crack initiation

Results showed that in 7075-T651 aluminum specimens, the addition of surface etching and IVD coating reduced the fatigue life. In as-reamed open hole IVD specimens the life was reduced by 37% compared to the baseline bare specimen similar to previously tested anodized specimens. The addition of IVD to cold expanded specimens reduced the life by 76%. However, even with this reduction in life, the cold expanded specimens had a minimum fatigue life improvement of 5 times the fatigue life of the non-cold expanded specimens. For the specimens tested in this program, the results showed that it was better to cold expand the holes after the parts were processed with IVD coating.

Recent Applications of Cold Expansion on In-Service Aircraft P-3
During full scale testing of the US Navy P-3 aircraft, fatigue cracks were discovered in the lower wing skin. The cracks were located at riveted nutplate locations common to wing skin to engine pylon fairing attachments. FTI ForceTec rivetless nutplates were incorporated into the test article to repair damaged holes and to prevent damage to other existing locations. Based on the results of this testing, the US Navy has incorporated the use of FTI's ForceTec rivetless nutplate as a repair and preventative modification to the P-3 wing skin

Helicopter Fatigue Critical Locations
Several helicopter manufacturers have recently incorporated the use of FTI's ForceMate high interference fit bushing process to fatigue critical components. The fatigue strength improvement of the ForceMate process allowed optimum design and in some cases allowed the OEM to achieve damage tolerance airworthiness requirements. The first helicopter certified under damage tolerance requirements utilized the benefits of a high interference fit bushings to prevent bushing fretting, a common origin of fatigue cracking and corrosion on helicopter components.

9.11.3 Crack-Bulging Effects on Repairs in a Pressurized Narrow-Body Aircraft Fuselage
John G. Bakuckas, FAA

The damage tolerance design philosophy requires realistic stress-state determinations in the vicinity of cracks in airframe fuselages. Longitudinal cracks in pressurized aircraft fuselages are subjected to hoop and bending loads. The interaction of these two loadings can cause the skin to bulge, which can significantly elevate the stress-intensity factor (SIF) at a crack tip and reduce the residual strength. One way to quantify the effect of bulging is the bulging factor. The bulging factor is the ratio of the mode I SIF at the tip of a longitudinal crack in a curved panel to that for the same crack in an infinite flat plate. Few studies have been done to study the bulging effects for cracks in narrow-body fuselage structures that represent commuter-sized aircraft, and the consequence of not including these effects in the stress

predictions and subsequent damage tolerance analysis. Of particular concern is a fuselage that has been repaired. Repairs add new flaw initiation sites to the structure and also alter its bulging response. (Figure 9.11.3.1)

To examine the effect of bulging on SIF and residual strength calculations in a repaired fuselage, the bulging factors were calculated using a nonlinear finite element analysis. The crack tip SIFs were calculated using the Modified Crack Closure Integral (MCCI) method.

A typical commuter fuselage with a 40-in. radius was modeled using the finite element method. A 16- × 12-in. cutout was modeled in the fuselage. The cutout was repaired by a 28- × 24-in. internal doubler. A crack of half length a was introduced into the outermost rivet row. The model was loaded with internal pressure p. The bulging effects were studied by varying the pressure p, the crack half-length a, and the stiffening of the fuselage.

Typical results are shown in Figure 9.11.3.2 where the bulging factor is plotted as a function of internal pressure for stiffened and unstiffened fuselages. The crack length was such that $a/L = 1.2$. One can see that the bulging factor is lower for the stiffened fuselage; however, it is still significant and should not be neglected. For the case shown here, the crack-tip mode I SIF for a fuselage stiffened both with frames and longerons (fully stiffened case)is 50% higher than a crack with the same length in an infinite unstiffened flat plate (unstiffened without repair case). The mode I SIF will be even higher when compared to an equivalently stiffened flat plate.

The MCCI method employed here allows one to partition the strain energy and to isolate the SIF for different modes. (Figure 9.11.3.3)

The studies completed up to this point have established the need to account for bulging factors in narrow-body aircraft in general and in repairs of narrow-body aircraft in particular. Further work to calculate and develop a database of bulging factors for narrow-body aircraft fuselages will continue.

9.11.4 Repair of Transport Aircraft Using Composite Doublers

David Galella, FAA

Bonded composite doublers offer airline maintenance facilities a cost-effective way to safely extend the lives of their aircraft. Instead of riveting multiple-steel or -aluminum plates to repair an aircraft, it is now possible to bond a single boron-epoxy composite doubler to the damaged structure. However, before this advanced aircraft repair technique could be accepted for commercial use, uncertainties surrounding the application, nondestructive inspection (NDI), and long-term endurance of composite doublers had to be addressed.

The FAA's Airworthiness Assurance NDI Validation Center (AANC) has completed an experimental project where composite repair doublers were installed on in-service commercial aircraft. The project validated a family of generic composite patches to be used to repair various types of damage to metallic structures caused by dents, dings, lightning strikes, corrosion grind outs, and certain cracks in nonpressurized areas. The project also identified necessary guidance data needed to assure the continued airworthiness of composite doublers.

In conducting this program, the AANC focused their attention only on the DC-10/MD-11 aircraft and worked collaboratively with FedEx, Boeing Long Beach, and Textron Specialty Materials. To a large extent, the project built upon a foundation established during a previous project where the AANC worked with Delta Airlines to validate the use of a composite reinforcement on an L-1011 doorframe corner.

In the current project, the first composite patches were installed to repair impact damage on two FedEx aircraft in July 2000. Those installations marked the first use of bonded composite doublers as permanent repairs for skin damage in a U.S.-operated commercial aircraft. To date, repairs have been installed using a phosphoric acid-anodized surface preparation method, although future efforts will investigate a simpler procedure using Sol-Gel. After each installation, the doublers were inspected using AANC-developed ultrasonic inspection procedures. The inspections ensured that there were no interply delaminations or disbonds between the composite patch and the underlying metallic structure. As part of the project, the inspections were conducted after 30 days, 6 months, and 1 year of service after installation. After 1 year, the inspection of the doubler was coordinated into the airplanes' heavy maintenance or D-check schedule.

One key element of the experimental project was to demonstrate that aircraft maintenance personnel could be trained to install and inspect the composite doubler repairs. As a result, workers from the FedEx composite and NDI shops were key participants in the repair installation and inspection. AANC personnel gradually reduced their role in the composite doubler installations until FedEx personnel were able to safely apply and inspect them without supervision. Overall, seven composite doubler repairs were installed on FedEx aircraft and, to date, each has successfully passed the applied NDI tests.

The project included developing the appropriate technical data that can be used in an FAA advisory circular on installing and inspecting composite repairs. The data needed to develop a Boeing Material Specification to formally adopt the material allowables for the boron-epoxy composite material was also formulated. The adoption of the material allowables is the last step necessary before a revision can be made to the manufacturer's Structural Repair Manual (SRM). The ultimate outcome of this project is to have composite doubler repairs conveniently specified in the manufacturer's SRMs.

Future users of this technology are all the airlines and maintenance depots that currently apply metallic repairs. Industry interest in using composite doubler repair has grown considerably since the results from this study have shown that the finished doublers are lighter in weight, corrosion resistant, stronger, and faster to install than a typical riveted aluminum plate repair.

Figures 9.11.4.1 and 9.11.4.2 show examples of the installation and inspection of a composite doubler repair on a FedEx DC-10 aircraft.

9.11.5 Laser Additive Manufacturing of Titanium for Rapid Fabrication of Spare Parts

M.H. Bohun, University of Dayton Research Institute; K.T. Slattery and S.S. Fields, The Boeing Company; P.A. Kobryn, Air Force Research Laboratory; and W. Leng, H.J. Ford and R.B. Ivey, Warner Robins ALC

Overview

A novel production method known as laser additive manufacturing (LAM) has the potential to greatly reduce the manufacturing lead time for select titanium components by eliminating the need for hard tooling and greatly reducing the volume of feedstock required. The LAM fabrication method can be used to manufacture metallic preforms directly from computer-generated 3D drawings (see Figure 9.11.5.1)). In this process, metallic powder is directed toward a substrate and melted by a laser beam. Parts are built up layer by layer by moving the laser and powder source across the surface of the underlying material. In this manner, free-standing shapes are generated without molds or dies. Conventional techniques are then used to machine the preform to the final part geometry. [1-4,6,7]

Tensile Strength, Crack Initiation and Crack Growth

The averaged ultimate tensile strength properties of LAM are within the limits of conventional forged Ti-6Al-4V alloys (see Table 9.11.5.1). The yield strength and total elongation values are near the lower

bound of conventional wrought Ti-6Al-4V behavior. Both open hole and shallow gradient fatigue crack initiation testing was conducted using a fighter aircraft wing root bending moment spectrum. In both cases it was shown that the LAM material met or exceeded the wrought product form design curves. In general, the LAM material also exhibited superior crack growth behavior compared to mill annealed, equivalent behavior to recrystallized annealed, and higher growth rates compared to beta annealed. [5]

Technology Development

While the initial results applying LAM to non-critical aerospace components are promising; significant work is required to provide designers with enough information to be able to predict the structural performance of LAM material with enough fidelity to trust its use for the production of structurally critical components.[8] As production of non-critical components proceeds, many questions regarding the consistency of the LAM process and the underlying supply chain can be answered (provided that the proper data are collected during manufacturing). As the number of different part geometries being produced increases, empirical correlations between mechanical properties and deposit geometry / deposition path can be explored. The Air Force is currently pursuing the use of LAM to produce Ti-6Al-4V preforms for certain non-critical components and developing a strategy to expand the applicability of LAM to increasingly complex and critical components.[9]

REFERENCES

[1] "Aging of U.S. Air Force Aircraft" Final Report: National Research Council, National Academy Press, 1997.

[2] D. Abbott and F. Arcella, 1998, Laser Forming Titanium Components, *Advanced Materials & Processes*, ASM International, Vol. 153, No. 5, pp. 29 to 31.

[3] DARPA "Flexible Fabrication in Titanium (FFTi)" Program, U.S. Government Contract Number N00014-95-C-0029.

[4] CAD-Driven Laser Forming Process May Eliminate Costly Manufacturing Practices, 1999, Office of Naval Research News Release, 2 August 1999.

[5] K.T. Slattery, The Boeing Company, unpublished research, 1998-2002.

[6] T. Bayha, D. Evans, D. Furrer, and A. Poole, 2002, Metals Affordability Initiative Consortium, *Advanced Materials & Processes*, ASM International, Vol. 160, No. 5, pp. 30 to 32.

[7] "Parts Shortages Are Impacting Operations and Maintenance Effectiveness," United states General Accounting Office Report to Congressional Committees, GAO-01-587, June 2001.

[8] W.E. Frazier, D. Polakovics, and W. Koegel, 2001, Qualifying of Metallic Materials and Structures for Aerospace Applications, *JOM*, TMS, Vol. 53, No. 3, pp.16 to 18.

[9] K.T. Slattery, P.A. Kobryn, S.Kidd, and F.G. Arcella, 2002, Use of Laser Additive Manufacturing for Spare Part Fabrication, at Aeromat 2002.

9.11.6 Structural Life Enhancement for Fighter Aircraft

J. McFarland and R. Perez, The Boeing Company

Fatigue and corrosion damage are issues in the USAF aging fighter aircraft fleet. Periodic inspections and replacements of the damaged components have solved many of these problems, but this approach is expensive and significantly reduces aircraft availability. In addition, damage can reoccur requiring the same repair to be performed several times. Alternative structural life extension technologies exist which offer more efficient solutions.

Recent modifications to the F-15 airframe structure have taken place or are under consideration to reduce honeycomb water corrosion, reduce maintenance costs, quickly produce spares, provide technology demonstration for future aircraft, and eliminating/reducing maintenance, including NDI inspections and problem fatigue cracking issues.

Included in this paper are the results of a recent study conducted for the United States Air Force Research Laboratory at Wright-Patterson Air Force Base, to identify the problem areas on the F-15 structure and determine appropriate solutions. This study provided an assessment of available structural life extension technologies and was focused on technologies that can be applied on existing structure. In addition to this study, recent technological upgrades to the F-15 as spares, technology demonstrators, corrosion enhancements, or resolutions to fatigue areas of concern have been included. The recommendations in the plan address solutions that can be integrated into an overall life extension plan for fighter aircraft.

These technologies include;

a) Mature Technologies - Cold Working, Interference Fit Fasteners, Shot Peening, and Fleet Monitoring
b) Near General Application - Corrosion Prevention, Damped Bonded Patch, Composite Patches, Grid-Lok, Laser Formed Titanium (Figure 9.11.6.1), and Material Substitutions
c) Needs Additional Work - Advanced Riveting Technology, Active Vibration Suppression, Laser Shock Processing, Friction Stir Welding, and Health Monitoring

REFERENCE

[1] J. McFarland and R. Perez, “Structural Life Enhancement for Fighter Aircraft,” 2002 Aircraft Structural Integrity Program Conference, Savannah, Ga.

9.11.7 Development of a Damaged Metallic Part Database for Rotorcraft

Dy Lee, FAA

One of the tasks identified in the consensus rotorcraft damage tolerance roadmap developed by the FAA and Rotorcraft Industry Technology Association (RITA), is to develop a database structure to capture, store, and manipulate data on damaged metallic parts. RITA, under the National Rotorcraft Technology Center’s (NRTC) umbrella, is conducting the research. The objective is to provide a tool for analyzing sources and consequences of damage (initiated both during manufacture and in the field), as well as assessing the significance of various threats and quantifying inspection capabilities.

The structure of this Microsoft Access database has been defined and much of the user interface has been developed. (Figure 9.11.7.1) This database has 87 fields or attributes that cover data relating to the

aircraft model and part, material description, damage details, and documentation and part disposition. Damage description attributes are available for detected, initial, and consequential damages. The definitions of these damages are provided within the user interface.

All of the features have been implemented except for the Reports function that needs to be integrated with Microsoft Excel for graphing selected data. The main data screen is shown below from the data-viewing mode. This same screen is also used, with minor modification, for data editing (password protected), entry of new records into the database, and displaying search or query results. Many of the entry boxes have pull-down lists of commonly used entries to reduce the amount of input typing and to help standardize entry syntax.

In order to query the database, a search screen is provided. (Figure 9.11.7.2) Any combination of attributes may be used as search criteria, and pull-down lists are again used.

In addition to those described above, there are other screens that provide ancillary information. This information includes definitions of various damage terms such as scratch, nick, and gouge. The database is also able to store photos of the damage.

9.12. NON-DESTRUCTION INSPECTION

9.12.1 Innerlayer Crack Experiment

David Galella, FAA

Investigators from the FAA's Airworthiness Assurance Nondestructive Inspection Validation Center (AANC) recently completed an experiment to assess the reliability of a sliding probe eddy-current procedure for its effectiveness in finding second- and third-layer cracks in certain Boeing 737 lap splice joints. The task was undertaken at the request of the FAA's Seattle Aircraft Certification Office.

The experiment used well-characterized test panels that simulated the lap splice joint shown in Figure 9.12.1.1. Each test specimen consisted of one mock doubler, four mock tear straps, and two aluminum skins riveted together with a 3-inch overlap that included the doubler. Fatigue cracks were grown in the aluminum sheets and placed in the lower skin, requiring inspection through either 0.072 or 0.080 inch of combined upper skin and doubler material. The spacing of the tear straps was varied to simulate manufacturing tolerances. Since the tear straps create a major source of noise for the eddy-current inspection, the number of tear straps per unit length of lap splice was doubled for this experiment. The fatigue cracks were created from starter notches at select locations. The lower skin panels were then cycled until the desired length of crack was reached. The starter notches were then removed by drilling the final holes for fastener installation. Individual eddy-current signals were verified to simulate signals from aged aircraft. Cracks were of varying lengths and some of the rivet locations had cracks emanating from both sides of the rivet hole. In total, there were 360 rivet sites to inspect as part of the experiment.

The AANC researchers traveled with the test panels to eight different inspection facilities where 56 inspectors participated in the experiment. Inspectors were asked to conduct the inspections following Boeing's procedure 53-30-11 using the eddy-current instruments and probes available at their facilities.

The results from the experiment are shown in the probability of detection curves in Figure 9.12.1.2.

Analysis conducted to date has revealed several observations. First, as is often the case, there was substantial inspector-to-inspector variation in this experiment. This variation indicates that fundamentally different inspections are being carried out from one inspector to another. Many of the inspectors failed to closely follow the Boeing procedures and only a few implemented the checks that were included in the procedures to give better inspections in the presence of tear straps. Second, many of the inspectors only used an absolute threshold of the maximum signal height and did not include calls based on signal loop width, as called for in the Boeing procedure. Third, many of the inspectors did not use a nonconducting straight edge to aid in keeping the sliding probe centered over the rivets, a factor which can mask crack signal indications.

FAA certification personnel and Boeing NDI procedure developers were briefed on these findings and will take them into consideration when issuing revisions and future lap splice inspection procedures.

9.12.2 Automated Nondestructive Inspection of Multi-Layer Structures in the C-130 Center Wing

Eric Lindgren, Michael Concordia, John Mandeville, David Judd and Tim MacInnis, SAIC Ultra Image International; and John Aldrin, Computational Tools

SAIC Ultra Image International is developing an ultrasonic inspection technique that will inspect the sections of the center wing of the C-130 Hercules aircraft [1]. The two-layered structures to be inspected include the fastener sites that join the wing planks and the stringers, plus the wing plank and the rainbow fittings. The rainbow fittings are components of the joint between the center and outer wings. A key

aspect of this inspection technique is that the inspection can be completed without the removal of any fasteners, which greatly reduces the time required to perform the inspection. The work described is being completed under a task from the Warner Robins Air Logistics Center (WR-ALC) of the US Air Force and builds on previous work completed for inspection procedures for the C-141 and C-130 aircraft [2, 3], which were supported by WR-ALC and the USAF Aging Aircraft Office. This crosscutting technology has applications to multiple aircraft and is currently being applied to the B-1B Lancer.

The C-130 inspection of the center wing stringers is for over 18,000 fasteners and the rainbow fitting inspection is for over 900 fasteners. The technique being developed uses automated ultrasonic scanning and automated interpretation of the ultrasonic images, or C-scans. The data are acquired from the exterior surfaces of the wing structure, eliminating the need for internal wing access. Ultrasonic inspection of multi-layer structures requires adequate sealant between the faying surfaces to couple the ultrasonic signal from one layer to the next. In addition, flush head (countersunk) and raised head fasteners are used to join the layers. Figure 9.12.2.1 is a photograph of the inspection system positioned to collect data on the upper surface of the center wing.

Typical ultrasonic C-scan results of data collected with the Ultra Image IV imaging system are shown in Figure 9.12.2.2. The sample that was inspected is a set-up standard for the stringer and wing plank inspection. The image shows time-of-flight (ToF) data with a dark red background and peak amplitude data with an orange background. In the ToF scan, the fasteners and notches are clearly shown with the gradient scale corresponding to decreasing ToF, red to green. In the amplitude scan, the notches can be distinguished by their lateral position aft and forward of the fastener holes (top and bottom in this image). Note that the fastener holes appear elongated due to the extended gate used to capture the data from both layers of the structure.

The output of the Automated Defect Analysis (ADA) software is shown in Figure 9.12.2.3. The software provides the inspector with near-instantaneous results that indicate the presence of a fatigue crack by a fastener. This data can be stored electronically for easy archiving. A Probability-of-Detection (PoD) experiment is being executed using the geometry and materials of the structure on the aircraft to validate the detection of the fatigue cracks to the desired goal of detecting 0.070" fatigue cracks in each surface of the two layers. The estimated cost savings for this inspection has not yet been calculated, but a high return on investment is anticipated.

REFERENCES

[1] E.A. Lindgren, et. al., "Enhanced Nondestructive Inspection Techniques for the C-130 Center Wing", 6th Joint DoD/NASA/FAA Aging Aircraft Conference, Sept. 2002, San Francisco, CA

[2] T.J. MacInnis, et. al., "C-130 Center Wing Stringer Second Layer Ultrasonic Fatigue Crack Inspection," 4th Joint DoD/NASA/FAA Aging Aircraft Conference, May 2000, St. Louis, MO

[3] J. Aldrin, et. al., "Case Study of the Implementation of an Automated Ultrasonic Technique to Detect Fatigue Cracks in Aircraft Weep Holes," Mat. Eval., 59, (2001).

9.12.3 Aircraft Inspections Using Computer-Aided Tap Test (CATT)

David Galella, FAA

The coin tap test method has a long history of being a simple, low cost, and reasonably effective means for inspecting adhesively bonded metal structures and composite parts of aircraft. Tap tests are usually used for the detection of voids, disbonds, and delaminations in the structures based on their acoustic

response to a tap. Qualitatively, a tap on a structurally sound region produces a characteristic resonant sound, whereas a tap on a defective or damaged region will produce a dull or dead sound. In aircraft inspection, a tap test is usually applied when the composite part shows visual indications of damage or there is reason to suspect subsurface damages. A strictly manual tap test relies on the human ear to discriminate between the sound of a good region and a defective region. This is subjective, operator dependent, and susceptible to false calls, especially in a noisy environment. It is also often difficult to ascertain the size, shape, and severity of flaws or damages.

Funded as part of the FAA's Airworthiness Assurance Center of Excellence (AACE) program, Iowa State University has developed a Computer-Aided Tap Tester (CATT) for the inspection of damage, flaws, and repairs in sandwich structures on aircraft, including composite and aluminum honeycomb sandwiches. (Figuire 9.12.3.1) The CATT system provides C-scan images depicting local part stiffness that can be used to reveal the size, shape, and severity (percentage reduction of stiffness) of the defective or damaged area. The system has the advantages of being operator independent, portable, and easy to use.

The system actually measures the time of contact between an accelerometer and the surface of the test component. A novel magnetic cart is used for maneuvering the accelerometer by hand across a surface. As the cart is pushed, a wheel containing permanent magnets forces the accelerometer to contact the surface at a predetermined linear distance, e.g., every centimeter. A portable laptop computer records the impact duration and position for each tap. Microsoft Excel software is used to produce a C-scan image of the inspected area.

Based on a simple spring model, to which a wide variety of sandwich components on aircraft conform, the time of contact image is then converted into an image of the local stiffness. The image of local stiffness reveals not only the presence of defects or damages, but also the normal substructures and reinforcements.

The CATT system was evaluated quantitatively for its sensitivity and range of applications, using composite standards from the Commercial Aircraft Composite Repair Committee (CACRC). Using these standards, the stiffness measured by the tap test is compared to that obtained directly from mechanical loading tests; the agreement is found to be quite good. (Figure 9.12.3.2) The system has also been tested in more than 15 field trials at airline maintenance facilities, military depots, and original equipment manufacturers on a variety of composite and aluminum sandwich structures. Since using the CATT, field test results have been obtained for a wide array of applications, including repairs on composite rotor blades, engine fan cowlings, trailing-edge flaps, aluminum heater blankets, petal door, pylon fairing, and impact damages in foam-cored composites.

9.12.4 Composite Reference Standards for NDI

David Galella, FAA

Since the inception of its National Aging Aircraft Research Program (NAARP) in 1988, the FAA has been conducting nondestructive inspection (NDI) research and validation studies. Although originally focused on aging metal aircraft structures, the scope of the NAARP eventually grew to encompass inspection and repair issues related to the use of composites and advanced materials as well. In 1993, the FAA established its Airworthiness Assurance NDI Validation Center (AANC) at the Albuquerque International Airport as a resource where current and emerging NDI technologies could be evaluated, validated, and transferred to the aviation industry. Operated and staffed by Sandia National Laboratories under an interagency agreement, the FAA AANC has since conducted numerous NDI validation projects for the FAA – most with excellent industry support and cooperation. One recent project has resulted from the FAA AANC's collaboration with the Society of Automotive Engineers' (SAE) Commercial Aircraft

Composite Repair Committee (CACRC) Inspection Task Group, an international committee consisting of composite inspection experts from the airlines, and aircraft manufacturers.

A virtue of fabricating aircraft components from composite materials is that the designer is afforded significant flexibility to vary materials, adhesives, ply lay-ups, cell-size, core thickness, etc., to best optimize the component's weight and load-carrying performance. The same wide range of variables that is so appealing to the designer, however, can cause significant concern to the NDI practitioner who must buy or fabricate calibration standard samples for each type of structure encountered when conducting comparative-type NDI tests.

In an effort to keep the required number of composite calibration standards manageable, the FAA AANC worked closely with the CACRC to define specifications for a minimum set of honeycomb and composite laminate calibration standards for damage assessment and post repair inspection of those composite structures.

For nonmetallic honeycomb structures, an initial set of variables was identified that resulted in the fabrication of 64 unique honeycomb panels, each possessing combinations of the identified variables. These 64 panels were then inspected using a wide array of currently available NDI techniques. From an analysis of the results, it was determined that certain construction variables affected the outcome of the NDI inspections more than others. By identifying these variables, the team was able to design a smaller subset of standards using only those variables that truly impact NDI, thus eliminating unnecessary standard configurations. A series of subsequent tests determined that the minimum honeycomb reference standard set was able to fully support inspections over the full range of honeycomb construction scenarios encountered in the field. For solid composite laminate structures (i.e., composite skins without honeycomb), the FAA-AANC/CACRC team identified G11 Phenolic as a generic laminate material that sufficiently replicates certain material properties found in carbon graphite and fiberglass laminates. Those tests determined matches in key velocity and acoustic impedance properties, as well as low attenuation relative to carbon laminates. Further, comparisons of resonance testing response curves from the G11 Phenolic prototype standard were found to be very similar to the resonance response curves measured for carbon and fiberglass laminates. The G11 material improves on existing solid laminate standards because it is inexpensive, can be consistently manufactured, and is easily machined into laminate thickness standards. See Figure 9.12.4.1.

As a result of this project, two SAE Aerospace Recommended Practice (ARP) documents (ARP 5605 and ARP 5606 for honeycomb and solid laminate reference standards, respectively) were developed and published. The major airframe manufacturers of the CACRC committee, including Boeing, Airbus, British Aerospace, and Embraer, have indicated that they will reference these documents when specifying their composite inspection procedures. Other manufacturers who are currently reviewing these standards for possible adoption include Fokker, Bombardier, and Raytheon.

9.12.5 Engineering Studies of Cleaning and Drying Process for Fluorescent Penetrant Inspection

Paul Swindell, FAA

Fluorescent penetrant inspection (FPI) is a widely used inspection method for detecting surface cracks in engine and airframe components. Most parts will receive an FPI as part of the production process while the parts are still in a pristine condition. For critical engine hardware, components will also be inspected during their service life, which includes the additional challenge of field-generated conditions. Figure 9.12.5.1(a) shows a part to which the penetrant has been applied. The penetrant solution enters the defect, excess penetrant is removed from the surface, and a developer is applied to draw the penetrant back out of

the flaw so it is more readily visible to the inspector under blacklight. Figure 9.12.5.1(b) shows an example of a crack indication.

For the penetrant process to be effective, the part must be clean and dry, i.e., the crack must be open to the surface and empty of contaminants so the penetrant can enter the flaw. Contaminants can include service-induced conditions such as oxide, soot, scale, or coke and varnish conditions that are generated at high temperatures. Contamination can also come from the processes used to prepare the part for inspection, e.g., fluids or blast media from the cleaning processes. In recent years, the requirements for improved environmental protection have led to modifications in the cleaning processes used in preparation for FPI. Because of these changes, engineering data is needed to understand the impact of the various cleaning and drying processes being used. Starting in February 2000, the Engine Titanium Consortium (ETC) evaluated two approved drying methods and a range of chemical and mechanical cleaning methods. The project was completed in July 2002.

The primary effort of the program focused on comparisons of oven and flash drying methods and the evaluation of the effect of eight chemical and six mechanical cleaning methods on FPI response. A set of samples that contained low-cycle fatigue cracks ranging from 20 to 150 mils, with most being in the 60 to 80 mil range, were produced in titanium and nickel. Samples were baselined at Iowa State University where FPI brightness was measured and digital images of the ultraviolet indications were captured. Following the laboratory characterization, the samples and measurement equipment were shipped to Delta Airlines' engine maintenance facility in Atlanta, Georgia. Three separate 1-week studies were conducted at the Delta facility. Delta provided access to their cleaning, drying, and fluorescent penetrant inspection facilities for these studies, a major contribution to the program. After the cleaning process and prior to FPI, the parts are dried using either an oven dryer like the one shown in Figure 9.12.5.2(a) or by flash dry as shown in Figure 9.12.5.2(b). Flash dry involves placing the part in water at a temperature of 150° to 200°F, allowing the part to come to temperature, and then removing the part to allow the water to flash from the surface. A comparison of the two methods was completed and led to the conclusion that for the crack sizes and temperatures evaluated in the study, there are no statistical differences between the two methods. Additional efforts to understand the effect of part size, i.e., thermal mass, on the inspection sensitivity are needed. Data for the two methods are shown in Figure 9.12.5.3.

A range of chemical cleaning methods, including aqueous and alkaline cleaning processes, were used to evaluate their effectiveness to remove oil; service coatings such as antigallant compound and high-temperature sealant; and baked-on contamination such as oxide, scale, varnish, and soot. In addition, six mechanical-blasting processes were evaluated: plastic media, wet glass bead, aluminum oxide at three grit sizes (500, 320, and 240), and walnut shell. The purpose of the cleaning studies was to determine if cleaning methods were effective in removing the contaminants and whether those cleaning processes had an impact on the FPI response. The results indicated that some of the cleaning methods were effective for the range of contaminants, but in some cases, the FPI indications were reduced. As an example, using wet glass bead led to surface changes and reduction in FPI response, including no FPI indication in some samples. An example of the results for one sample of a nickel specimen is shown in Figure 9.12.5.4. The photograph on the far left shows the sample surface of a pristine crack. The top center image shows the baseline FPI response for the sample. The indication was not found after wet glass bead but was partially restored after alkaline cleaning. The right image shows the final surface condition. Based on the results of this research, it is recommended that wet glass bead not be used prior to FPI. Further details and conclusions of the study will be published as a final report in 2003. Continued assessment of the FPI process is underway in an FAA program being performed by Iowa State University.

9.12.6 Inspection Development for Nickel Billet

Paul Swindell, FAA

In November 2001, the Engine Titanium Consortium (ETC)—an FAA-funded consortium comprised of General Electric, Honeywell, Iowa State University, and Pratt & Whitney—completed initial testing of a new ultrasonic inspection system for nickel alloys used in jet engines. These tests, demonstrated to the billet manufacturers at the GE facility in Cincinnati, revealed that the new inspection system, which is based on the ETC's multizone ultrasonics for titanium billet, has improved sensitivity to material anomalies that can reduce the durability of critical rotating components.

Using the new system, ETC researchers, working together with billet manufacturers, will inspect 25,000 pounds of Waspaloy and 75,000 pounds of Inconel 718, two of the most common alloys used for high-temperature rotating components such as turbine disks, by February 2003. Figure 9.12.6.1 shows a multizone inspection system with five transducers, each focused on a different depth along a radius of the circular cross section of the billet. As the billet spins, each transducer sweeps an annular section with greater precision than the existing conventional system, which relies on a single transducer to inspect along the entire radius.

The original program goal was to develop and validate an inspection system with the capability of finding flaws of a cross-sectional area four times smaller than what can be found by conventional systems. As shown in Figures 9.12.6.2 and 9.12.6.3, this goal was substantially exceeded. While conventional inspection of Inconel 718 is capable of detecting a flaw that is the size of a flat bottom hole (FBH) with a diameter of 1/32-inch (#2 FBH), the new system is, in some zones, capable of detecting a 1/128-inch diameter flat bottom hole (#1/2 FBH)). In no case is the new system's inspection of Inconel 718 billet less sensitive than a #1 FBH (1/64-inch-diameter flat bottom hole)—a six-fold improvement over the conventional system. For Waspaloy, the conventional two-transducer inspection is calibrated to detect a #5 FBH (5/64-inch flat bottom hole), while the new inspection system is capable of finding a #1 FBH. The new inspection system is designed to handle billets up to 10 inches in diameter.

9.12.7 Development and Validation of the Excited Dielectric Test Technique for Aircraft Electrical System Nondestructive Inspection

Robert Pappas, FAA

In April 2000, the FAA issued a broad agency announcement to support the development of advanced testing and inspection systems, technology, and techniques that characterize and identify material flaws in aircraft wiring. Of specific interest to the FAA and industry were test methods that can be used to detect the presence of nicked and chafed insulation.

In response to this announcement, CM Technologies Corporation proposed a new test technology, known as the Excited Dielectric Technique (EDT). CM Technologies asserted that the lumped impedance associated with a material flaw in aircraft wiring could be manipulated (i.e., made to increase or decrease) using an alternating current stimulus or an electrical forcing function. Furthermore, if the impedance of a material flaw were manipulated during a time domain reflectometery (TDR) test, the material flaw would appear more pronounced on the resultant TDR signature. A contract was awarded to CM Technologies in October 2000 to develop the concept for measuring flaws in wire insulation.

The EDT method exploits the basic property of polar insulation materials that some small amount of current will flow through all insulation materials when exposed to an alternating electric field. The magnitude of the current varies with the frequency of the applied electric field. In a polar insulation material, there is a frequency at which a maximum current occurs (usually less than 1 Hz for most

materials). As a practical consideration, this current is often expressed in terms of the phase angle, δ, between the applied voltage and the resultant current. The tangent of δ is known as the dissipation factor (DF).

The other aspect of the EDT test method is TDR. Aircraft wiring can be modeled as a classical transmission line (i.e., a continuous structure of resistors, inductors, and capacitors). Assuming this model, the electrical characteristics of the wire (e.g., impedance, capacitance, DF, and resistance) can be thought of as distributed elements. TDR has been shown to be extremely effective in measuring the distributed characteristics of wiring.

The EDT method is based on the combination of DF and TDR measurement theory. An alternating electric field, known as a forcing function, is applied to the wire under test at a frequency that creates the maximum DF. A TDR signature is acquired and stored under this excitation. The frequency of the forcing function is then changed, and a second TDR signature is acquired and stored. The signatures are then compared and areas where the signatures separate represent the wire's weakest insulation. Polyimide and cross-linked ethylene tetraflouroethylene (ETFE) were the insulation materials studied under this research effort.

Laboratory evaluation of the technique, Figure 9.12.7.1, was completed at the William J. Hughes Technical Center in March 2002. Field-testing of a system based on the EDT method was performed on a DC-9 aircraft prior to lab evaluation.

The following is a summary of the important results of this project:

- The theory associated with EDT was proven and demonstrated in the lab and in the field.

- The EDT method can detect and locate a variety of defect types including abrasions, fluid contamination, and thermal degradation. Slight damage to the wire's insulation is more easily detected when contaminates are also present.

- The EDT method has demonstrated that no historical data (i.e., baseline TDR signatures) are required for the technique to be effective.

- Expert data interpretation can be used but automated analysis is needed to advance the technology.

More EDT and materials testing is needed using other insulation types to better understand the effects that various defect types have on the electrical properties of a wire. Further development of the EDT technique is required before it can be introduced into service. However, the results of this project validate the theory of the approach and have identified the improvements necessary to develop a field-ready system. The Office of Naval Research and the Naval Air Systems Command has awarded a follow-on contract to CM Technologies to continue development of the EDT system, including the incorporation of signal analysis software and to produce deployable EDT units.

9.13. ENGINES

9.13.1 Debris Characterization and Vulnerability Analysis

Donald Altobelli, FAA

Uncontained turbine engine failures have caused catastrophic results to aircraft. The FAA saw a need to update advisory material relative to uncontained turbine engine failures.

As a result, the Aviation Rulemaking Advisory Committee (ARAC) was tasked to update Advisory Circular (AC) 20-128, "Design Considerations for Minimizing Hazards Caused by Uncontained Turbine Engine and Auxiliary Power Unit Rotor and Fan Failure." (Figure 9.13.1.1) This group determined that there was a need to better characterize the types of failures, number of fragments, velocity of fragments, and damage caused by these fragments.

Engine and airframe manufacturers, who considered this data to be proprietary, had collected much of the data needed to do this. In 1995, the FAA Technical Center entered into an interagency agreement with the Naval Air Warfare Center, Weapons Division (NAWCWD), China Lake, CA, to gather this data and conduct an analysis of the data, which could then be used to update AC 20-128. Data was given freely to the Navy for analysis because this organization had pre-existing nondisclosure agreements with most engine and airframe manufacturers and could therefore respect the proprietary nature of this data. This data has now been analyzed and the results have been made available in several reports on small- and large-engine failure events, which the ARAC members can use to update AC 20-128.

Additionally, this characterization is being used to prepare stochastic models of uncontainment events of various types to be used in conjunction with vulnerability assessment tools. These tools (FASTGEN 3 and COVART 4.0) have been used by the military to assess the vulnerability of their aircraft to hostile threats. By modifying this code for use by civilian airframe manufacturers, the vulnerability analysis of a threat from uncontained engine debris in a commercial airframe can be conducted.

Under FAA funding, NAWCWD has completed the code modifications identified by commercial airplane manufacturers. Boeing has conducted initial evaluations of the vulnerability assessment tools under contract from NAWCWD. Boeing provided recommendations that will improve the tools' ability to assess aircraft safety from an uncontained engine debris threat.

As suggested at the Fourth Uncontainment Workshop held in March 2000, NAWCWD created generic models of a business jet and a two-engine commercial transport aircraft. The resulting vulnerability assessment tools will enhance the safety of commercial aircraft by providing the means to critically examine the threat posed by uncontained engine debris and allow steps to be taken to mitigate the threat.

Several reports have been produced which document the work done in support of developing the revisions to AC 20-128 "Design Precautions for Minimizing Hazards to Aircraft from Uncontained Turbine Engine and Auxiliary Power Unit Rotor Failure." (Figure 9.13.1.2)

Two reports from the Naval Air Warfare Center, Weapons Division, China Lake, California, provide data on the historical events for large- and small-engine uncontained events, and a third report documents air-gun tests to refine penetration equations used for aircraft vulnerability analysis. These reports are DOT/FAA/AR-99/7, DOT/FAA/AR-99/11, and DOT/FAA/AR-99/19 respectively. The latest round of ballistic testing is summarized in report DOT/FAA/AR-01/27, "Engine Debris Fuselage Penetration Testing, Phase I."

9.13.2 Uncontained Engine Debris Damage Assessment Model (UEDDAM) Version 1.1 Released

Donald Altobelli, FAA

A second Interagency Agreement with Naval Air Warfare Center Weapons Division (NAWCWD) China Lake was signed in FY02. The existing tasks were expanded to continue the work started under Uncontained Engine Debris Damage Assessment Model (UEDDAM) and new tasks were added such as engine disk crack detection. Figure 9.13.2.1 shows a typical engine disk failure debris layout. Figure 9.13.2.2 shows how a typical spray pattern of debris would exit a turbine engine from a compressor disk failure.

In FY02 NAWCWD and their support contractor, Survice Engineering Company, delivered version 1.1 of UEDDAM. This code will help industry comply with a proposed revision to AC 20-128 currently in development by FAA rulemaking. Both of Boeing's commercial divisions have conducted initial evaluations of the vulnerability assessment tools in UEDDAM under contract from NAWCWD. Resulting recommendations will improve the tools' ability to assess aircraft safety to the uncontained engine debris threat.

As a result of the Fourth Uncontainment Workshop (March 2000), NAWCWD started developing generic models of a business jet and a commercial transport aircraft. Results were presented at the Aviation Rulemaking Advisory Committee (ARAC) Propulsion and Power Industry Harmonization Working Group (PPIHWG) meetings held in June 2001, October 2001, and July 2002.

The UEDDAM vulnerability assessment tools automate the analysis and allow airframe design trade studies to be performed. UEDDAM enhances the safety of commercial aircraft by providing the means to critically examine the threat posed by uncontained engine debris and determines steps that can be taken to mitigate the threat (see Figure 9.13.2.3).

The uncontainment research effort has produced several reports that are the result of years of effort in support of developing the revisions to AC 20-128, "Design Precautions for Minimizing Hazards to Aircraft From Uncontained Turbine Engine and Auxiliary Power Unit Rotor Failure." A compact disc with all reports was distributed at the 29th ARAC meeting in October 2001.

The ballistic testing is summarized in a series of reports DOT/FAA/AR-01/27 "Engine Debris Fuselage Penetration Testing, Phase I and II." A draft report for the generic twin transport airplane has been delivered along with the code. This code is currently being evaluated by the U.S. Navy, the U.S. Air Force, and Boeing Commercial Airplane Group.

9.13.3 Enhanced Turbine Rotor Material Design and Life Methodology

Joseph Wilson, FAA

Despite the current rigorous safe-life design approach for failure-critical rotating components, the commercial service experience of turbine-powered aircraft has shown that material and manufacturing anomalies can reduce the structural integrity of critical rotating components and increase the risk of failure.

A recent Advisory Circular (AC) 33.14-1, "Damage Tolerance for High-Energy Turbine Engine Rotors," introduces an enhanced rotor life management process and a new element, known as damage tolerance, to the engine manufacturers existing design and life management process. (Figure 9.13.3.1)

The enhanced process, detailed in AC 33.14-1, establishes a new standard for rotor design and life management of all titanium rotor components in new aircraft turbine engines. The new approach is a probabilistic fracture mechanics-based assessment process with the corresponding damage tolerance design targets. The engine manufacturers will use this new design philosophy to evaluate the acceptability of all future titanium rotor designs and life management plans.

The software tool Design Assessment of Reliability With Inspection (DARWIN) was developed by Southwest Research Institute (SwRI) under an FAA grant specifically to support this new design process. DARWIN is a probabilistically based damage tolerance design code used to determine the risk of fracture of turbine engine rotor disks containing undetected material anomalies. The DARWIN software integrates finite element stress analysis results, fracture mechanics-based life assessment for low-cycle fatigue, material anomaly data, probability of anomaly detection, and inspection schedules to determine the probability of fracture as a function of applied operating cycles. The code also indicates the regions of the disk most likely to fail and the sensitivity of the risk to inspection schedules.

The previous versions of DARWIN focused on the presence of the melt-related defect known as hard alpha found in titanium alloys. Version 4.0 of DARWIN includes new capabilities for probabilistic life prediction of rotor disks subjected to manufacturing and maintenance-induced surface damage. The photographs in Figure 9.13.3.2 show failures due to an abusively machined bolthole. The primary focus of the current version is on cracks that initiate at surfaces and corners associated with boltholes. Version 4.0 includes a number of new features to allow the user to directly define zone dimensions, stresses, temperatures, and stress gradients associated with surface damage problems.

9.13.4 Aircraft Material Penetration Analysis

Donald Altobelli, FAA

Lawrence Livermore National Laboratory (LLNL) and industrial partners Allied Signal Engines, Boeing Commercial Aircraft Group (BCAG), United Technologies, and Pratt & Whitney (P&W) showed the need for improved analysis tools for evaluating mitigation and containment in advanced turbofan engines. Although various experimental data have been obtained, a methodology has not yet been developed to implement a calibrated system for the design and certification for the various means of maximizing engine debris containment and minimizing uncontained engine debris hazards to aircraft. The development and validation of the tools necessary to implement an assessment by numerical simulation of containment and the vulnerability of aircraft to uncontained engine debris were the objectives of this effort. The numerical methodology will be based on a fundamental understanding of material properties, failure mechanisms, and structural dynamics, which will be validated by experimental data.

Testing, numerical simulation, elucidation of physics-material interaction mechanisms and necessary code development are being used to develop a verified methodology for design and development of containment and mitigation technology. This result will provide analytical tools that will be useful to engine, as well as airframe, manufacturers for predicting the design of a cost-effective aircraft structure mitigation and/or engine containment system. This verified toolbox would be applicable to vulnerability analysis of the overall system structure.

The developed computational tools will assess more general problems of single- or multiple-fragment effects. With sufficient industrial use and validation, this collection of robust simulation tools will form part of the certification process. The mechanism for the transition from simulation tools validated for use in design and the aviation community as a whole will determine analysis to the incorporation of simulation tools into a certification process.

Lawrence Livermore National Laboratory (LLNL) has completed its Hopkinson Bar and ballistic test series. The results showed that the existing Johnson –Cook Model was not accurate. LLNL updated the model and two reports summarizing this work were issued in FY-01 ("Ballistic Experiments With Titanium and Aluminum Targets," DOT/FAA/AR-01/21 and "Experimental Investigations of Material Models for Ti-6Al-4V Titanium and 2024-T3 Aluminum," DOT/FAA/AR-00/25).

The DYNA-3D material model update is scheduled to be issued by January 2002.

9.13.5 Armor Material Development and Analysis

Donald Altobelli, FAA

Over the years, several catastrophic civil aircraft accidents have occurred when fragments from in-flight engine failures damaged critical aircraft components. To reduce the probability of such incidents in the future, the Federal Aviation Administration (FAA) is sponsoring research to develop and apply advanced technologies and methods for mitigating the effects of uncontained engine bursts. Under FAA funding, SRI International is conducting a research program to evaluate the ballistic effectiveness of fabric structures made from advanced polymers and to develop a computational ability to design fragment barriers. See Figure 9.13.5.1 and Figure 9.13.5.2.

In the last year, SRI has solved several problems associated with the crimped geometry and interaction of woven yarns. When an orthotropic model is invoked and direction-dependent yarn properties are specified, the yarn, as it is loaded, exhibits no appreciable stiffness until it straightens. The calculational behavior of this model was examined in simple simulations of single-yarn response to axial and transverse loads and found acceptable. SRI evaluated the ballistic response of fabrics to fragment impact, examined the phenomenology of fabric deformation and failure by using quasi-static penetration tests, and measured the tensile properties of yarns and fibers. SRI focused on three commercially available high-strength polymer materials—PBO (Zylon), aramid (Kevlar), and polyethylene (Spectra).

Several reports were published to document the progress made in modeling and designing armor fabric barriers to protect aircraft systems from the majority of fragments liberated from an uncontained engine failure. These reports are "Improved Barriers to Turbine Engine Fragments: Interim Report," DOT/FAA/AR-99/8 Part I and II. A full-scale test of fabrics in an aircraft structure is described in "Full-Scale Tests of Lightweight Fragment Barriers on Commercial Aircraft," DOT/FAA/AR-99/71.

The majority of fragments, as described in the Naval Air Warfare Center-Weapons Division (NAWCWD) reports, are relatively small and can be defeated with ballistic fabrics in combination with the existing structure.

The largest fragments, like the disc found in the farmers field from the Sioux City accident, would not be stopped by these materials. However, the loss of all hydraulic systems in that accident was attributed to smaller debris liberated by the failure rather than a direct hit by the large piece

In 2000 and 2001, the research included full-scale testing of fabric barriers at NAWCWD and SRI. The testing concentrated on fabric attachment problems and solutions. This work is summarized in DOT/FAA/AR-99/8 III, "Improvement Barriers to Turbine Engine Fragments: Interim Report III."

The final results of this effort in Uncontained Turbine Engine Research will be a validated tool kit to improve the certification process and provide a means of compliance with the proposed revision to AC20-128 that will include design for a multiple-fragment threat.

9.13.6 Improved Barriers to Turbine Engine Fragments Phase II Completed

Donald Altobelli, FAA

Over the years, several civil aircraft accidents with catastrophic consequences have occurred when fragments from in-flight engine failures damaged critical aircraft components. To reduce the probability of such incidents in the future, the FAA is sponsoring research to develop and apply advanced technologies and methods for mitigating the effects of uncontained engine bursts. The largest fragments, like the compressor disc segment from the Sioux City accident, would not be stopped by improved barrier materials. However, the loss of all hydraulic systems in that accident was attributed to smaller debris liberated by the failure rather than a direct hit by the large piece. Under FAA funding, SRI International has completed an evaluation of the ballistic effectiveness of fabric structures made from advanced polymers and has developed a computational ability to design fragment barriers.

SRI evaluated the ballistic response of fabrics to fragment impact, explained the phenomenology of fabric deformation and failure using quasi-static penetration tests, and measured the tensile properties of yarns and fibers. Figures 9.13.6.1 and 9.13.6.2 show model printouts from this work. SRI focused on three commercially available high-strength polymer materials—PBO (Zylon), aramid (Kevlar), and polyethylene (Spectra).

The FAA research on armor barriers for uncontainment has produced a series of reports that documents the progress made in modeling and designing armor fabric barriers to protect aircraft systems from the majority of fragments liberated from an uncontained engine failure. The majority of fragments are relatively small and can be defeated with ballistic fabrics in combination with the existing structure.

Published reports from this work (including Parts IV and V published in 2002) are titled “Improved Barriers to Turbine Engine Fragments,” DOT/FAA/AR-99/8, Part I through V. Parts IV and V complete the planned work and includes extensive testing and analysis on fabric attachment methods. This research included a full-scale test of fabrics in an aircraft structure, which is described in report DOT/FAA/AR-99/71, “Full-Scale Tests of Lightweight Fragment Barriers on Commercial Aircraft.”

The research included full-scale testing of fabric barriers at both Naval Air Warfare Center Weapons Division and SRI International. Figure 9.13.6.3 shows how the fabric barrier was attached to the aircraft fuselage. During full-scale testing a fan blade fragment weighing 0.37 pound was shot at a fuselage wall containing three layers of Zylon fabric. The initial velocity was 622 feet per second, and the Zylon stopped the fragment in the wall (see Figure 9.13.6.4). Additional aircraft fuselage testing concentrated on fabric attachment problems and solutions. This work was summarized in DOT/FAA/ AR-99/8 III, “Improved Barriers to Turbine Engine Fragments: Interim Report III,” published in 2001.

To allow for the end user to design fabric barriers with reasonable computer time, SRI converted the detailed model to a simplified shell model.

Currently, there are two programs being conducted that are working to transfer the technology from the fabric barrier research to commercial use. The University of California Berkeley is currently working with SRI International and Boeing to develop fuselage barriers, while Arizona State University is currently working with SRI and Honeywell Engines to develop improved engine containment.

9.13.7 Multiaxial Effects on Fatigue

David W. Hoeppner, University of Utah-QIDEC Laboratories

Dr. Hoeppner participated in a research program for Sverdrup Technologies and USAF on multiaxial effects on fatigue of aircraft gas turbine materials. The Principal Investigator on the program is Dr. Charles Elliott and the co-principal investigator is Dr.Hoeppner.

9.14. FIGURES/TABLES

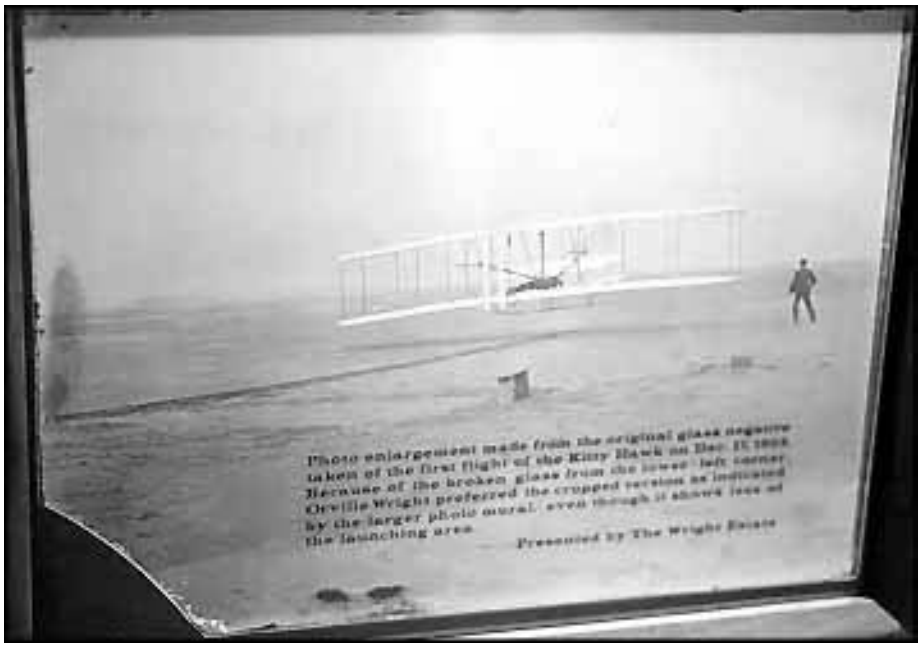

Figure 9.2.1.1 The First Flight of the Wright Flyer I

Figure 9.2.1.2 Ohio $.25 Coin

Figure 9.2.1.3 North Carolina $.25 Coin

821,393

THE UNITED STATES OF AMERICA

TO ALL TO WHOM THESE PRESENTS SHALL COME:

Whereas Orville Wright and Wilbur Wright
Dayton, Ohio

had presented to the **Commissioner of Patents** a petition praying
for the grant of Letters Patent for an alleged new and useful improvement in

Flying Machines,

a description of which invention is contained in the specification of which a copy is hereunto annexed and made a part hereof, and have complied with the various requirements of Law in such cases made and provided, and

Whereas upon due examination made the said Claimants are adjudged to be justly entitled to a patent under the law.

Now therefore these **Letters Patent** are to grant unto the said
Orville Wright and Wilbur Wright, their heirs or assigns
for the term of Seventeen years from the twenty-second day of
May One Thousand Nine Hundred and Six
the exclusive right to make, use and vend the said invention throughout the United States and the territories thereof.

In testimony whereof, I have hereunto set my
hand and caused the seal of the **Patent Office**
to be affixed at the City of Washington
(on the) Twenty-Second day of May
(in the) year of our Lord one Thousand nine
hundred and six and of the
Independence of the United States of America
the one hundred and thirtieth
[Signed]
Commissioner of Patents

Figure 9.2.1.4 Transcript of Patent

SIGNAL CORPS SPECIFICATION, NO. 486.

ADVERTISEMENT AND SPECIFICATION FOR A HEAVIER-THAN-AIR FLYING MACHINE.

TO THE PUBLIC:

Sealed proposals, in duplicate, will be received at this office until 12 o'clock noon on February 1, 1908, on behalf of the Board of Ordnance and Fortification for furnishing the Signal Corps with a heavier-than-air flying machine. All proposals received will be turned over to the Board of Ordnance and Fortification at its first meeting after February 1 for its official action.

Persons wishing to submit proposals under this specification can obtain the necessary forms and envelopes by application to the Chief Signal Officer, United States Army, War Department, Washington, D. C. The United States reserves the right to reject any and all proposals.

Unless the bidders are also the manufacturers of the flying machine they must state the name and place of the maker.

Preliminary.—This specification covers the construction of a flying machine supported entirely by the dynamic reaction of the atmosphere and having no gas bag.

Acceptance.—The flying machine will be accepted only after a successful trial flight, during which it will comply with all requirements of this specification. No payments on account will be made until after the trial flight and acceptance.

Inspection.—The Government reserves the right to inspect any and all processes of manufacture.

GENERAL REQUIREMENTS.

The general dimensions of the flying machine will be determined by the manufacturer, subject to the following conditions:

1. Bidders must submit with their proposals the following:
   - (a) Drawings to scale showing the general dimensions and shape of the flying machine which they propose to build under this specification.
   - (b) Statement of the speed for which it is designed.
   - (c) Statement of the total surface area of the supporting planes.
   - (d) Statement of the total weight.
   - (e) Description of the engine which will be used for motive power.
   - (f) The material of which the frame, planes, and propellers will be constructed. Plans received will not be shown to other bidders.

2. It is desirable that the flying machine should be designed so that it may be quickly and easily assembled and taken apart and packed for transportation in army wagons. It should be capable of being assembled and put in operating condition in about one hour.

3. The flying machine must be designed to carry two persons having a combined weight of about 350 pounds, also sufficient fuel for a flight of 125 miles.

4. The flying machine should be designed to have a speed of at least forty miles per hour in still air, but bidders must submit quotations in their proposals for cost depending upon the speed attained during the trial flight, according to the following scale:

   40 miles per hour, 100 per cent.
   39 miles per hour, 90 per cent.
   38 miles per hour, 80 per cent.
   37 miles per hour, 70 per cent.
   36 miles per hour, 60 per cent.
   Less than 36 miles per hour rejected.
   41 miles per hour, 110 per cent.
   42 miles per hour, 120 per cent.
   43 miles per hour, 130 per cent.
   44 miles per hour, 140 per cent.

5. The speed accomplished during the trial flight will be determined by taking an average of the time over a measured course of more than five miles, against and with the wind. The time will be taken by a flying start, passing the starting point at full speed at both ends of the course. This test subject to such additional details as the Chief Signal Officer of the Army may prescribe at the time.

6. Before acceptance a trial endurance flight will be required of at least one hour during which time the flying machine must remain continuously in the air without landing. It shall return to the starting point and land without any damage that would prevent it immediately starting upon another flight. During this trial flight of one hour it must be steered in all directions without difficulty and at all times under perfect control and equilibrium.

7. Three trials will be allowed for speed as provided for in paragraphs 4 and 5. Three trials for endurance as provided for in paragraph 6, and both tests must be completed within a period of thirty days from the date of delivery. The expense of the tests to be borne by the manufacturer. The place of delivery to the Government and trial flights will be at Fort Myer, Virginia.

8. It should be so designed as to ascend in any country which may be encountered in field service. The starting device must be simple and transportable. It should also land in a field without requiring a specially prepared spot and without damaging its structure.

9. It should be provided with some device to permit of a safe descent in case of an accident to the propelling machinery.

10. It should be sufficiently simple in its construction and operation to permit an intelligent man to become proficient in its use within a reasonable length of time.

11. Bidders must furnish evidence that the Government of the United States has the lawful right to use all patented devices or appurtenances which may be a part of the flying machine, and that the manufacturers of the flying machine are authorized to convey the same to the Government. This refers to the unrestricted right to use the flying machine sold to the Government, but does not contemplate the exclusive purchase of patent rights for duplicating the flying machine.

12. Bidders will be required to furnish with their proposal a certified check amounting to ten per cent of the price stated for the 40-mile speed. Upon making the award for this flying machine these certified checks will be returned to the bidders, and the successful bidder will be required to furnish a bond, according to Army Regulations, of the amount equal to the price stated for the 40-mile speed.

13. The price quoted in proposals must be understood to include the instruction of two men in the handling and operation of this flying machine. No extra charge for this service will be allowed.

14. Bidders must state the time which will be required for delivery after receipt of order.

JAMES ALLEN,
Brigadier General, Chief Signal Officer of the Army.

SIGNAL OFFICE,
WASHINGTON, D. C., *December 28, 1907.*

Figure 9.2.1.5 Signal Corps Specification, No. 486

Form No. 18.

Signal Corps, United States Army.

These Articles of Agreement entered into this ------tenth--------- day of February---, nineteen hundred and-eight--, between ----Chas. S. Wallace----, Captain----------, Signal Corps, United States Army, of the first part, and

Wilbur and Orville Wright, trading as Wright Brothers, of 1127 West Third Street, Dayton,

in the county of-------Montgomery----------, State of------Ohio----------, of the second part, Witnesseth, that in conformity with copy of the advertisement, specifications, and proposal hereunto attached, and which, in so far as they relate to this contract, form a part of it, the said ----------Chas. S. Wallace, Captain,---------- Signal Corps, United States Army, for and in behalf of the United States of America, and the said ----------Wright Brothers---------- (hereinafter designated as the contractor) do covenant and agree, to and with each other, as follows, viz:

Article I. That the said contractor shall manufacture for and deliver to the United States of America,

One (1) heavier-than-air flying machine, in accordance with Signal Corps Specification No. 486, dated December 23, 1907.

Art. II. That the deliveries of the supplies and materials herein contracted for shall be made in the manner, numbers, or quantities, and for each number or quantity, on or before the date specified therefor, as follows, viz:

That complete delivery shall be made on or before August 28, 1908.

Art. III. All supplies and materials furnished and work done under this contract shall, before being accepted, be subject to a rigid inspection by an inspector appointed on the part of the Government,

3—1190

Figure 9.2.1.6a Contract

and such as do not conform to the specifications set forth in this contract shall be rejected. The decision of the Chief Signal Officer, United States Army, as to quality and quantity shall be final.

ART. IV. That for and in consideration of the faithful performance of the stipulations of this contract, the contractor shall be paid at the office of -----the Chief Signal Officer---------of the Army---------, at-----Washington, D. C.---, for all supplies and materials delivered in conformity with the requirements of this contract, on or before the dates above specified (Article II, *supra*) *and accepted*, the following prices, viz:

One (1) heavier-than-air flying machine at a total cost of twenty-five thousand ($25,000) dollars.

to be paid as soon as practicable after the acceptance of the same, in funds furnished by the United States for the purpose, reserving per cent from each payment until final settlement, on completion of the contract or otherwise.

ART. V. It is further agreed that for all supplies and materials which shall not be delivered in conformity with the requirements of this contract on or before the dates prescribed therefor in Article II, above, but which shall be subsequently delivered and accepted, the prices shall be as follows:

5-1388

Figure 9.2.1.6b Contract (Continued)

ART. VI. That in case of the v of the said contractor to perf he stipulations of this contract within the time and in the manner specified above, Articles I to III, inclusive, the said party of the first part may, instead of waiting further for deliveries under the provisions of the preceding article, supply the deficiency by purchase in open market or otherwise, at such place as may be selected (the articles so procured to be the kind herein specified, as near as practicable); and the said contractor shall be charged with the increased cost of the supplies and materials so purchased over what they would have cost if delivered by the contractor on the date they were received under such open-market purchase.

ART. VII. It is further agreed by and between the parties hereto that until final inspection and acceptance of, and payment for, all of the supplies and materials and work herein provided for, no prior inspection, payment, or act is to be construed as a waiver of the right of the party of the first part to reject any defective articles or supplies or to require the fulfillment of any of the terms of the contract.

ART. VIII. The contractor further agrees to hold and save the United States harmless from and against all and every demand, or demands, of any nature or kind for, or on account of, the use of any patented invention, article, or process included in the materials hereby agreed to be furnished and work to be done under this contract.

ART. IX. Neither this contract nor any interest herein shall be transferred to any other party or parties, and in case of such transfer the United States may refuse to carry out this contract either with the transferor or the transferee, but all rights of action for any breach of this contract by said contractor are reserved to the United States.

ART. X. No Member of or Delegate to Congress, nor any person belonging to, or employed in, the military service of the United States, is or shall be admitted to any share or part of this contract, or to any benefit which may arise therefrom.*

ART. XI. That it is expressly agreed and understood that this contract shall be noneffective until an appropriation adequate to its fulfillment is made by Congress and is available.

ART. XII. That this contract shall be subject to approval of the Chief Signal Officer, United States Army.

IN WITNESS WHEREOF the parties aforesaid have hereunto placed their hands the date first hereinbefore written.

WITNESSES:

John J Mullaney as to
Albert Lawrence as to
C. E. Taylor as to
H. H. Hoffman as to

Signal Corps, U. S. Army.

Wright Brothers,
by Orville Wright

APPROVED: FEB 28 1908 , 190

Brigadier General,
Chief Signal Officer of the Army.

*Here add to any contract made with an incorporated company for its general benefit the following words, viz: "But this stipulation, so far as it relates to Members or Delegates to Congress, is not to be construed to extend to this contract." See section 3740, Revised Statutes.

(EXECUTED IN QUINTUPLICATE.)

Figure 9.1.2.6c Contract (Continued)

Figure 9.2.1.7 Wright 1979 Military Flyer

Figure 9.2.1.8 Hawthorne Hill Residence of the Wright Family

Figure 9.2.1.9 Wright Memorial Located on Wright Brothers Hill

Figure 9.2.1.10 Huffman Prairie Flying Field Interpretative Center

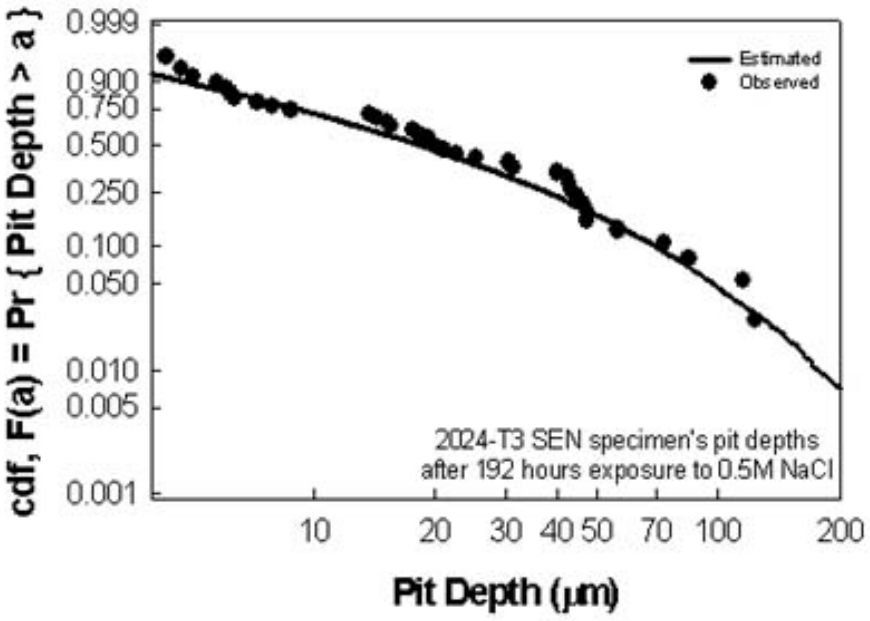

Figure 9.2.2.1 Comparison between observed distribution in pit sizes with that predicted from a model for constituent-particle induced pitting in a 2024-T3 aluminum alloy (after 192 h immersion in 0.5 M NaCl solution at room temperature

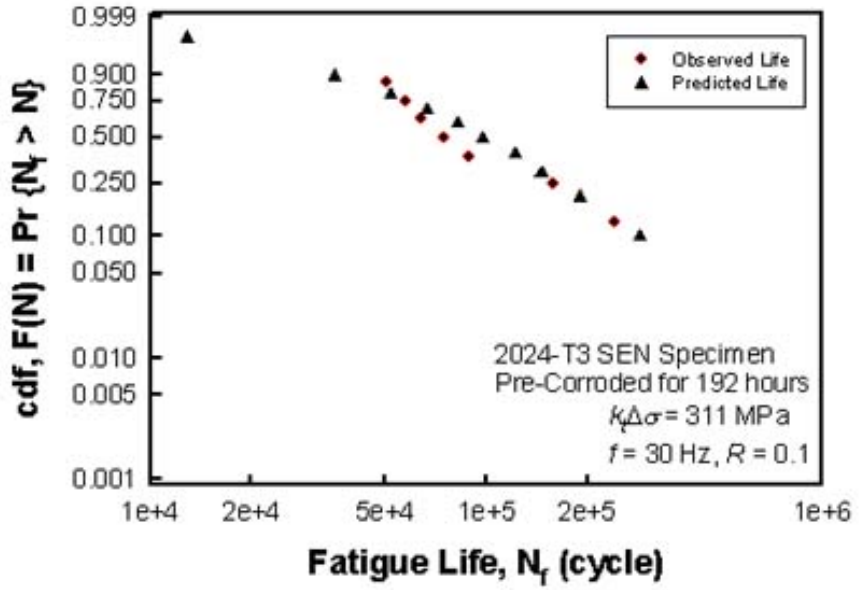

Figure 9.2.2.2 Comparison between the observed fatigue lives in pre-corroded specimens and that predicted from the expected distribution in pit sizes shown in Figure 9.2.2.1

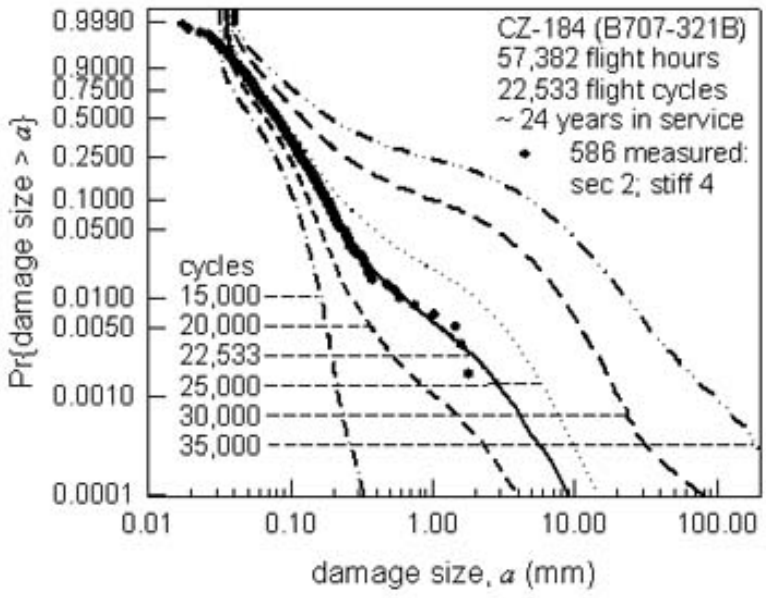

Figure 9.2.2.3 Comparison between model prediction (solid line) and observed distribution of damage in the fattener holes of the lower wing skin panels from a B-707 aircraft that had been in commercial service for 22,533 flight cycles over about 24 years, and the model estimations of evolution in damage distribution with flight cycles (broken lines)

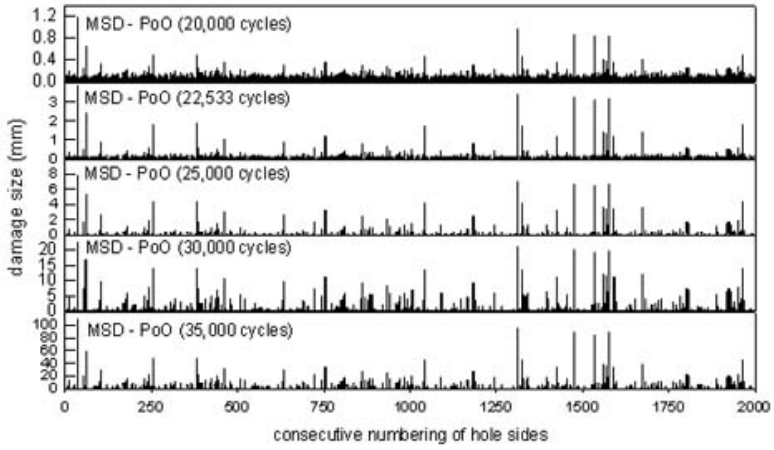

Figure 9.2.2.4 Successive simulation of the evoluation and distribution in damage over 1,000 fastener holes, based on the distributions shown in Figure 9.2.2.3, and the formation of significant areas of MSD

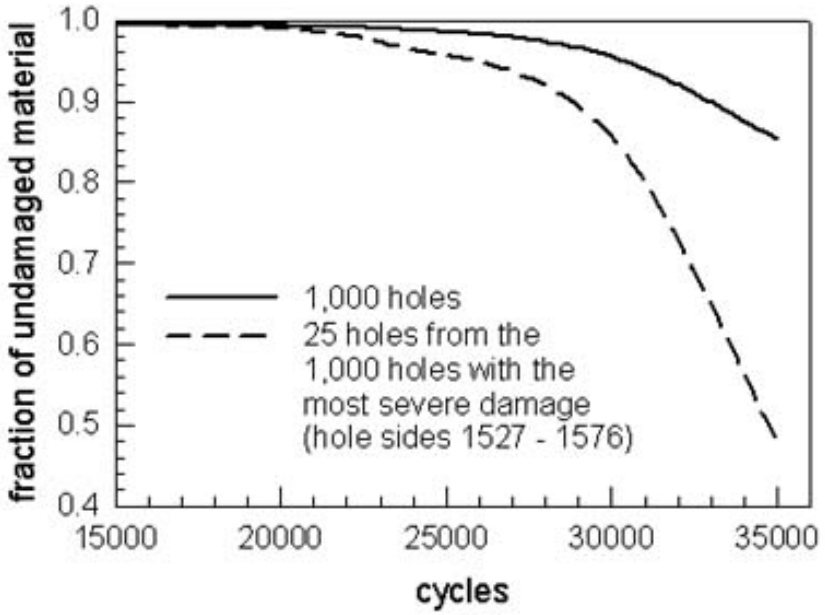

Figure 9.2.2.5 Impact of damage reflected by the decrease in the fraction of load carrying material with flight cycles; over 1,000 holes (solid line) and over the most severely damaged holes (dashed line) (see Figure 9.2.2.4)

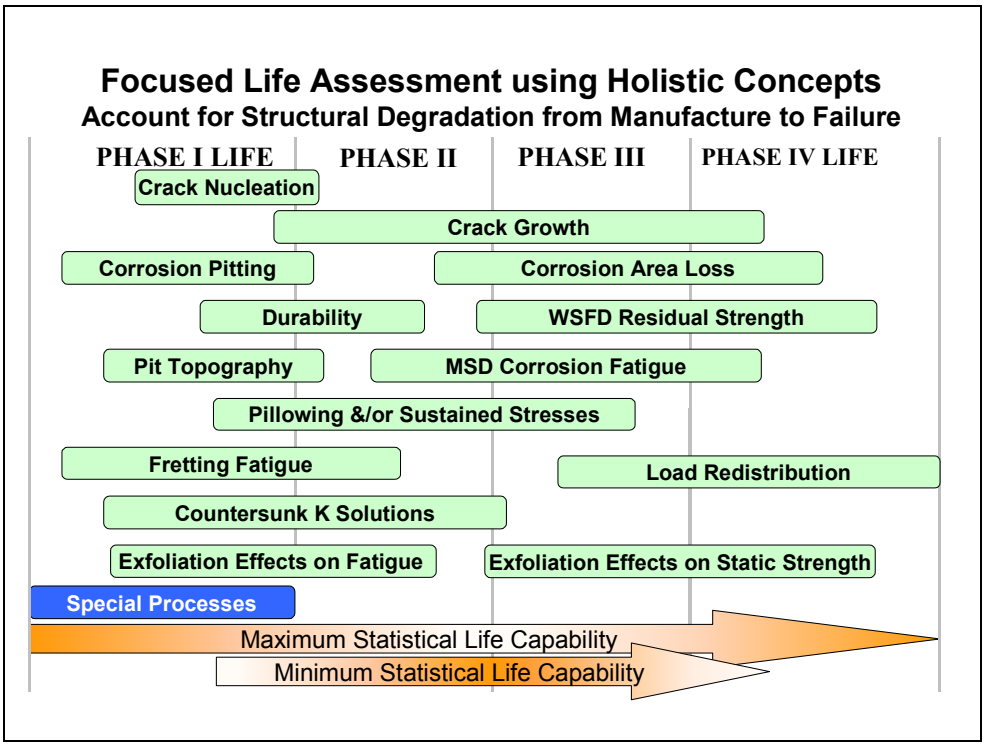

Figure 9.2.3.1 Holistic life methodology makes “cradle-to-grave” damage progression assessments

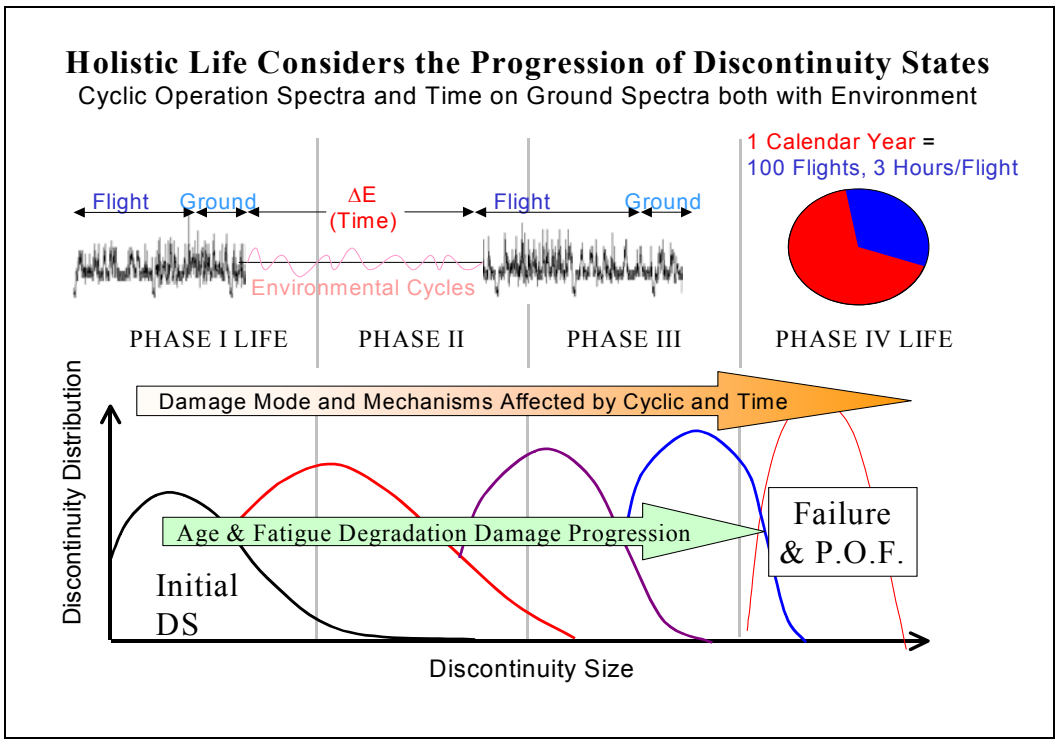

Figure 9.2.3.2 Holistic life assessments consider both fatigue and environmentally driven damage

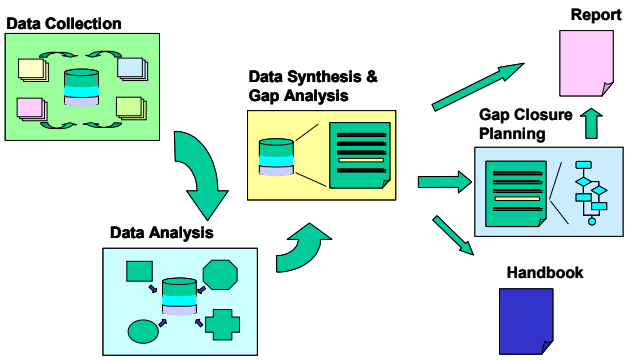

Figure 9.2.5.1 Overall research effort design

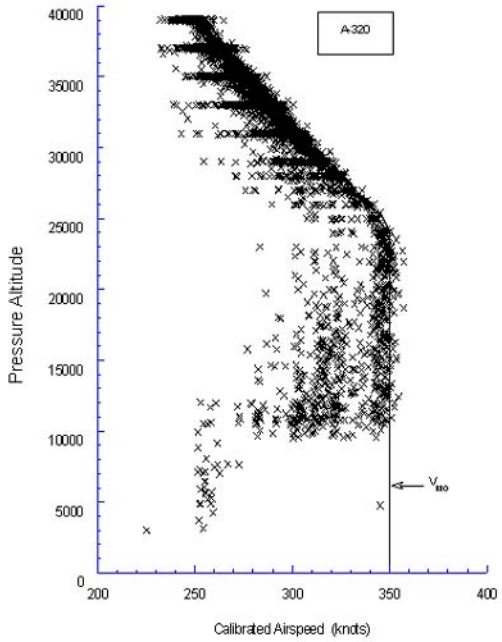

Figure 9.3.1.1 A-320 data

Figure 9.3.2.1 Video landing survey facility

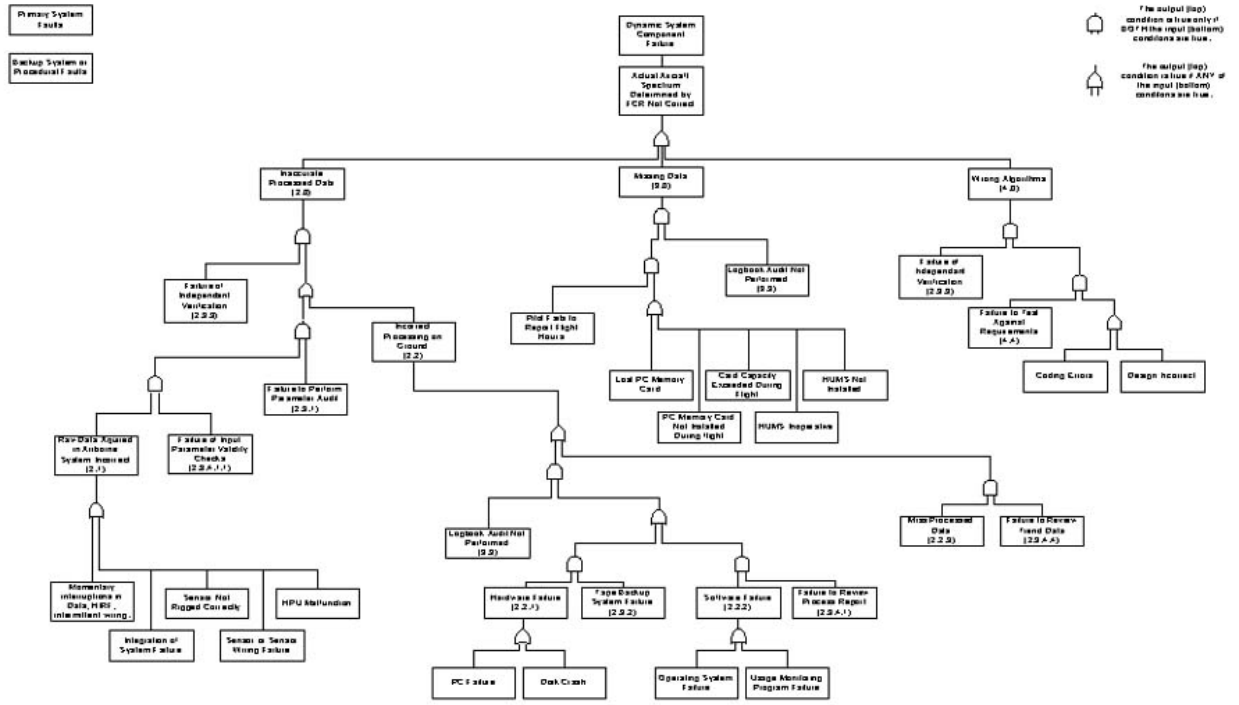

Figure 9.3.3.1 Fault tree

Table 9.3.4.1 Summary of fatigue lives using mini-HUMS and complete HUMS

Life Calculation Method	REPHASE LEVER Fatigue Life (Hrs)	COLLECTIVE LEVER Fatigue Life (Hrs)	MAIN ROTOR SPINDLE Fatigue Life (Hrs)	MAIN ROTOR YOKE Fatigue Life (Hrs)
- Certification Spectrum - No Altitude Breakdown - Certification Gross Weight Breakdown	**5000**	**10,000**	**10,000**	**5,000**

Concept \ HUMS Mission Profile	GCM	ASHM	UMMC	GCM	ASHM	UMMC	GCM	ASHM	UMMC	GCM	ASHM	UMMC
Mini HUMS Concept 1 - Certification Spectrum - Mission Altitude Breakdown - Certification Gross Weight Breakdown	**12,910**	**80,320**	**21,030**	**20,730**	**45,170**	**27,607**	**19,000**	**33,090**	**23,563**	**5,760**	**5,460**	**5275**
Mini HUMS Concept 2 - Certification Spectrum but with actual Level Flight from Mission Spectrum - Mission Altitude Breakdown - Certification Gross Weight Breakdown	**16,176**	**53,604**	**31,547**	**30,972**	**56,341**	**45,097**	**23,445**	**20,480**	**35,185**	**11,045**	**5,250**	**11,826**
Mini HUMS Concept 3 - Certification Spectrum but with actual Level Flight, Turns & Pullups from Mission Spectrum - Mission Altitude Breakdown - Certification Gross Weight Breakdown	**40,592**	**21,031**	**34,799**	**32,415**	**72,364**	**46,654**	**33,103**	**22,678**	**32,506**	**9,814**	**3,735**	**9486**
Complete HUMS Package - Mission Spectrum (including unrecognized) - Mission Altitude Breakdown - Mission Gross Weight Breakdown	**24,610**	**15,620**	**20,850**	**27,410**	**174,220**	**34,830**	**28,840**	**32,810**	**18,850**	**26,510**	**4,760**	**20,030**

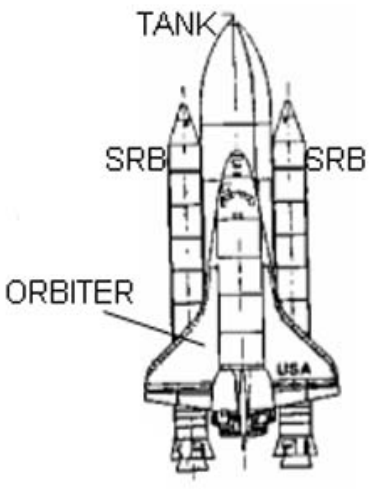

Figure 9.3.5.1 Space shuttle

Figure 9.3.6.1 Deicing from a deicing bucket

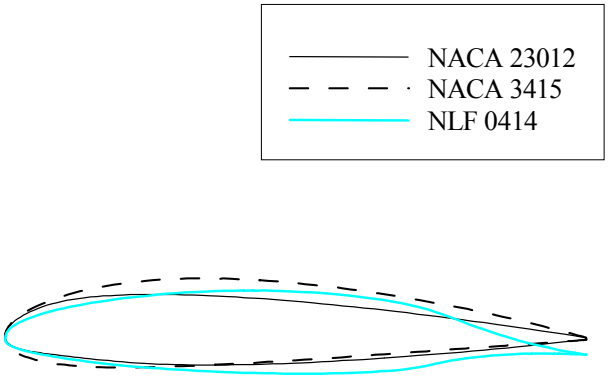

Figure 9.3.8.1 Comparison of the three airfoil geometries

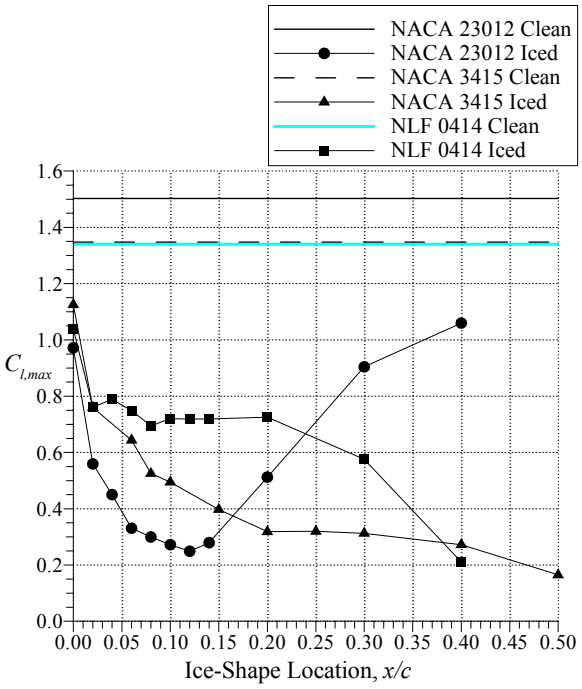

Figure 9.3.8.2 Summary of maximum lift effects from a simulated ice accretion located at various chorwise locations

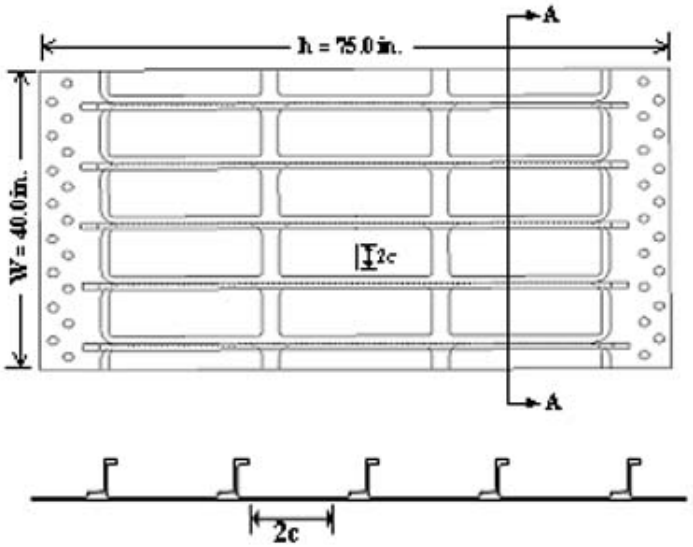

Figure 9.4.1.1 Integrally stiffened 40-inch-wide panel with a single lead crack

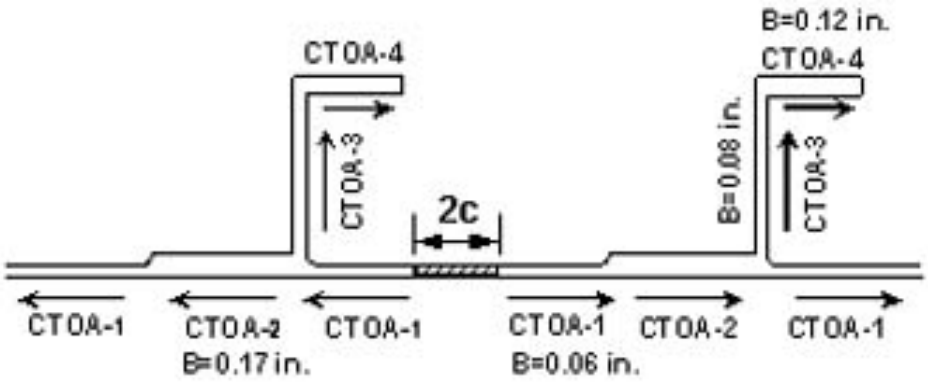

Figure 9.4.1.2 Schematic representations of crack branching for an integrally stiffened panel with a CTOA criterion.

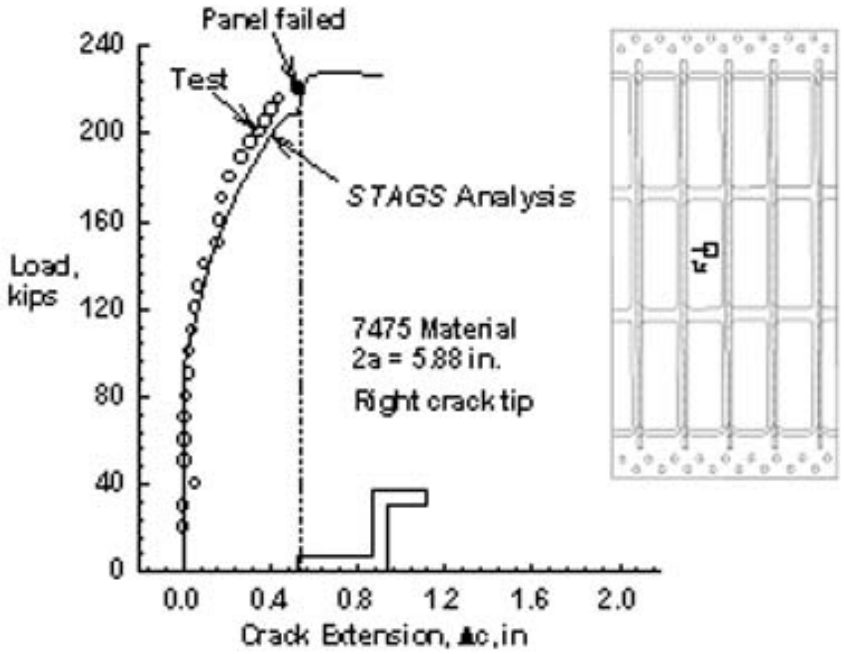

Figure 9.4.1.3 Comparison of load-crack extension data for a 40-inch-wide integral panel

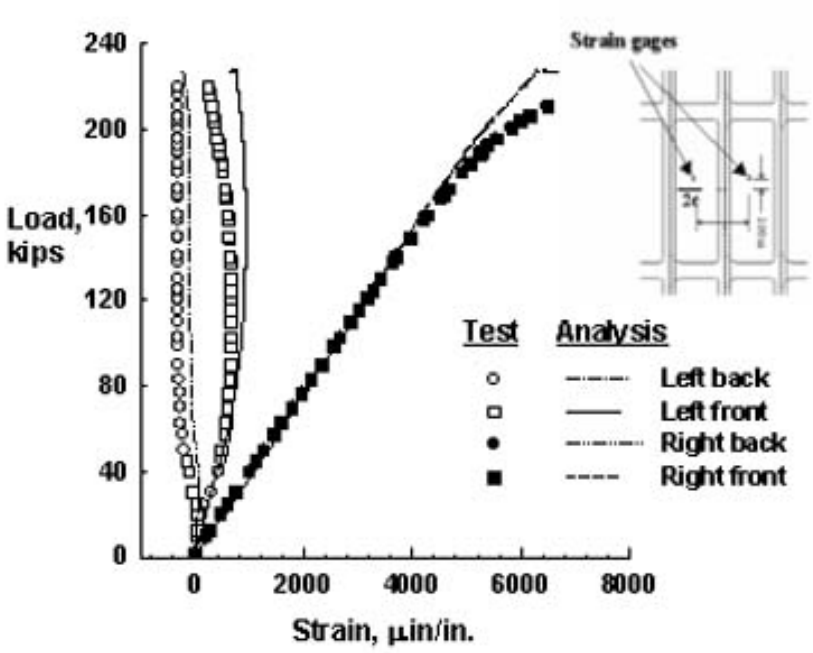

Figure 9.4.1.4 Measured and predicted load vs. strain variation near the initial crack tip locations

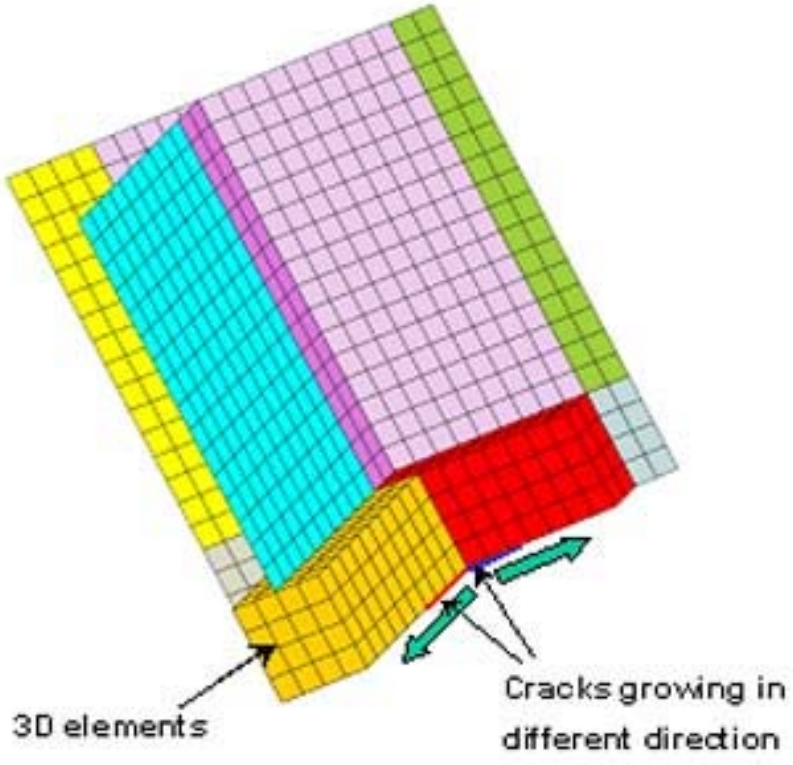

Figure 9.4.1.5 Typical STAGS finite element model of an integrally stiffened panel with solid and shell elements

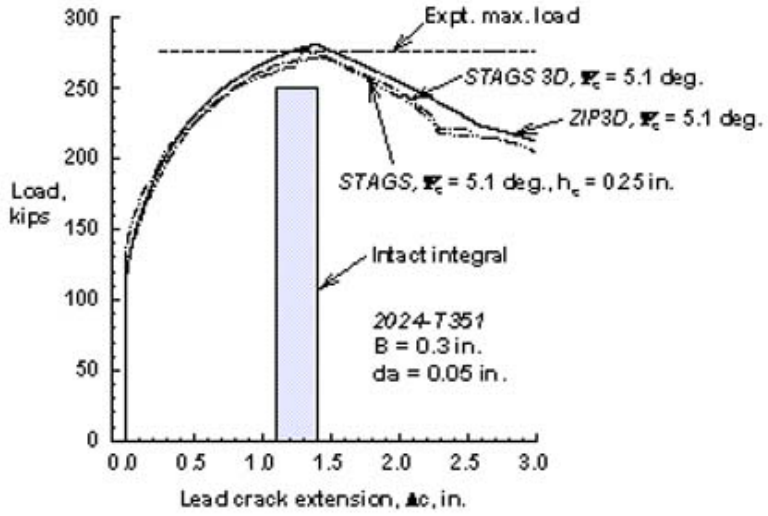

Figure 9.4.1.6 Comparison of load-crack extension data for a 20-inch-wide integral panel

Crack Growth & Advanced Stress Intensities

Feasibility Study: Interacting AFGROW with External K-Solvers

Integration Code Drives

Examples: ***Assembly of K-Solver Handbooks & AFGROW Models, 2nd Generation ECLIPSE***

- Built-up or Integral Structure or Compounding Solutions
- Crack Transitions from 2-D to 3-D and Back Again
- Integrator Must Ensure Robust Handbook Limits, Solutions, and Transitions Between Models

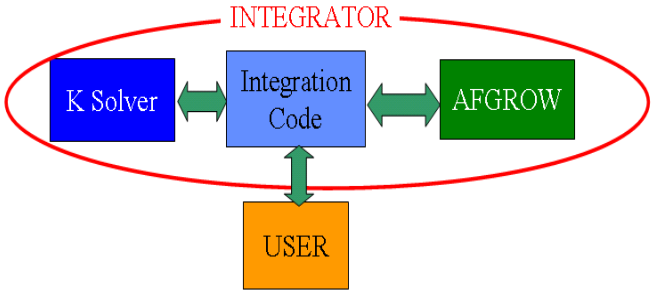

NEW PROBLEM CLASSES

- Handbook
- Integral or Mixed Structure & Residual Strength
- Built-up Structure & Residual Strength
- Repairs & Patches
- Multiple Cracking
- Geometry Variation (Age Degradation)
- Load Variation
- Compound Solutions
- Crack Link-up
- Failure Analyses
- Gradient Following

Figure 9.4.2.1 Solution approach and defined problem classes

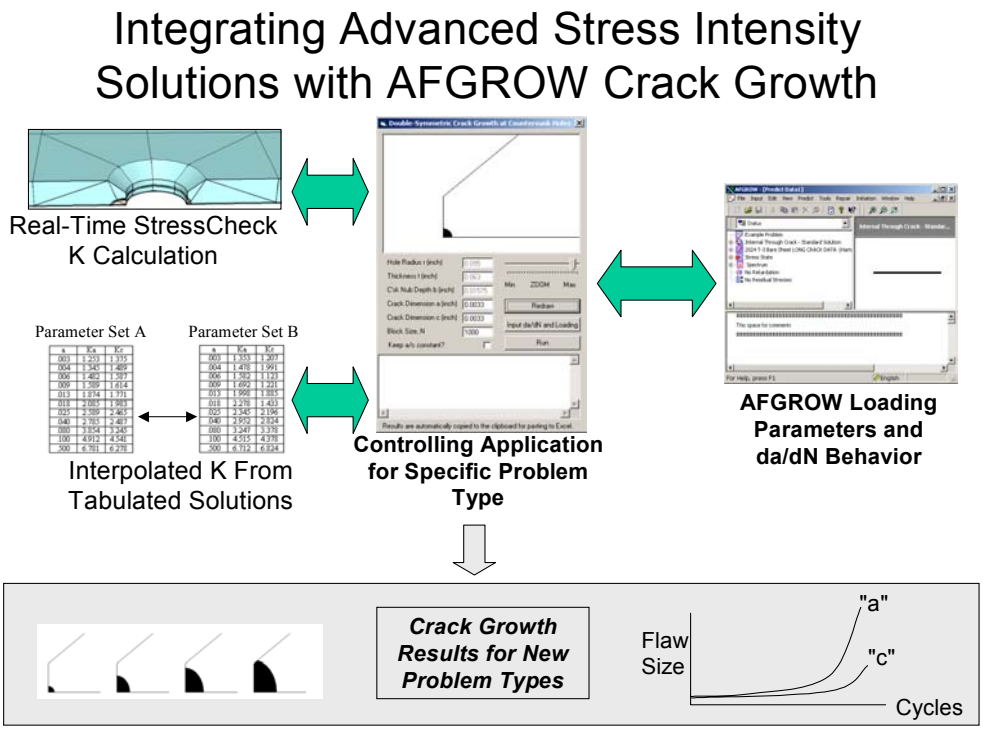

Figure 9.4.2.2 Technology is feasible for many problem types

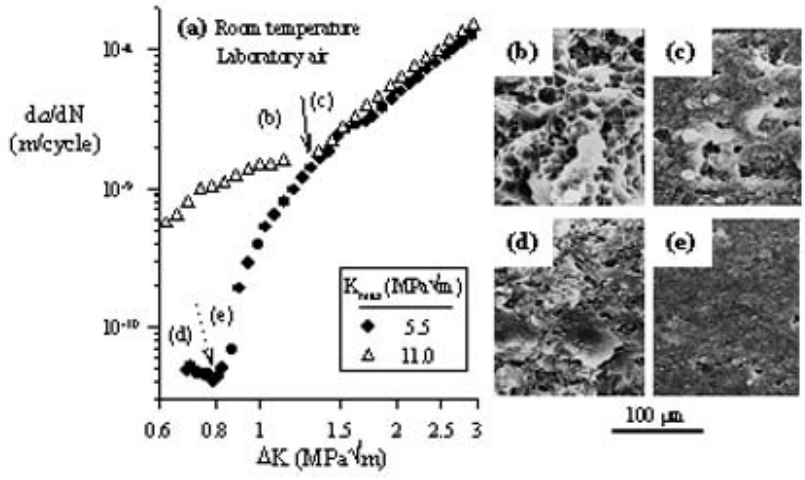

Figure 9.4.3.1 (a) Constant-K_{max} = 5.5 and 11.0 MPa√m FCG data (f = 10 Hz). FCG Transitions (arrows) coincide with changes in crack surface morphology. (b and c) Micro-void crack surface produced at K_{max} = 11.0 MPa√m and $\Delta K < 1.3$ MPa√m and a flat surface produced at $\Delta K > 1.3$ MPa√m, respectively. (d and e) Micro-void crack surface produced at K_{max} = 5.5 MPa√m and $\Delta K < 0.8$ MPa√m and a flat surface produced at $\Delta K > 0.8$ MPa√m, respectively.

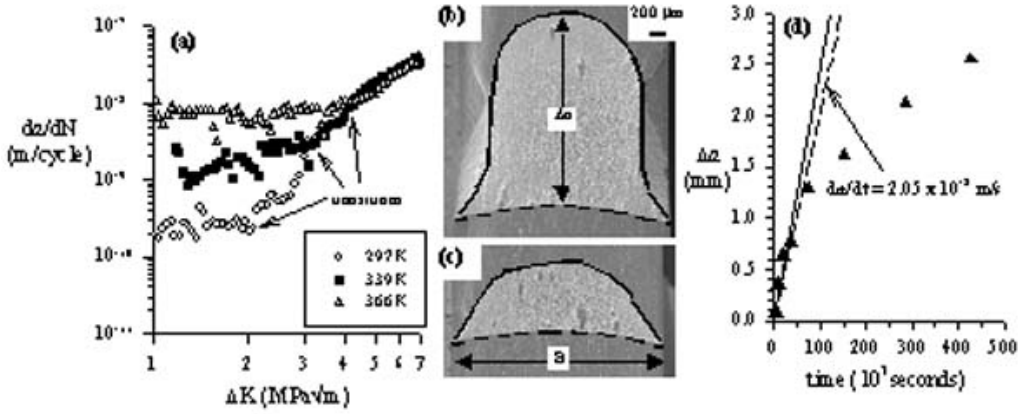

Figure 9.4.3.2 (a) UHV constant- K_{max} = 7.7 MPa√m FCG data (f = 10 Hz) are shown for three temperatures (297 K, 339 K, and 366 K). (b and c) Shown are tunneled crack surface produced by constant load time dependent crack growth during a 43-hour test and 10-hour test, respectively. The specimen thickness in "B" and the direction of crack growth is from the bottom to the top of the figures. (d) The plot shows crack growth at the specimen centerline, Δa, versus time for eight experiments performed at times ranging from 1 hour to 120 hours.

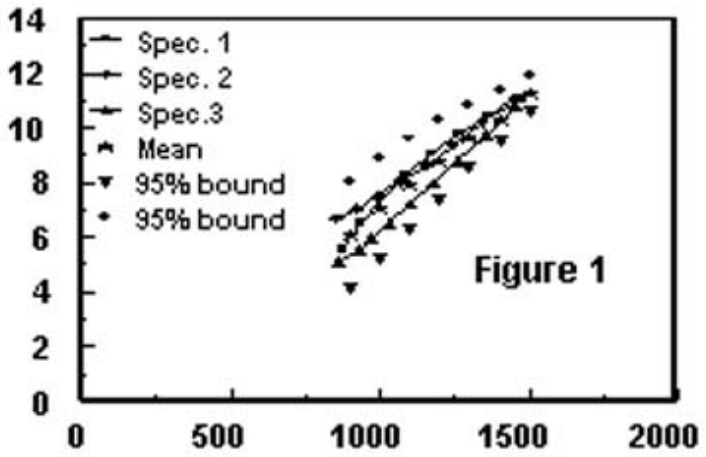

Figure 9.4.4.1 Y axis---da/dN, nm per cycle. X axis---a, crack length, microns

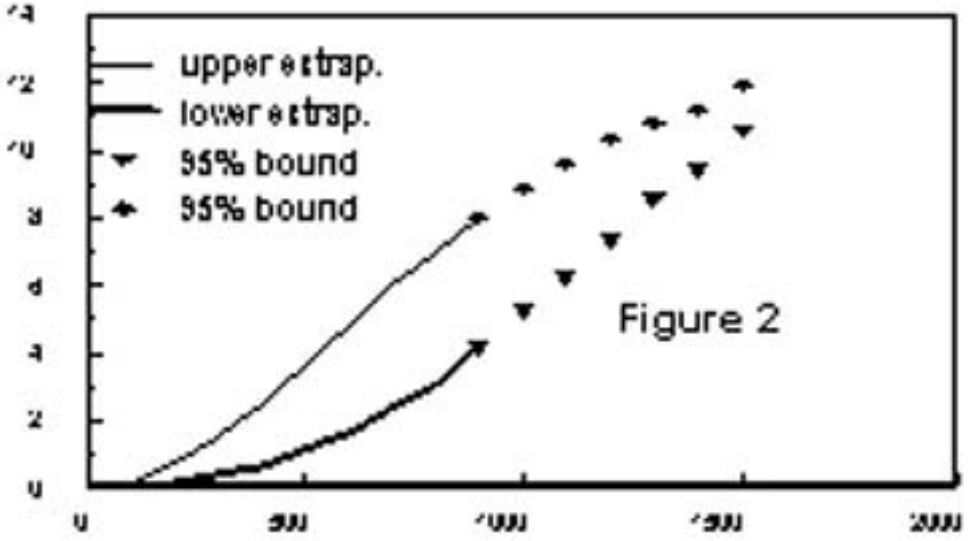

Figure 9.4.4.2 Y axis---da/dN, nm per cycle. X axis---a, crack length, microns

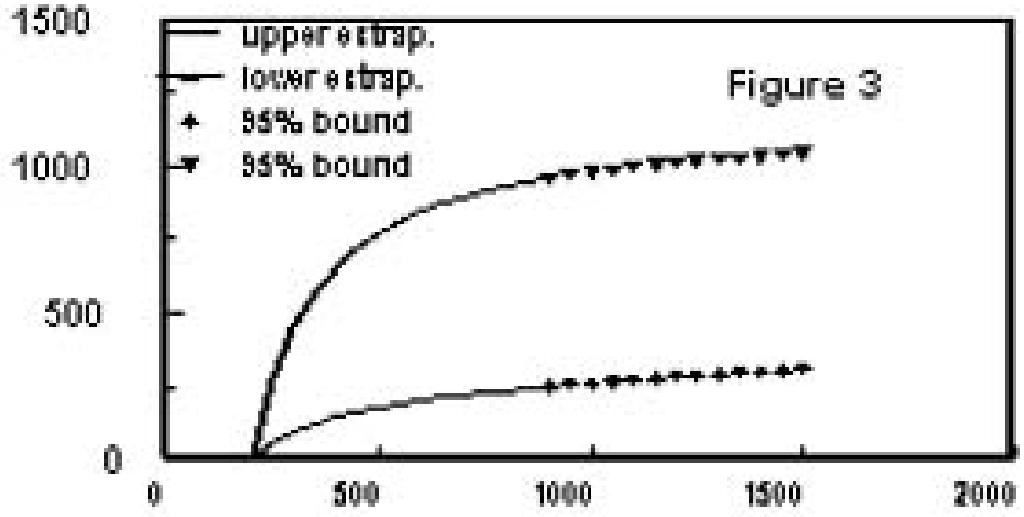

Figure 9.4.4.3 Y axis---N, kilocycles. X axis---a, crack length, microns

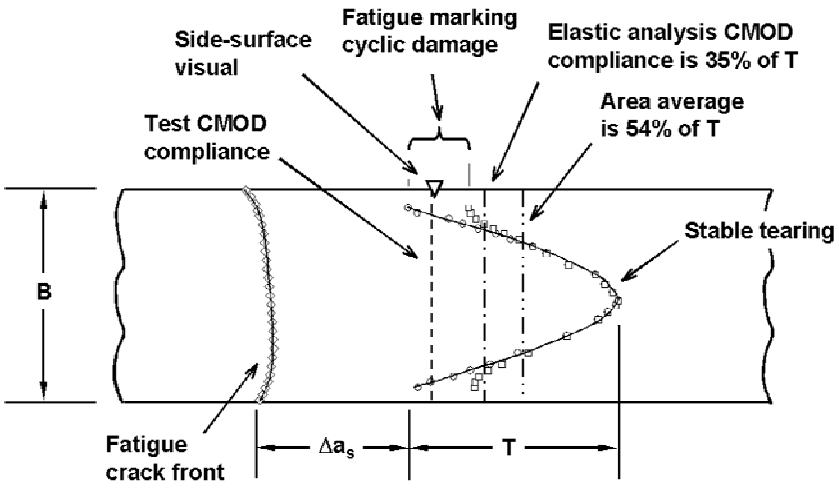

Figure 9.4.6.1 Scale drawing of crack length measures compared with a tunneling crack front shape

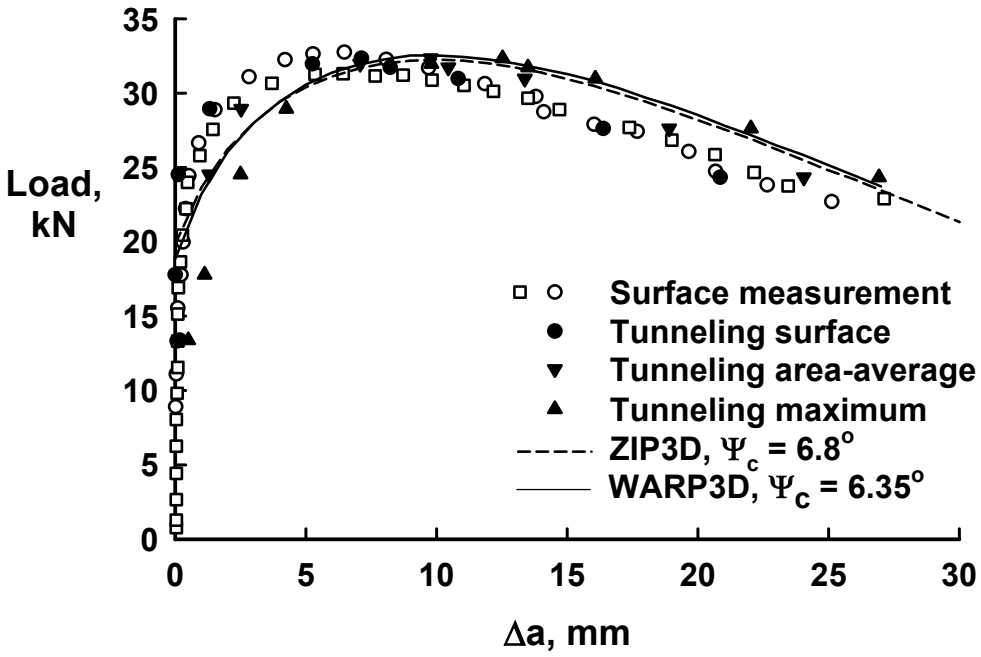

Figure 9.4.6.2 Comparison of tunneling results with and analysis results

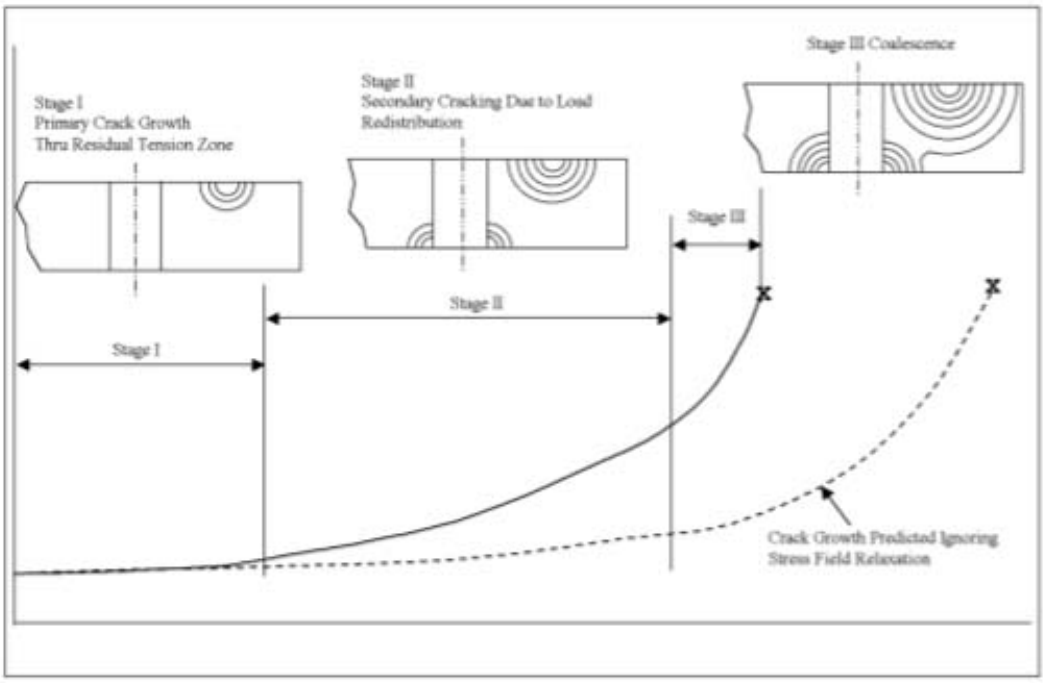

Figure 9.4.7.1 Multi-stage crack growth in cold-worked holes

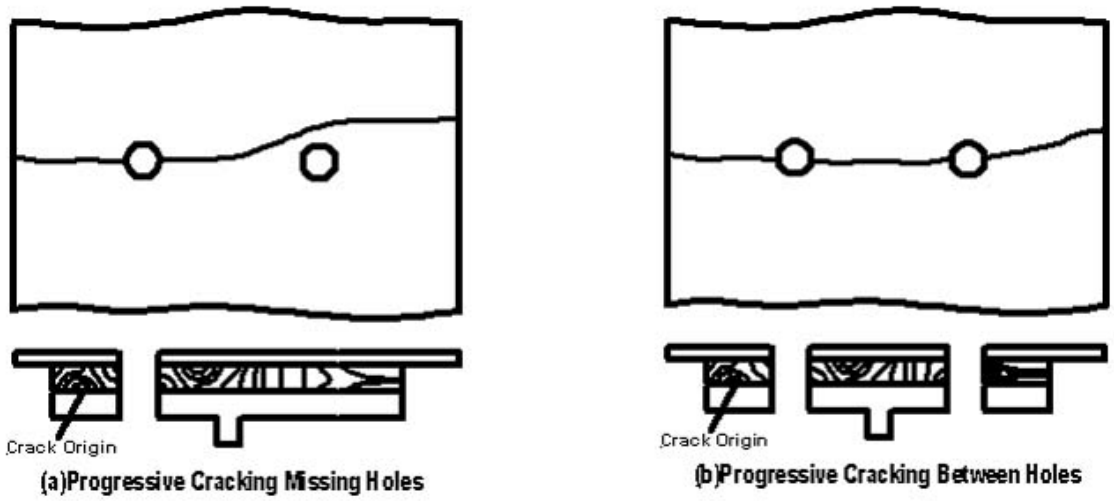

Figure 9.4.7.2 The system architecture is designed to handle complex crack growth scenarios

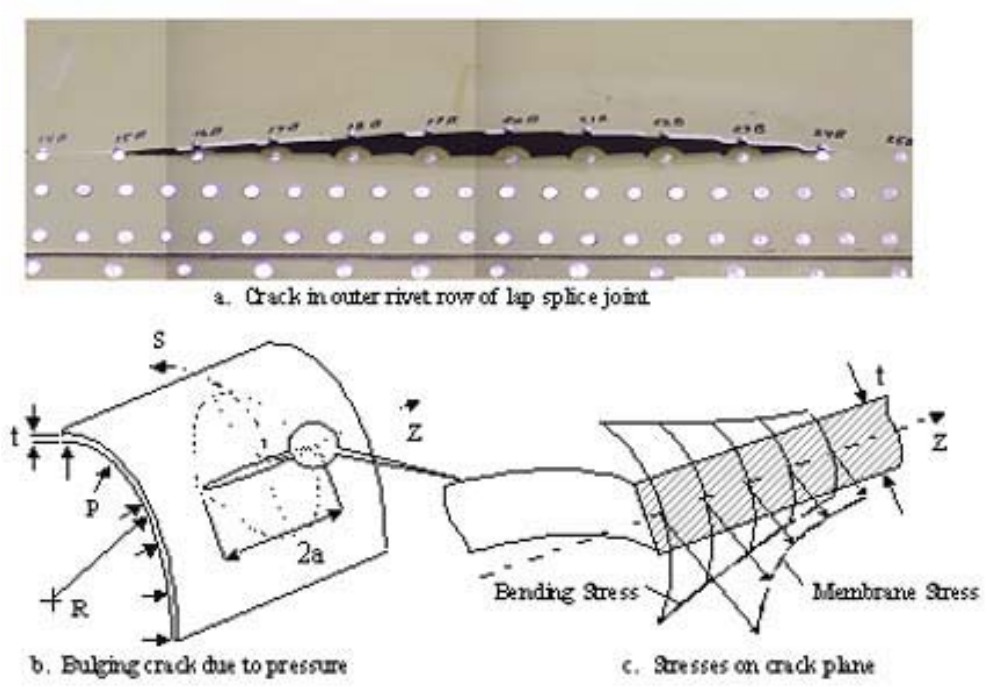

Figure 9.4.8.1 Crack bulging phenomena

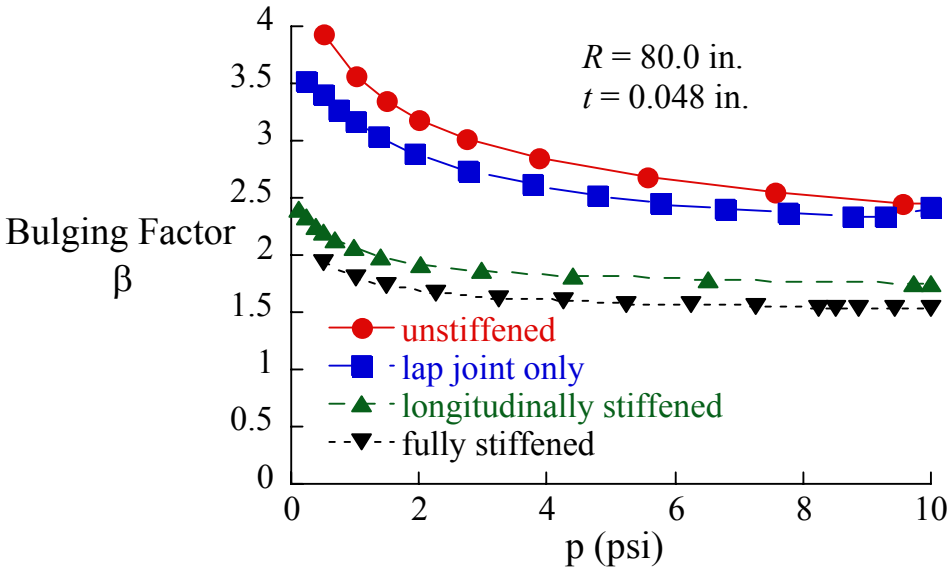

Figure 9.4.8.2 Bulging factor for the configurations analyzed

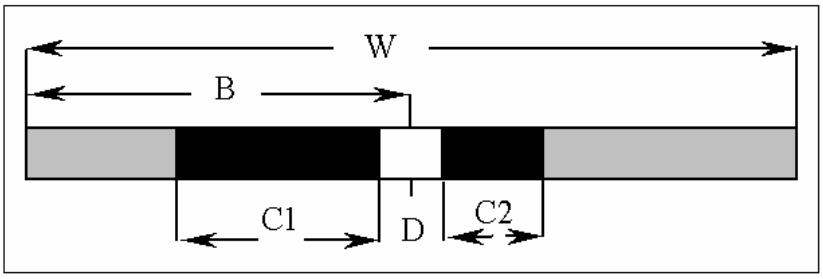

Figure 9.4.9.1 Two, unequal cracks growing from a single, centered hole

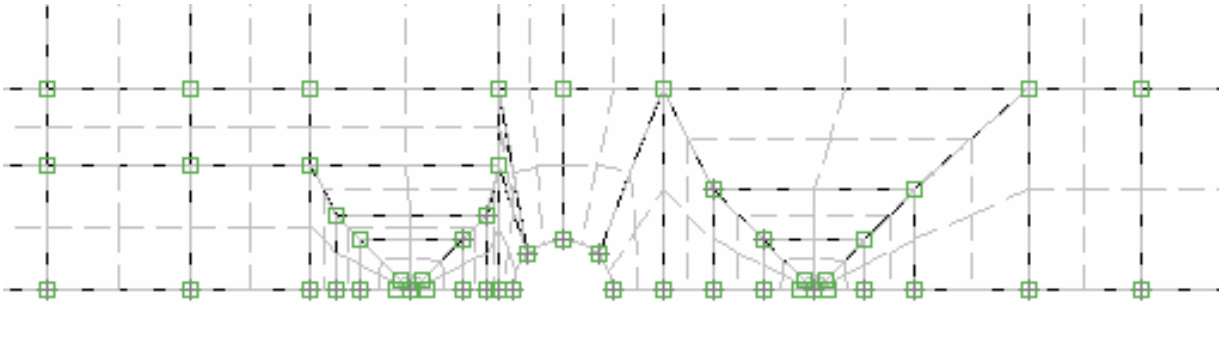

Figure 9.4.9.2 Finite element mesh

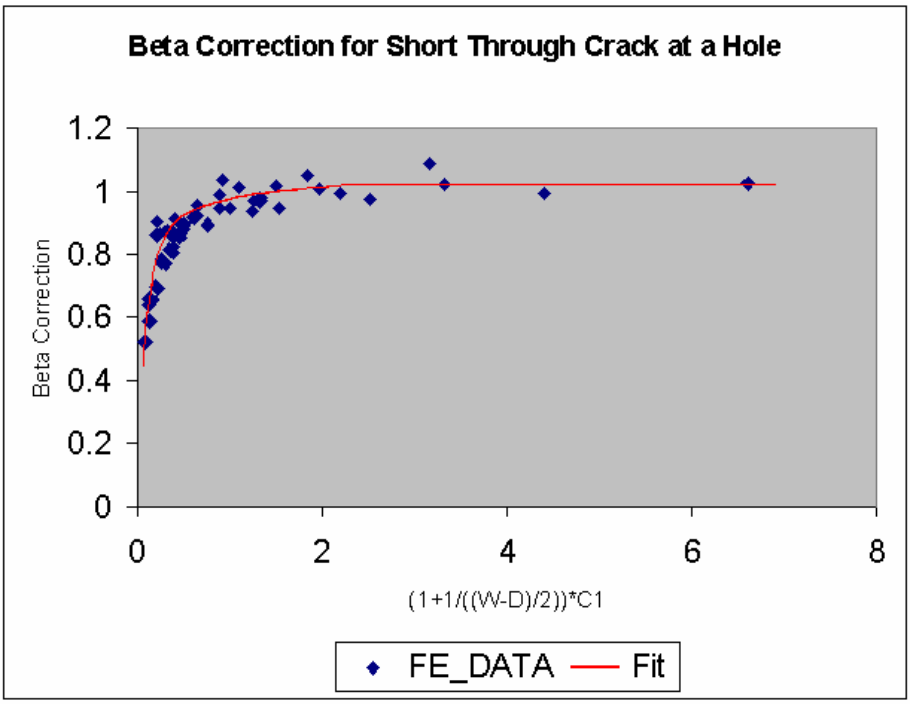

Figure 9.4.9.3 Sample finite width correction factor

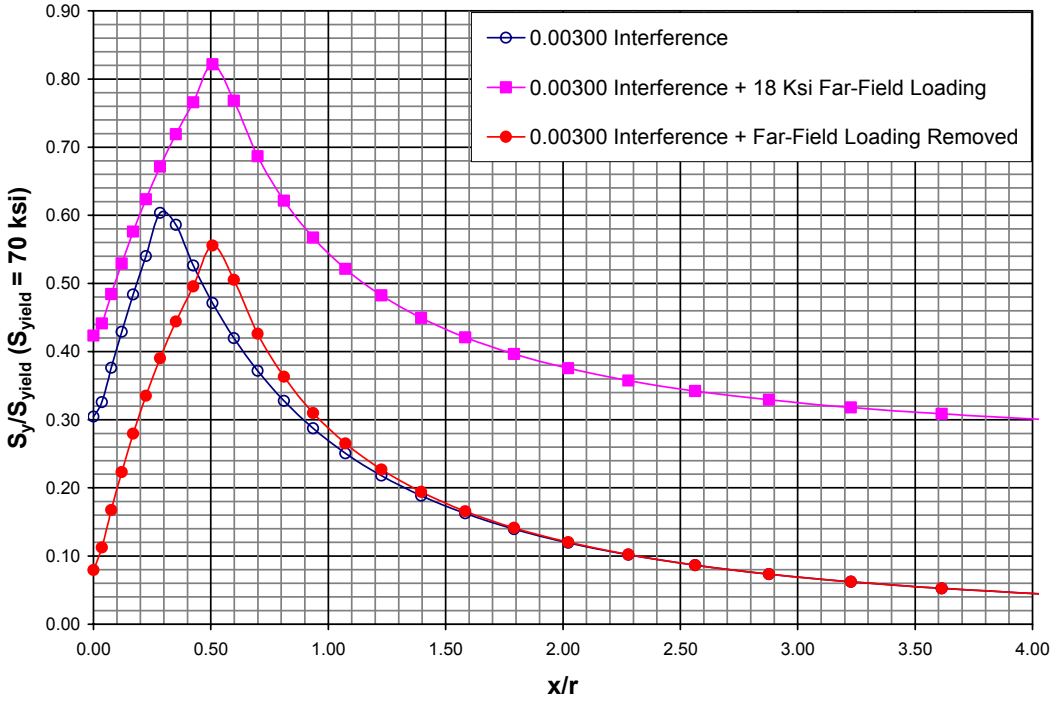

Figure 9.4.10.1 Tangential stress distribution – specimen A -0.00300 in. interference – 18 ksi applied far-field stress

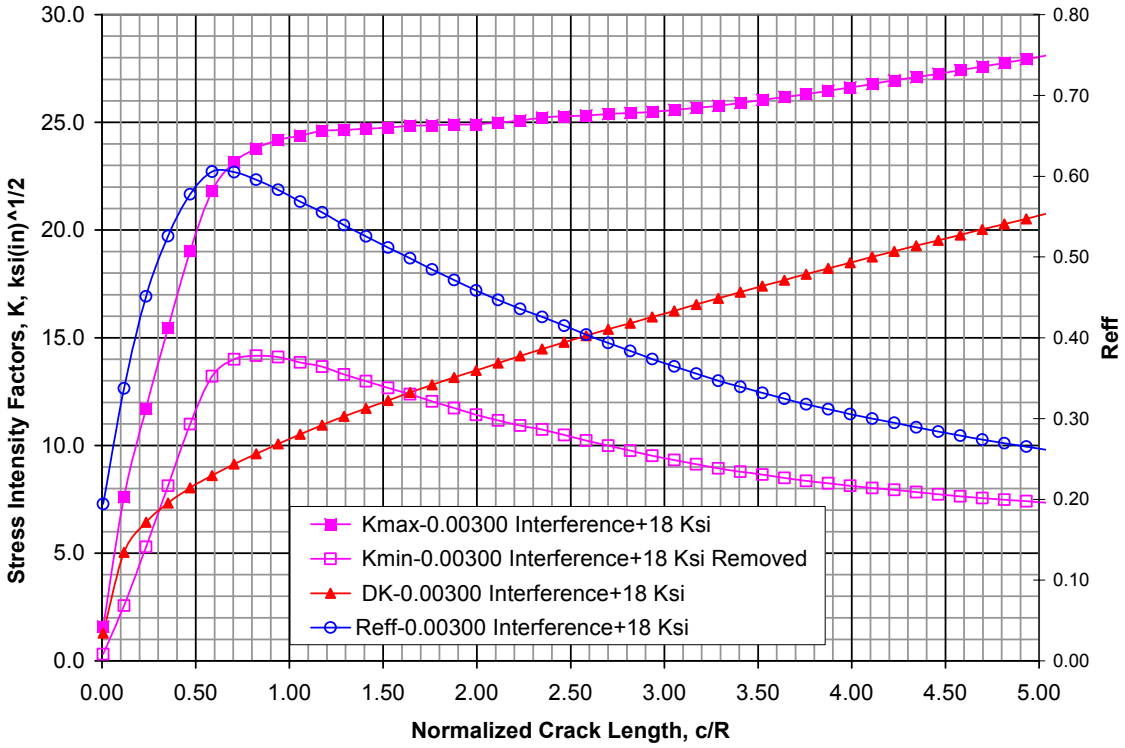

Figure 9.4.10.2 Stress intensity factors for specimen A -0.00300 in. interference – applied far-field stress of 18 ksi and subsequent unloading

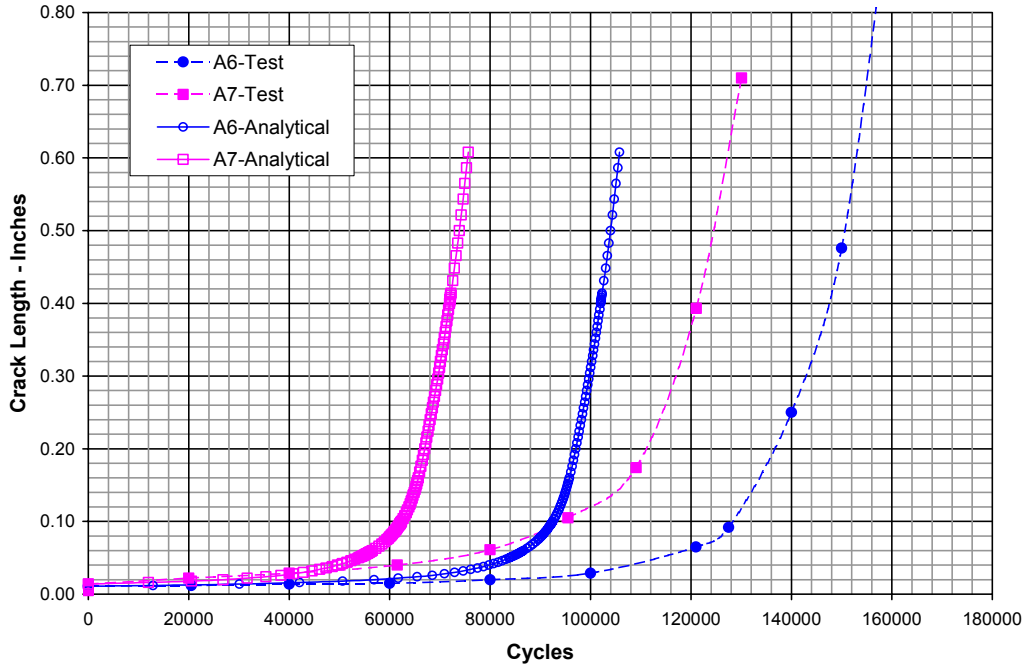

Figure 9.4.10.3 Comparison of test and analytical data – specimen A – S_{max} = 18 ksi, R = 0.10

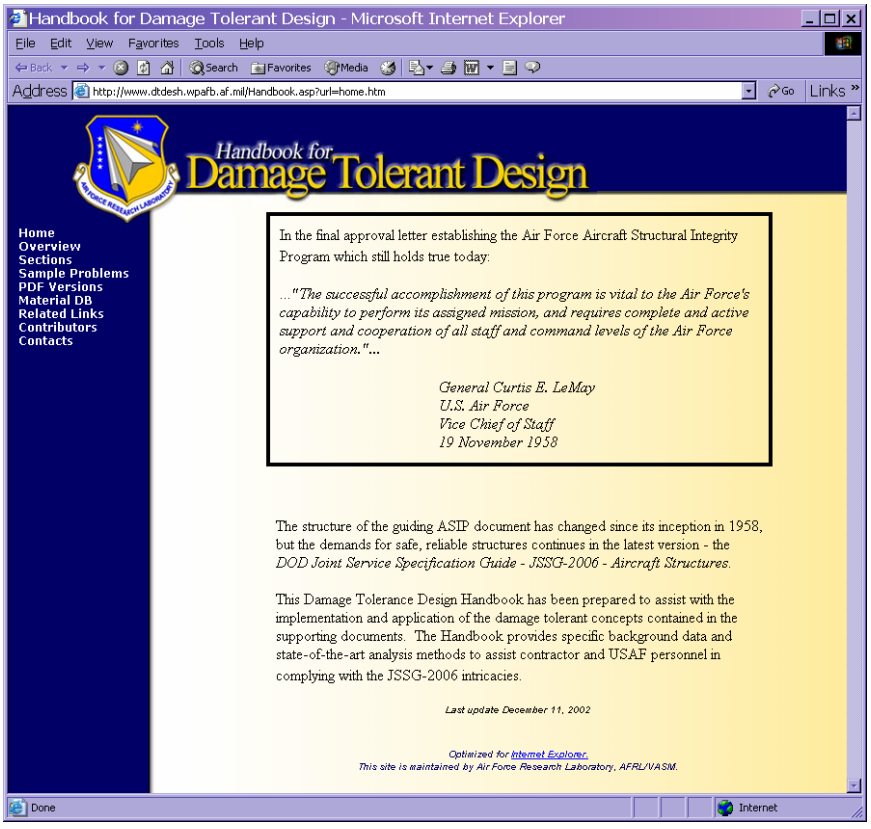

Figure 9.5.1.1 Damage Tolerant Design Handbook

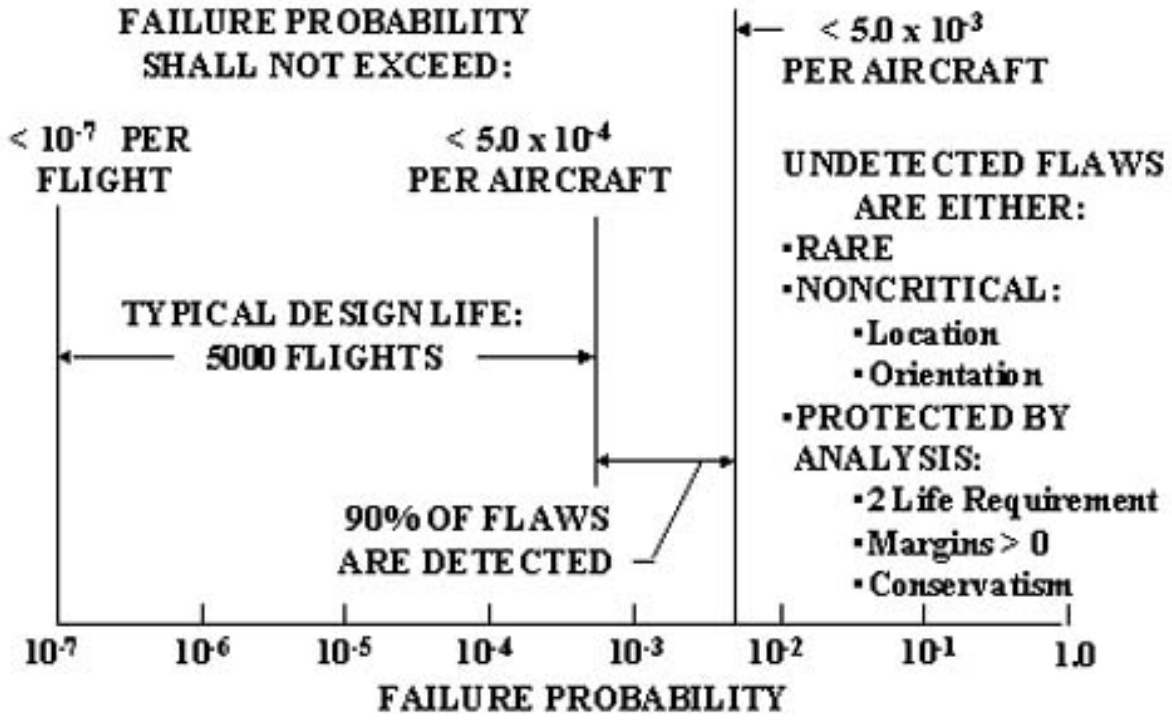

Figure 9.5.2.1 How damage tolerance design assures $<<10^{-7}$ probability of failure

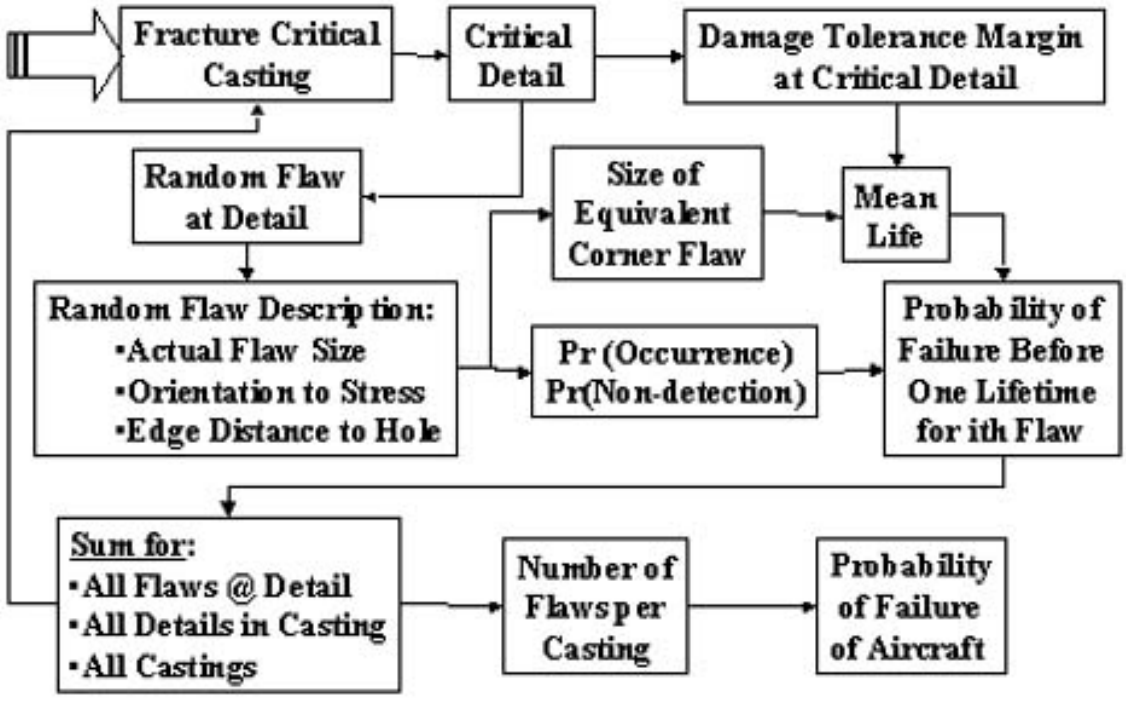

Figure 9.5.2.2 Summary: probability of failure analysis

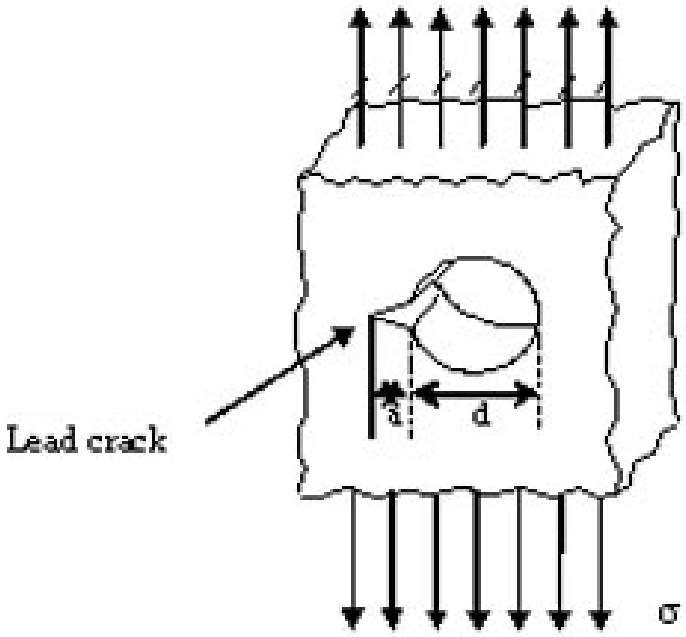

Figure 9.5.3.1 Initial crack configuration, Case 1

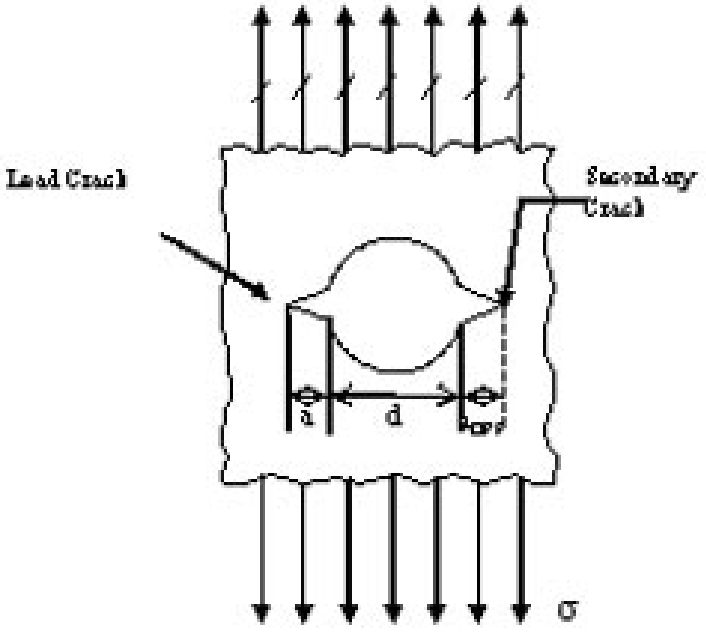

Figure 9.5.3.2 Local MSD crack configuration, Case 2

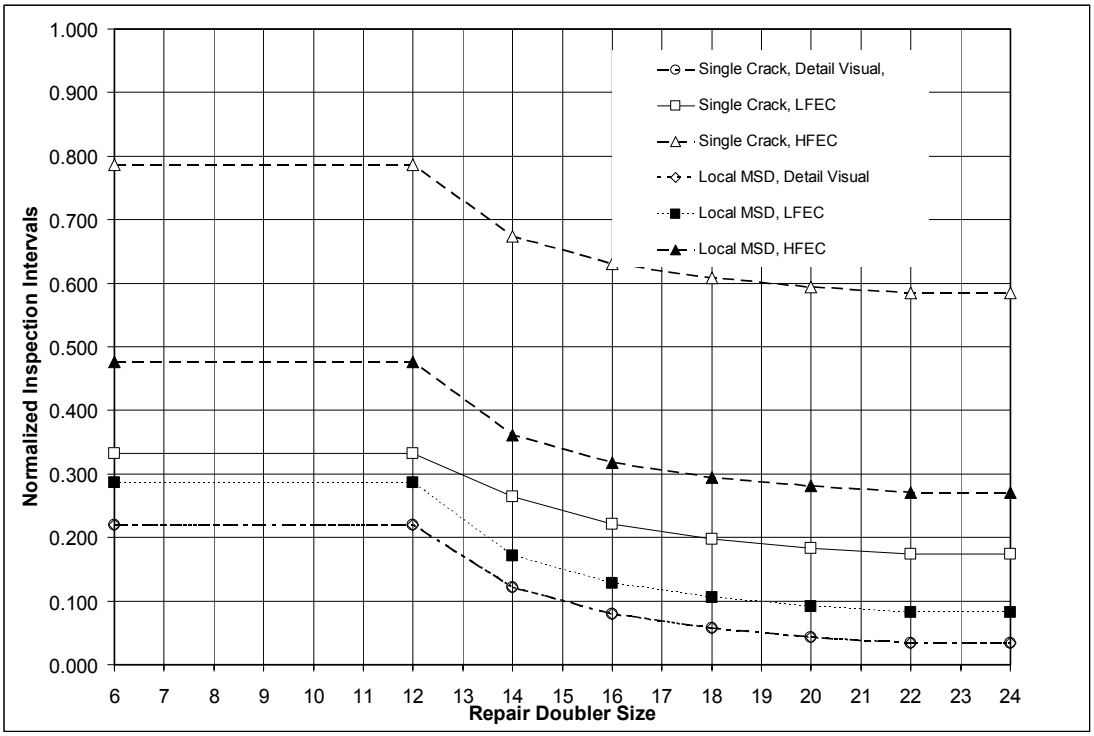

Figure 9.5.3.3 Influence of local MSD consideration on the repeat inspection intervals of various inspection techniques

Structural Element	Repair Ref.	Inspections Intervals	Options
Fuselage skin in AREAs 1 and 3 excluding areas described on page 19	727 SRM: External skin repair • On lower cargo door skins: 52-00-3 (Fig. 3) 52-00-3 (Flg. 4) • Between stringers: 53-30-3 (Fig. 1) • At stringers: 53-30-3 (Fig. 3) • At lap splice: 53-30-3 (Fig. 5) 53-30-3 (Flg. 12) 53-30-3 (Flg. 14) 53-30-3 (Fig. 15A) 53.30-3 (Fig. 24) SB: See Section 2.3.4 for affected service bulletins. See Ref. 1	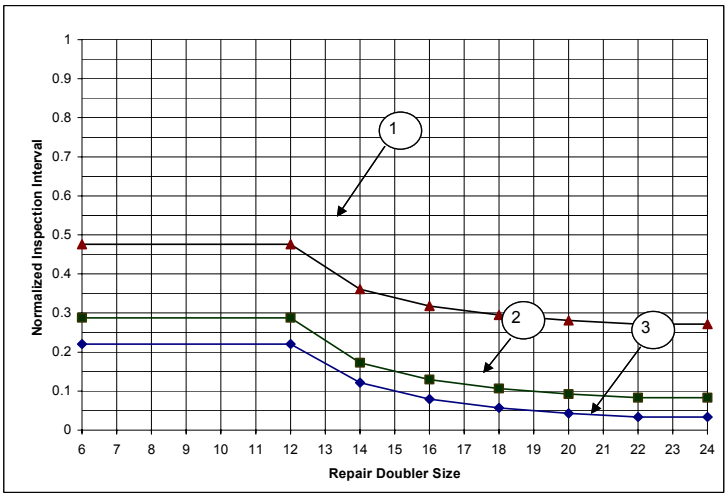	Option A Internal MFEC in accordance with curve 1 on skin at all fastener locations at critical rows. Option B External LFEC inspect through repair on skin at all critical rows in accordance with curve 2 Option C Internal Detailed Visual Inspect on skin at critcal rows in accordance with curve 3 Notes: 1) NDT procedures in accordance Table 4

Figure 9.5.3.4 Typical repair assessment chart for 727 freighter conversions based on local MSD consideration

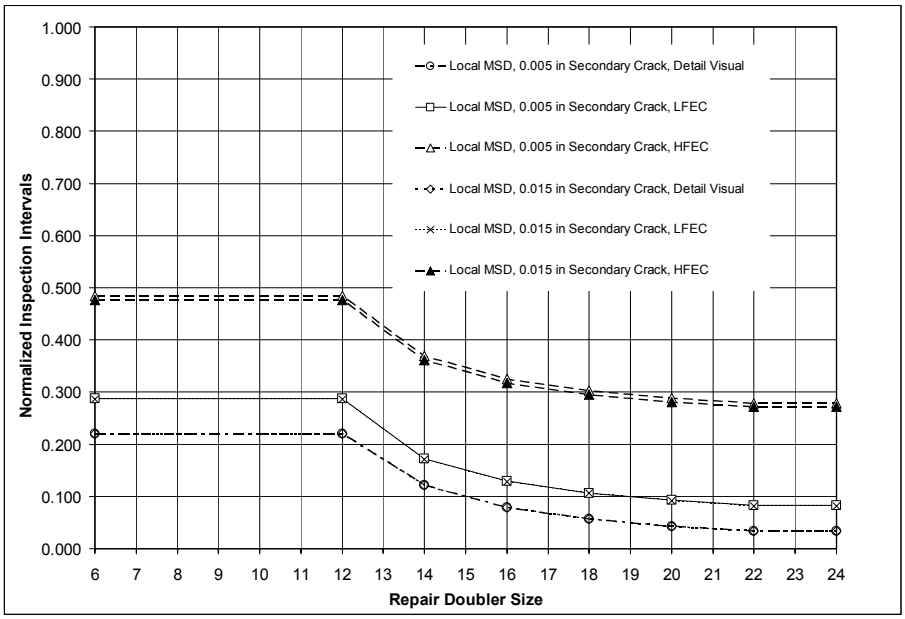

Figure 9.5.3.5 Influence of secondary crack sizes on the repeat inspection intervals

Multiple Crack Growth Analysis Manager

	CRACK A	CRACK B	CRACK C	CRACK D	CRACK E	CRACK F	CRACK G	CRACK H
Nasgro File Name	S02-0A	S02-0B						
	Load Data	Load Data	Load Data	Load Data	Load Data	Load Data	Load Data	Load Data
	view model	view model						
Structure Name	crown skin	crown skin						
Crack Type	CC02	CC02						
Interaction Type	F_int	F_int						
Spectrum Name	CONS2	CONS2						
Material Code	M2EA1	M2EA1						
Inititial Crack Length	0.05	0.005						
Aspect Ratio (a/c)	1	1						
Hole Diameter d	0.188	0.188						
Hole Edge Distance B	1	1						
Plate Thickness t	0.056	0.056						
Plate Width W	2	2						
Ref. Stress S0	16.088	16.088						
Ref. Stress S1	0	0						
Ref. Stress S2	0	0						
Ref. Stress S3	14.548	14.548						
Limit Stress So	18.5	18.5						
Limit Stress S1	0	0						
Limit Stress S2	0	0						
Limit Stress S3	16.7	16.7						
Schedules to apply	1	1						
Blocks to apply	500	500						
Cycles to apply	1	1						
Matl. Poisson Ratio	0.33	0.33						
% delta Ca per block	0.05	0.05						
Multiple Crack Run	Run NASGRO	Run NASGRO	Run NASGRO	Run NASGRO	Run NASGRO	Run NASGRO	Run NASGRO	Run NASGRO

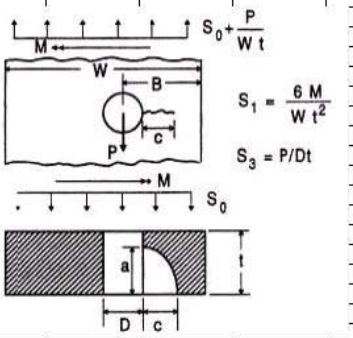

Figure 9.5.3.6 Excel based multiple crack growth analysis interface with NASGRO code

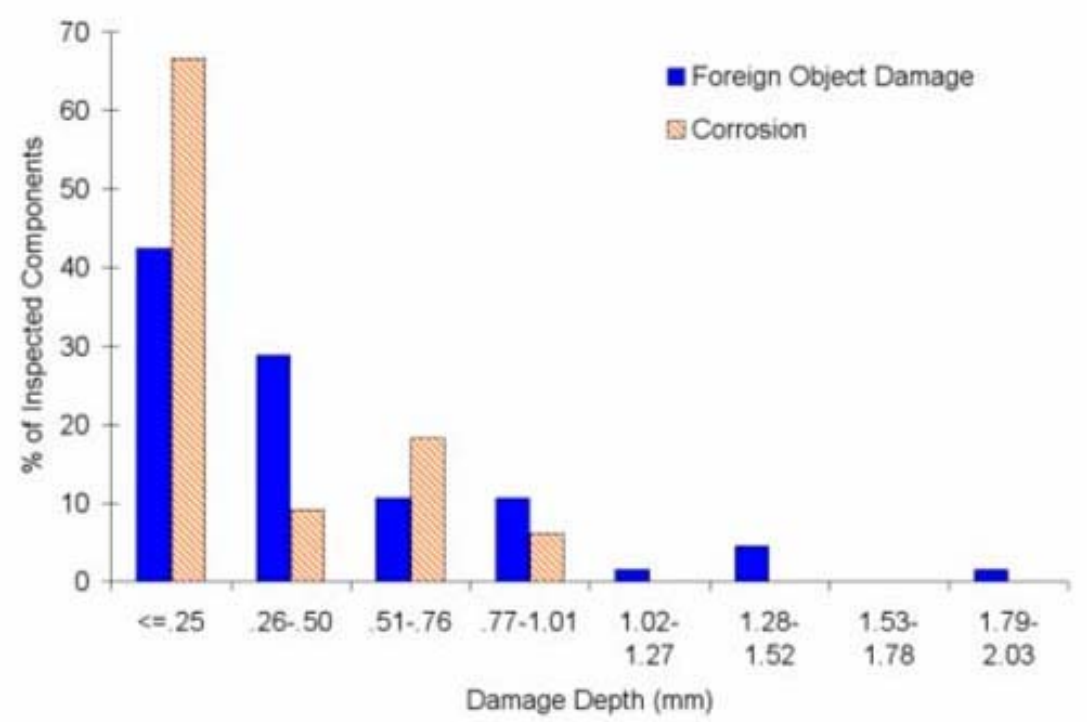

Figure 9.5.4.1 Survey of field damage for rotorcraft structure

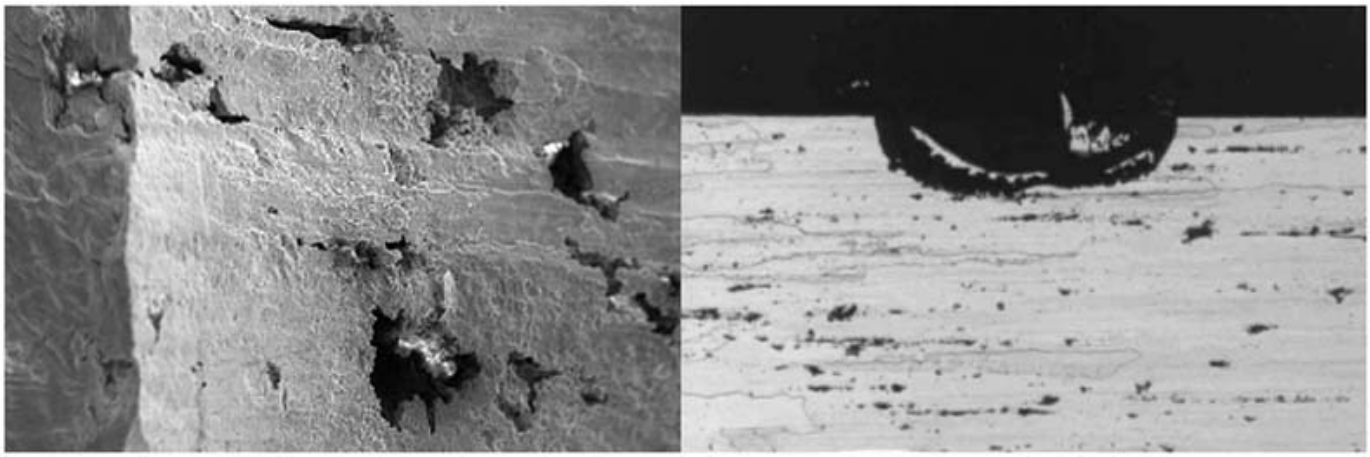

Figure 9.5.4.2 Photographs of field and laboratory corrosion damage

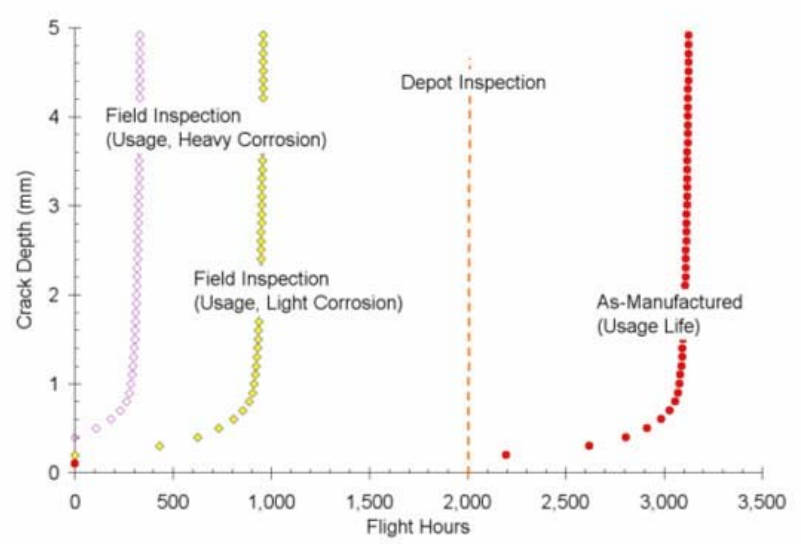

Figure 9.5.4.3 Life management for the fault-tolerance method

Table 9.5.4.1 Spindle lug economics of ownership (Figures in $1,000's)

	Safe-life	Flaw-tolerance	Damage-tolerance	Fault-tolerance
Original design cost	125	122	148	137
Original inspection cost	Not Applicable	60	240	240
New design cost	875	172	148	137
New inspection cost	Not Applicable	300	300	300
Probability of Failure	71%	93%	50%	60%

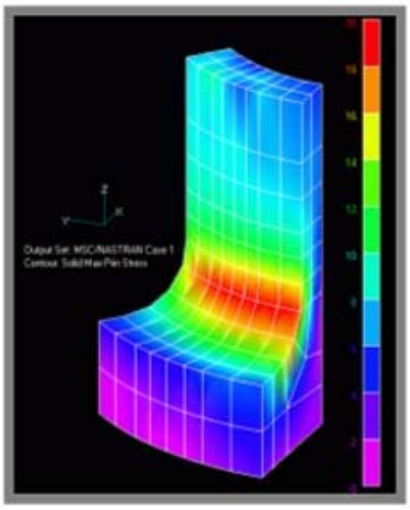

Figure 9.5.5.1 Local model analysis

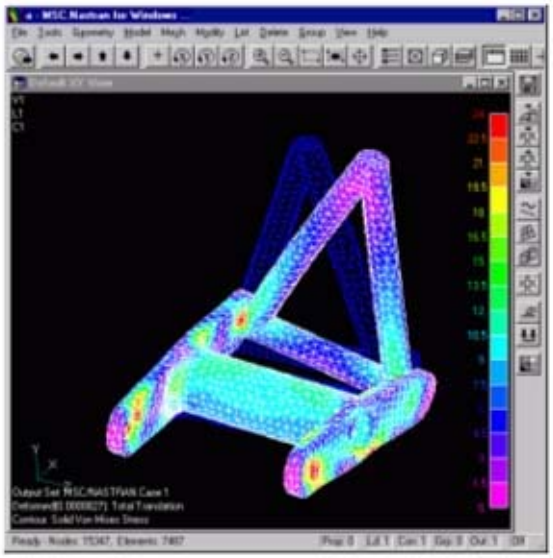

Figure 9.5.5.2 Global model solved using MSC NASTRAN

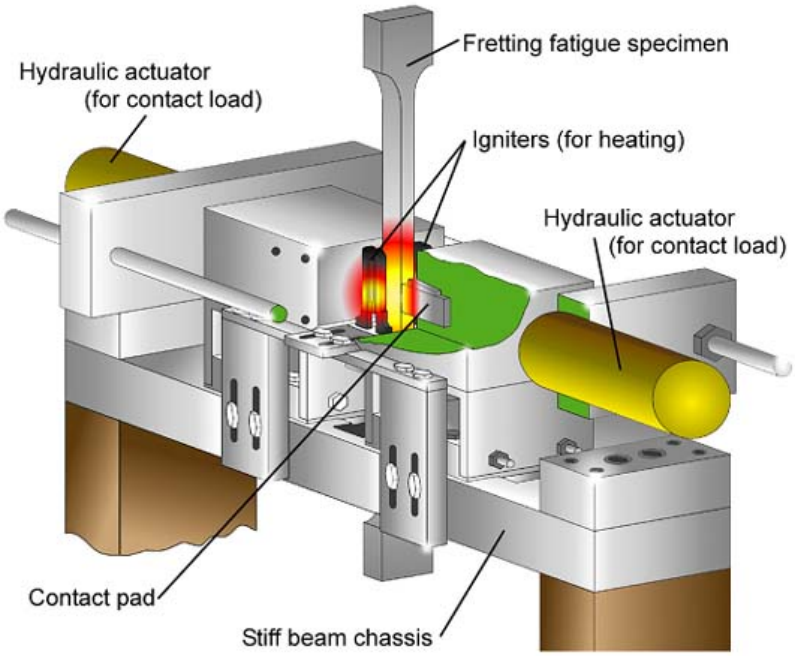

Figure 9.6.1.1 Schematic representations of Purdue test apparatus designed to study attachment fatigue at elevated temperature. The fretting fatigue specimen is clamped between two contact pads and then loaded with a remote cyclic load that leads to eventual specimen cracking and failure

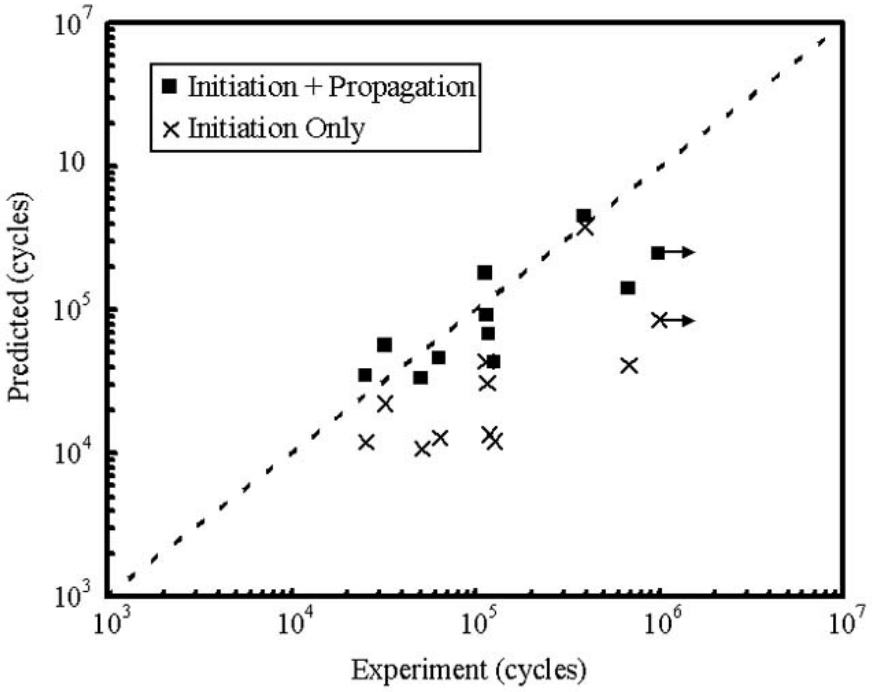

Figure 9.6.1.2 Comparison of total fatigue life calculations with experimental results for Inco718 on Ti-6Al-4V fretting fatigue tests (x's are predictions for crack formation life only, white square symbols include predictions for crack propagation in the total fatigue life)

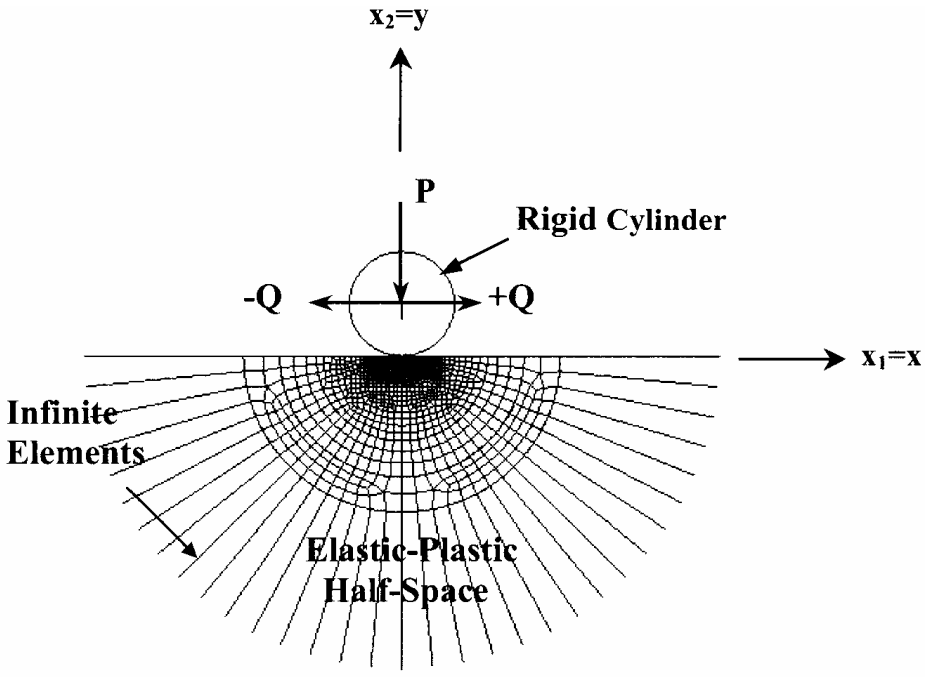

Figure 9.6.2.1 Finite element model of fretting contact

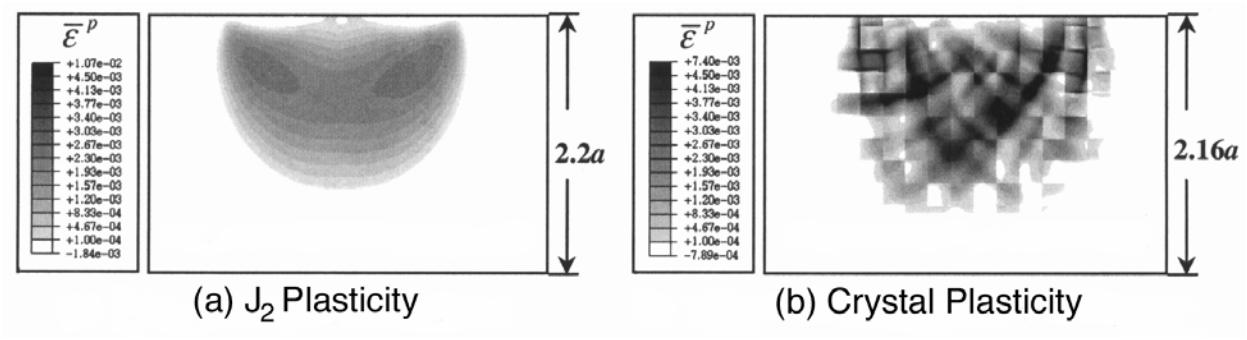

Figure 9.6.2.2 Distributions of cumulative effective plastic strain for Q/P_y – 0.3, P/P_y – 15, μ = 1.5 using (a) homogeneous elastic-plastic (J_2) material model and (b) crystal plasticity material model

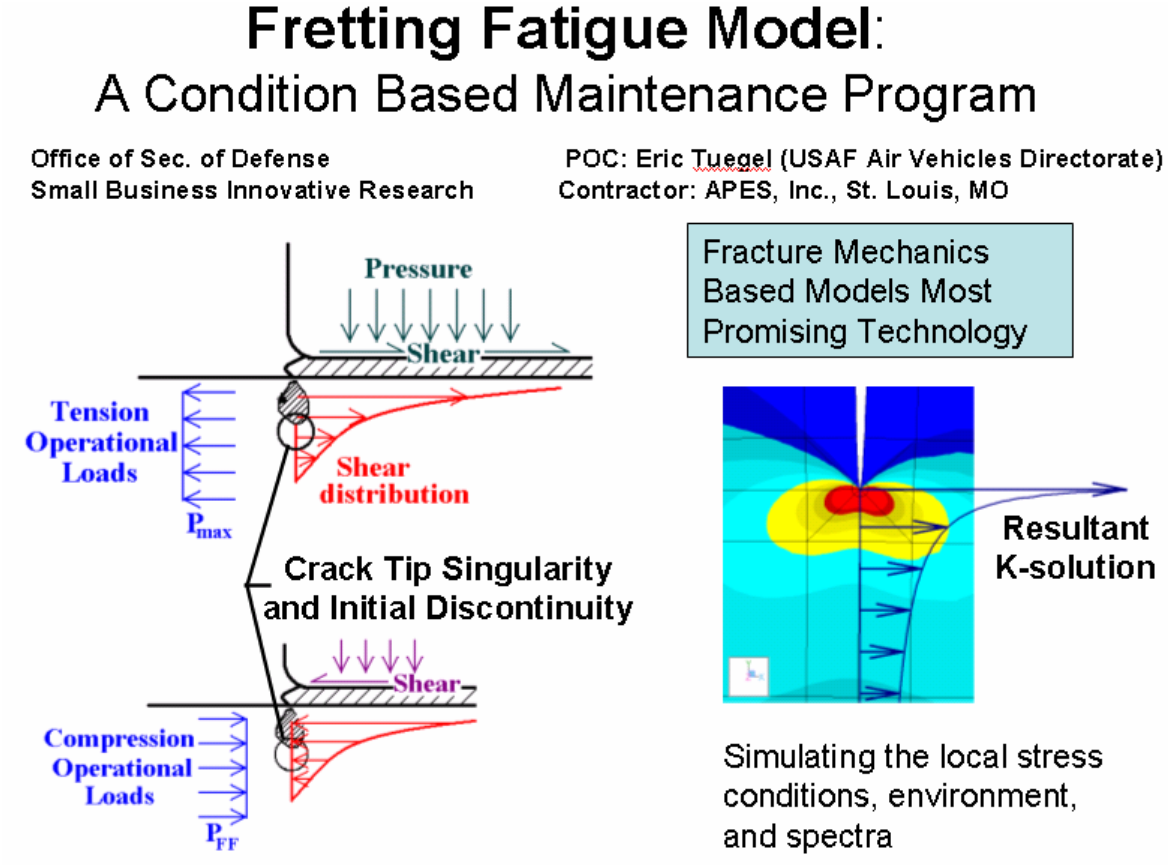

Figure 9.6.3.1 Fretting model examines fretting damage modes

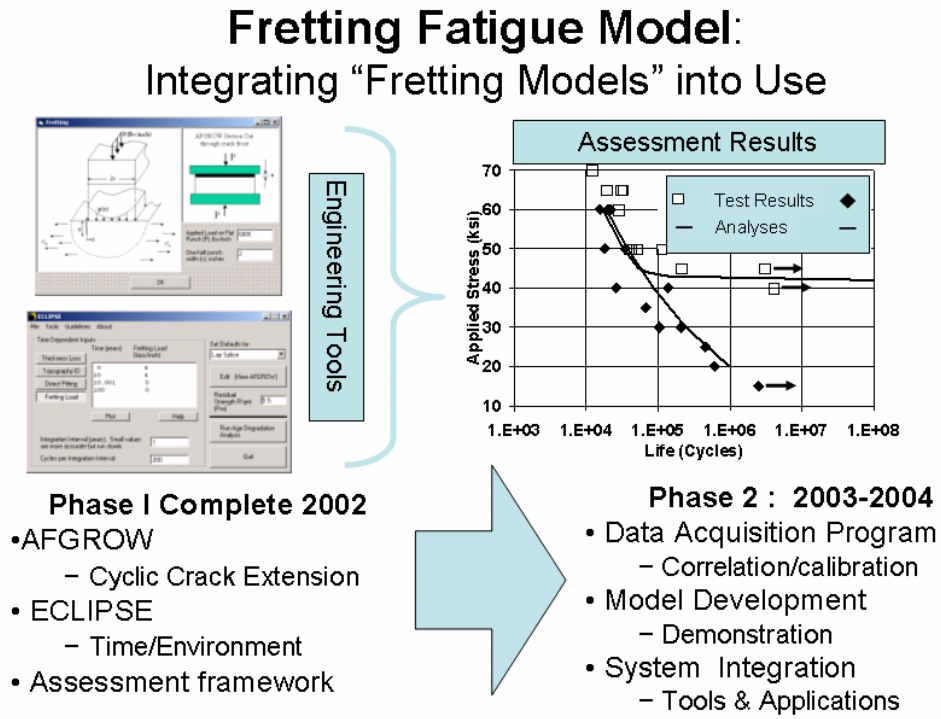

Figure 9.6.3.2 Holistic fretting model will be correlated with experimental data

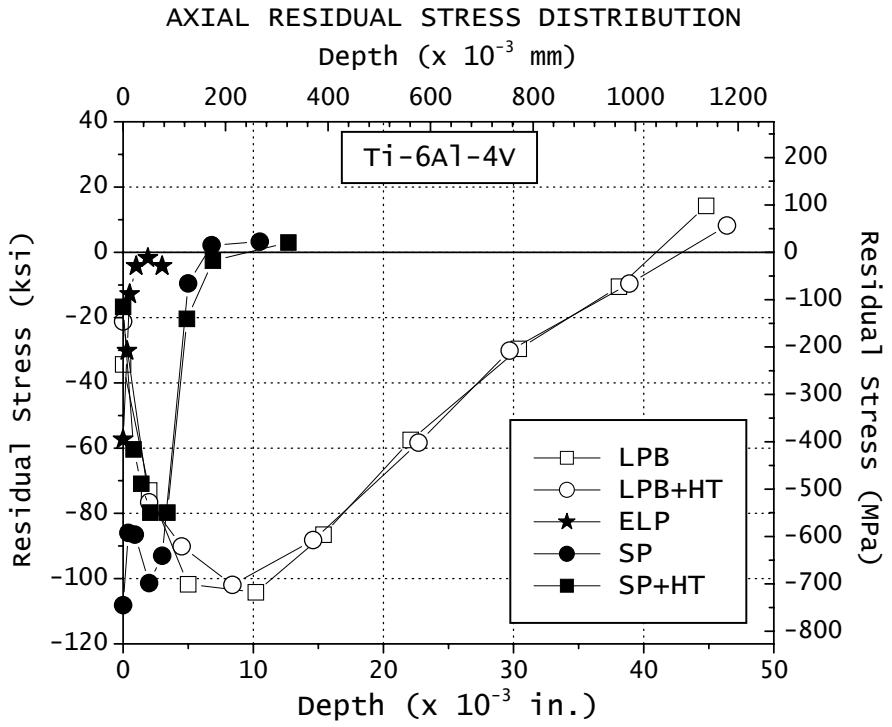

Figure 9.6.4.1 Residual stress and cold work profile indicating depth of compression for LPB, SP, and ELP specimens. (HT indicates heat treatment of 375°C for 10 hours)

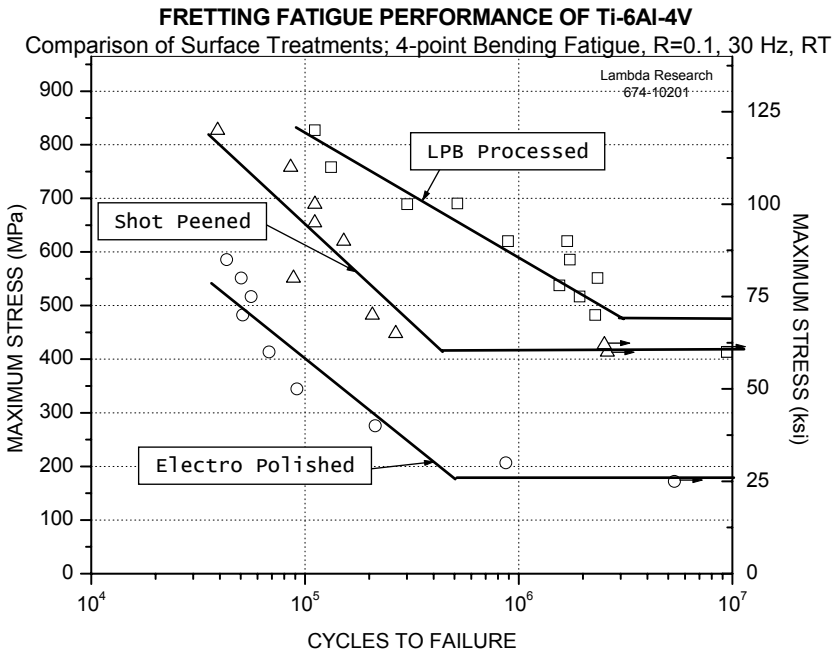

Figure 9.6.4.2 Comparison of fretting HCF data for ELP, Sp and LPB treated specimens. Clearly while SP shows some benefits, LPB is superior both in HCF performance and endurance limit. A note should be made that due to the specimen design used here, all LPB specimens failed from subsurface crack initiation and not from fretting, while all SP and ELP specimens failed from fretting.

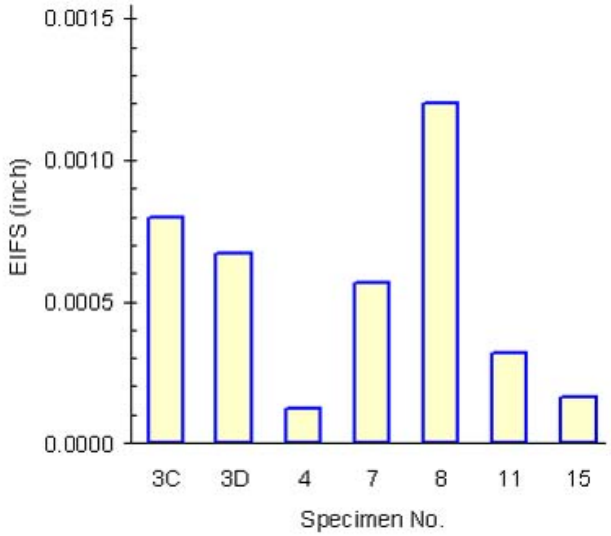

Figure 9.7.1.1 Equivalent initial flaw-size data

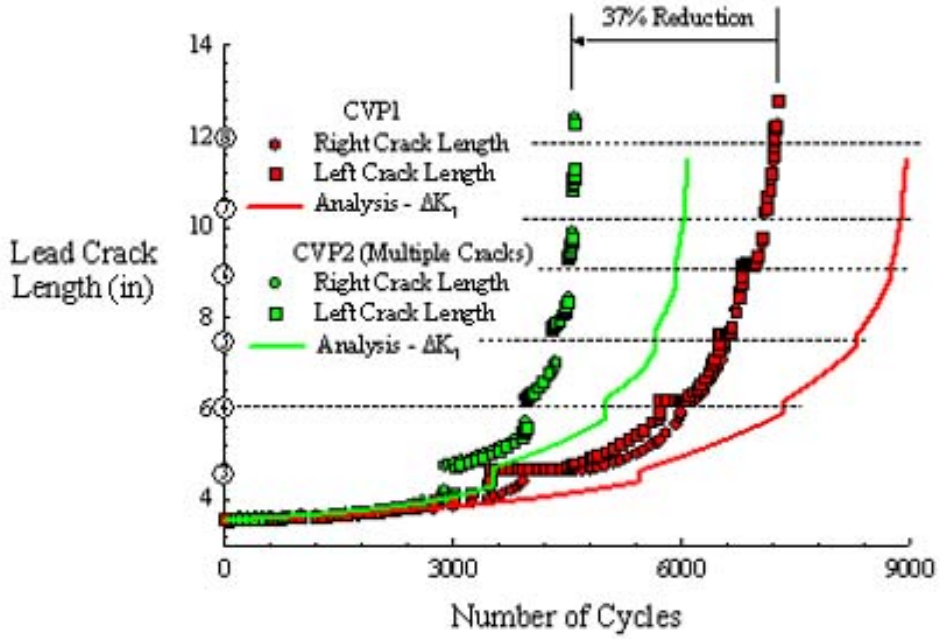

Figure 9.7.1.2 Effect of MSD on lead crack growth

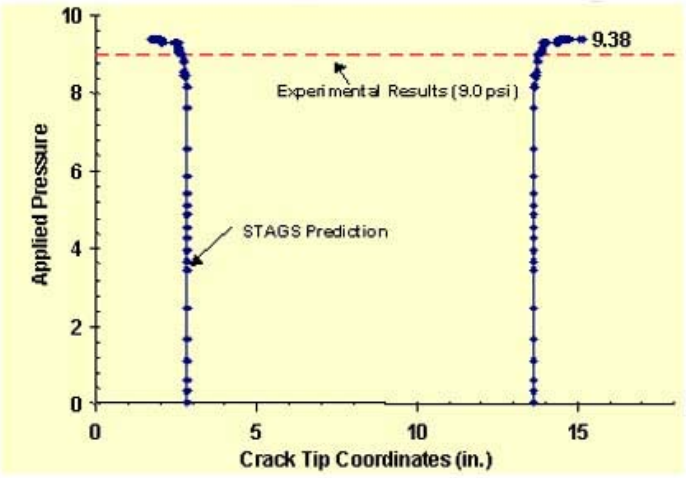

Figure 9.7.1.3 Residual strength of aft pressure bulkhead

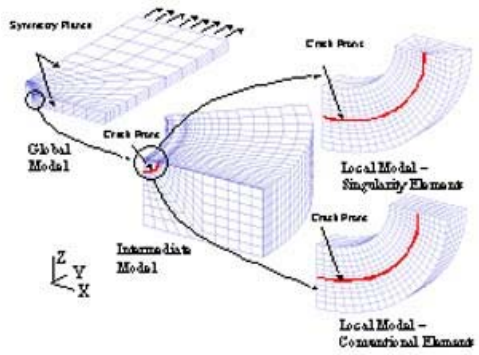

Figure 9.7.2.1 Global-intermediate-local hierarchical approach

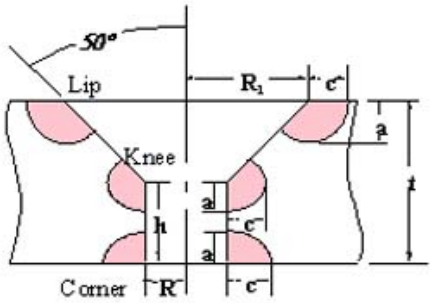

Figure 9.7.2.2 Center-crack configurations for first group

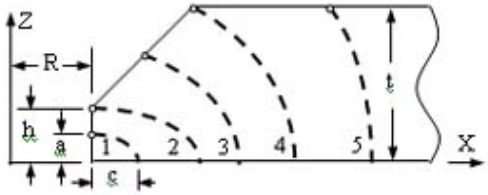

Figure 9.7.2.3 Crack configurations for second group

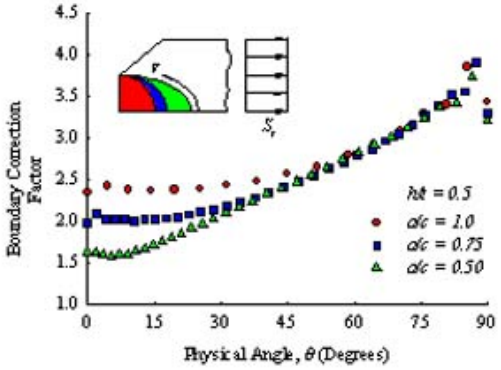

Figure 9.7.2.4 Effect of crack shape

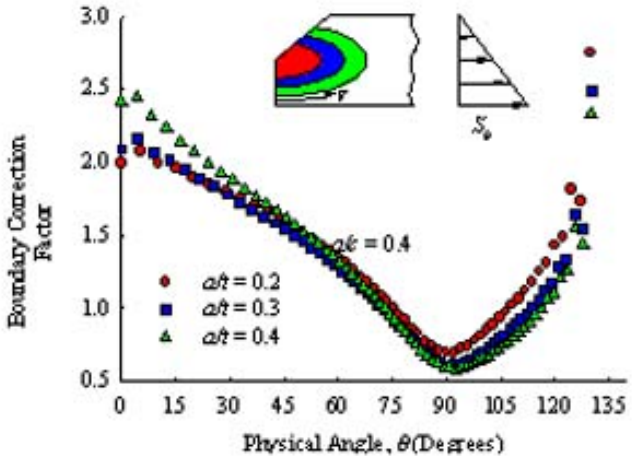

Figure 9.7.2.5 Effect of crack size

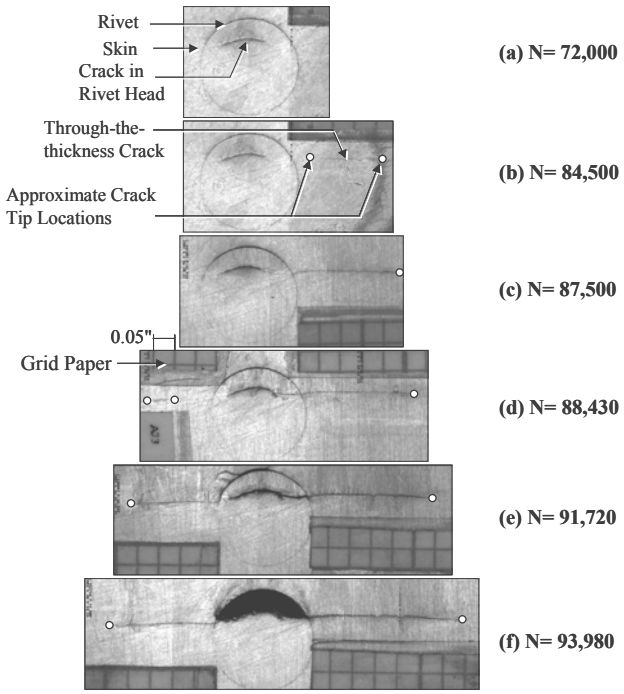

Figure 9.7.3.1 Crack growth process in outer critical rivet row

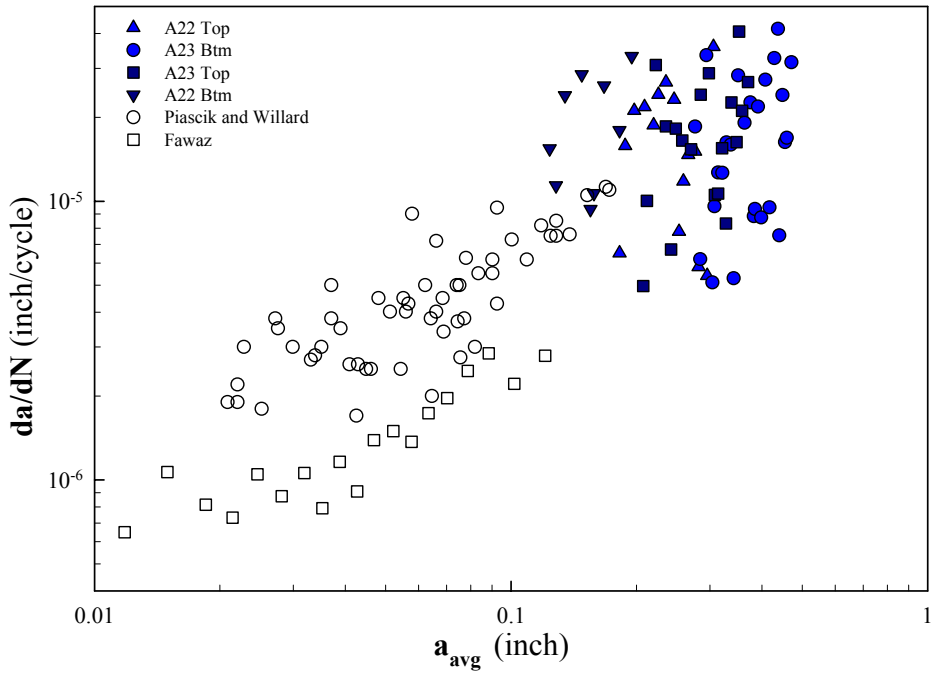

Figure 9.7.3.2 Fatigue crack growth characteristics

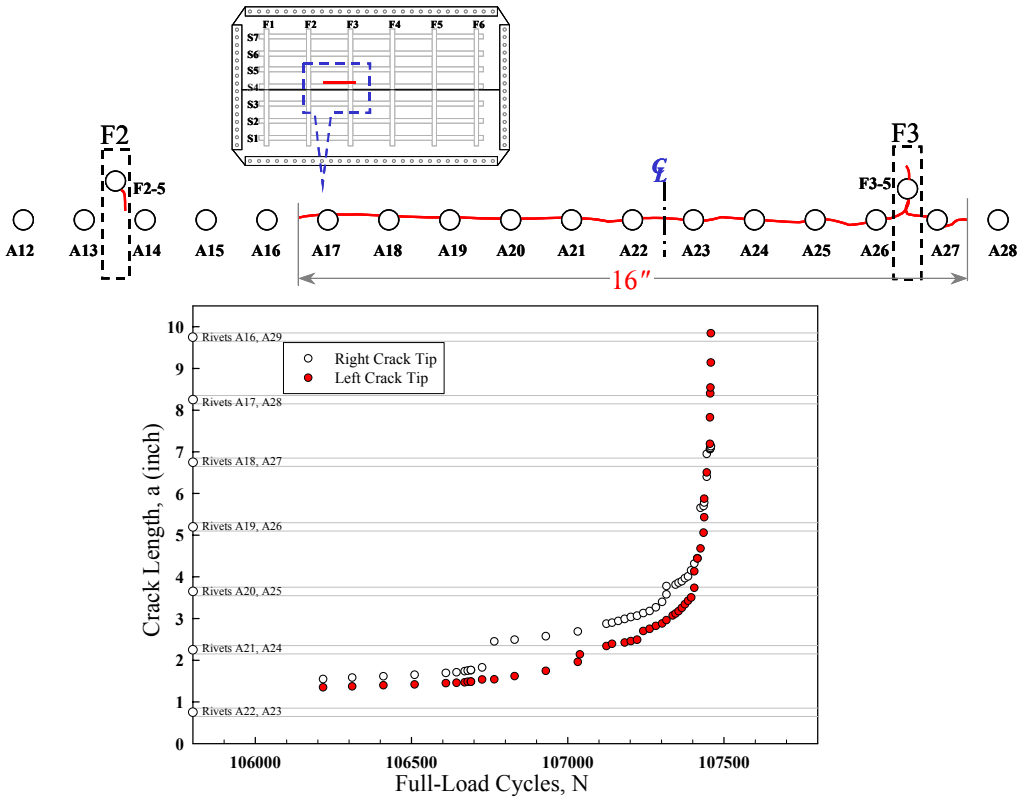

Figure 9.7.3.3 Lead crack length as a function of fatigue cycles

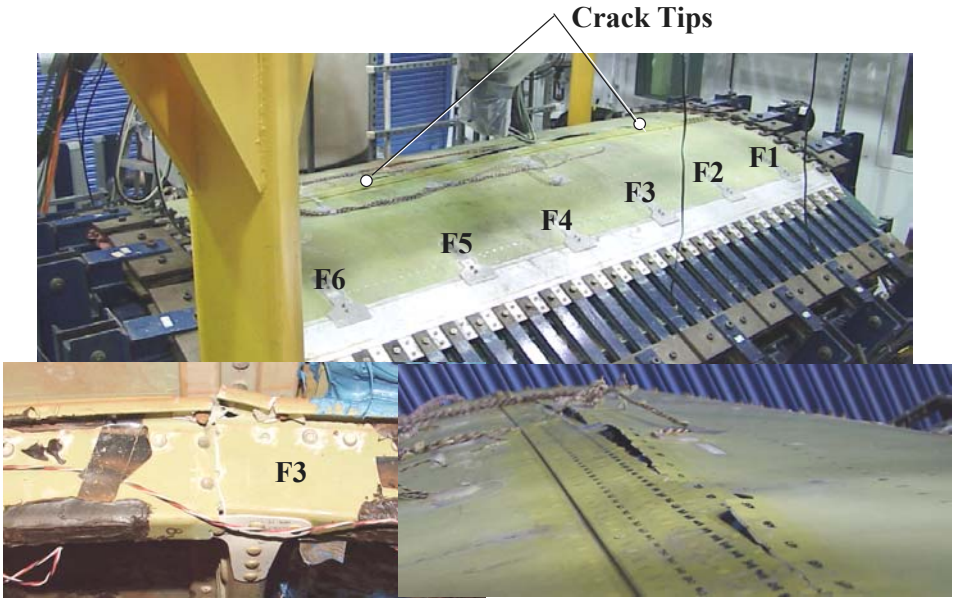

Figure 9.7.3.4 Failed panel with final crack

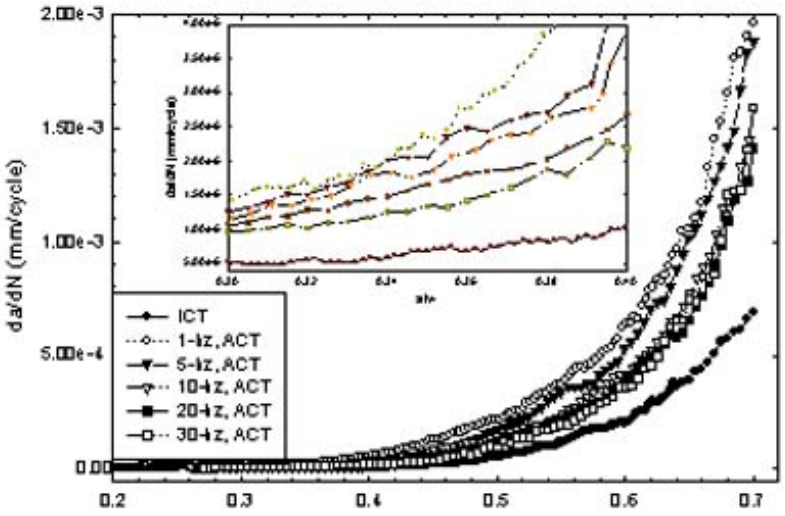

Figure 9.8.2.1 Comparison of fatigue CGR results for tests conducted at different frequencies

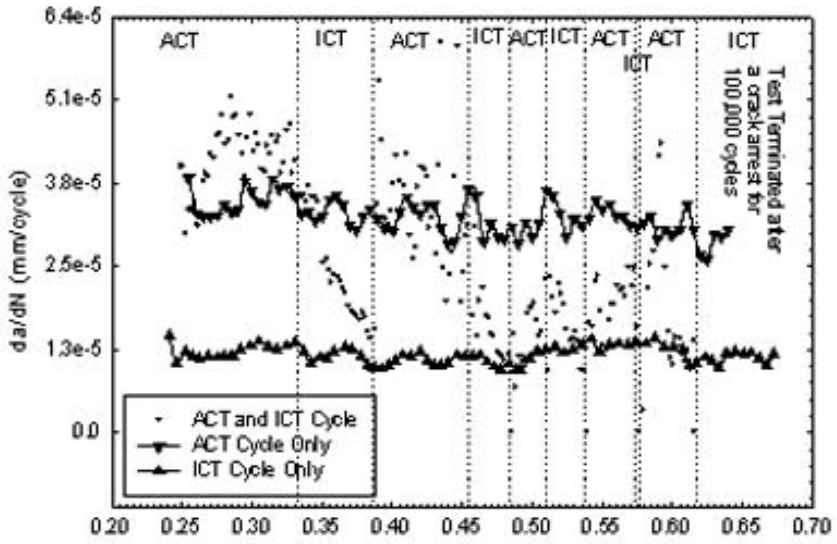

Figure 9.8.2.2 Test conducted under alternating ACT (in the presence of electrolyte) and ICT (dry air) environment under constant stress intensity condition

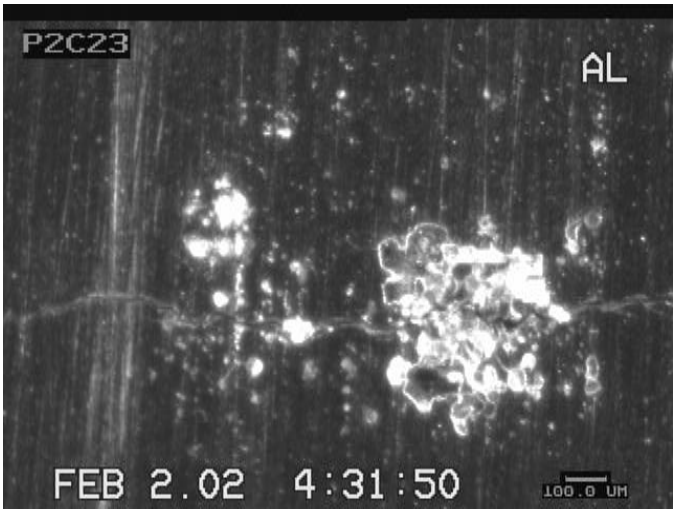

Figure 9.8.3.1 Example of crack originating at a corrosion pit

Figure 9.8.3.2 Example of damage found in fuselage panel rivet holes

Figure 9.9.1.1 S-3B Viking wing/fuselage test airframe installed in reaction frame – Lockheed Martin Structural Test Laboratory, Marietta, Georgia – Fatigue testing span: 17 September 2001 to 11 November 2002

Figure 9.9.1.2 S-3B Viking empennage test airframe installed in reaction frame (vertical tail shown partially folded for inspection) – Lockheed Martin Structural Test Laboratory, Marietta, Georgia – Fatigue testing span: 13 December 2001 to 21 August 2002

Figure 9.9.2.1 P-3C wing/fuselage test airframe mounted on structural test floor – Lockheed Martin Structural Test Laboratory, Marietta, Georgia – Fatigue testing span: 30 October 2001 to 2 December 2002

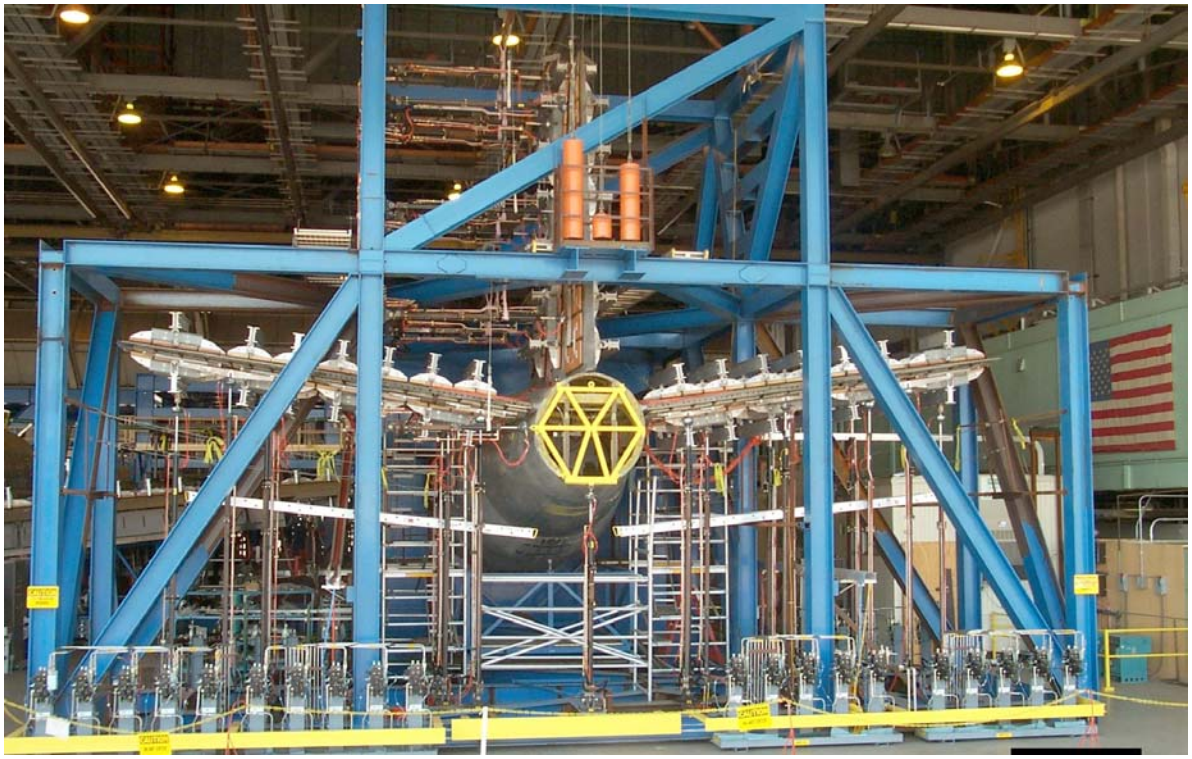

Figure 9.9.2.2 P-3C Empennage test airframe installed in reaction frame – Lockheed Martin Structural Test Laboratory, Marietta, Georgia – Fatigue testing span: 24 April 2001 to 30 October 2002

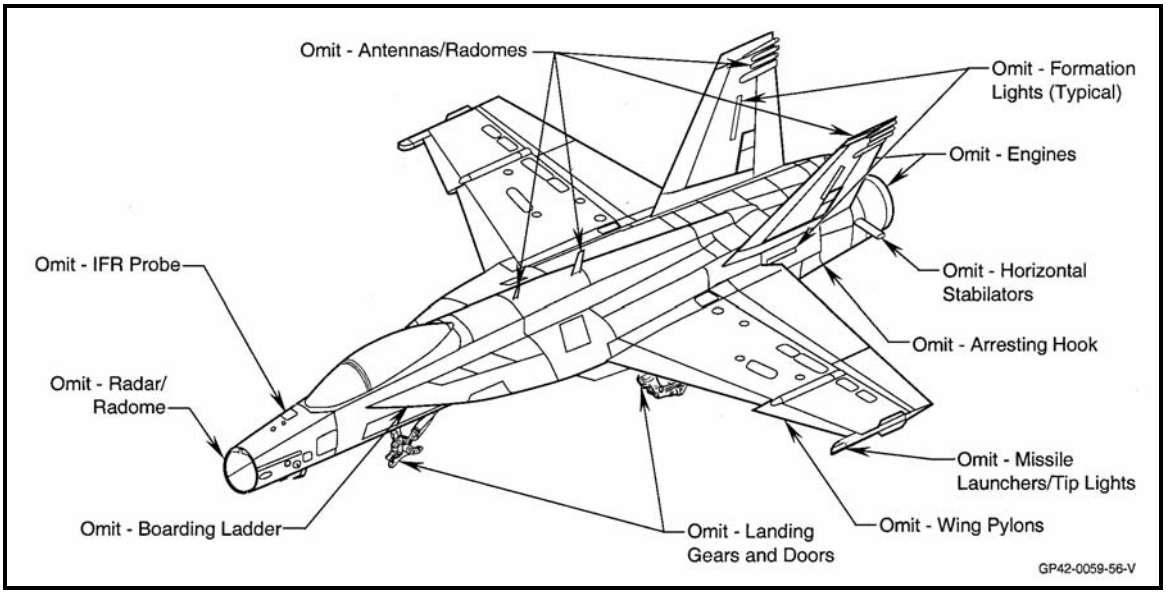

Figure 9.9.3.1 F/A-18E/F full-scale static and fatigue test article structural configuration

Figure 9.9.3.2 F/A-18E/F full-scale fatigue test article in the test fixture

Figure 9.9.4.1 Fuselage prior to drop test

Figure 9.9.4.2 Results of fuselage drop test

Figure 9.9.5.1 Photo of onboard oxygen analysis system

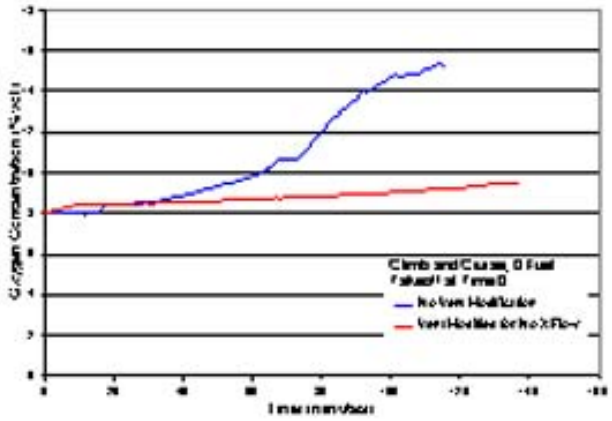

Figure 9.9.5.2 Average fuel tank oxygen concentration during a typical 2-hour flight for different venting configurations

Figure 9.9.6.1 NAPTF test vehicle

Figure 9.9.6.2 Results after repeated passes of the test vehicle

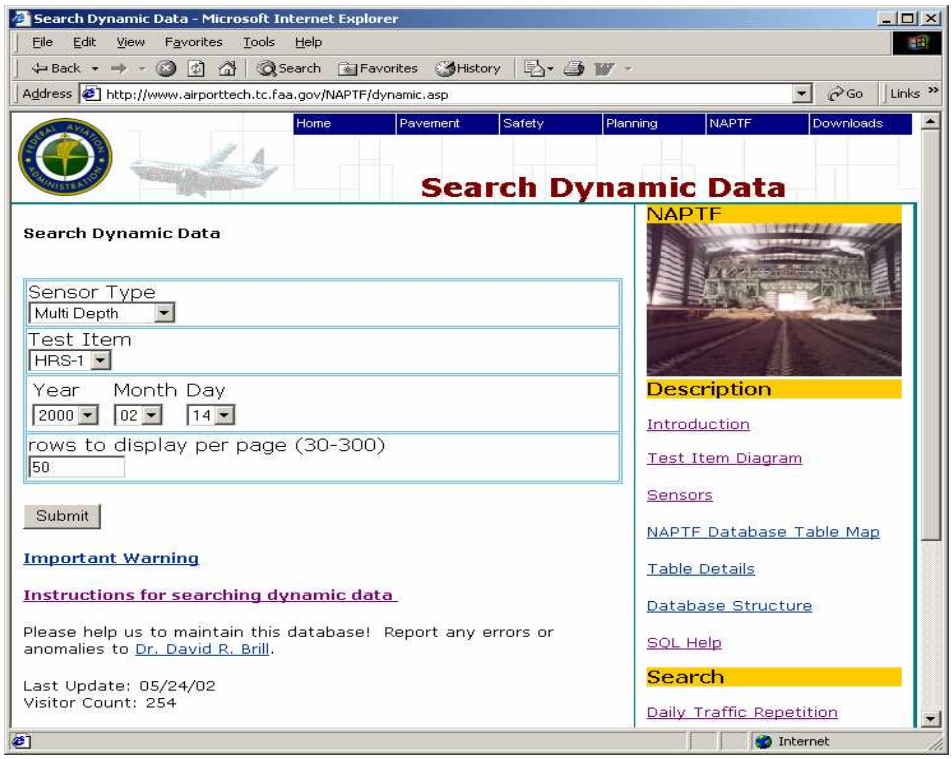

Figure 9.9.7.1 On-line data base

Figure 9.9.8.1 Aerospace vehicles

Figure 9.9.8.2 Test capabilities of the CASRL

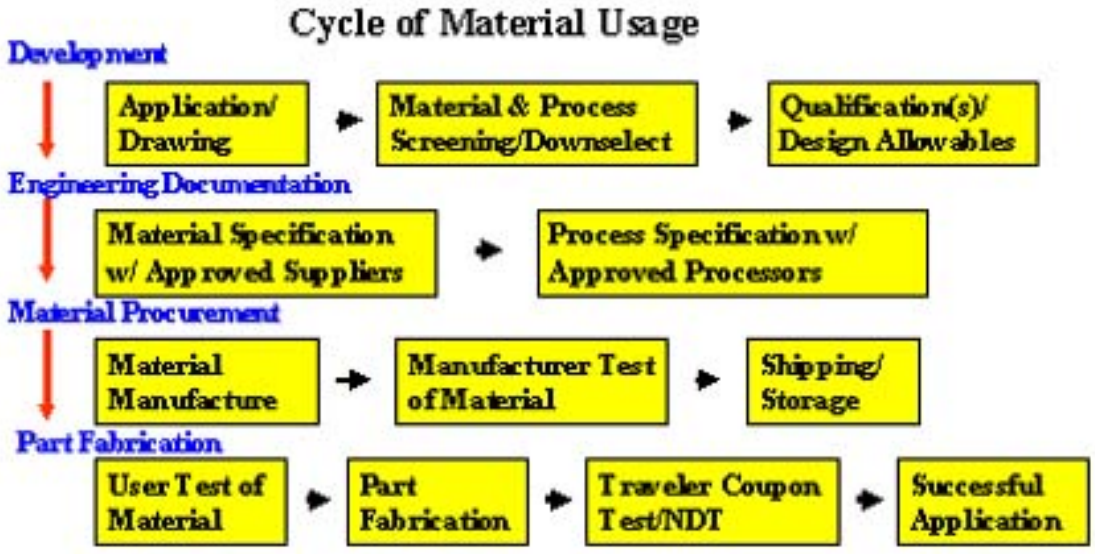

Figure 9.10.1.1 Life cycles for composite materials

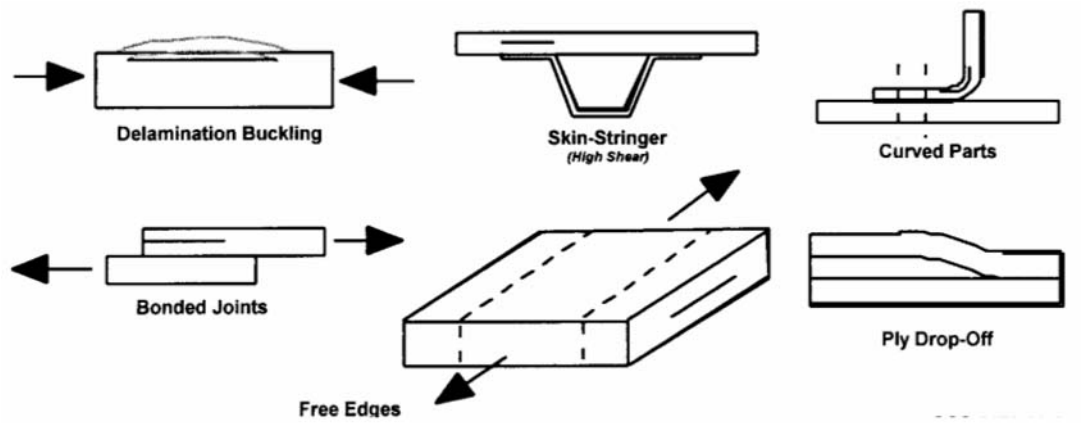

Figure 9.10.2.1 Locations for possible delamination initiations

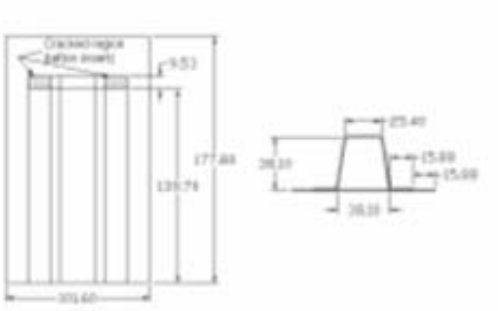

Figure 9.10.2.2 Skin-stringer geometry considered (all dimensions in mm)

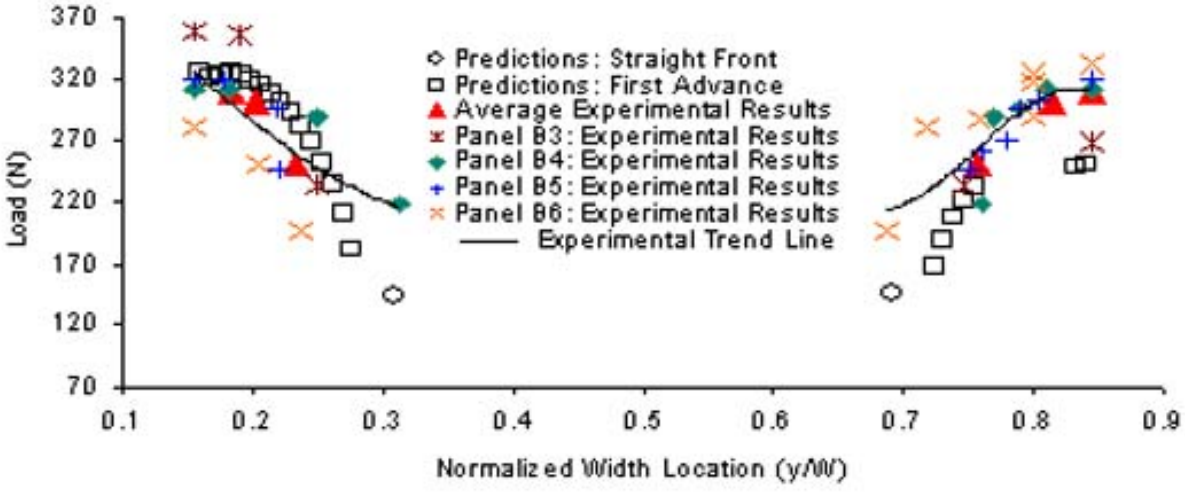

Figure 9.10.2.3 Comparison of predicted and observed results for the bending panels

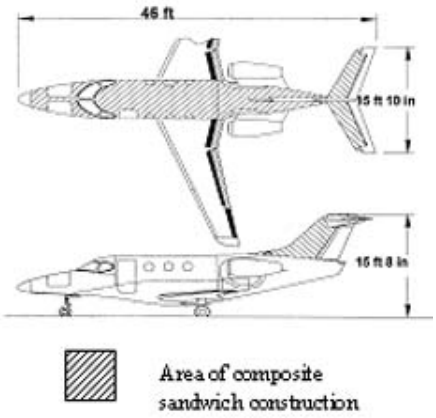

Figure 9.10.3.1 Composite sandwich applications by Raytheon

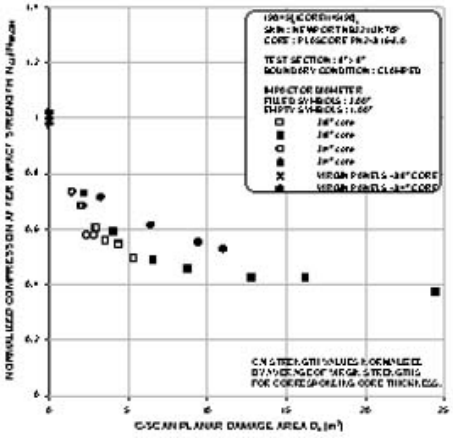

Figure 9.10.3.2 Compression after impact strength versus planar damage area for $[(90/45)_2/\text{core}/(45/90)_2]$ panels

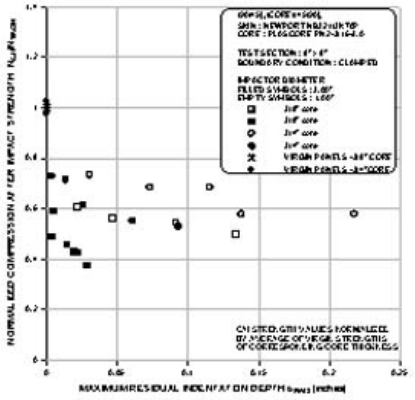

Figure 9.10.3.3 Compression after impact strength versus maximum dent depth for $[(90/45)_2/\text{core}/(45/90)_2]$ panels

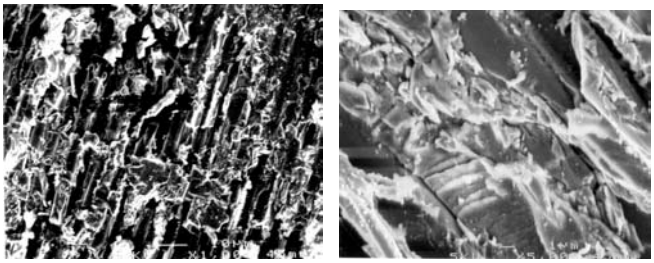

1000x 5000x

FEP, blast
Matrix morphology extremely jagged & random
Carbon fiber orientation visible but fibers unbroken

Figure 9.10.4.1 SEM images of surfaces cured against FEP release film and blasted

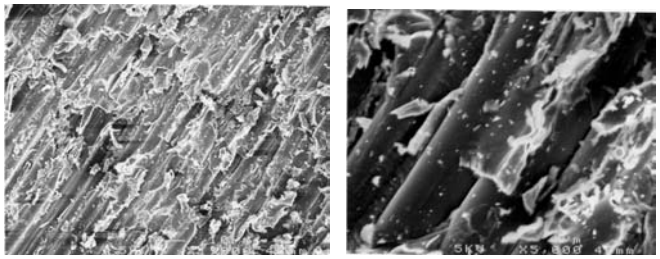

1000x 5000x

NAT, blast
Peel ply fiber impression no longer visible
Carbon fiber pattern exposed but fibers apparently not broken
Matrix extremely broken and jagged

Figure 9.10.4.2 SEM images of surfaces cured against NAT peel ply and blasted

Figure 9.10.5.1 BlackglasTM/Nextel 312 panel mounted to shaker for test

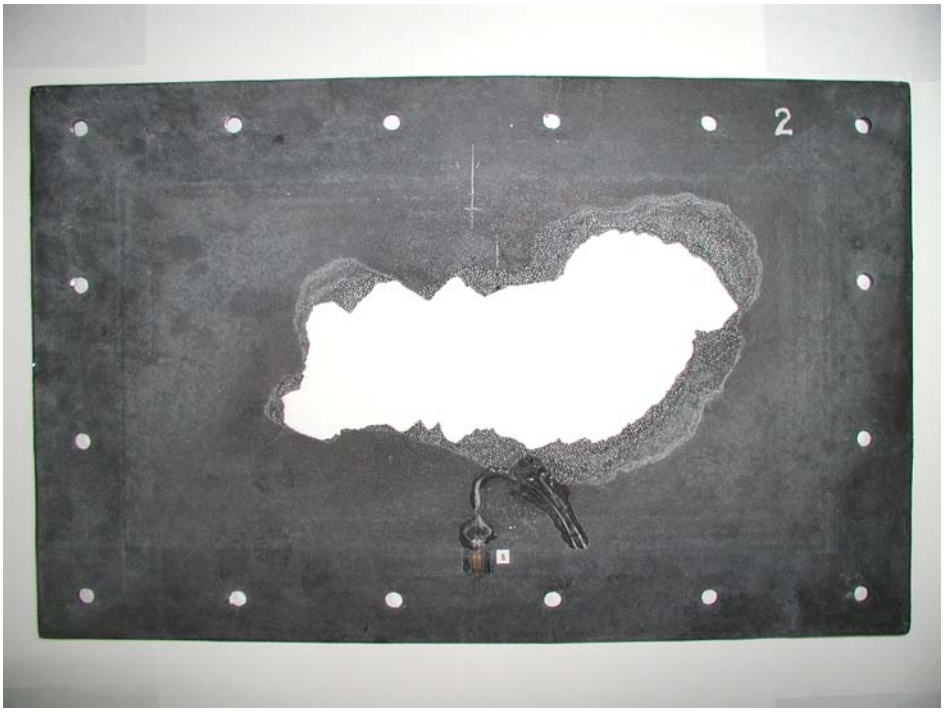

Figure 9.10.5.2 Room temperature test of ceramic matrix composite panel in traveling wave tube. List of publications for 2001

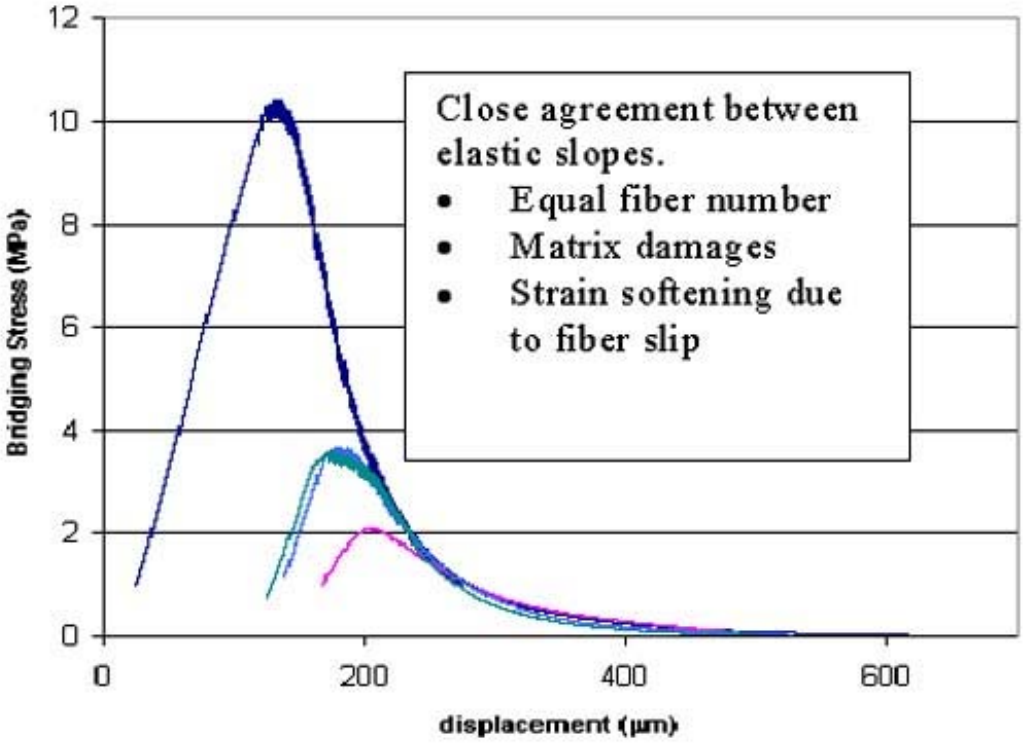

Figure 9.10.6.1 Family of PFT curves

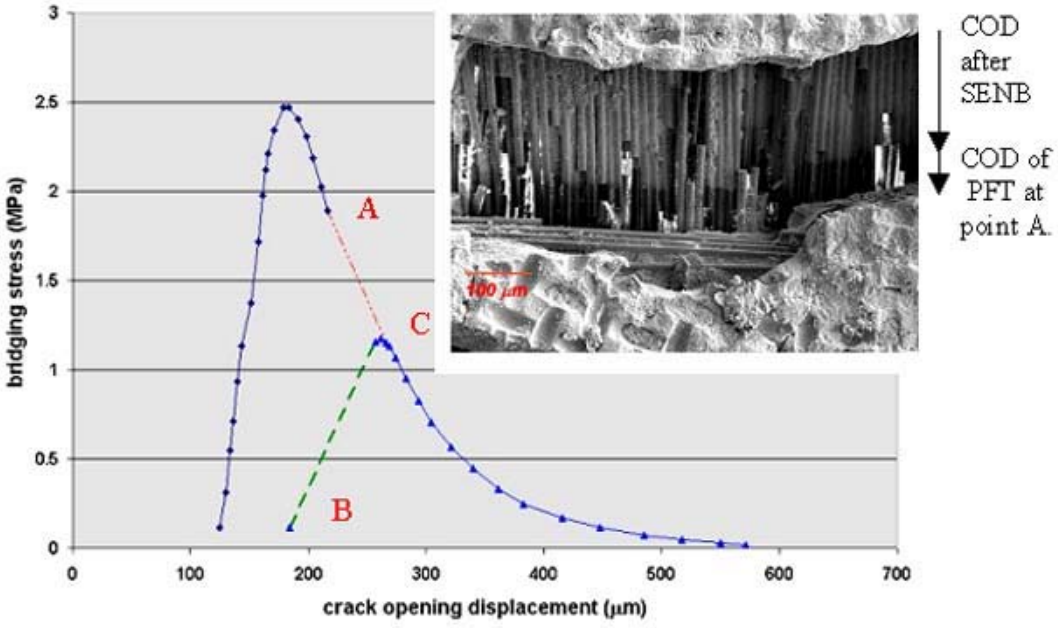

Figure 9.10.6.2 PFT loading/reloading

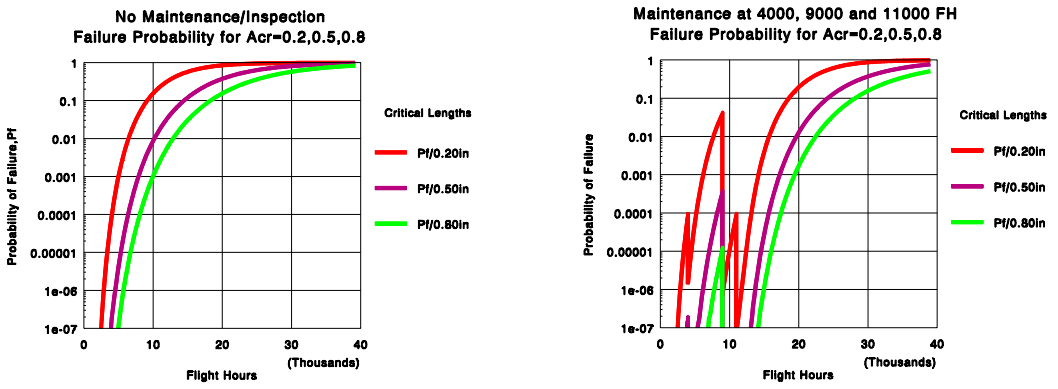

Figure 9.11.1.1 Failure probability evolution: (a) no inspection, (b) with inspections

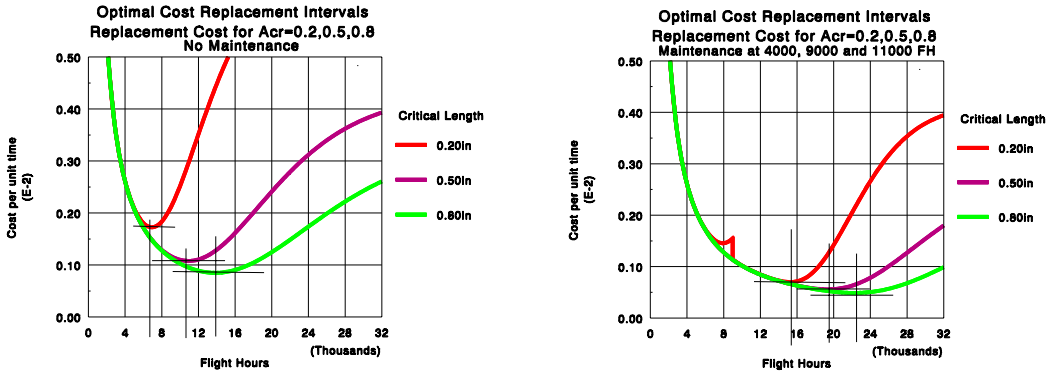

Figure 9.11.1.2 Maintenance cost versus removal time: (a) no inspection, (b) with inspections

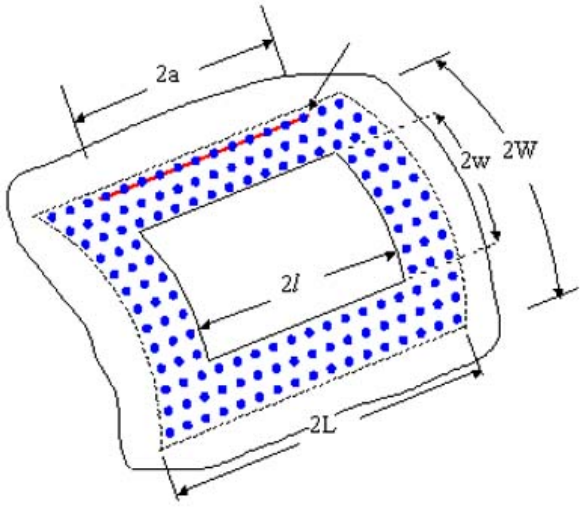

Figure 9.11.3.1 Repair patch configuration

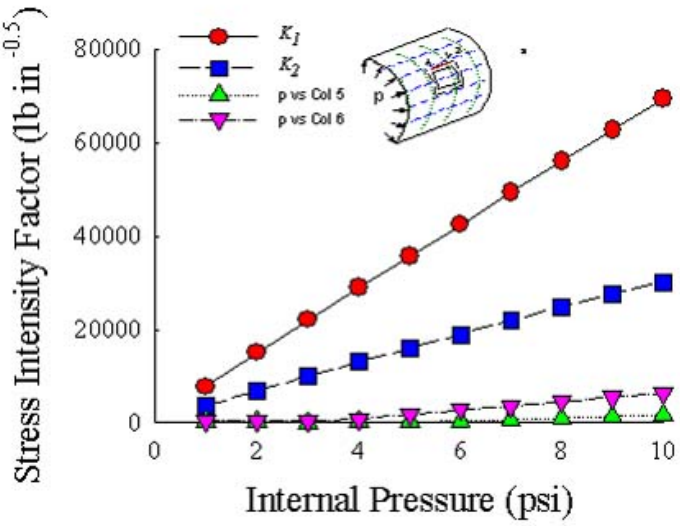

Figure 9.11.3.2 Mixed-mode stress-intensity factors

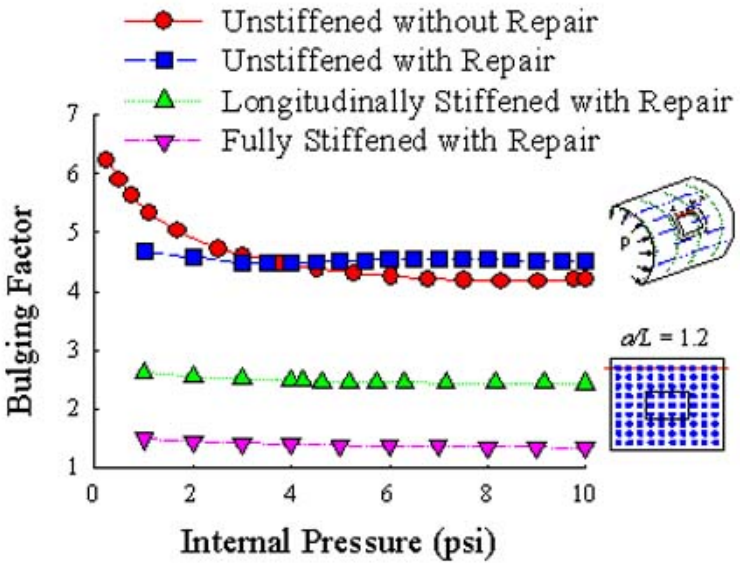

Figure 9.11.3.3 Effect of configuration on bulging factor

Figure 9.11.4.1 Composite doubler during cure cycle

Figure 9.11.4.2 Ultrasonic inspection of repair

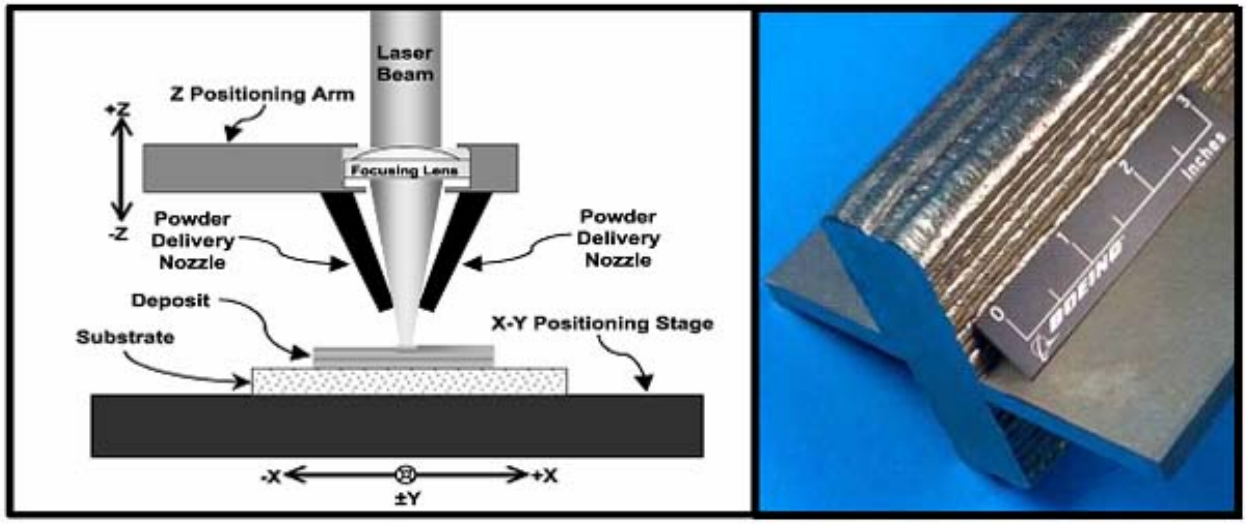

Figure 9.11.5.1 Schematic diagram of the LAM process and actual LAM'ed part

Table 9.11.5.1 Typical properties for Aeromet LAM

DIRECTION	NUMBER OF TESTS	STRENGTH (ksi)		E	ELONGATION (%)	
		UTS	0.2% YS	(Msi)	TOTAL	R.A.
X	256	138.4	125.3	17.2	11	24
Y	59	140.4	127.6	17.1	11	22
X&Y Combined	315	138.8	125.8	17.2	11	24
Z	169	134.6	120.7	16.9	15	38
XZ - 45°	8	146.0	131.1	18.2	11	18
YZ - 45°	8	141.0	127.5	18.4	10	15
Substrate - Heat Treated	26	144.2	132.0	18.7	15	27
Substrate - Heat Affected Zone	29	136.1	121.9	17.5	15	
Wrought Mill Annealed		145.0	130.0	16.9	14	

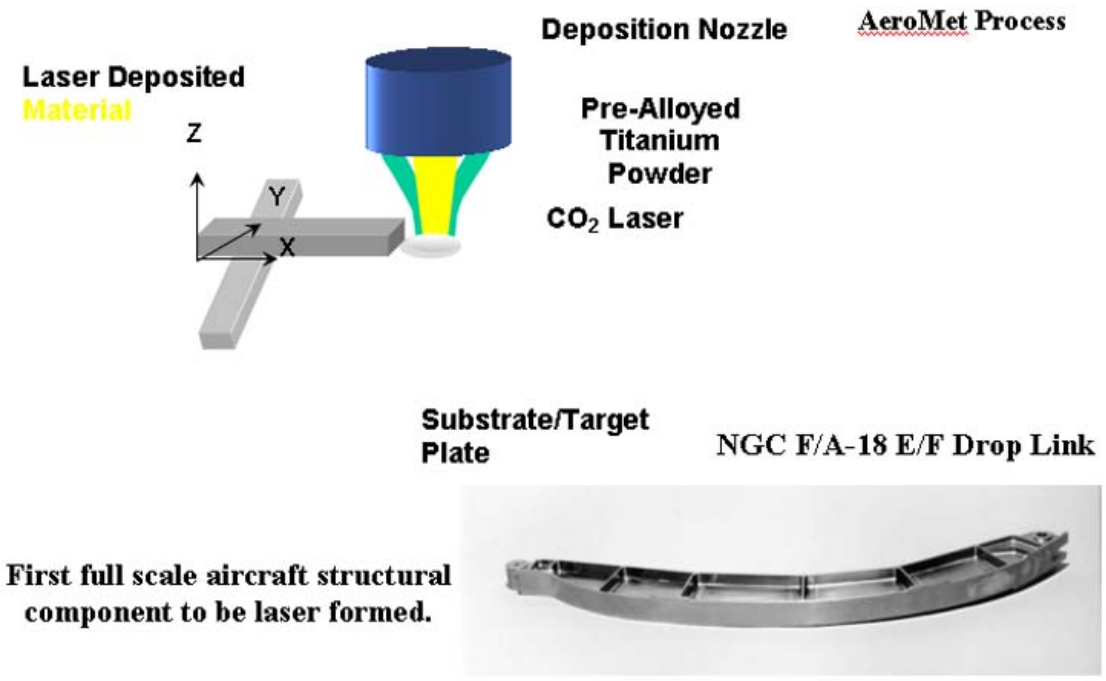

Figure 9.11.6.1 Laser formed titanium

Figure 9.11.7.1 Main data screen

Figure 9.11.7.2 Main user screen

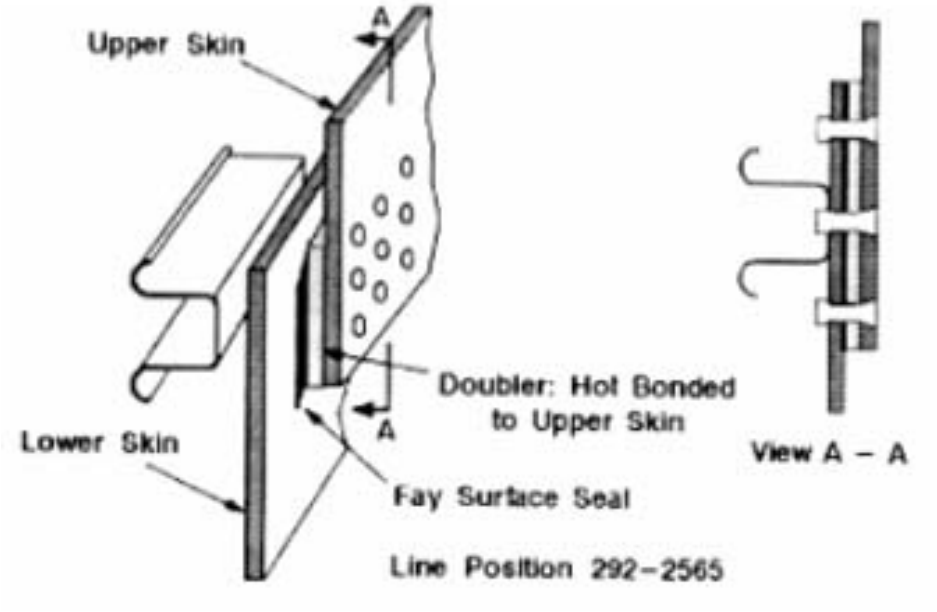

Figure 9.12.1.1 Boeing lap splice joint configuration

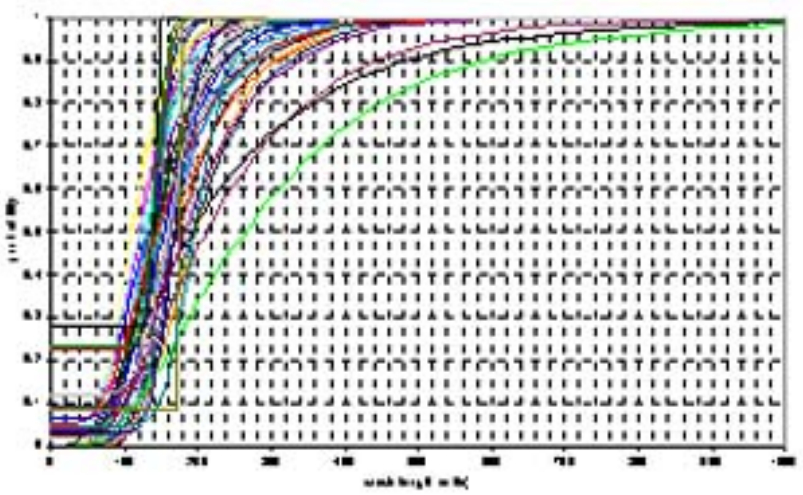

Figure 9.12.1.2 Probability of detection curves for 56 inspectors

Figure 9.12.2.1 Ultra Image IV inspecting the upper wing plank/stringer of the C-130 Center Wing

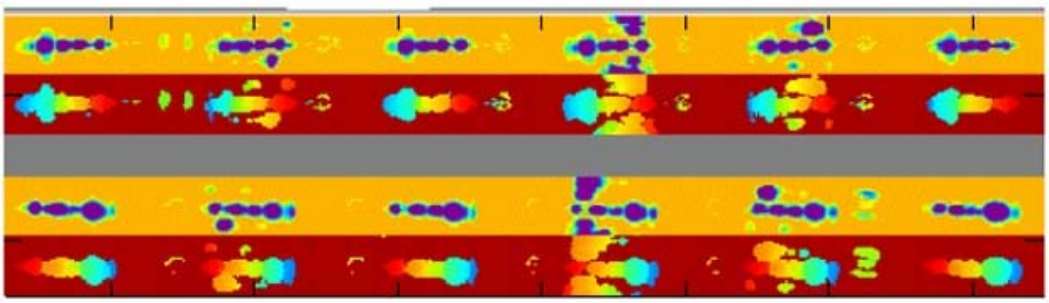

Figure 9.12.2.2 Ultrasonic C-scan image from inspecting the wing plank/stringer flange set-up sample

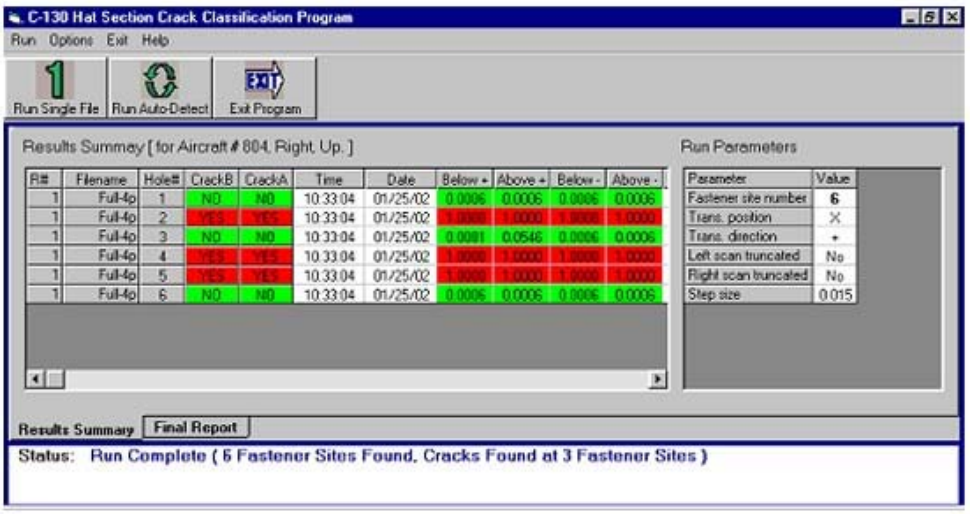

Figure 9.12.2.3 ADA results from the two channels of ultrasonic data in Figure 9.12.2.2. The ADA software successfully identifies all the defects in the set-up sample

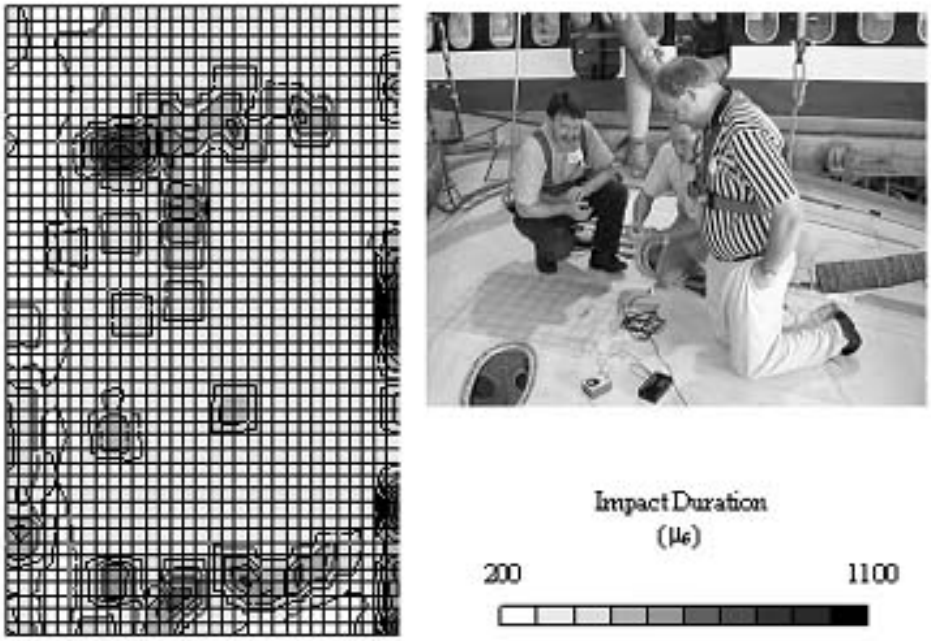

Figure 9.12.3.1 CATT image of MD80 heater

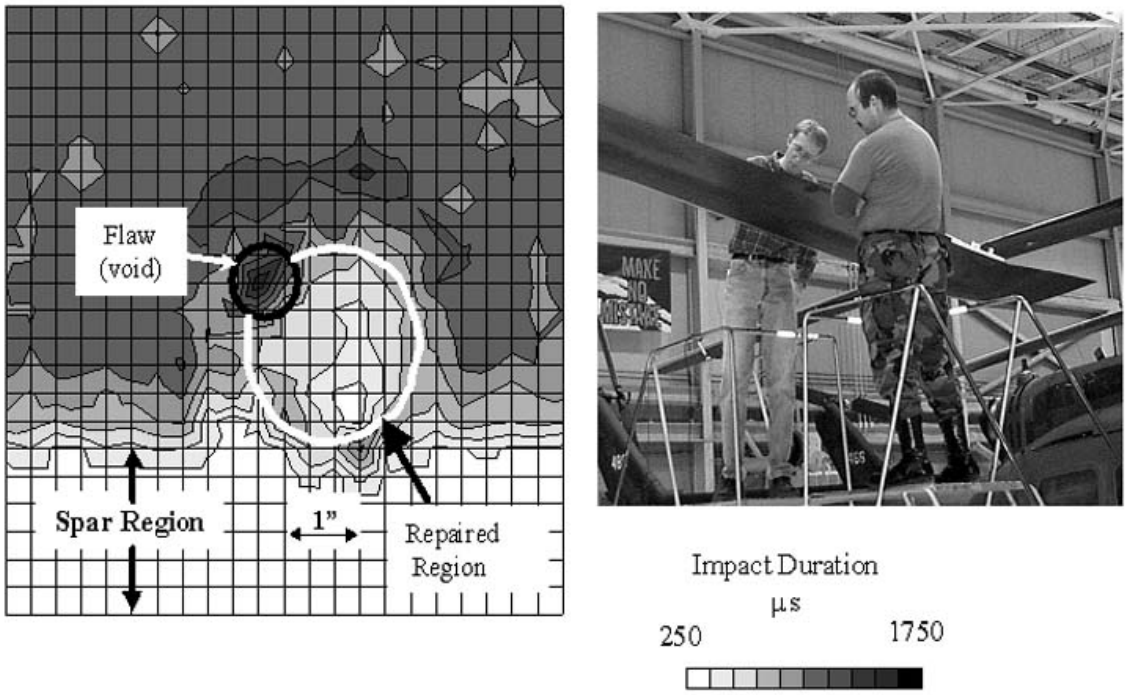

Figure 9.12.3.2 A 22cm x 22cm tap test scan image of a repair on a Black Hawk helicopter rotor blade

Figure 9.12.4.1 Front and back photos of G11 solid laminate set

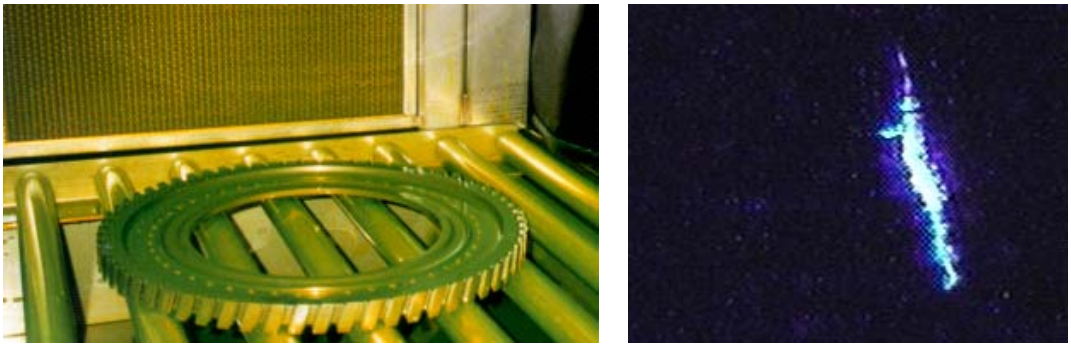

Figure 9.12.5.1 (a) Typical engine part with fluorescent penetrant solution applied to the part and (b) Example of the FPI response of a 60-mil crack captured using digital imaging as part of the FPI studies

Figure 9.12.5.2 (a) Oven dryer that contains three furnaces and (b) Flash-dry tank used to process components prior to FPI

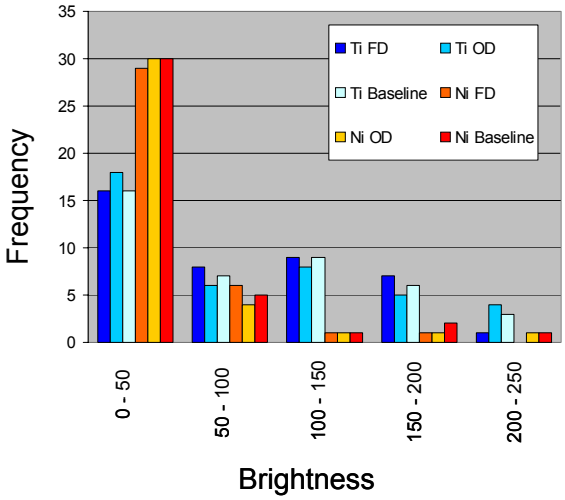

Figure 9.12.5.3 Brightness histograms comparing flash dry and oven dry results to the baseline brightness for titanium and nickel samples

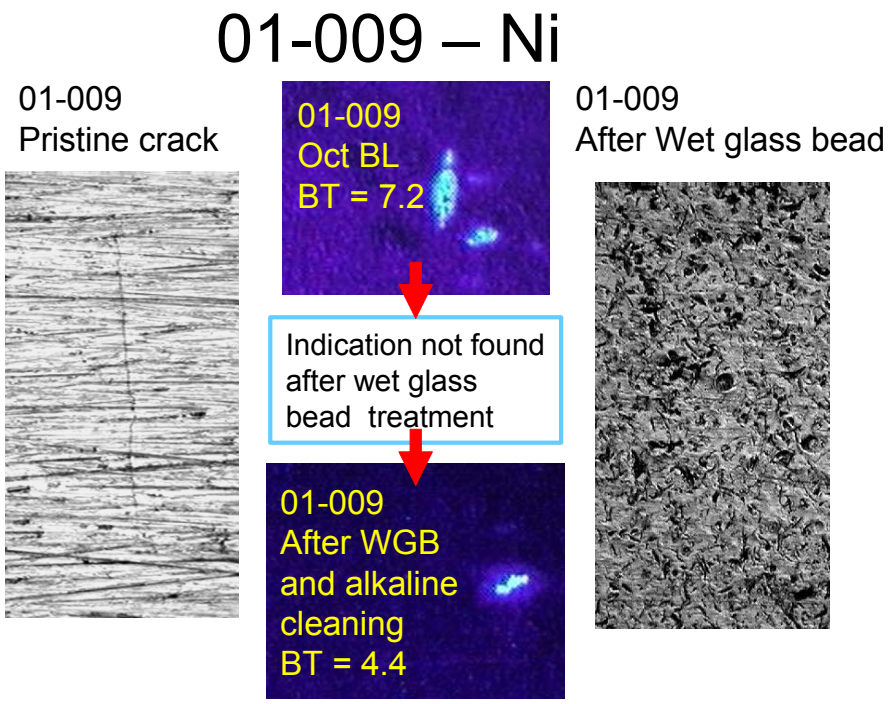

Figure 9.12.5.4 Results for nickel sample 01-009

Figure 9.12.6.1 Nickel billet ultrasonic inspection demonstration

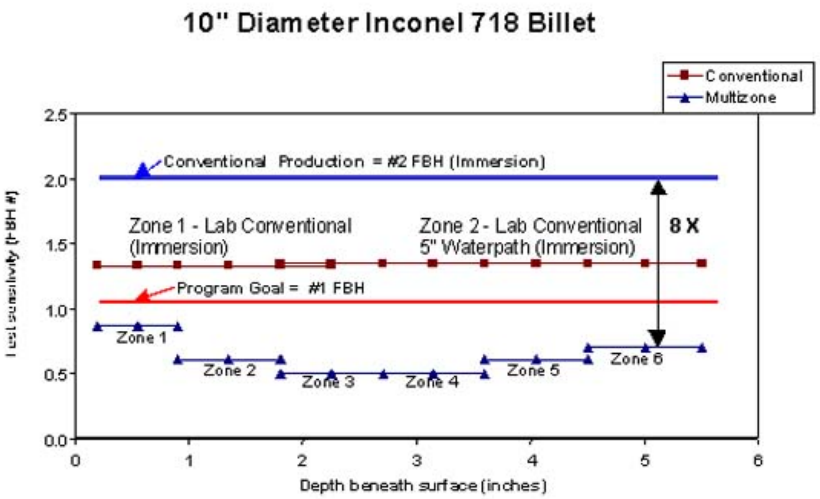

Figure 9.12.6.2 Comparison of conventional and multizone inspection of Inconel 718

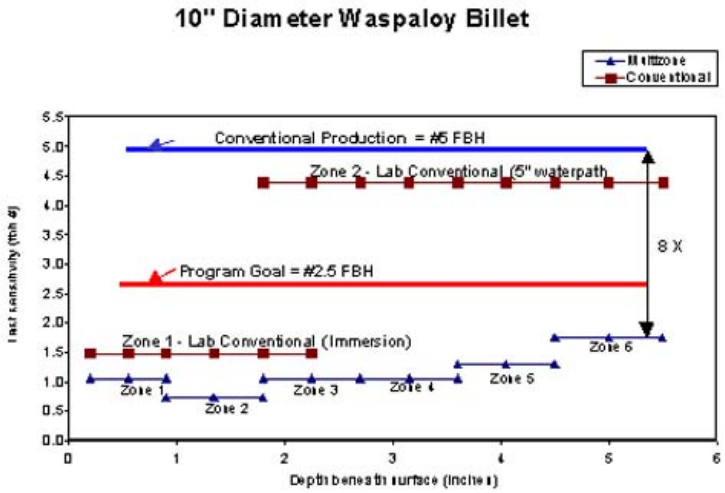

Figure 9.12.6.3 Comparison of conventional and multizone inspection of Waspaloy

Figure 9.12.7.1

Figure 9.13.1.1 Uncontained engine fan disk

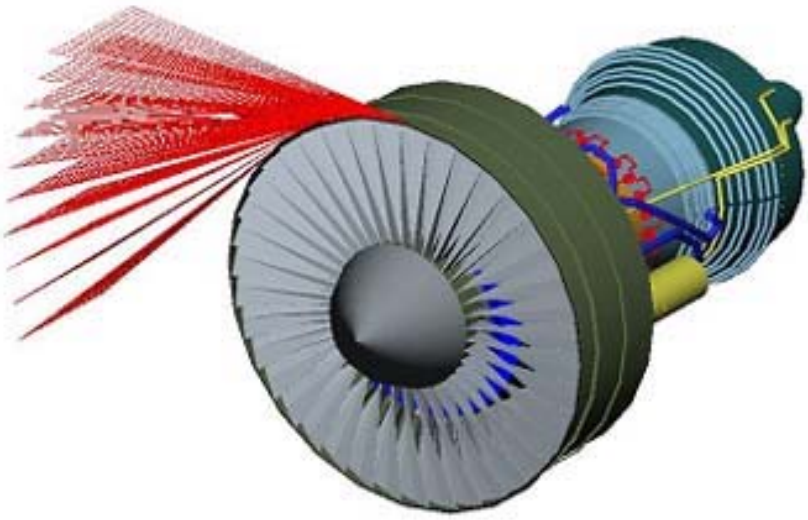

Figure 9.13.1.2 Uncontained engine failure model

Figure 9.13.2.1 Uncontained engine fan disk debris

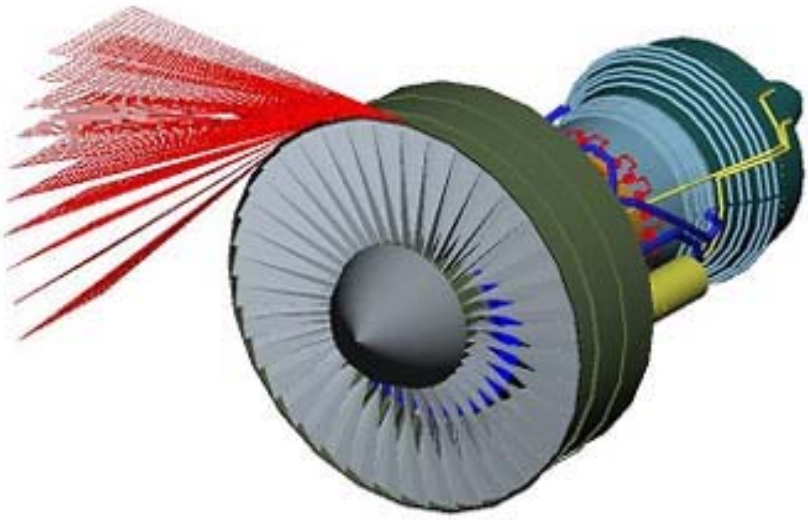

Figure 9.13.2.2 Uncontained engine failure model

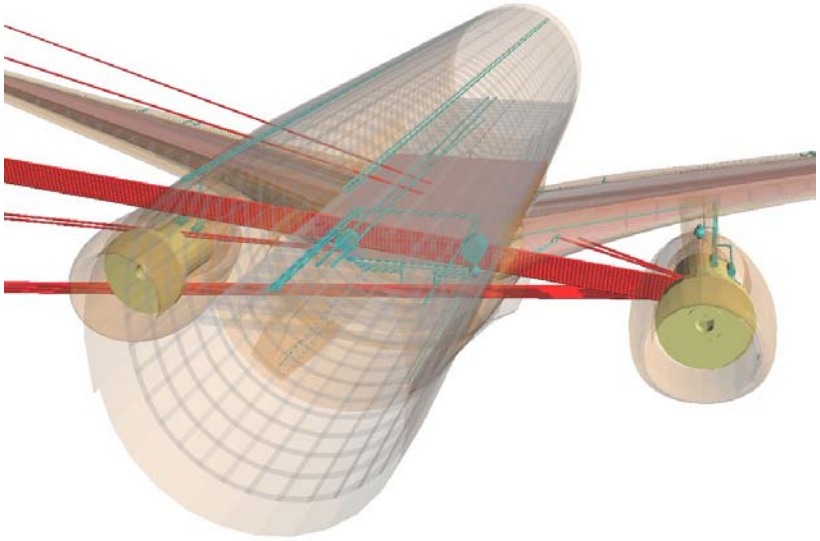

Figure 9.13.2.3 UEDDAM disk burst analysis

Figure 9.13.3.1

Figure 9.13.3.2 Uncontained fan disk failure due to an abusively machined bolthole

Figure 9.13.4.1 Fuselage air-gun test facility

Figure 9.13.4.2 Photograph of Ti-6Al-4V sample after testing

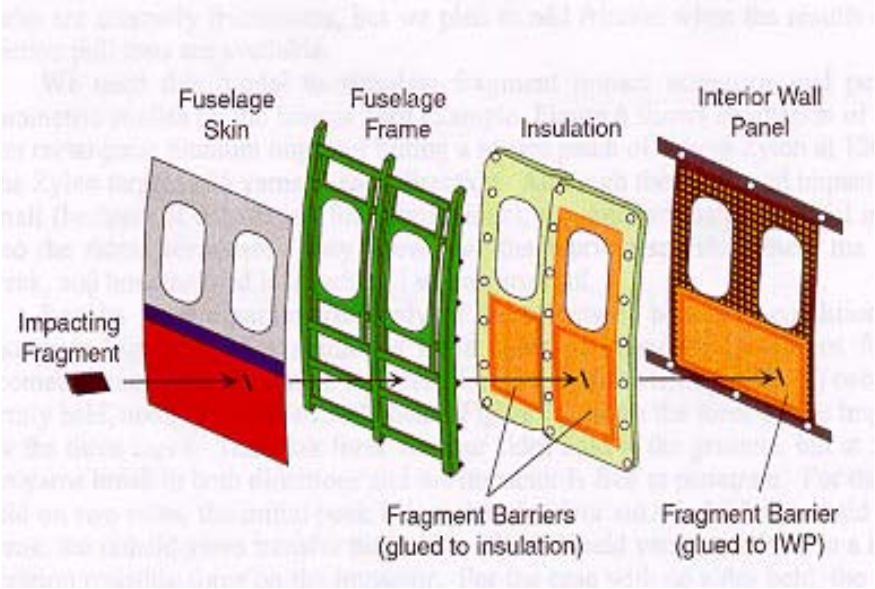

Figure 9.13.5.1 Armor fabric installation schematic

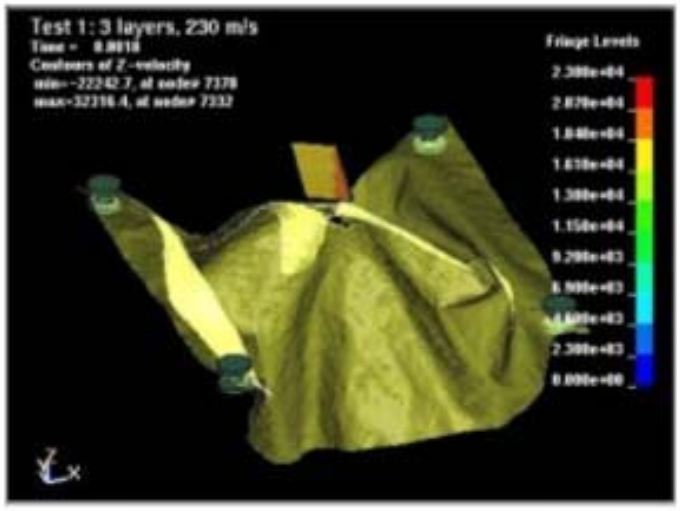

Figure 9.13.5.2 Simplified model - ballistic simulation

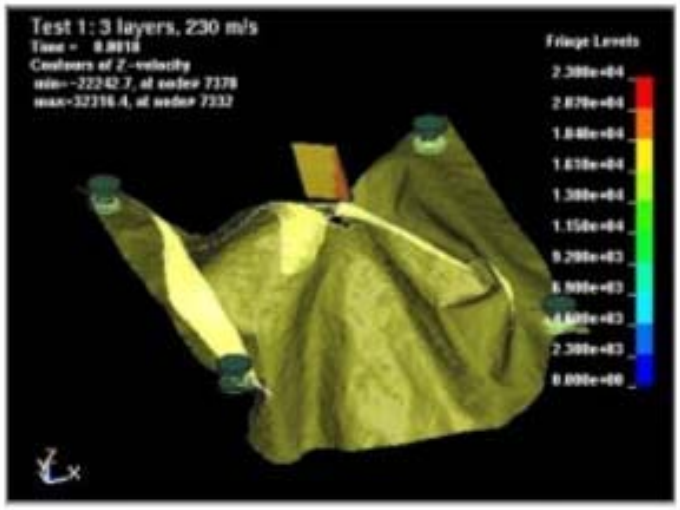

Figure 9.13.6.1 Simplified model – ballistic simulation

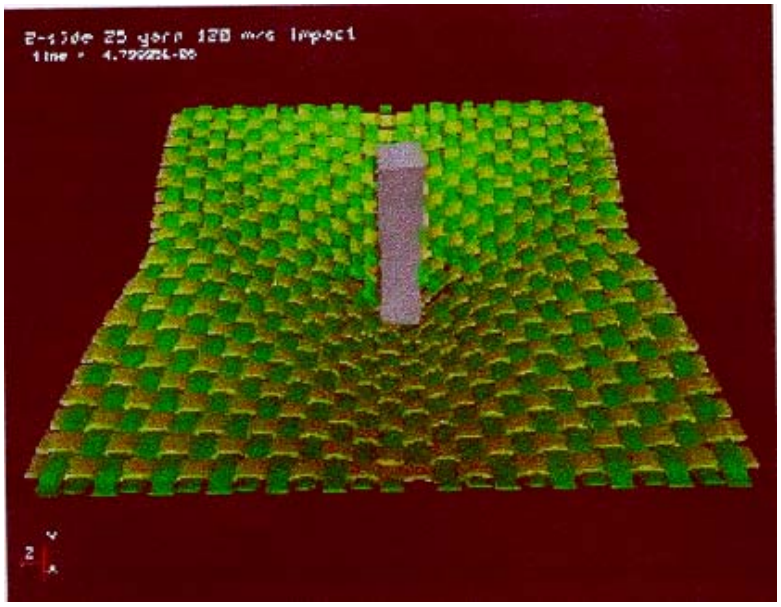

Figure 9.13.6.2 Model of fabric impact by debris

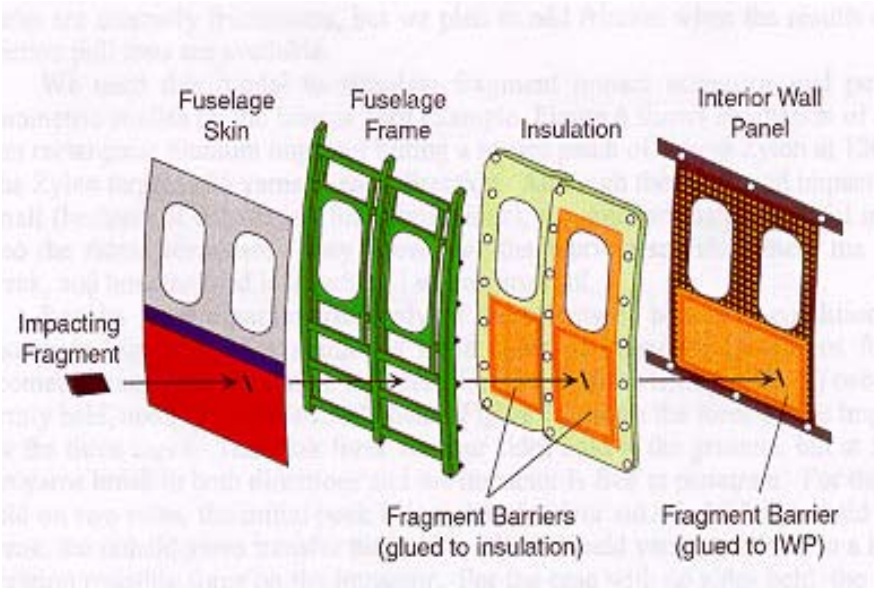

Figure 9.13.6.3 Armor fabric installation schematic